

**LIPID-BASED NANOPARTICLES FOR TOPICAL  
DELIVERY OF HAIR GROWTH THERAPEUTIC  
MOLECULES**

**NORHAYATI MOHAMED NOOR**

**Thesis submitted in accordance with the requirements of UCL for the degree of  
Doctor of Philosophy**

**October 2017**

**UCL School of Pharmacy  
29 – 39 Brunswick Square  
London WC1N 1AX  
United Kingdom**

# Declaration

This work has been conducted at The School of Pharmacy, University College London between April 2014 and October 2017 under the supervision of Professor Kevin M.G. Taylor, Dr Satyanarayana Somavarapu and Dr Khalid Sheikh.

I, Norhayati Mohamed Noor certify that research described is original. I certify that I have written all the text and that all source materials, which have already appeared in the publication, have been clearly acknowledged by suitable citations.

Signature: \_\_\_\_\_

Date: \_\_\_\_\_

*Dedicated to my husband, Mohd Husni Yusoff  
and my children, Iman Syakirin and Nur Damia Safrina*

# Acknowledgments

First and foremost, I would like to thank God the Almighty for giving me the strength, energy, good health, ability and idea that keep me going and completed my PhD study. Without His blessings, I would not be able to finish my study.

I would like to express my appreciation to Universiti Teknologi Malaysia (UTM) and Malaysian Government for sponsoring and giving me an opportunity to further my study abroad. They have put trust on me to let me do research and obtain experiences from the expertise around the world so that I can use the knowledge back home.

I would like to convey my greatest gratitude to my first supervisor, my mentor, Professor Kevin MG Taylor for his continuous patient, guidance, valuable advice and comments, encouragement and support in many ways throughout this research work. It was a great honour for me to be given an opportunity to work under his supervision. Without his continuous support and interest, my thesis would not have been the same as presented here.

I also would like to express my appreciation to my other supervisors, Dr Khalid Sheikh and Dr Satyanarayana Somavarapu for giving me an opportunity to further my PhD study at UCL School of Pharmacy and also giving ideas, suggestions and advices during my entire PhD study.

I indebted to Institute of Bioproduct Development (IBD) especially to Prof Ramlan Aziz, Professor Dr Mohamad Roji Sarmidi, Miss Rohaizan Khairul Anuar and all the entire staff for their encouragement and moral support.

My sincere appreciation specially goes to my 402 lab mates, Dr Zahra Merchant, Miss Noratiqah Mohtar, Miss Nattika Nimmano and Mr Acom Sornsute for contributing ideas, sharing knowledge and never stopped giving me an abundance of moral supports. For me, they are my family members who are always being here when I was in happy and sad situations. For my other SoP friends, Mina, Mandana, Maria, Fon, Pedro, Sarah, Francesca, Dr Tony, Dr Andre, Yacine, thank you so much for your attendance. I am truly glad for being surrounded by these wonderful people.

I would like to offer my special thanks to my other Malaysian colleagues especially to Dr Mohd Mukrish, Mrs Wan Azrina, Mr Muhammad Fauzi, Dr Erazuliana Abd. Kadir, Dr Awis Sabere, Dr Choon Fu Goh and Dr Nor Liyana for the moral support, knowledge and encouragement during my stay in London. Special thanks to Dato' Yunus Rais, my English teacher in London, for sharing his valuable knowledge especially on the English culture, history, poems and general knowledge.

My great special thanks extended to the staff of UCL School of Pharmacy, especially to Ms Isabel Goncalves, Ms Catherine Baumber, Ms Kate Keen, Ms Alison Dolling, Mr David Mc Carthy, Ms Satinder Sembi, Dr Sunny Hardyal Gill, Mr John Frost, Mr Rob Wittwer, Dr Renu Datta, Mr Chris Cook, Mr Elias Skourletos and Mr Victor Diran for their help and contribution that made my PhD journey smoothly and so valuable. Without their contribution, I am not able to complete my PhD study.

I would like to express my lovely thanks to my family members for their loving support and encouragement throughout the work. To my husband, Mr Mohd Husni Yusoff, thank you so much for your continuous support, especially on managing the house chores. Without you, I would not be able to concentrate and complete my study. And for my two children, Iman Syakirin and Nur Damia Safrina, both of you are awesome. Thank you so much for sacrificing your comfort zone in Malaysia and be with me in the UK. I am so sorry; I could not be with you all the time. Wearing two hats at once was so challenging, which taught me how to manage time properly. Not to forget, my mom, Mrs Wan Norhani Wan Mustaffa, and my dad, Mr Mohamed Noor Yunus, my mother in law, Mrs R Normala Puasa and father in law, Mr Yusoff Md Elah and all my family members, thank you so much for their continuous encouragement, prays and supports.

Finally, I would like to acknowledge Doctorate Research Group members in the social media that are always giving information, knowledge, tips, and ideas. Last but not least, to everyone who directly or indirectly helped me along my PhD journey.

Thank you, thank you, thank you. Love you all!

# Abstract

**Introduction:** Androgenic alopecia (AA) patients usually have high levels of dihydrotestosterone on their balding scalp area. Currently, dutasteride (DST) is given orally and has systemic adverse effects; diminished sexual desire, increased depression and ejaculation disorder. Topical administration of DST is an appropriate drug-delivery strategy with the potential to reduce systemic side effect, skin irritation and cytotoxicity effects.

**Materials and method:** Chitosan oligomer (CSO) conjugated with stearic acid (SA) or lauric acid (LA) was synthesised and characterised. Dutasteride-loaded nanostructured lipid carriers (DST-NLCs) were prepared using a melt-dispersion ultrasonication method. DST-NLCs were optimised using a design of experiments approach. DST-NLCs, uncoated and coated with CSO-SA or CSO-LA were characterised for particle size distribution, surface charge and morphology. *In vitro* release and permeation studies were performed. Cytotoxicity was investigated using human hair follicle dermal papilla cells, and skin irritation was performed using an EpiDerm™ RHE model. Cou-6 loaded NLCs were prepared and characterised before proceeding with the cell and skin uptake study.

**Results:** CSO-SA and CSO-LA were successfully synthesised; confirmed using <sup>1</sup>H NMR and FTIR. The mean size of DST-NLCs was significantly increased ( $p < 0.05$ ) when coated with 5% CSO-SA but not with 5% CSO-LA ( $p > 0.05$ ). The zeta potential changed from negative to positive charge when coating DST-NLCs with CSO-SA or CSO-LA. All formulations were physically stable over six months when stored at 4-8°C. However, DST-NLCs coated with CSO showed aggregation. All formulations exhibited rapid drug release. No dutasteride permeated through pig ear skin after 48 h for all formulations. The cytotoxicity (IC<sub>50</sub>) for DST nanoparticles, coated and uncoated, was greater than for DST alone ( $p < 0.05$ ). The *in vitro* skin irritation study indicated no irritation for all nanoparticle preparations. For the cell and skin uptake studies, all samples showed time-dependent skin and cell uptake.

**Conclusions:** These stable, low cytotoxic and irritant, positively-charged DST-NLCs with CSO-SA or CSO-LA, represents a promising strategy for topical/ transfollicular delivery of DST.

# Research Impact Statement

Androgenic alopecia is a common disorder affecting almost 50% of men in their lifetime due to the androgen effect. Based on the Euromonitor market study predicted in 2013, it was expected that the hair loss treatment would attract up to US\$100 million in sales globally by 2016. Even though hair loss is not a life-threatening disease, but it has a psychological and emotional effect, especially in young people. This study aims to prepare and characterise dutasteride-loaded nanostructured lipid carriers (DST-NLCs), coated with chitosan oligomer conjugated with stearic acid, and lauric acid to enhance local drug delivery and reduce toxicity.

This study will help in our understanding of the potential of nanoparticle formulations for topical delivery of hair growth molecules, which will benefit society especially, androgenic alopecia patients, improving their quality of life. Currently, few products are available in the markets which are prescribed for the androgenic alopecia patient. Due to their systemic adverse effects, the delivery of dutasteride for promoting hair growth using topical route would be a great advance. Phase III clinical studies on the use of dutasteride for promoting hair growth have shown significant hair growth for the people with hair loss. Unfortunately, no topical product based on dutasteride has been approved.

This research can generate good networks between researchers in the academia and people from industries whereby they can exchange the idea, skills and knowledge on the research and business areas. Also, this research can be one of the platforms for other molecules to be applied for topical or non-topical applications. A trained and skilled researcher who has cross-disciplinary generated from this study would be one of the main impacts on the academic area. In term of the economic, it would generate a knowledge transfer between researchers and industrial people who will lead to spin out companies, and the creation of new processes and products.

# Table of Contents

<b>Declaration</b>	<b>2</b>
<b>Acknowledgments</b>	<b>4</b>
<b>Abstract</b>	<b>6</b>
<b>Research Impact Statement</b>	<b>7</b>
<b>Table of Contents</b>	<b>8</b>
<b>List of Tables</b>	<b>14</b>
<b>List of Figures</b>	<b>17</b>
<b>Abbreviations and symbols</b>	<b>23</b>
<b>Chapter 1 Introduction</b>	<b>25</b>
1.1 Skin structure and function .....	26
1.2 Hair.....	27
1.3 Hair growth cycles .....	29
1.4 Mechanism of hair loss .....	30
1.5 Anti-androgenic activity for treating hair loss .....	31
1.6 Market overview of hair loss products.....	33
1.7 Delivery of drugs to the skin.....	34
1.8 Drugs used for treating hair loss .....	38
1.8.1 Minoxidil .....	38
1.8.2 Finasteride.....	40
1.8.3 Dutasteride .....	41
1.9 Positively-charged nanoparticles.....	44
1.10 Chitosan.....	45

1.10.1	Hydrophobic derivatives of chitosan .....	46
1.11	Nanoparticulate dermal drug delivery .....	47
1.11.1	Liposomes .....	48
1.11.2	Polymer-based carrier for drug delivery .....	50
1.11.3	Lipid nanocarriers .....	52
1.12	Aim of the study .....	55
1.13	Objectives of study .....	57
<b>Chapter 2</b>	<b>Conjugation of chitosan oligomer with different types of fatty acids</b>	<b>58</b>
2.1	Conjugation of chitosan oligomer with stearic acid (CSO-SA).....	59
2.1.1	Introduction.....	59
2.1.2	Materials .....	59
2.1.3	Synthesis of chitosan oligomer-stearic acid (CSO-SA).....	60
2.1.4	Characterisation of chitosan oligomer-stearic acid (CSO-SA).....	62
2.1.5	Statistical analysis.....	65
2.2	Conjugation of chitosan oligomer with lauric acid (CSO-LA).....	65
2.2.1	Introduction.....	65
2.2.2	Synthesis and characterisation of chitosan oligomer-lauric acid (CSO-LA) .....	66
2.3	Preparation and characterisation of selected CSO-SA or CSO-LA micelles.....	66
2.3.1	Measurement of particle size distribution of selected CSO-SA or CSO-LA micelles .....	66
2.3.2	Measurement of zeta potential of selected CSO-SA or CSO- LA micelles.....	67
2.3.3	Determination of micelles morphology by transmission electron microscope .....	67

2.3.4	Measurement of critical micelle concentration (CMC) using UV spectrophotometer of selected CSO-SA and CSO-LA .....	68
2.3.5	Statistical analysis.....	68
2.4	Results and discussion.....	69
2.4.1	Conjugation between chitosan oligomer and stearic acid (CSO-SA).....	69
2.4.2	Conjugation between chitosan oligomer and lauric acid (CSO-LA).....	79
2.4.3	Size distribution, surface charge and morphology of CSO-SA and CSO-LA micelles.....	83
2.4.4	Critical micelles concentration (CMC) of selected CSO-SA and CSO-LA .....	86
2.5	Conclusions .....	88
<b>Chapter 3 Preparation of dutasteride-loaded nanostructured lipid carriers coated with chitosan oligomer-fatty acid</b>		<b>89</b>
3.1	Preparation and characterisation of dutasteride-loaded nanostructured lipid carrier coated with chitosan oligomer-stearic acid.....	90
3.1.1	Introduction.....	90
3.1.2	Method development and validation using reverse-phase high-performance liquid chromatography (RP-HPLC) assay for quantification of dutasteride .....	90
3.1.3	Preparation of dutasteride-loaded nanostructured lipid carriers (DST-NLCs) .....	94
3.2	Preparation and characterisation of dutasteride-loaded nanostructured lipid carriers coated with chitosan oligomer-lauric acid .....	102
3.3	Thermal behaviour and viscosity of DST-NLCs, uncoated and coated with 5% CSO-SA and 5% CSO-LA .....	103

3.3.1	Freeze drying of DST-NLCs, uncoated and coated with 5% CSO-SA and 5% CSO-LA.....	103
3.3.2	Determination of crystallinity using x-ray powder diffractometer (XRPD) .....	103
3.3.3	Determination of the thermal behaviour of formulations using differential scanning calorimetry (DSC) .....	104
3.3.4	Measurement of dynamic viscosity using a micro viscometer .....	104
3.4	Statistical analysis .....	105
3.5	Results and discussion.....	105
3.5.1	Validation of RP-HPLC method for assay of dutasteride .....	105
3.5.2	Preparation and characterisation of dutasteride-loaded nanostructured lipid carrier coated with chitosan oligomer- stearic acid .....	107
3.5.3	Preparation and characterisation of dutasteride-loaded nanostructured lipid carrier coated with chitosan oligomer- lauric acid.....	130
3.6	Conclusions .....	140

**Chapter 4 *In vitro* characterisation of nanostructured lipid carrier formulations 143**

4.1	Introduction .....	144
4.2	Materials and methods .....	145
4.2.1	Materials .....	145
4.2.2	<i>In vitro</i> release and permeation studies of DST from solution, DST-NLCs, uncoated and coated with CSO-SA, CSO-LA, and CSO.....	145
4.2.3	<i>In vitro</i> proliferation and cytotoxicity of DST-NLCs/empty NLCs, uncoated and coated with 5%CSO-SA and 5% CSO- LA .....	151

4.2.4	<i>In vitro</i> skin irritation study using EpiDerm™ SIT 3D reconstructed human epidermis (RHE) .....	155
4.2.5	Formulation of coumarin-6 loaded NLCs, uncoated and coated with 5% CSO-SA and 5% CSO-LA .....	158
4.2.6	Preparation of Cou-6 loaded NLCs, uncoated and coated with 5% CSO-SA and 5% CSO-LA .....	160
4.3	Statistical analysis .....	162
4.4	Results and discussion.....	162
4.4.1	<i>In vitro</i> release of DST from solutions, NLCs, uncoated and coated with CSO-SA or CSO .....	162
4.4.2	<i>In vitro</i> permeation study of DST from solution, DST-NLCs, uncoated and coated with CSO-SA, CSO-LA and CSO .....	165
4.4.3	Optimisation of methodology for cytotoxicity studies .....	170
4.4.4	<i>In vitro</i> cytotoxicity study of DST-NLCs, uncoated and coated with 5% CSO-SA and 5% CSO-LA .....	172
4.4.5	Evaluation of <i>in vitro</i> skin irritation using 3D Reconstructed Human Epidermis (RHE) .....	176
4.4.6	Method development and validation of a coumarin-6 assay using RP-HPLC .....	178
4.4.7	Characterisation of Cou-6-loaded NLCs, uncoated and coated with 5% CSO-SA or 5% CSO-LA.....	181
4.4.8	Skin uptake of Cou-6 in solution and Cou-6-loaded NLCs, uncoated and coated with 5% CSO-SA and 5% CSO-LA .....	183
4.4.9	Cell uptake of Cou-6 in solution and Cou-6-loaded NLCs, uncoated and coated with 5% CSO-SA and 5% CSO-LA .....	186
4.5	Conclusions .....	188
<b>Chapter 5 General discussion and future work</b>		<b>190</b>
5.1	Summary .....	191
5.2	General conclusions .....	196

5.3 Future work .....	200
<b>References</b>	<b>202</b>
<b>Appendix A</b>	<b>220</b>
<b>Appendix B</b>	<b>222</b>
<b>Appendix C</b>	<b>223</b>
<b>Publications and Presentations</b>	<b>224</b>

# List of Tables

Table 1.1	Published studies on the delivery of dutasteride using different types of nanocarriers.....	44
Table 1.2	Chitosan conjugation with different type of fatty acids and their application.....	46
Table 2.1	Design of experiments for preparing CSO-SA using a 2 <sup>3</sup> full factorial design .....	62
Table 2.2	Value and coded units of the 2 <sup>3</sup> full factorial design for conjugation of chitosan oligomer with stearic acid.....	62
Table 2.3	Slope, percent of free amine groups and degree of substitution based on ninhydrin assay .....	77
Table 2.4	Analysis of variance (ANOVA) for a 2 <sup>3</sup> factorial design on degree of substitution (%DS).....	78
Table 2.5	Size distribution and surface charge of CSO–SA and CSO-LA micelles (n=3, mean ± SD) .....	83
Table 3.1	HPLC chromatographic condition for determination of dutasteride .....	92
Table 3.2	Description of main materials used in the nanoparticle preparation.....	95
Table 3.3	Value and coded units of a 2 <sup>3</sup> full factorial design for preparation of DST-NLCs.....	97
Table 3.4	Design of experiments for formulation of dutasteride-loaded nanostructured lipid carrier (DST-NLCs) using 2 <sup>3</sup> factorial design .....	98
Table 3.5	Before (x) and after scale-up (3x) contents of DST-NLCs .....	99
Table 3.6	Regression characteristics and validation parameters of dutasteride using HPLC .....	106
Table 3.7	Particle size distribution of DST-NLCs at day 1 and 14 stored at 4°C (n=3, mean ± SD).....	108

Table 3.8	Analysis of variance (ANOVA) for a 2 <sup>3</sup> factorial design for hydrodynamic diameter at day 14 (storage at 4°C).....	110
Table 3.9	Analysis of variance (ANOVA) for 2 <sup>3</sup> factorial design for polydispersity index at day 14 (storage at 4°C) .....	112
Table 3.10	Analysis of variance (ANOVA) for a 2 <sup>3</sup> factorial design for zeta potential at day 14.....	116
Table 3.11	Entrapment efficiency and drug loading of DST-NLCs at day 1 (n=3, mean ± SD) .....	118
Table 3.12	Analysis of variance (ANOVA) for a 2 <sup>3</sup> factorial design for entrapment efficiency at day 1 .....	119
Table 3.13	Analysis of variance (ANOVA) for a 2 <sup>3</sup> factorial design on drug loading at day 1 .....	120
Table 3.14	Hydrodynamic diameter, PDI and zeta potential of DST-NLCs after scaled-up (day 1) (n=3, mean ± SD) .....	121
Table 3.15	Size distribution and surface charge for DST-NLCs before and after coating with different concentrations of CSO-SA and CSO (n=3, mean ± SD) .....	123
Table 3.16	Size distribution and surface charge of DST-NLCs, uncoated and coated with CSO-SA or CSO (n=3, mean ± SD) .....	125
Table 3.17	Size distribution and surface charge for DST-NLCs before and after coating with different concentrations of CSO-LA (n=3, mean ± SD) .....	130
Table 3.18	Size distribution and surface charge of DST-NLCs, uncoated and coated with CSO-LA at day 1, 30, 60 and 180 stored at 4-8°C (n=3, mean ± SD) .....	132
Table 3.19	Viscosity of DST-NLCs uncoated and coated with CSO-SA or CSO-LA at different temperature and angles (n=3, mean ± SD) .....	139
Table 4.1	Interpretation of results of skin irritation study (OECD, 2015) .....	158
Table 4.2	HPLC chromatographic condition for determination of Cou-6 .....	159
Table 4.3	Formulation of Cou-6-loaded nanostructured lipid carrier (Cou-6-NLCs) .....	160

Table 4.4	Permeation parameters of DST from DST-NLCs using Strat- M® membrane after 48 h (n=4, mean ± SD) .....	166
Table 4.5	Permeation parameters of DST from solution, DST-NLCs, uncoated and coated with CSO-SA, CSO-LA and CSO using pig ear skin after 48 h (n=4, mean ± SD) .....	167
Table 4.6	Regression characteristics and validation parameters of Cou- 6.....	180

# List of Figures

Figure 1.1	Structure of skin (adapted from MacNeil, 2007) .....	26
Figure 1.2	Skin structure and layer (redrawn from Bensouilah and Buck, 2006).....	27
Figure 1.3	Structure of the hair follicles (adapted from Adolphe and Wainwright, 2005) .....	28
Figure 1.4	The hair follicle growth cycle (adapted from Randall and Botchkareva, 2009) .....	30
Figure 1.5	Hair loss cycle in patients with male pattern baldness (adapted from Randall, 2010).....	31
Figure 1.6	The action of androgen in the hair follicle (redrawn from Randall and Botchkareva, 2009) .....	32
Figure 1.7	Size of the global hair care market in 2006, 2011 and the estimated market in 2016 (in billion U. S. dollars) (adapted from Euromonitor International, 2013).....	33
Figure 1.8	Schematic illustration of the potential penetration pathways of drugs through the skin (redrawn from Patzelt and Lademann, 2013).....	35
Figure 1.9	The occlusion factor of lipid nanoparticles depends on different sizes (redrawn from Escobar-Chávez et al., 2012).....	36
Figure 1.10	Fluorescence intensity of different sizes of nanoparticles (without removing the stratum corneum) (modified from Campbell et al., 2012) .....	37
Figure 1.11	Mechanism of drug permeation by NLCs (redrawn from Fang et al., 2014).....	37
Figure 1.12	Chemical structure of minoxidil.....	38
Figure 1.13	Chemical structure of finasteride .....	40
Figure 1.14	Chemical structure of dutasteride.....	42
Figure 1.15	Structure of chitosan oligomer .....	45

Figure 1.16	Schematic representation of a liposome, showing the location of entrapped drugs (redrawn from Lembo and Cavalli, 2010).....	48
Figure 1.17	Different structures of nanocarriers (redrawn from Janssen et al., 2014).....	51
Figure 1.18	Schematic illustration of SLN and NLC structures (modified from Beloqui et al., 2016) .....	54
Figure 1.19	Schematic representation of DST-NLCs coated with CSO-SA or CSO-LA to be prepared and characterised in this project .....	55
Figure 1.20	Schematic diagram of overall preparation, characterisation and <i>in vitro</i> study of dutasteride-loaded nanostructured lipid carrier coated with chitosan oligomer-stearic or lauric acid .....	56
Figure 2.1	Conjugation between chitosan oligomer and stearic acid .....	60
Figure 2.2	Ninhydrin assay: Reaction of ninhydrin reagent with amine groups from CSO or CSO-SA or CSO-LA (colour of ninhydrin changes from light yellow (left) to purple (right)).....	64
Figure 2.3	FTIR spectra of chitosan oligomer-stearic acid from eight different condition of synthesis; varying ratio of SA:EDC.HCl/time of reaction (hours)/amount of stearic acid (g). S1 (1:5/6/0.5), S2 (1:10/6/0.5), S3 (1:5/24/0.5), S4 (1:10/24/0.5), S5 (1:5/6/1), S6 (1:10/6/1), S7 (1:5/24/1) and S8 (1:10/24/1.0).....	70
Figure 2.4	<sup>1</sup> H NMR spectra of chitosan oligomer-stearic acid from eight synthesis; varying ratio of SA: EDC.HCl/time of reaction (hours)/amount of stearic acid (g). S1 (1:5/6/0.5), S2 (1:10/6/0.5), S3 (1:5/24/0.5), S4 (1:10/24/0.5), S5 (1:5/6/1), S6 (1:10/6/1), S7 (1:5/24/1) and S8 (1:10/24/1.0) .....	71
Figure 2.5	Absorbance versus concentration from ninhydrin assay of D-glucosamine, CSO and different samples of CSO-SA (n=3, mean ± SD).....	75
Figure 2.6	FTIR spectra of lauric acid (LA), chitosan oligomer (CSO) and chitosan oligomer-lauric acid (CSO-LA) based on a	

	parameter of ratio 1:5; LA: EDC.HCl, 6 h reaction time and 0.5 g – lauric acid .....	79
Figure 2.7	<sup>1</sup> H NMR spectra of lauric acid (A), chitosan oligomer (B) and CSO-LA (C) based on ratio LA: EDC.HCl/time of reaction (hours)/amount of lauric acid (g), 1:5/6/0.5).....	81
Figure 2.8	Graph of absorbance versus concentration from ninhydrin assay of D-glucosamine, CSO and CSO-LA (n=3, mean ± SD) .....	82
Figure 2.9	Transmission electron micrographs of CSO-SA and CSO-LA micelles at 5 mg/mL in acetic acid solution.....	85
Figure 2.10	Absorbance of pyrene versus logarithm of chitosan oligomer-stearic acid (CSO-SA) concentration (A) and chitosan oligomer-lauric acid (CSO-LA) concentration (B) (n=3, mean ± SD) .....	86
Figure 3.1	Schematic diagram of preparation and characterisation of dutasteride-loaded nanostructured lipid carriers (DST-NLCs) .....	96
Figure 3.2	Peak area versus time for the dutasteride solution (A), NLCs without dutasteride (B), NLCs with dutasteride (C) .....	105
Figure 3.3	Calibration curve of dutasteride; peak area versus concentration (n=4, mean ± SD) .....	106
Figure 3.4	3D figure of interaction between stearic acid (A) and Lutrol® micro 68 (B) for hydrodynamic diameter at day 14.....	111
Figure 3.5	Normal percent probability versus studentized residuals (A) and predicted versus actual value for hydrodynamic diameter at day 14 (B).....	112
Figure 3.6	3D plot of interaction between stearic acid (A) and Lutrol® micro 68 (B) (above), and stearic acid (A) and Phosal® 53 MCT (C) (bottom) for the polydispersity index at day 14. ....	114
Figure 3.7	Normal percent probability versus studentized residuals (A) and predicted versus actual value for polydispersity index at day 14 (B).....	115

Figure 3.8	Zeta potential measurement of DST-NLCs at day 1 and 14 stored at 4-8°C (n=3, mean ± SD).....	117
Figure 3.9	3D plot of stearic acid (A) and Lutrol® micro 68 (B) for the entrapment efficiency (%).....	120
Figure 3.10	Entrapment efficiency and drug loading of DST-NLCs with different amounts of dutasteride (15, 17.5 and 20 mg) (n=3, mean ±SD).....	122
Figure 3.11	Entrapment efficiency of DST-NLCs uncoated at day 1, 30, 60, 90 and 180 stored at 4-8°C (n=3, mean ± SD).....	128
Figure 3.12	TEM images of DST-NLCs, uncoated (A), coated with; 5% CSO (B), 5% CSO-SA (C) and 10% CSO-SA (D).....	129
Figure 3.13	TEM images of DST-NLCs, uncoated (A), coated with; 2.5% CSO-LA (B), 5% CSO-LA (C) and 10% CSO-LA (D).....	134
Figure 3.14	X-ray diffractograms of dutasteride, physical mixture and freeze-dried formulations DST-NLCs uncoated and coated with CSO-SA and CSO (carriers: stearic acid, Phosal® 53 MCT, Lutrol® micro 68) .....	136
Figure 3.15	DSC thermograms of dutasteride, physical mixture and freeze-dried formulations DST-NLCs uncoated and coated with CSO-SA and CSO (carriers: stearic acid, Phosal® 53 MCT, Lutrol® micro 68) .....	138
Figure 4.1	Pig ear skin used for the permeation studies (A) and visualised using a light microscope after being cryotomed at 50 µm thickness (B) .....	148
Figure 4.2	In-house set-up of Franz diffusion cells for permeation study (modified from Verkhovskiy et al., 2015).....	149
Figure 4.3	Hair follicle dermal papilla cells (A) and cells with coumarin-6 dye (B).....	152
Figure 4.4	Chemical structure of MTT and MTT formazan (A) and absorption spectra of MTT in water and MTT formazan in sunflower oil (modified from Stockert et al., 2012).....	154

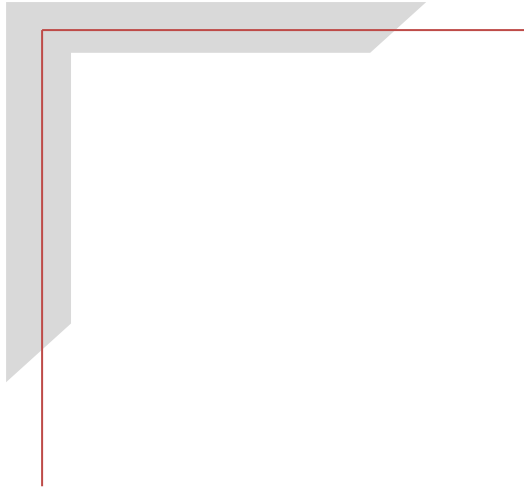
Figure 4.5	EpiDerm™ SIT (EPI-200) tissues in the medium for skin irritancy testing.....	156
Figure 4.6	Protocol of skin irritation studies using 3D reconstructed human epidermis skin.....	157
Figure 4.7	Dutasteride release from different DST-NLC formulations and control (dutasteride in ethanol) (n=3, mean ± SD).....	164
Figure 4.8	Percentage cell viability for different cell densities of dutasteride in DMSO after 5 days (n=4, mean ± SD).....	170
Figure 4.9	Cell viability study of dutasteride alone in DMSO at different days (n=4, mean ± SD).....	171
Figure 4.10	Cytotoxicity of dutasteride alone (A), empty NLCs uncoated and coated with 5% CSO-SA and 5% CSO-LA and DST-NLCs uncoated and coated with 5%CSO-SA and 5%CSO-LA (B) on hair follicle dermal papilla cells (n=4, mean ± SD).....	173
Figure 4.11	Cell proliferation study of lauric and stearic acids on hair follicle dermal papilla cells (n=4, mean ± SD).....	175
Figure 4.12	Skin irritation results for different formulations on 3D reconstructed human epidermis (RHE) (n=3, mean ± SD).....	177
Figure 4.13	Peak area versus time for the NLCs with Cou-6 (A) and Cou-6 in ethanol, 10 µg/mL (B).....	179
Figure 4.14	Calibration curve of Cou-6, peak area versus concentration (n=4, mean ± SD).....	180
Figure 4.15	Hydrodynamic diameter and polydispersity index for Cou-6-NLCs for different contents of Cou-6 (n=3, mean ± SD).....	181
Figure 4.16	Entrapment efficiency for Cou-6 loaded NLCs (n=3, mean ± SD).....	182
Figure 4.17	Hydrodynamic diameter and polydispersity index for Cou-6-NLCs, uncoated and coated with 5% CSO-SA and 5% CSO-LA (n=3, mean ± SD).....	183
Figure 4.18	Skin uptake of Cou-6 in full thickness pig ear skin (cryostat was set at 50 µM thickness) from Cou-6-loaded NLCs,	

	uncoated and coated with 5% CSO-SA and 5% CSO-LA and Cou-6 in solution.....	184
Figure 4.19	Cell uptake study of Cou-6 in hair follicle dermal papilla cells from Cou-6-loaded NLCs, uncoated and coated with 5% CSO-SA and 5% CSO-LA and Cou-6 in solution .....	187
Figure 5.1	Schematic diagram of preparation of lipid nanoparticles for topical delivery of hair growth therapeutic molecules and potential future work .....	199

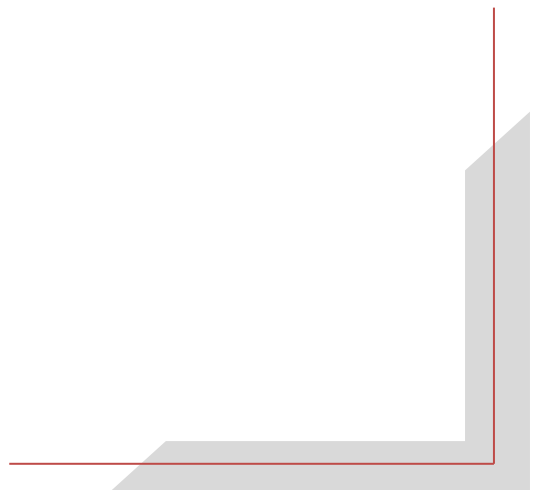
# Abbreviations and symbols

<b>ANOVA</b>	analysis of variance
<b>Avodart®</b>	dutasteride based medication
<b>BBB</b>	blood-brain barrier
<b>BCS</b>	biopharmaceutics classification system
<b>BPH</b>	benign prostatic hyperplasia
<b>CAGR</b>	compound annual growth rate
<b>Cou-6</b>	coumarin-6
<b>CSO</b>	chitosan oligomer
<b>Da</b>	Dalton
<i>df</i>	degree of freedom
<b>DHT</b>	dihydrotestosterone
<b>DL</b>	drug loading
<b>DLS</b>	dynamic light scattering
<b>DoE</b>	design of experiment
<b>DS</b>	degree of substitution
<b>DST</b>	dutasteride
<b>EDC</b>	1-ethyl-3-(3-(dimethylamino) propyl) carbodiimide
<b>EE</b>	entrapment efficiency
<b>FDA</b>	food and drug administration
<b>FT-IR</b>	Fourier Transform Infrared Spectroscopy
<b>GSK</b>	GlaxoSmithKline
<b>HCl</b>	hydrochloric acid
<b>HF<sub>s</sub></b>	hair follicles
<b>HLB</b>	hydrophobic-lipophilic balance
<b>HPLC</b>	high performance liquid chromatography
<b>ICH</b>	International Conference on Harmonisation
<b>LA</b>	Lauric acid
<b>LOD</b>	limit of determination
<b>Log P</b>	partition coefficient
<b>LOQ</b>	limit of quantification
<b>Lutrol® micro 68</b>	Poloxamer 188

<b>MR</b>	magnetic resonance
<b>MW</b>	molecular weight
<b>NLCs</b>	nanostructured lipid carriers
<b>NMR</b>	Nuclear Magnetic Resonance Spectroscopy
<b>PDI</b>	polydispersity index
<b>PEG</b>	polyethylene glycol
<b>Phosal® 53 MCT</b>	53% of phosphatidylcholine and medium chain triglyceride
<b>PLGA</b>	poly(lactic-co-glycolic acid)
<b>R<sup>2</sup></b>	coefficient of determination
<b>Rogaine®</b>	minoxidil based medication
<b>RP</b>	reverse phase
<b>RSD</b>	relative standard deviation
<b>SA</b>	stearic acid
<b>SC</b>	stratum corneum
<b>SD</b>	standard deviation
<b>Sephadex®</b>	cross-linked dextran
<b>SLNs</b>	solid lipid nanoparticles
<b>SMEDDS</b>	self-emulsifying drug delivery system
<b>T</b>	testosterone
<b>TEM</b>	transmission electron microscope
<b>TFA</b>	trifluoroacetic acid
<b>TNBS</b>	trinitrobenzene sulfonic acid
<b>UV/Vis</b>	ultraviolet-visible spectroscopy
<b>XPRD</b>	X-ray powder diffractometer
<b>ZP</b>	zeta potential



# Chapter 1 Introduction



## 1.1 Skin structure and function

Skin is the largest, heaviest and most versatile organ of the human body. The vital roles of the skin are the protection of the body, regulation of body temperature and sensory perception. The skin protects the body from water loss and the possibility of access by potentially toxic compounds, allergens, irritants and microbes (Bartosova and Bajgar, 2012). To ensure these diverse functions can be fulfilled, healthy skin is needed. For an adult, the skin surface area is approximately 1.8 - 2.0 m<sup>2</sup> (Uchechi et al., 2014). Figure 1.1 shows the structure of the skin.

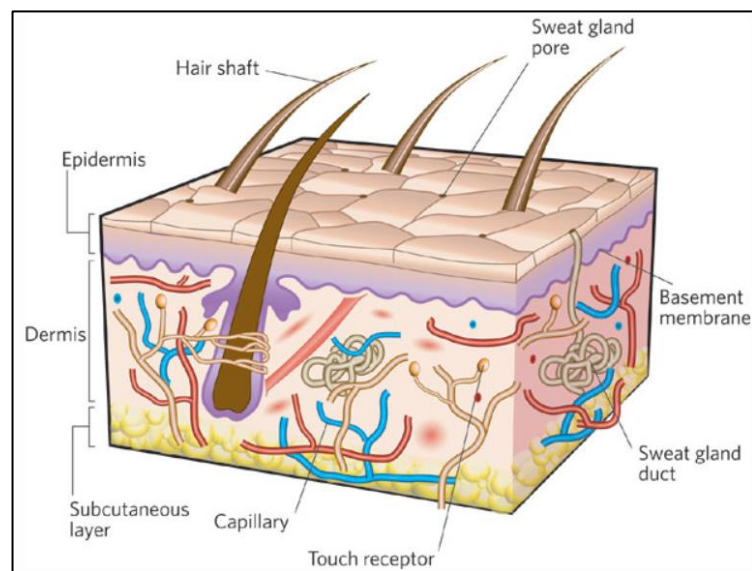


**Figure 1.1 Structure of skin** (adapted from MacNeil, 2007)

The skin consists of three main layers (Figure 1.2). The outermost layer is the epidermis which is made up of stratum corneum, stratum lucidum, stratum granulosum, stratum spinosum and stratum basal (Williams, 2018). The barrier properties of the skin are due to the stratum corneum. The stratum corneum is a very hydrophobic layer, comprising differentiated non-nucleated cells, corneocytes, filled with keratins embedded in the lipid domain (Godin and Touitou, 2007). The lipid domain is composed of equal proportions of ceramides, cholesterol and free fatty

acids (Pappas, 2009). The synthesis of these three components promotes the acidic condition of the skin.

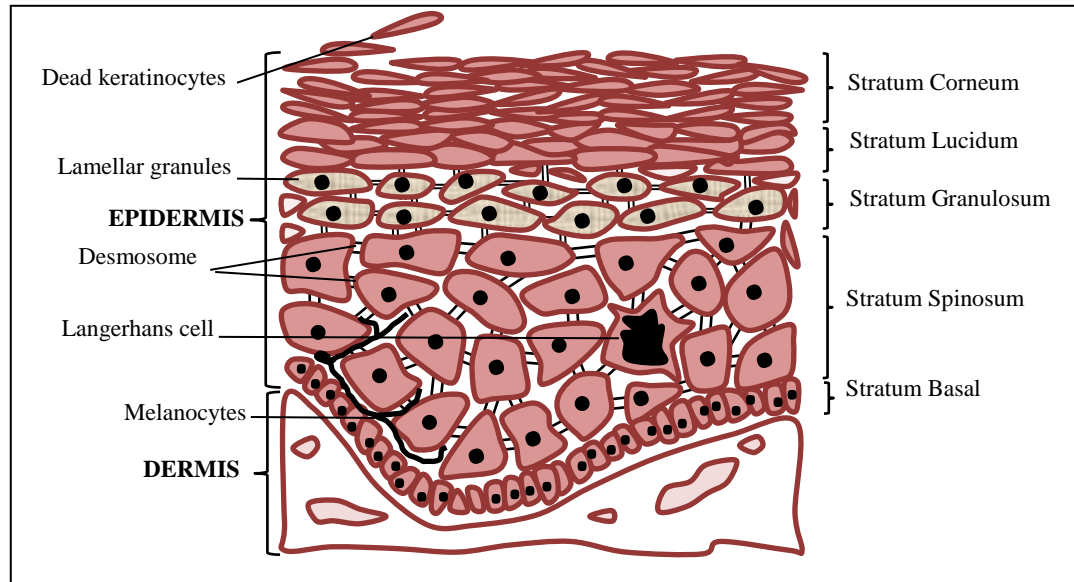


**Figure 1.2 Skin structure and layer** (redrawn from Bensouilah and Buck, 2006)

The second layer is dermis. The dermis is composed of connective tissues such as collagen fibrils and elastic tissues that mostly provide support, mechanical strength, elasticity and flexibility of the skin. The dermis is supplied with a reticulate network of blood vessels, lymphatic vessels, nerve endings, hair follicles, sebaceous glands and eccrine glands (Thakur et al., 2008).

Finally, the inner layer of the skin is subcutaneous tissue or hypodermis which contains adipose cells in and between the connective tissue. The primary function of subcutaneous tissue is to provide insulation to the body (Williams, 2018).

## 1.2 Hair

The largest appendages, which consist of hair follicles and sebaceous glands, can provide ‘short cut’ routes which drugs can pass across the stratum corneum barrier (Williams, 2018). The hair follicle is an organ and part of the skin. It starts in

the dermis and goes through the outer part of the skin to the epidermis layer (Figure 1.3). Hair consists of proteins, lipids, water, trace elements and pigments (Robbins, 2012). The hair protein is called keratin. Hair can be divided into two types. First is vellus hair, appearing on the body, or hair that changes to terminal hair at puberty. The second is called terminal hair. Terminal hair may be short (eyebrows, ears, nose) and long (head hair, beard, underarm, pubic area).

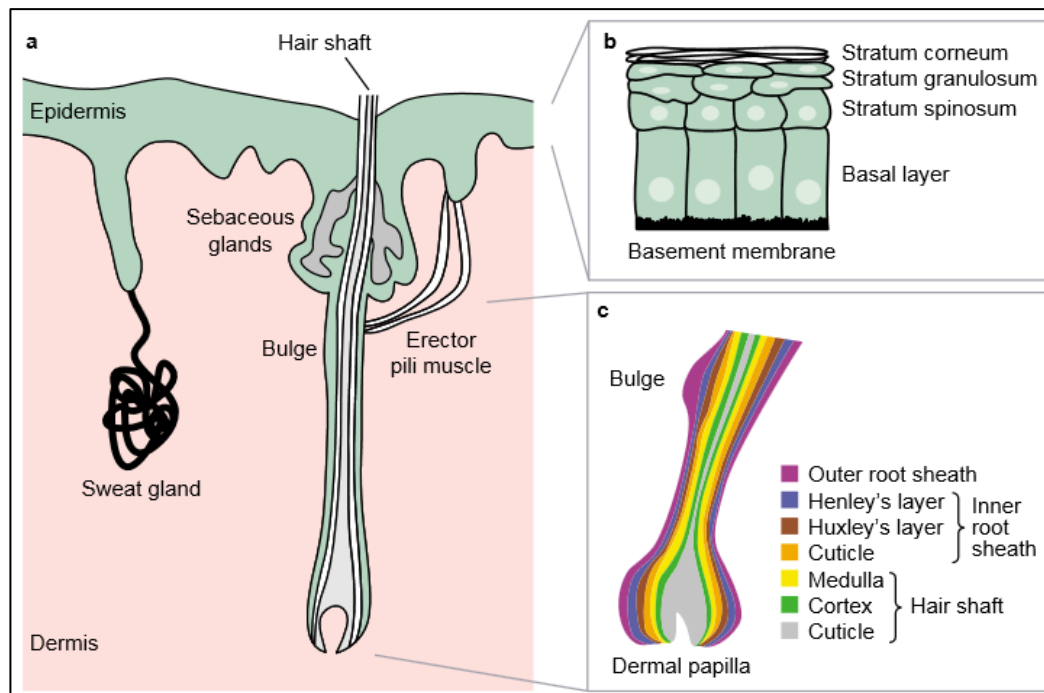


**Figure 1.3 Structure of the hair follicles** (adapted from Adolphe and Wainwright, 2005)

Hair that is visible above the skin is called the hair shaft. It consists of cuticle, cortex and medulla. Previous studies have found the hair diameter on the scalp and face differ (Tolgyesi et al., 1983). The normal adult hair shaft diameter (Caucasian) is approximately 70  $\mu\text{m}$ , whereas in the beard it is 126  $\mu\text{m}$ . These have made skin appendages (sweat gland and hair follicle) which is only 0.1% to 1% of the area of the skin (Schaefer and Redelmeier, 2001) used as a follicular route for targeted delivery of drugs.

Hair that is invisible or within the skin is called the hair root. The bulbous end of the hair root is called the hair bulb (Williams, 2018). All biological processes including cell division happen in this part. The hair bulb is positioned in a tubular pocket called the hair follicle. Human hair follicles are one of the organs that are affected by hormones such as androgens (Randall et al., 1991). Androgen promotes hair growth and also sometimes inhibits scalp hair growth causing androgenetic alopecia (AGA). As it is specific to the hair follicle itself, the response to androgens varies with the body site. In the case of AGA, androgens cause the miniaturisation of the scalp hair follicle (Hibberts et al., 1998).

### 1.3 Hair growth cycles

Hair is produced by the hair follicle and undergoes a cycle with different phases. It starts at the anagen phase, then passes through catagen and lastly telogen phases. All hair growth phases in the body occur at the same time; one hair might be in the anagen phase and others in the catagen or telogen phase. The original lower follicle will be destroyed, and the new follicle will regenerate to form a new hair (Randall and Botchkareva, 2008).

Figure 1.4 shows the cycles of hair growth in the normal human body. Different areas have different hair growth cycle. Hair is produced in the anagen phase or so-called growth phase. Scalp follicles have the longest anagen phases, lasting up to several years (Randall, 2008). Once hair reaches its full length in the anagen phase, then the catagen phase (regression) will take place, in which cell proliferation, differentiation, and pigmentation will stop, and extensive apoptosis occurs, and the dermal papilla shrinks (Randall, 2008). The catagen phase normally takes 1 to 2 weeks. In the catagen stage, the hair is fully keratinised and a specialised structure, the club hair is formed and moves upwards (Randall and Botchkareva, 2008). After this, the telogen phase takes over, which lasts for several months. During the telogen phase, the round-shaped dermal papilla is closely situated near to the secondary hair germ keratinocytes containing hair follicle stem cells. In an early-mid anagen phase, a new lower follicle develops inside the same dermal sheath, and the new hair grows into the original upper follicle, and the existing hair ejected (Randall and Botchkareva, 2008).

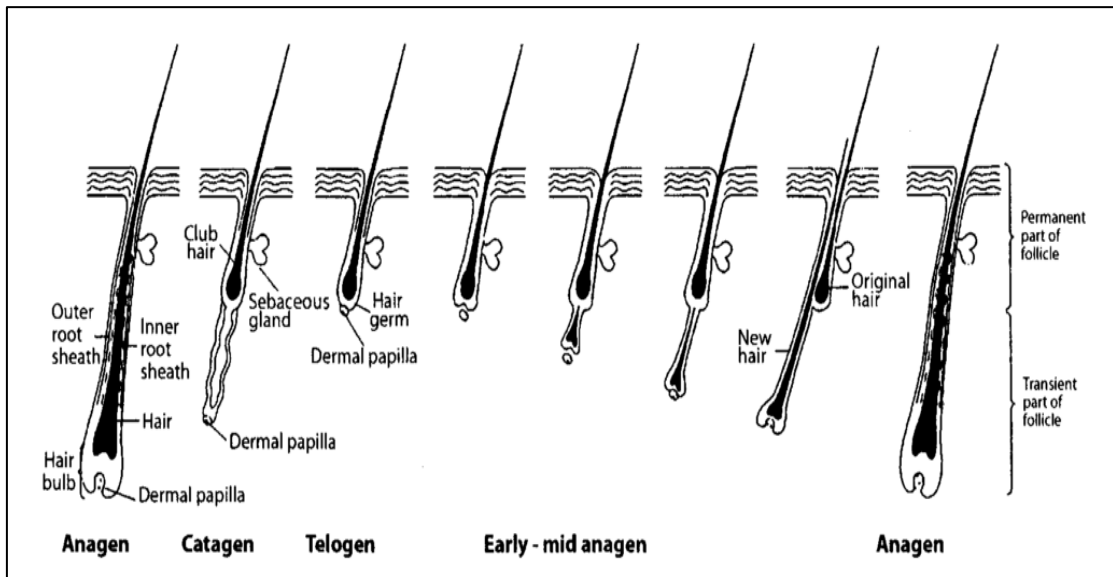


**Figure 1.4** The hair follicle growth cycle (adapted from Randall and Botchkareva, 2009)

#### 1.4 Mechanism of hair loss

Most problems associated with hair relate to either hirsutism (excessive hair growth) or alopecia. Alopecia is a common medical term for hair loss or baldness. Baldness which is affected by androgens is called AGA, also known as male pattern hair loss (MPHL) or female pattern hair loss (FPHL) (Kaufman, 2002). Testosterone and dihydrotestosterone are the major androgens that regulate the hair growth.

Dihydrotestosterone (DHT) has approximately a five-fold greater affinity for the androgen receptor than testosterone (Kaufman, 2002). In hair loss patients, the  $5\alpha$ -reductase enzyme acts as a catalyst that converts testosterone, which is the primary androgen, to the more potent androgen, DHT which makes the hair follicle miniaturise and shed hair (Olsen et al., 2006).

Figure 1.5 shows the hair loss cycle for a patient with hair loss. Due to the effect of the potent androgen (DHT), their normal hair starts as long, thick and pigmented, then changes to be thin, short and less pigmented at the end of the process. The new hair colour becomes less pigmented from one cycle to another, the hair shaft becomes thinner, and there is the appearance of baldness. Two isozymes

participate in androgen synthesis; namely, Type I  $5\alpha$ -reductase isozyme which is present in the skin, hair follicles and sebaceous glands, liver, prostate, and kidney and Type II  $5\alpha$ -reductase isozyme which is present in hair follicles, male genitalia and the prostate (Russell and Wilson, 1994; Kandavilli et al., 2010). Both these isozymes are involved in steroid metabolism and interact with the androgen receptors. In androgen synthesis, the  $5\alpha$ -reductase enzyme acts as catalyst converting testosterone to the more potent dihydrotestosterone. By introducing a  $5\alpha$ -reductase inhibitor, the conversion of testosterone to DHT can be decreased and reduce hair loss.

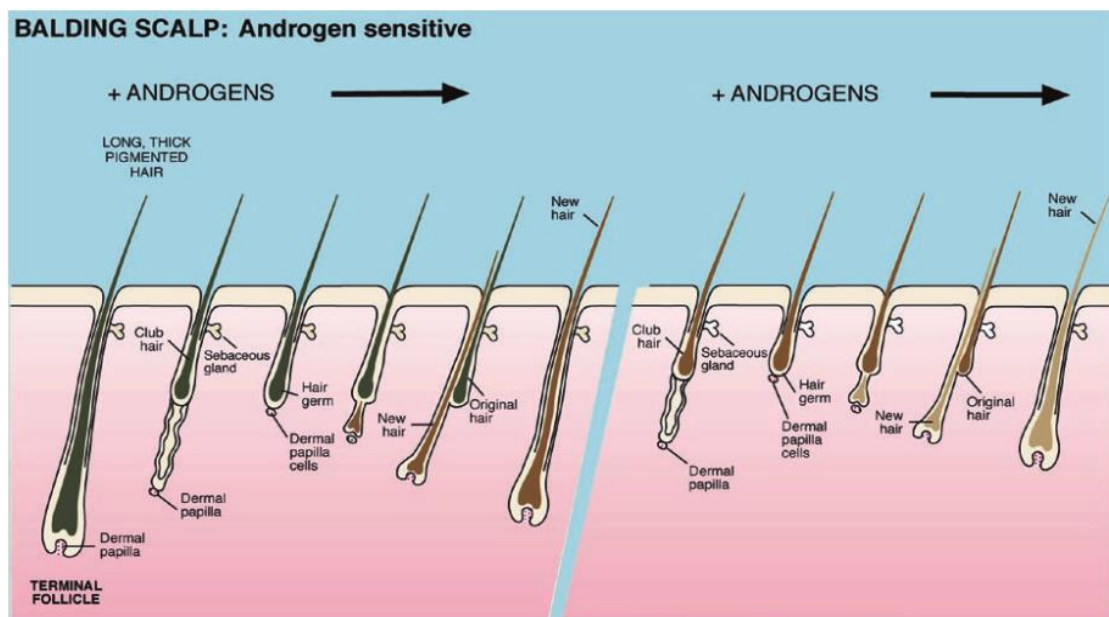


**Figure 1.5 Hair loss cycle in patients with male pattern baldness** (adapted from Randall, 2010)

### 1.5 Anti-androgenic activity for treating hair loss

Hair loss is not a life-threatening disease, but has an emotional impact and affects certain individuals, especially young people and they may experience psychological distress (Hunt and Mchale, 2005). Androgenic alopecia (male pattern baldness) is a common disorder affecting almost 50% of men in their life (Yassa et al., 2011) due to effect from androgen. Androgen is one of the prerequisites for male pattern baldness (Randall and Botchkareva, 2008). Normally, patients with androgenic alopecia have higher levels of DHT (dihydrotestosterone) and  $5\alpha$ -reductase enzyme activity on their balding scalp area than those with a non-balding

scalp area (Hibberts et al., 1998). Figure 1.6 shows the circulation of androgens in the hair follicles. Testosterone (T) is mainly secreted by the Leydig cells of the testes of males and a lesser amount by the ovaries of female (Brownlee et al., 2005).

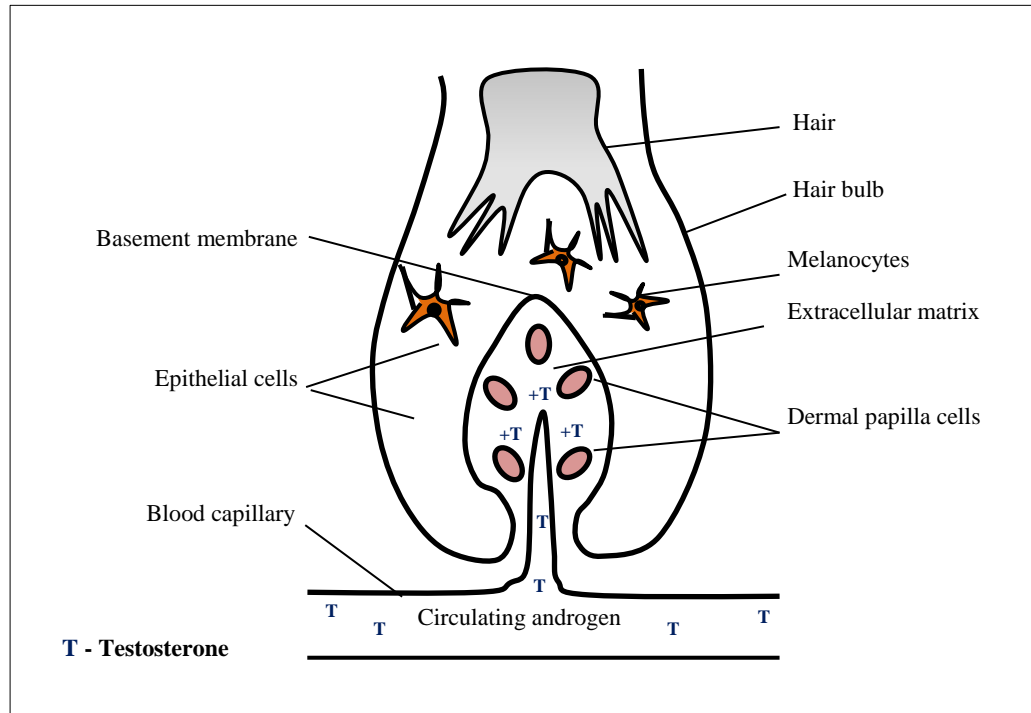


**Figure 1.6 The action of androgen in the hair follicle** (redrawn from Randall and Botchkareva, 2009)

Testosterone will circulate in the blood and enter the hair follicle through the dermal papilla's blood supply and interact with the androgen receptors in the dermal papilla cells. Several studies have focussed on the inhibition of the activity of the  $5\alpha$ -reductase enzyme, either by using natural extracts or drugs. One example of natural extract for  $5\alpha$ -reductase inhibitor was the use of fatty acids (Liu et al., 2009); those with  $C_{12}$ - $C_{16}$  and  $C=C$  double bond which enhanced Type II  $5\alpha$ -reductase inhibition activity. Finasteride which has Type II  $5\alpha$ -reductase inhibitor activity is approved by the FDA to treat benign prostatic hyperplasia and male pattern baldness. Dutasteride is approved for treating benign prostatic hyperplasia (BPH) and has both Types I and II  $5\alpha$ -reductase inhibitor. Finasteride and dutasteride are discussed in detail in Section 1.8.2 and 1.8.3 respectively.

## 1.6 Market overview of hair loss products

Figure 1.7 shows the estimated size of the global hair care market in 2013 from 2006 to 2016 (Euromonitor International, 2013). Hair care products comprise products that promote health; hair nourishment, prevention of hair damage and hair loss treatment.

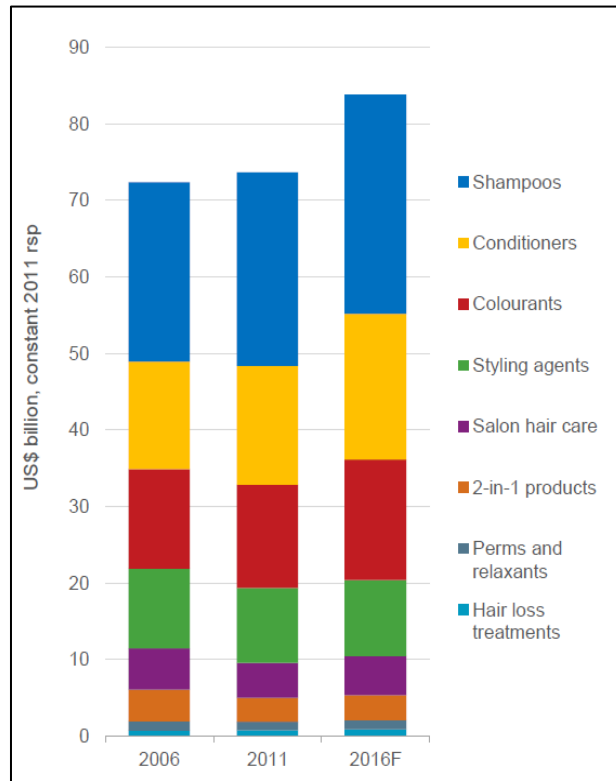


**Figure 1.7 Size of the global hair care market in 2006, 2011 and the estimated market in 2016 (in billion U. S. dollars)** (adapted from Euromonitor International, 2013)

From this data, the sales of the hair loss treatments are dominated by minoxidil (Regaine®, Johnson and Johnson) which exhibits a significant sales growth especially in Western Europe (Euromonitor International, 2013). Minoxidil is an over-the-counter drug and has been approved for treating hair loss in both men and women. However, some people use cosmetic products to treat hair loss rather

than pharmaceutical products due to their adverse effects. In this case, cosmetics are defined in Regulation (EC) No. 1223/2009 as:

"any substance or mixture intended to be placed in contact with the external parts of the human body (epidermis, hair system, nails, lips and external genital organs) or with the teeth and the mucous membranes of the oral cavity with a view exclusively or mainly to cleaning them, perfuming them, changing their appearance, protecting them, keeping them in good condition or correcting body odours." (European Commission, 2009).

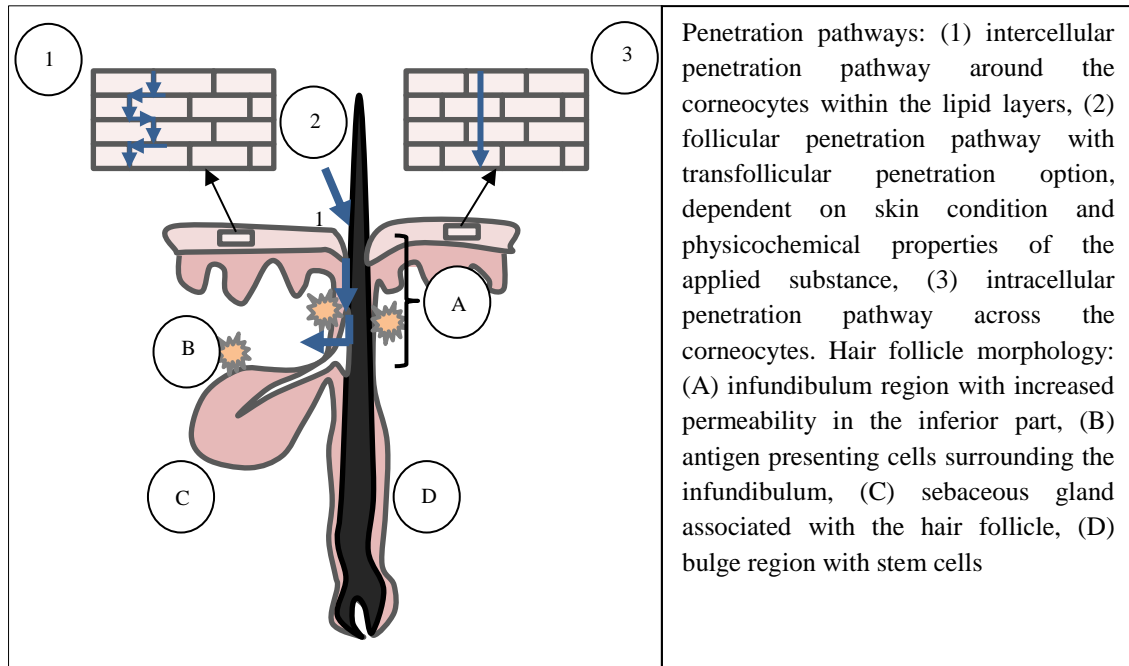
Cosmetics or drugs used for treating hair loss are not permanent and their activity is reversible, which means when someone uses the product; hair loss will decrease or stop, but when they stop using the product, then the hair loss returns. To reduce this problem, an effective delivery system for a drug acting as a potential hair growth promoter should be designed to have a long-lasting effect such as having controlled release properties which is targeted to the hair follicle area and at the same time reduce the adverse effects.

## **1.7 Delivery of drugs to the skin**

Many studies have been conducted to deliver drugs to the transfollicular region (Bhatia et al., 2013; Mittal et al., 2015). Figure 1.8 shows the potential penetration pathways of a drug through the skin. The drug can pass either through the skin barrier (No. 1 - 3) or to the transfollicular area (A - D). Drug delivery through the skin offers convenience to the patient, is pain-free and allows self-administration, and may eliminate frequent administration especially when long-term treatment is needed (Paudel et al., 2010).

The transfollicular route has shown promise for delivery; particulate delivery would be ideal by allowing deep intrafollicular penetration, sustained release and selectively targeted delivery (Patzelt and Lademann, 2013). The size of particulate materials is one of the key criteria to deliver the drug to the transfollicular area. Hair follicles have a size range from 10 - 70  $\mu\text{m}$  depending on the hair type, location and race (Singh et al., 2000) making it a suitable site for delivering nanoparticles to the dermal papilla cells for hair growth products.

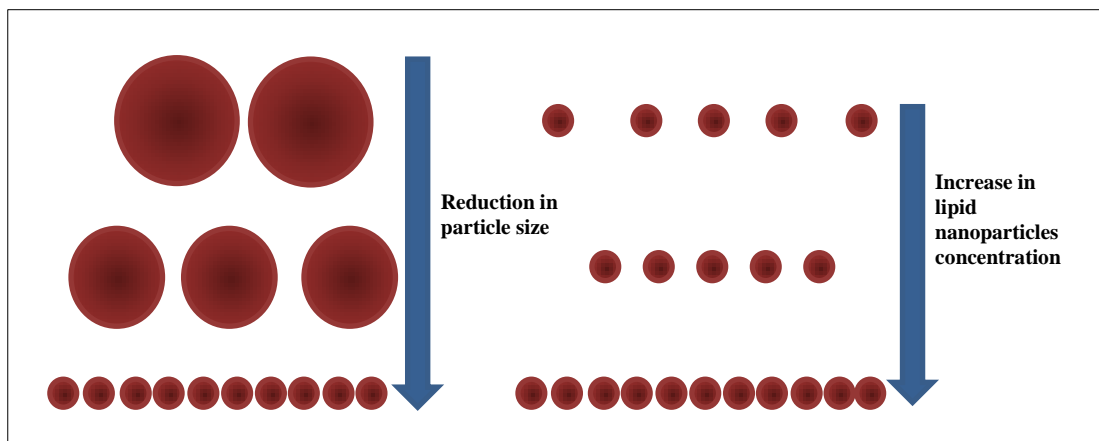
Previous research has found that, applying 320 nm fluorescence dye-containing nanoparticles, and massaging the area enhanced the penetration for up to 10 days (Lademann et al., 2007); with nanoparticulates of dye penetrating deeper than the dye in solutions.



**Figure 1.8 Schematic illustration of the potential penetration pathways of drugs through the skin** (redrawn from Patzelt and Lademann, 2013)

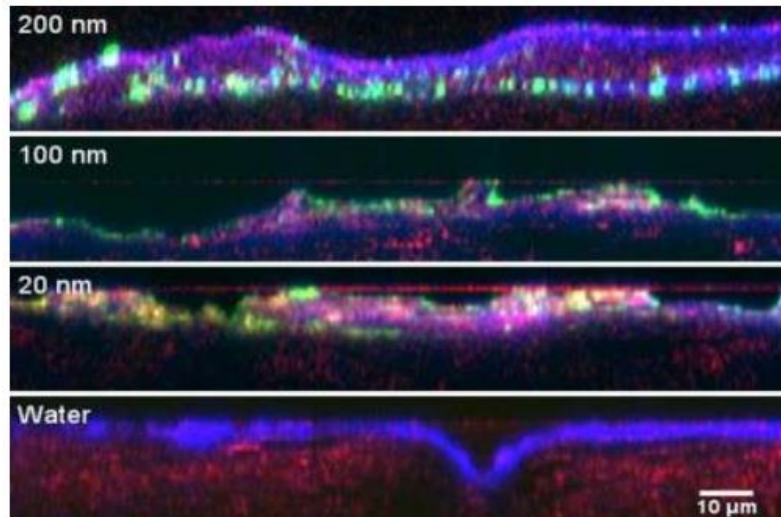
Lipophilic vehicles rather than hydrophilic are able to improve the delivery of drug to the skin (Motwani et al., 2004), and many studies have been conducted using lipid-based vehicles for dermal delivery (Doktorovova et al., 2011; Wang et al., 2012; Uprit et al., 2013; Montenegro et al., 2016). Due to the occlusive properties of lipid nanoparticles, an increased skin hydration effect is observed (Hommos, 2008). Previous studies found that a lipid film formed on the top of the skin, and the subsequent occlusion effect was reported for lipid nanoparticles (Müller et al., 2002; Wissing and Müller, 2003; Escobar-Chávez et al., 2012). Particles smaller than 400 nm containing at least 35% lipid of high crystallinity have been most effective for the occlusive properties (Wissing and Müller, 2003).

Figure 1.9 shows that the occlusion factor of lipid nanoparticles depends on the sizes; reducing the particle size leads to an increase in particle number, the film becomes denser (left) and therefore the occlusion factor increases. Other criteria on the occlusion factor have been considered, such as identical lipid content; increasing the lipid concentration increases particle number and density of the film (right) which also leads to a higher occlusion factor (Pardeike et al., 2009). In solid lipid nanoparticles (SLN) or nanostructured lipid carriers (NLC) system, the skin hydration after applying these nanoparticles leads to a reduction of corneocytes packing and an increase in the size of the corneocytes gaps and facilitate the percutaneous absorption and drug penetration to the deeper skin layers (Hommos, 2008).



**Figure 1.9** The occlusion factor of lipid nanoparticles depends on different sizes (redrawn from Escobar-Chávez et al., 2012)

Campbell et al., (2012) investigated the deposition of nanoparticles in mammalian skin and found that nanoparticles (mean size of 20 – 200 nm) cannot penetrate beyond the superficial layers of the barrier. Figure 1.10 shows the intensity of fluorescence nanoparticles at different sizes. Even at the smallest mean size of nanoparticles (20 nm), there is no penetration of nanoparticles to the deeper layer of the skin. This result proved that nanoparticles could not penetrate the skin barrier, but it is useful as skin surface reservoirs to control the drug release over time (Campbell et al., 2012).



**Figure 1.10** Fluorescence intensity of different sizes of nanoparticles (without removing the stratum corneum) (modified from Campbell et al., 2012)

Fang et al. (2014) reported the mechanism of skin permeation by drug-loaded NLCs (Figure 1.11). As mentioned before, occlusion factor which increases hydration of the stratum corneum (SC) become the main factor that can reduce the corneocytes packing and increase drug permeation (Fang et al., 2014). These findings suggest that nanoparticles could go deep in the skin and systemic circulation through transfollicular region as seen in Figure 1.11.

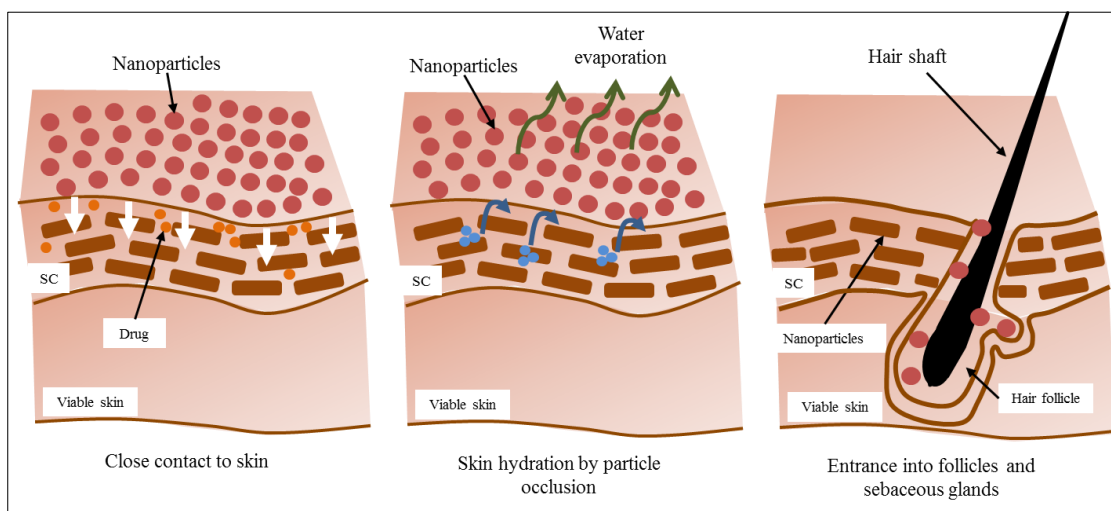


**Figure 1.11** Mechanism of drug permeation by NLCs (redrawn from Fang et al., 2014)

## 1.8 Drugs used for treating hair loss

### 1.8.1 Minoxidil

For many years, minoxidil has been the first-choice for topically applied drug recommended by medical practitioners to treat hair loss for both men and women. Currently, Rogaine® (USA) or Regaine® (Europe and UK) is an approved hair-loss product based on minoxidil which is available on prescription and as an over-the-counter medication. Minoxidil (Figure 1.12), a pyridine derivative drug was used in the 1970s as a treatment for hypertension in patients where therapy had failed with multidrug regimens (Messenger and Rundegren, 2004; Sica, 2004). In 1988, 1% minoxidil mixed with an alcohol-based carrier was approved by the FDA to treat alopecia in men.

In a 12-month randomised double-blind trial of 150 men, 82% of the minoxidil group increased hair count (Kreindler, 1987). Sato et al., (1999) used cultured human dermal papilla cells from the balding scalp and found that minoxidil increased  $17\beta$ -hydroxysteroid dehydrogenase activity by approximately 40% but had an insignificant effect on  $5\alpha$ -reductase activity and such as the mechanism of minoxidil action remains unknown (Silva et al., 2009). Another study (Han et al., 2004) found minoxidil prolonged the anagen phase where the dermal papilla cells proliferated and had an anti-apoptotic effect on dermal papilla cells.

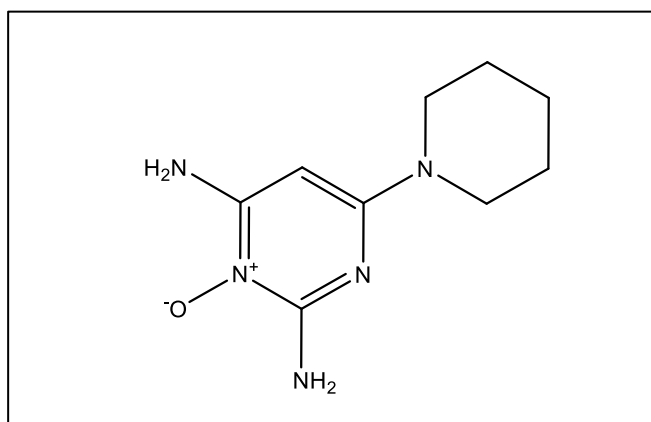


**Figure 1.12 Chemical structure of minoxidil**

### 1.8.1.1 Nanocarrier delivery of minoxidil and minoxidil derivatives

In order to overcome the severe adverse reaction such as scalp dryness, irritation from propylene glycol-water-ethanol ingredients in the current minoxidil products, several studies have investigated the delivery of minoxidil using nanoparticle formulation. Nanostructured Lipid Carrier (NLCs) have been used for the delivery of minoxidil (Silva et al., 2009) for promoting hair growth, with a particle size of approximately 250 nm before adding to a hydrogel; particles remained below 500 nm when incorporated in the hydrogel. These formulations of minoxidil-NLCs hydrogel were a promising alternative to the conventional alcoholic solutions, as the drug is physically entrapped within the lipid matrix which can be useful to increase the bioavailability for skin delivery (Silva et al., 2009). No efficacy study on hair growth activity between the minoxidil-NLCs hydrogel and conventional minoxidil solutions was conducted. However, this formulation approach would help in reducing the risk of occurrence of adverse side effects, such as skin dryness and irritation.

The Globally Harmonized System of Classification and Labeling of Chemicals (GHS) defines skin irritation as “the production of reversible damage to the skin following the application of a test substance for up to 4 hours” and skin corrosion as “the production of irreversible damage to the skin; namely, visible necrosis through the epidermis and into the dermis, following the application of a test substance for up to 4 hours” (United Nations, 2013). Padois et al., (2011) used solid lipid nanoparticles (SLNs) as a carrier for minoxidil and found SLNs suspensions which was approximately 190 nm of particle size proved efficient as commercial solutions for skin penetration; and were non-corrosive while commercial solutions presented a corrosive potential.

Some examples of minoxidil-loaded nanoparticulate carriers include research by Aljuffali et al. (2014), which used squalene-based NLCs for targeted drug delivery, known as “squarticles” and delivered minoxidil together with diphenylprone. The size was approximately 177 nm for the NLCs-based carrier. The encapsulation efficiency and zeta potential for minoxidil-loaded squalene NLCs were 63.3% and -54.0 mV respectively. They found that compared to the free control (drugs in 30% propylene glycol in water), squarticles-NLCs reduced minoxidil

penetration through the skin, indicating minimised absorption in the systemic circulation. The result also showed an improvement of drug deposition by 2-fold in the skin, using an *in vitro* skin absorption test and good tolerability of squarticles to skin based on the *in vitro* papilla cell viability and *in vivo* skin irritancy tests in nude mice.

Matos et al. (2015) formulated minoxidil sulphate-loaded chitosan nanoparticles (MXS-NP) which demonstrated sustained drug release (5-fold) compared to drugs in solutions. The MXS-NP formulation (chitosan/MXS; 1:1 w/w) had mean diameter 236 nm and positive zeta potential. They found that the drug permeation studies through the skin *in vitro* showed that MXS-NP application resulted in a 2-fold increase in MXS in uptake hair follicles after 6 h in comparison to the control solution.

### 1.8.2 Finasteride

Finasteride, (Figure 1.13) an anti-androgen steroidal drug has been used widely to treat patients with benign prostatic hyperplasia. A clinical open, randomised, parallel-group study for 12 months on 100 male patients with androgenic alopecia to investigate the efficacy of oral finasteride (1 mg per day), topical 2% minoxidil solution and topical 2% ketoconazole shampoo alone and in combination was conducted (Khandpur et al., 2002). The results demonstrated a significant increase in hair growth between a combination group having finasteride orally (1 mg) and 2% minoxidil (topically) and finasteride (orally) alone (Khandpur et al., 2002).

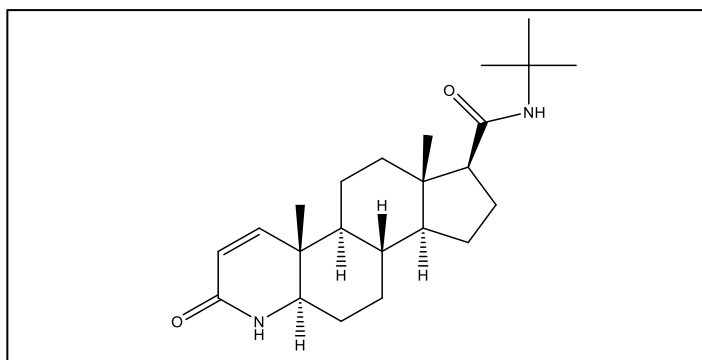


**Figure 1.13 Chemical structure of finasteride**

### 1.8.2.1 Nanocarrier delivery of finasteride

Several studies have been conducted using nanoparticle formulations of finasteride for topical delivery. Madheswaran et al., (2013) prepared liquid crystalline nanoparticles from monoolein, with size 154 – 170 nm which showed a potential for topical delivery of finasteride. The addition of different types of additives (glycerol, propylene glycol, and polyethylene glycol 400) had little or no influence on the size. The formulations produced slow release profiles and high permeation to the dermis. The release profile was significantly altered with the addition of different additives. Formulation with monoolein exhibited skin permeation which increased significantly with the inclusion of glycerol, propylene glycol, and polyethylene glycol 400, while it decreased with the addition of oleic acid. The release rate of finasteride increased when glycerol, propylene glycol, or polyethylene glycol 400 was added and decreased with the addition oleic acid.

Gomes et al. (2014) formulated lipid nanoparticles of finasteride with mean size around 200 nm and stable up to 28 days. Penetration studies using pig ear skin found that only a small amount of finasteride crossed the skin, suggesting the suitability of this formulation for dermal delivery of anti-alopecia active compounds.

Caon et al. (2014) found chitosan coated polymersomes of finasteride interacted more strongly with the skin components than non-coated formulations due to the positive surface charge. It was observed that the addition of chitosan contributed to an increase in the accumulation of finasteride in the epidermis. It was proposed that the particles (mean diameter of 180 - 404 nm) were preferentially accumulated in the follicular openings and that follicular localization was favoured by the smaller particle size, which would be more easily transported via the follicular route than the larger size.

### 1.8.3 Dutasteride

Dutasteride, approved for treating benign prostatic hyperplasia also affects hair growth. Due to its androgenic activity, dutasteride can only be taken by male patients. Dutasteride (MW = 528.5 g/mol) (Figure 1.14) is classified as Class II/IV in the Biopharmaceutics Classification System (BCS) (Tiwari et al., 2014). It has very

low water solubility (0.038 ng/mL, Log P = 5.09 and  $pK_a = 13.5$ ) and high solubility in ethanol (44 mg/ml) and methanol (64 mg/ml) at 25° C and has a half-life of approximately 3-5 weeks (GlaxoSmithKline Inc., 2013).

In 2009, dutasteride (0.5 mg daily orally intake) was approved in Korea for treating hair loss in men (Harcha et al., 2014), but until now no dutasteride-based product been approved for androgenic alopecia in Europe or USA. However, it is commonly prescribed as an off-label for hair loss treatment (oral administration) in the USA and Europe. This product is swallowed without chewing, crushing, or opening the capsule because it might irritate the lips, mouth, and throat. The prescribed dosage for treating benign prostatic hyperplasia (BPH) is 0.5 mg per day (GlaxoSmithKline Inc., 2013).

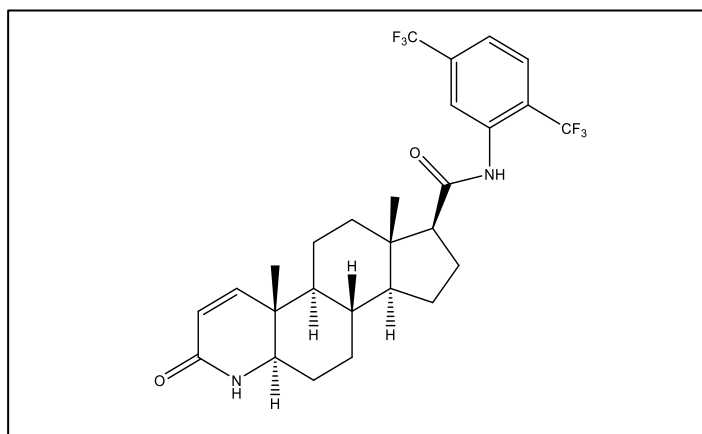


**Figure 1.14 Chemical structure of dutasteride**

Olsen et al. (2006) found dutasteride increased scalp hair growth in men with hair loss, at 2.5 mg of dutasteride (orally), it and was superior to finasteride (5 mg) (orally) at 12 and 24 weeks. Eun et al. (2010) used dutasteride for treating hair loss in male patients at 0.5 mg daily orally and reported that the dutasteride group had significant hair growth compared to the placebo group within six months. Another study (Stough, 2007) reported evidence that dutasteride significantly reduced hair loss progression in men with male pattern hair loss when tested in a randomised study in 17 pairs of identical twin males for 1 year period. They found that treatment with dutasteride (0.5 mg/day orally) slowed the progression of hair loss and enhanced hair growth compared to treatment with placebo. In 2014, a randomised, active- and

placebo-controlled study of dutasteride versus placebo and finasteride in the treatment of 917 male subjects with androgenetic alopecia was conducted by Harcha et al. (2014). They found that dutasteride 0.5 mg significantly increased the hair count, width diameter and improved hair growth at week 24 compared with finasteride and placebo.

### 1.8.3.1 Nanocarrier delivery of dutasteride

Based on the summary of product characteristics for oral dutasteride (Avodart®), the side effects of taking oral dutasteride are: it may increase the risk of development of high-grade prostate cancer, decrease libido, and may cause breast enlargement and ejaculation disorders (GlaxoSmithKline Inc., 2013). Dutasteride has a toxicity effect on the skin, with multiple red areas produced in the skin (animals at 40 mg/kg) suggesting that dutasteride is a dermal irritant (GlaxoSmithKline Inc., 2013). In order to reduce these side effects, drug delivery with sustained release should preferably target the skin, especially to the hair follicle. Delivery of dutasteride using nanocarriers has been studied by the oral route with little research of topical delivery (Table 1.1).

Previous research on topical delivery has used a liposome system (Sharma et al., 2011). The liposomes produced significantly higher skin permeation of dutasteride through excised abdominal mouse skin compared to a hydro-alcoholic solution and conventional gels. Ansari et al. (2013) prepared different ratios of oleic acid and eucalyptus oil to prepare nanoemulsion to deliver dutasteride to the skin. The mean size range was around 18 - 213 nm, no measurements were undertaken on zeta potential, entrapment efficiency, and drug loading. Madheswaran et al. (2015) used monoolein to produce dutasteride nanoparticles, with their surface modified using different concentrations of chitosan (low molecular weight) to give a positive charge. The particle size was 239 - 259 nm, with mean zeta potential of +19.8 to +48.5 mV. The surface modified liquid crystalline nanoparticles enhanced transdermal delivery of dutasteride and increased the permeation of dutasteride using a porcine skin (700 – 800  $\mu\text{m}$  thickness). Release studies on this formulation produced the cumulative amount of dutasteride released only about 5% after 24 h. The highly lipophilic nature of dutasteride, which had a stronger interaction with

lipid inside the nanoparticles produced slower release compared to finasteride (Madheswaran et al., 2015).

**Table 1.1 Published studies on the delivery of dutasteride using different types of nanocarriers**

Delivery system	Particle Size	Application	Authors
Liposome	$1.82 \pm 0.15 \mu\text{m}$	Topical for dermal delivery	Sharma et al. (2011)
Eudragit E® nanoparticles	62.2 – 180.6 nm	Oral	Park et al. (2013)
Hydroxypropyl- $\beta$ -cyclodextrin nanostructures	<160 nm	Oral	Kim, (2013)
Self-microemulsifying drug delivery system (SMEDDS)	43.9 nm	Oral	Kim et al. (2015)
Self-microemulsifying drug delivery system (SMEDDS)	35.3 nm	Oral	Choo et al. (2013)
Nanoemulsion	58.8 – 88.7 nm	Topical for systemic delivery	Sajid et al. (2014)
Liquid crystalline nanoparticles	$197.9 \pm 2.5 \text{ nm}$	Topical for dermal delivery	Madheswaran et al. (2015)

### 1.9 Positively-charged nanoparticles

Nanoparticles having a positive surface charge have received great interest in drug delivery, especially for topical and transfollicular delivery, where hair and the lipid layer in the SC contain high ratio of negatively-charged lipids (Bhushan, 2010; Madheswaran et al., 2015). For instance, the anionic surfactant is often added in shampoos to remove grease from the hair. The surfactant has two different regions; one region is soluble in water (hydrophilic) and the other region is soluble in the greasy material (lipophilic). The lipophilic/hydrophobic part will encircle the greasy

matter, and the other part (negative-charged) will repel the fibres because hair fibres are negatively-charged, and remove the greasy material easily.

On the other hand, cationic surfactants are normally added to hair conditioners to neutralise the charge of hair after washing. Based on this, many studies on positively-charged nanoparticles have been undertaken in order to promote interaction with the negative target site, especially for dermal/transdermal and transfollicular delivery (Şenyiğit et al., 2010; Gelfuso et al., 2011; Ridolfi et al., 2012; Özcan et al., 2013; Madheswaran et al., 2015).

### 1.10 Chitosan

Chitosan is a natural polymeric material being used increasingly by the pharmaceutical industry. It contains free amine groups, and this makes it is insoluble in water (water-soluble only at  $\text{pH} < 6$ ) (Sogias et al., 2010). Chitosan oligomers or chitosan oligosaccharide (Figure 1.15) are the hydrolysates of chitosan, mainly made up of -1,4 linked D-glucosamine and partially of -1,4 linked N-acetyl-D-glucosamine (Ibrahim et al., 2016). Chitosan oligomer has been used widely for different bioactivity such as antibacterial (No et al., 2002; Merchant et al., 2014; Yildirim-Aksoy and Beck, 2017), antitumour activity (Jeon and Kim, 2002; Hu et al., 2009; Xie et al., 2012), anti-cancer activity (Nam et al., 2007a; 2007b), wound healing activity (Kang et al., 2016) and antioxidant activity (Sun et al., 2007).

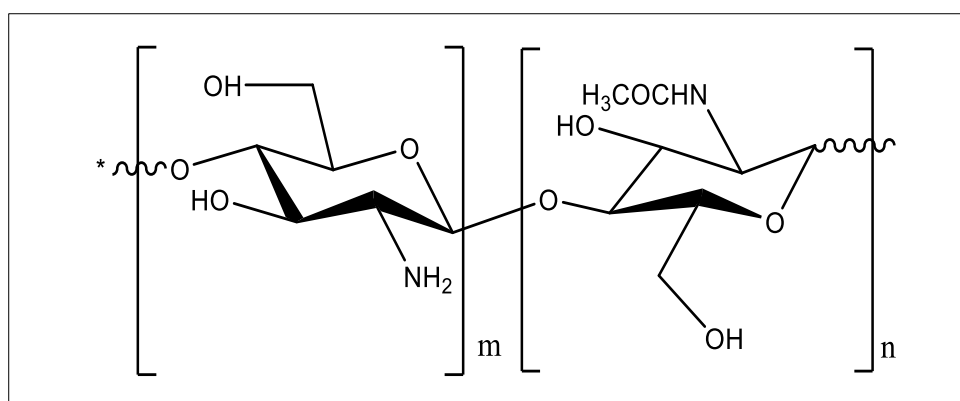


**Figure 1.15 Structure of chitosan oligomer**

In this project, chitosan oligomer (Carbosynth Ltd, United Kingdom) with molecular weight less than 3 kDa and 85% deacetylation degree was chosen. This chitosan is positively charged, which is likely to be advantageous for skin and hair, such skin and hair are negatively charged and will be attracted to positively charged moieties (Bhushan, 2010). Mittal et al. (2015) demonstrated that a nanoparticle formulation of antigen ovalbumin with chitosan increased follicular uptake when compared to a nanoparticle formulation without chitosan.

### 1.10.1 Hydrophobic derivatives of chitosan

Table 1.2 shows the potential delivery of drugs by using different types of chitosan conjugated with a hydrophobic chain (fatty acid). From Table 1.2, it can be seen that chitosan conjugated with fatty acid has been employed in many areas using nanoparticles and micellar systems.

**Table 1.2 Chitosan conjugation with different type of fatty acids and their application**

<b>Delivery system</b>	<b>Chitosan and Fatty acid</b>	<b>Application</b>	<b>Authors</b>
<b>Micelles</b>	Chitosan 18 kDa and stearic acid	Brain targeting	Xie et al. (2012)
<b>Immobilization</b>	Chitosan LMW and lauric acid	Osteoblast proliferation and antibacterial	Zhao et al. (2014)
<b>Micelles</b>	Chitosan 5 kDa and stearic acid	Oral delivery	Li et al. (2010)
<b>Micelles</b>	Chitosan 9.2 kDa and stearic acid	Anti-tumour activity	Hu et al. (2009)
<b>Nanoparticles</b>	Chitosan 9.2 kDa and oleic acid	Optical MR/Imaging	Lee et al. (2011)
<b>Micelles</b>	Glycol chitosan different MWs with palmitic acid (GCPQ)	Oral, ocular, parenteral	Uchegbu et al. (2014)

The surface activity of chitosan (non-conjugated) is low as it does not possess any hydrophobic portions and can be improved by chemical modifications at its glucosidic group with a hydrophobic substituent (Cheung et al., 2015). Szymańska and Winnicka (2015) reported chemical crosslinking with chitosan as a strategy to increase the stability of chitosan, whereby the stability of modified chitosan was based on the covalent bonds, and also interactions—hydrogen or hydrophobic bonds.

Xie et al. (2012) prepared chitosan oligosaccharide (MW 18 kDa) conjugated with stearic acid (CSO-SA) for brain targeting. The blood-brain barrier (BBB), makes it difficult for the drug to penetrate, however, the delivery of doxorubicin in a CSO-SA micellar system was beneficial. The micellar system (22 nm sizes; zeta potential +36 mV) demonstrated high drug loading and a slow release pattern. High amounts of doxorubicin were found in the brain and low amounts accumulated in the heart. This result was due to the ability of micelles to transport across the blood-brain barrier and into the brain (Xie et al., 2012). The lower toxicity of CSO-SA/doxorubicin micelles than doxorubicin in solutions might be relevant with a slow release of doxorubicin from micelles (Xie et al., 2012).

### **1.11 Nanoparticulate dermal drug delivery**

Topical application of drugs has many advantages especially reducing systemic effects and targeting affected local areas, such as for skin diseases. The stratum corneum (SC) provides the main barrier function of skin, limiting the loss of essential substances from inside the body and reducing chemically or toxic materials entering the body (Trommer and Neubert, 2006). Even though the drug in the formulation for hair loss therapy should ideally target the transfollicular region, drugs will also likely permeate through the dermal or transdermal regions which represent the main permeation pathways. Due to the limited permeability of the SC (the drug should be in low molecular weight and moderate lipophilicity), several methods have been employed to enhance the delivery of the drugs to the skin. These include chemical permeation enhancers such as fatty acids, urea, phospholipids, alcohols, amide, and sulfoxides and physical permeation enhancement such as iontophoresis, sonophoresis, ultrasound and microneedles (Finnin and Morgan, 1999; Pathan and Setty, 2009; Akhtar et al., 2011; Shaji and Varkey, 2012).

Other skin penetration enhancers, more recently investigated are micro or nanoscale size drug formulations, such as liposomes, polymeric nanoparticles, nanoemulsions, solid lipid nanoparticles and nanostructured lipid carriers (Müller et al., 2002; Sintov and Shapiro, 2004; Guterres et al., 2007; Escobar-Chávez et al., 2012; Wang et al., 2012; Gomes et al., 2014). Mahe et al., (2009) found the particles of approximately 200 nm mean sizes applied to the skin were found around the hair follicles. Further studies reported that particles with a size approximately 300 nm were found in the transfollicular region (Mittal et al., 2015). These studies suggest to deliver the drug into the hair follicle regions, a size of particles in the range of 200-300 nm is appropriate.

### 1.11.1 Liposomes

Liposomes, sphere-shaped vesicles with mean size 30 nm to several micrometres, produced by self-forming enclosed lipid bilayers upon hydration consisting of one or more phospholipid bilayers, were first described in the mid-60s (Akbarzadeh et al., 2013). Liposome formulations consist of one or more non-toxic natural phospholipids such as soy phosphatidylcholine and egg phosphatidylcholine or a synthetic phospholipid such as distearoyl-phosphatidylcholine (Figure 1.16).

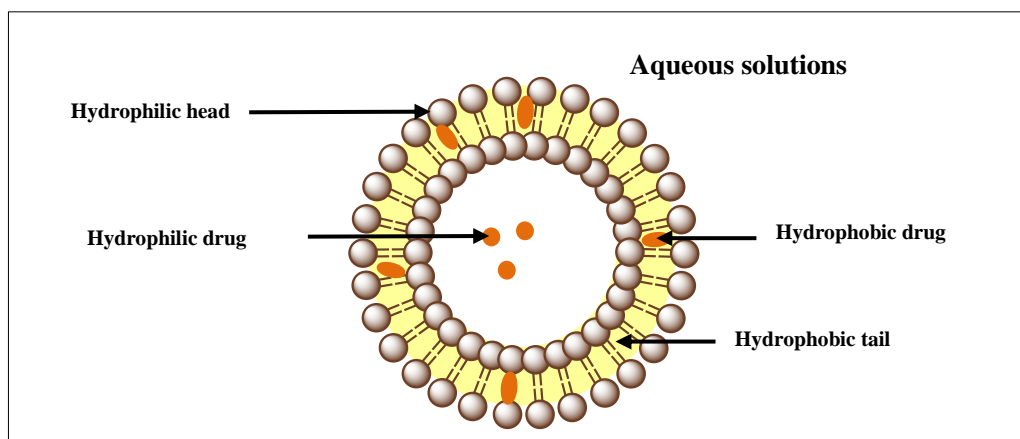


**Figure 1.16 Schematic representation of a liposome, showing the location of entrapped drugs (redrawn from Lembo and Cavalli, 2010)**

Liposomes differ based on the different type of phospholipid used, lipid composition, method of preparation, surface charge, lamellarity and size (Du Plessis et al., 1994). Liposomes have a characteristic  $T_c$  (phase transition temperature), at which the liposome membranes transit from the gel phase to liquid crystalline phase, and the encapsulated drugs are released from the vesicles (Li et al., 2015). The  $T_c$  depends on the nature of the polar head group, the length of the hydrocarbon chains, the degree of saturation of the hydrocarbon chains and the purity of phospholipids (Li et al., 2015). In liposomes system, hydrophobic drugs will be encapsulated in the hydrophobic region of the phospholipid bilayers whereas hydrophilic drugs will be entrapped in the aqueous core and between bilayers. The ‘rigidity’ or ‘fluidity’ and the charge of the bilayer of the liposome are dependent on the bilayer components (Akbarzadeh et al., 2013).

Liposomes have been widely used for dermal and transfollicular delivery of drugs. Du Plessis et al. (1994) found that the particle size influenced the deposition of drugs in the skin, for a liposome preparation containing ciclosporin as a model drug. They found the intermediate particle size (0.3  $\mu\text{m}$ ) studied resulted in the highest amount of drug in the deeper skin strata and the receiver chamber for both hamster and hairless mouse skin except the pig skin after 24 h using Franz diffusion cells. The same was not seen for pig skin because of the lipophilic nature of both ciclosporin and the pigskin with the release of ciclosporin to the receiver retarded (Du Plessis et al., 1994).

Esposito et al. (1998) found the permeability of a liposome preparation of methyl nicotinate through a synthetic membrane was influenced by the charged particles, a higher amount of phosphatidylcholine, the smaller size of particles and also the higher viscosity of the samples. In the case of the non-extruded sample, the permeability was affected by the vesicle size, where smaller size increased the permeability rather than the viscosity. However, for extruded samples, the permeability was affected by the viscosity of the formulation.

Flexible liposomes, which are mixtures of lipids and surfactants have been studied in order to penetrate the SC (Cevc et al., 1998; Ogunsola et al., 2012). Cevc et al. (1998) prepared flexible liposomes, called as Transferosomes® containing

soybean phosphatidylcholine, sodium cholate and biocompatible surfactants produced liposome dispersion that passed through a filter of much smaller pore size.

Another study conducted by Ogunsola et al. (2012) prepared flexible liposomes with egg phosphatidylcholine and Tween 80 or sodium cholate or ethanol with the mean size range from 74 – 110 nm that passed through the filter with 50 nm pore size. *In vitro* penetration studies found that fluorescent-tagged lipid to liposomes with a higher amount of Tween 80 (60 or 68%) showed penetration of fluorescent-tagged lipid flexible liposomes into the epidermis of hairless guinea pig and excised human skin.

Although liposomes have been used for drug delivery to reduce the toxicity of drugs, increase efficacy and stability and site-specific drug delivery, there are also some disadvantages. Conventional liposomes have poor drug loading capacity, poor stability, production costs are high, and the use of volatile solvents are required in their preparation.

### 1.11.2 Polymer-based carrier for drug delivery

Figure 1.17 shows different types of the polymer-based carrier for drug delivery. Hydrogels are produced by a group of polymeric materials having a hydrophilic structure which is capable of holding large amounts of water in their three-dimensional networks (Ahmed, 2015). Drugs can be loaded into the gel matrix and the drug release rate is dependent on diffusion of the small molecule or macromolecule through the gel network (Hoare and Kohane, 2008). Many studies have reported incorporation of nanoparticles or microparticles into a hydrogel in order to improve dermal delivery. Bhaskar et al. (2009) produced flurbiprofen loaded SLNs or NLCs (average particles sizes of less than 300 nm) incorporated with a hydrogel and found that sustained drug release over a period of 24 h was higher with the SLNs and NLCs hydrogel compared to SLNs and NLCs without hydrogel.

Biodegradable polymers such as poly(D,L-lactic acid) (PLA), poly(D,L-lactic-co-glycolic acid) (PLGA), and poly( $\epsilon$ -caprolactone) (PCL) and their copolymers diblock or multiblock with poly(ethylene glycol) (PEG) have been commonly used to form polymeric nanocarriers (polymeric micelles, capsules,

spheres) in order to encapsulate a variety of therapeutic compounds (Chan et al., 2010). Polymeric nanocarriers such as micelles are formulated by self-assembly of block copolymers consisting of two or more polymer chains with different hydrophobicities (Chan et al., 2010) such amphiphilic polymers which have both hydrophilic blocks and hydrophobic blocks can be used for drug delivery where normally the hydrophobic blocks form the core to minimize their exposure to aqueous surroundings (Chan et al., 2010; Trivedi and Kompella, 2010).

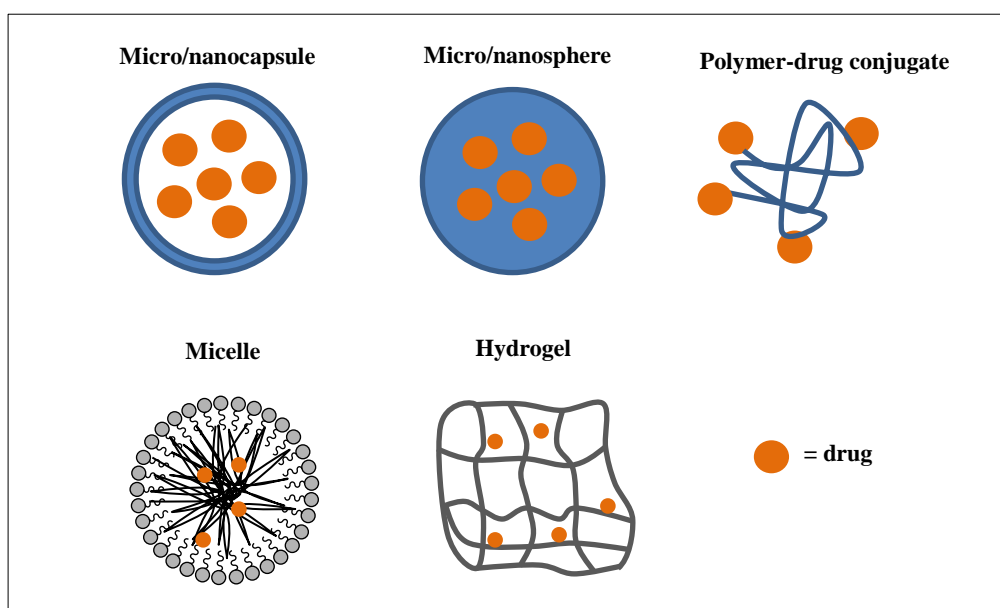


**Figure 1.17 Different structures of nanocarriers** (redrawn from Janssen et al., 2014)

Nanospheres (matrix system) or nanocapsules (reservoir system) are both in the polymeric nanoparticle group. Nanocapsules are polymeric nanoparticles containing either an oily or aqueous core surrounded by a polymeric shell (combination with a mixture of lipophilic and hydrophilic surfactants), whereas nanospheres are polymer-only matrix systems (Elmowafy et al., 2017). Nanospheres and nanocapsules are able to modify the activity of drugs, sustain and control drug release, and increase the drug adhesivity in the skin (Guterres et al., 2007).

Elmowafy et al. (2017) reported indomethacin loaded into polymeric nanocapsules and nanospheres produced a higher cumulative amount of drug in human skin compared to a marketed product (indomethacin in gel) at 24 h. They

found significantly higher skin permeation from nanocapsules of indomethacin compared to nanospheres. Even though nanocapsules had a larger particle size (186 – 193 nm) than nanospheres (138 - 142 nm), higher permeability was attributed to higher nanocapsules deformability than nanospheres (rigid matrix system).

Biodegradable, natural polymers are the first choice materials for producing polymeric nanoparticles, in order to minimise toxicity. In some studies, investigators have developed new compounds for nanoparticle production by conjugating the polymer with drugs especially for tumour targeting (Dragojevic et al., 2015). Ringsdorf (1975) introduced a model for pharmacologically active polymers, consisting of a biocompatible polymer backbone bound to three components; solubilizer, drug which is bound to the polymeric backbone via a linker, and a targeting moiety whose function is to provide transport to a desired physiological destination or to bind to a particular biological target (Larson and Ghandeharia, 2012). Castleberry et al. (2017) prepared all-trans retinoic acid conjugated with polyvinyl alcohol and produced sustained controlled delivery of active up to 10 days and significantly increased dermal accumulation of the all-trans retinoic acid in the pig skin. Polymer-conjugated drugs generally exhibit prolonged half-life, higher stability, water solubility, lower immunogenicity and antigenicity and often also specific targeting to tissues or cells (Pasut and Veronese, 2007).

The disadvantages of polymeric nanoparticles are the need for the approval by regulatory authorities on the safety issues, and also their high production costs (Bala et al., 2004).

### 1.11.3 Lipid nanocarriers

There are different types of lipid nanocarriers used for drug delivery system. Nanoemulsions comprise liquid mixtures of oil, water, surfactant and sometimes a co-surfactant having a droplet size in the range of 50 - 200 nm (Kong et al., 2011). In terms of production, the concentration of surfactant used is much lower (3-10%) compared to microemulsion preparation (more than 20%) (Bouchemal et al., 2004). Borges et al. (2013) found a dapsone-loaded nanoemulsion with isopropyl myristate as the oil phase promoted high *in vitro* epidermal permeation using Franz cells on

porcine ear epidermis. Hussain et al. (2016) formulated an amphotericin B-loaded nanoemulsion (mean droplet size 76 nm) and found a higher skin percutaneous permeation flux rate through rat skin as compared to drug solution using Franz diffusion cell. Amphotericin B in solution showed the highest release at 2 h, while amphotericin B-loaded nanoemulsion gel showed slower release compared to amphotericin B loaded-nanoemulsion alone. However, there are some disadvantages of nanoemulsions such as limited controlled release properties due to the liquid state of the carrier (Martins et al., 2007).

A second type of lipid-based nanocarriers is solid lipid nanoparticles (SLNs). In the 1990s, these were introduced as drug carrier system (Müller et al., 2002), and produced by replacing the liquid lipid (oil) of an emulsion by solid lipids or a blend of solid lipids (Müller et al., 2007). SLNs have a mean particle size of between 50 and 1000 nm (nanoparticles) (Müller et al., 2000). SLNs have been produced for pharmaceutical, traditional Chinese medicine and cosmetic applications. SLNs have been used to deliver bioactive ingredients such as vitamin A (Jenning et al., 2000), rifampicin, isoniazid and pyrazinamide (Pandey and Khuller, 2005), oridonin (Zhang et al., 2006), isotretinoin (Liu et al., 2007), *Artemisia arborescens* essential oil (Lai et al., 2007), repaglinide (Vijayan et al., 2010), virgin coconut oil (Noor et al., 2013), docetaxel (Naguib et al., 2014) and olanzapine (Iqbal et al., 2017). Different methods have been proposed in order to produce SLNs including high-pressure homogeniser, solvent evaporation, ultrasonication or melt dispersion techniques (Gasco, 1993; Müller et al., 2000; Trotta et al., 2003).

The second generation of SLNs is called as nanostructured lipid carriers (NLCs). NLCs are produced by incorporating blends of solid lipids and liquid lipids (oils) (Pardeike et al., 2009). Some examples of liquid lipid used in NLCs production are medium chain triglyceride such as oleic acid. Figure 1.18 shows the structural differences between SLNs and NLCs. Due to the main ingredients in SLNs being solid lipid (at room temperature), SLNs are in a highly crystalline form, limiting drug loading, whereas NLCs (combination of solid and liquid lipid) have a less crystalline structure, increasing drug loading. NLCs were introduced in order to overcome some of the problems associated with SLNs by increasing drug loading and reducing the burst release of drugs (Wissing and Müller, 2002; Hommos, 2008; Silva et al., 2009). The mean particle size for NLCs is usually less than 1000 nm.

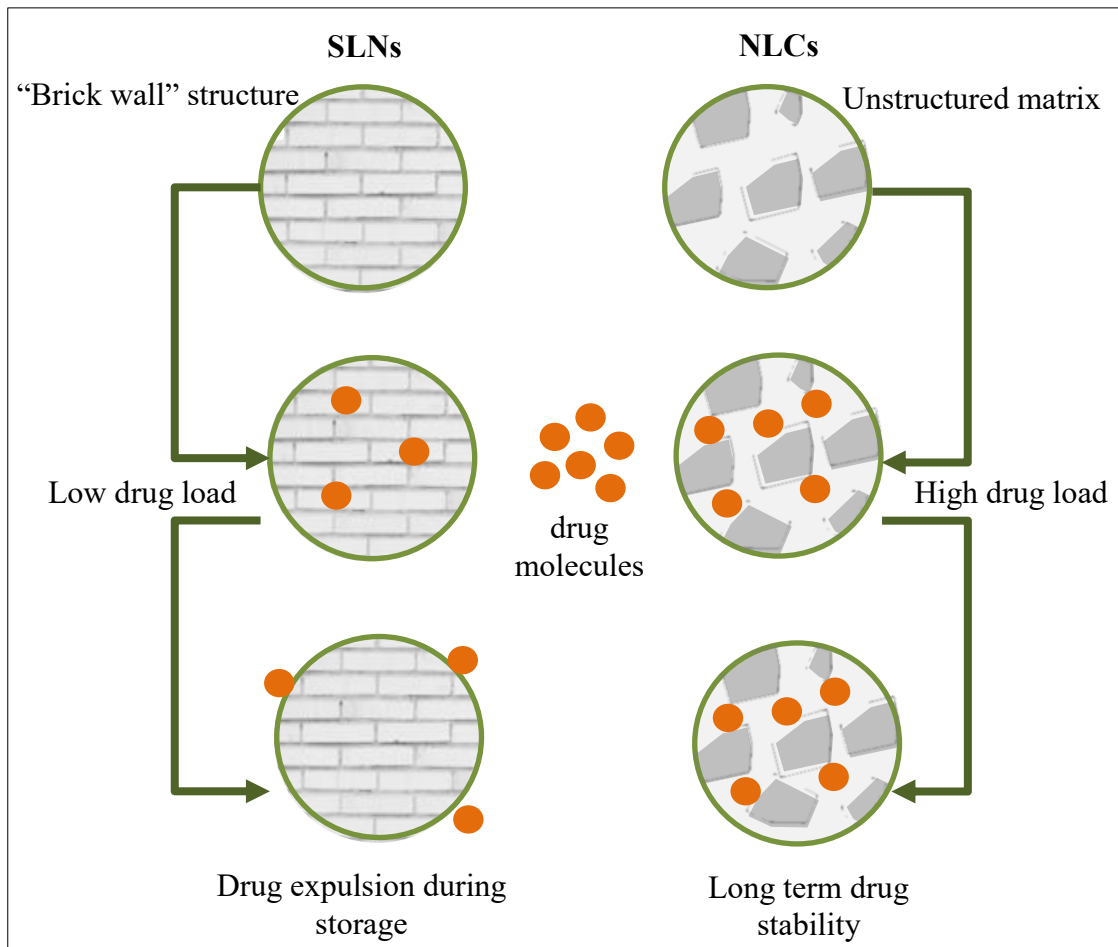


**Figure 1.18 Schematic illustration of SLN and NLC structures** (modified from Beloqui et al., 2016)

Several different types of solid lipid can be used in the production of SLNs and NLCs. The term ‘solid lipid’ includes fatty acids (e.g. myristic, stearic and palmitic acid), triglyceride (e.g. tripalmitin and tristearin), diglyceride (e.g. glyceryl behenate), monoglyceride (e.g. glyceryl monostearate), steroid (e.g. cholesterol) and waxes (e.g. cetyl palmitate and beeswax). Lipids used in SLNs or NLCs are generally regarded as safe (GRAS) (Attama et al., 2012). Different types of solid lipid have various degrees of crystallisation that may impact the drug entrapment efficiency and loading, size and charge of the resulted carriers. The lipid particle matrix is solid at both room and body temperatures (Müller et al., 2014).

### 1.12 Aim of the study

The aim of this project is to prepare and characterise dutasteride-loaded nanostructured lipid carriers (DST-NLCs), coated with chitosan oligomer conjugated with stearic acid, and lauric acid to enhance local drug delivery and reduce toxicity (Figure 1.19).

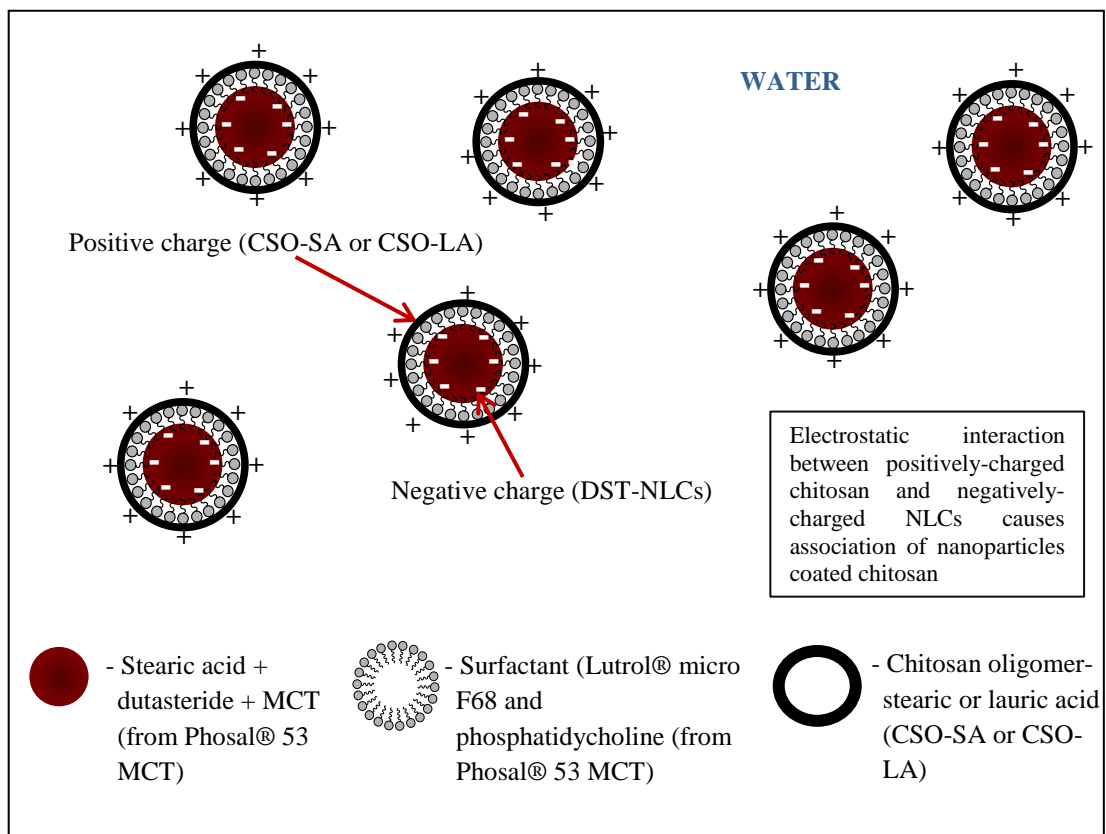


**Figure 1.19 Schematic representation of DST-NLCs coated with CSO-SA or CSO-LA to be prepared and characterised in this project**

Figure 1.20 shows the flow of the project outlined in this thesis. The project began with the conjugation and characterisation of CSO-SA and CSO-LA (Chapter 2). This was followed by optimisation of the formulation and manufacture of nanoparticles containing dutasteride and their characterisation (Chapter 3) and the *in vitro* studies (Chapter 4). Dutasteride was chosen as a drug having anti-androgenic activity, exhibiting Type I and Type II 5 $\alpha$ -reductase inhibitions.

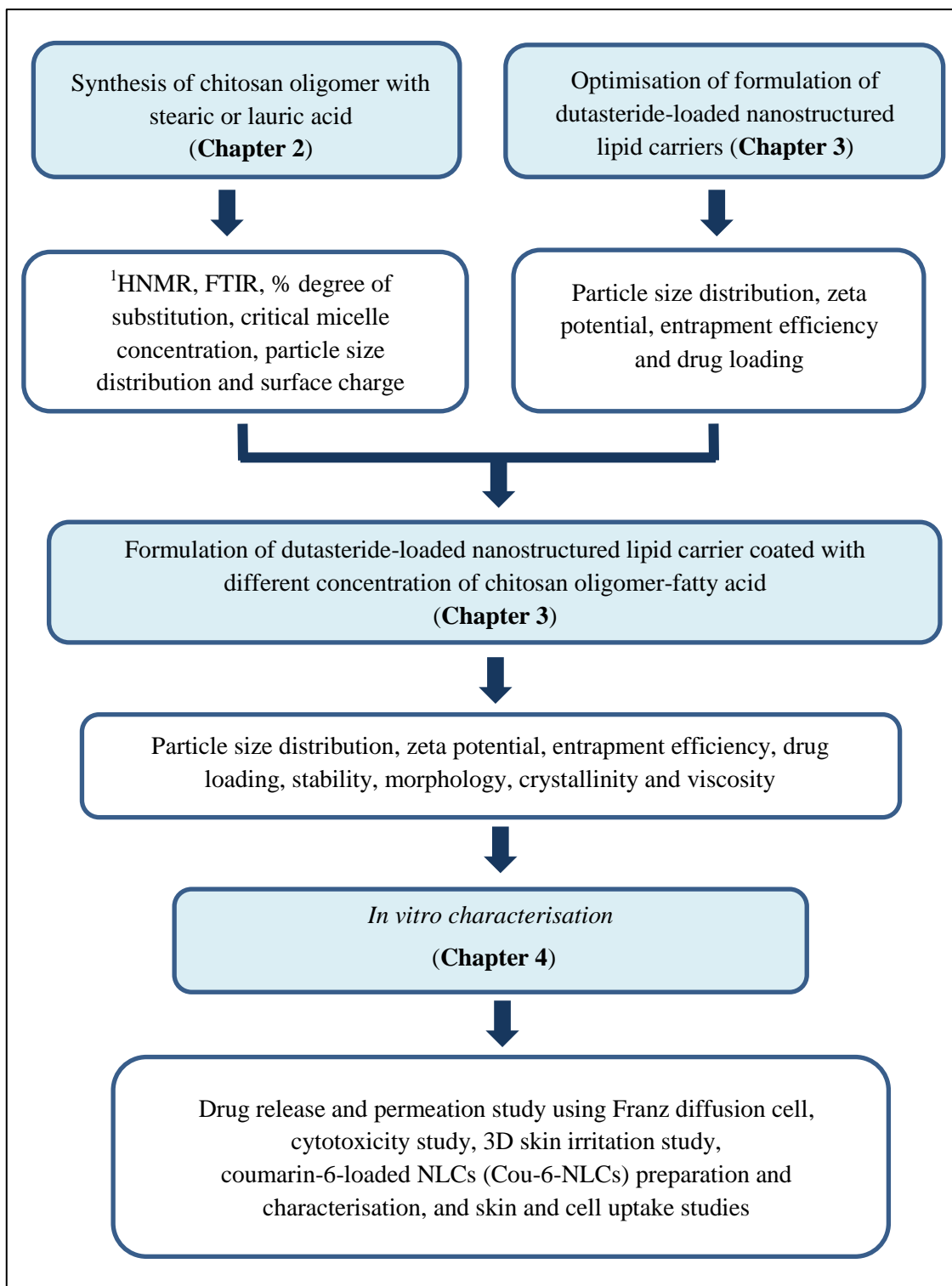


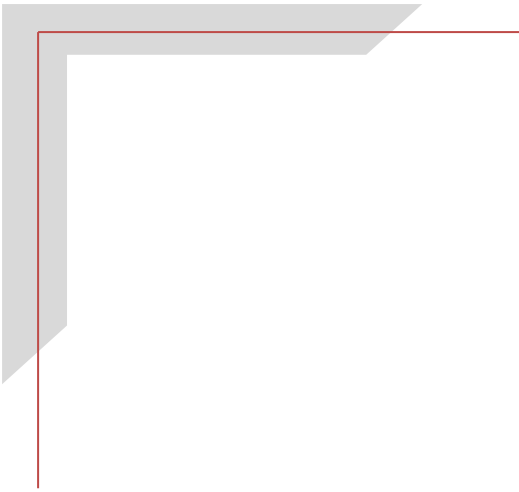
**Figure 1.20** Schematic diagram of overall preparation, characterisation and *in vitro* study of dutasteride-loaded nanostructured lipid carrier coated with chitosan oligomer-stearic or lauric acid

Moreover, the fatty acid used in the conjugation and DST-NLCs preparation also has 5 $\alpha$ -reductase inhibitor activity and may promote hair growth. The hypothesis of this project is that modifying the surface of NLCs with chitosan conjugated with CSO-SA or CSO-LA will enhance the stability of nanoparticles, delivery and safety of dutasteride. Delivering the NLC-drug system by topical application is hypothesised to enhance the retention of drug in the skin due to the particles' positive charge, achieve slow drug release, reducing toxicity and irritation.

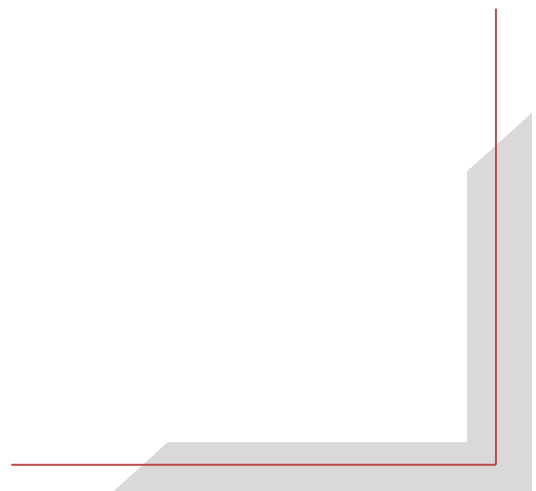
### 1.13 Objectives of study

In order to achieve the aim of the study, the specific objectives of the study are as follows:

- (i) To synthesis chitosan oligomer with stearic or lauric acid
- (ii) To develop, optimise and characterise DST-NLCs, uncoated and coated with chitosan oligomer-stearic or lauric acid, based on particle size distribution, surface charge, entrapment efficiency, drug loading, morphology, crystallinity and viscosity
- (iii) To determine *in vitro* drug release of DST-NLCs, uncoated and coated with different concentrations of chitosan oligomer-stearic or lauric acid
- (iv) To determine *in vitro* drug permeation through pig ear skin of DST-NLCs, uncoated and coated with chitosan oligomer-stearic or lauric acid
- (v) To investigate cell cytotoxicity and proliferation for hair follicle dermal papilla cells of DST-NLCs, uncoated and coated with chitosan oligomer-stearic or lauric acid
- (vi) To investigate skin irritation of DST-NLCs, uncoated and coated with chitosan oligomer-stearic or lauric acid using 3D Epiderm™ SIT tissue
- (vii) To formulate and develop Cou-6-loaded NLCs, uncoated and coated with chitosan oligomer-stearic or lauric acid (coumarin-6 as a model drug)
- (viii) To investigate cell and skin uptake using Cou-6-loaded NLCs uncoated and coated with chitosan oligomer-stearic or lauric acid



## **Chapter 2 Conjugation of chitosan oligomer with different types of fatty acids**



## 2.1 Conjugation of chitosan oligomer with stearic acid (CSO-SA)

### 2.1.1 Introduction

In this project, dutasteride was encapsulated in nanostructured lipid carriers (NLCs) which were then coated with chitosan oligomer-stearic acid, with the aim of increasing the stability of nanoparticles, sustaining the release of the drugs at the targeted area and prolonging the drug's residence in the epidermis/dermis layer of the skin. In this chapter, chitosan oligomer and stearic acid were chosen as a biodegradable polymer and lipid respectively, for conjugation. The experiments were designed in order to obtain the highest degree of substitution for use as a coating material. The independent variables were the different amount of stearic acid, different ratio of stearic acid and coupling reagent (1-ethyl-3-(3-(dimethylamino) propyl) carbodiimide, EDC) and different duration of reactions. The degree of substitution (%DS) was chosen as a dependent variable in order to calculate the amount of amine group substituted in the chitosan oligomer conjugated with stearic acid.

### 2.1.2 Materials

Stearic acid (purity > 98%) and lauric acid (purity > 98%) were purchased from the Tokyo Chemical Industry (TCI, UK). Chitosan oligomer (CSO) with molecular weight less than 3000 Da (deacetylation >85%) was obtained from Carbosynth Ltd (UK). Ethanol (96% v/v analytical grade), 1-(3-dimethylaminopropyl)-3-hydrochloride (EDC.HCl), acetic acid-d<sub>4</sub> (99.9 atom %D), ninhydrin, D-glucosamine, sodium acetate anhydrous (purity > 99%) and pyrene for fluorescence, ≥99.0% were obtained from Sigma-Aldrich Company Ltd (UK). Deuterium oxide (99.9 atom %D) was purchased from Cambridge Isotope Lab Inc (USA). Acetic acid glacial (analytical reagent) and acetone were purchased from Fisher Scientific (UK). Deionised water (PURELAB Option, ELGA, UK) was obtained on site from a water system.

### 2.1.3 Synthesis of chitosan oligomer-stearic acid (CSO-SA)

The free amine group of chitosan oligomer (CSO) was conjugated with the carboxyl group of the fatty acid in stearic acid (SA) using 1-(3-dimethyl aminopropyl)-3-ethyl carbodiimide hydrochloride (EDC.HCl) as a coupling reagent (Figure 2.1; Hu et al. (2009) and Xie et al. (2012)). Due to the long hydrocarbon chain, stearic acid has 5 $\alpha$ -reductase inhibitory activity, though less potent than shorter chain hydrocarbons (Liu et al., 2009). This strategy would provide potential inhibition activity and a synergistic effect at higher concentration when combined with dutasteride.

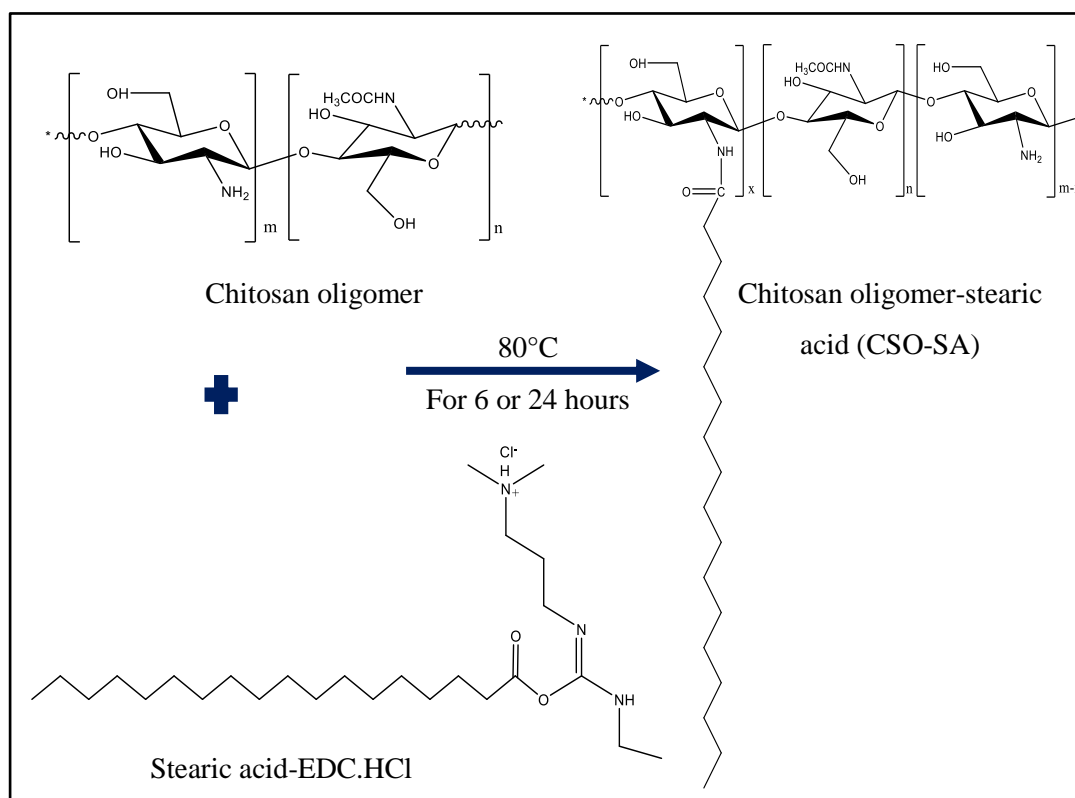


**Figure 2.1** Conjugation between chitosan oligomer and stearic acid

The hydrophobic region in chitosan oligomer-stearic acid would be expected to produce self-assembled nanoparticles in the aqueous phase. This would also result in more stable particles when coating the nanoparticles compared to chitosan

oligomer without conjugation because the surface activity of chitosan (non-conjugated) is low due to the absence of hydrophobic portions (Cheung et al., 2015).

CSO (1 g) was dissolved in 120 mL of deionised water using magnetic stirrer for 2 h at 80°C on a hot plate. On another hot plate, SA (0.5 or 1.0 g) was dissolved in ethanol (80 mL), heated at 60°C with constant stirring. SA solutions were then activated with EDC.HCl (1.68 or 3.37 g; molar ratio SA: EDC.HCl; 1:5 or 1:10) and stirred for 2 h at 60°C. The solutions of SA were added using a syringe with a needle (25 gauge, 5/8th inch, BD Microlance™ 3, Becton Dickinson, Spain) into the CSO solutions with continuous magnetic stirring for 6 or 24 h. To remove the unreacted EDC.HCl and SA in the solutions, dialysis (molecular weight size cut off 1000 Da, Spectrum Laboratories, USA) was undertaken. The product was evaporated to reduce volume (final volume is approximately 70 mL) under vacuum using rotary evaporator (Rotavapor® R-100, Buchi, Switzerland) at 70°C. After dialysis for two days, the product was precipitated using 300 mL acetone and filtered using filter paper (Fisherbrand QL100, Fisher Scientific, UK) to obtain the product. The product was dissolved in 10 mL of water and precipitated again with 300 mL acetone. This step was repeated for a further two times. Finally, the sample was stored in a desiccator prior to use.

The conjugation between chitosan oligomer and stearic acid was investigated using a design of experiments approach (Design Expert 6.0.8 Software, Stat-Ease, USA). The independent variables were the ratio of SA to EDC.HCl, time of reaction and the amount of SA used. The dependent variable selected was the degree of substitution (%DS). %DS was calculated in order to determine the amount of amine groups substituted with the stearyl chain. Table 2.1 shows the design of experiments for the synthesis, while the coded and value for the design of experiment are shown in Table 2.2.

**Table 2.1 Design of experiments for preparing CSO-SA using a 2<sup>3</sup> full factorial design**

Product	SA: EDC.HCl	Time (h)	Stearic acid (mg)
S1	1:5	6	0.5
S2	1:10	6	0.5
S3	1:5	24	0.5
S4	1:10	24	0.5
S5	1:5	6	1.0
S6	1:10	6	1.0
S7	1:5	24	1.0
S8	1:10	24	1.0

**Table 2.2 Value and coded units of the 2<sup>3</sup> full factorial design for conjugation of chitosan oligomer with stearic acid**

Variables	Coded	Level	
		Low (-1)	High (+1)
Molar ratio SA:EDC.HCl	A	5	10
Time of reaction (hours)	B	6	24
Stearic acid (mg)	C	0.5	1.0

#### 2.1.4 Characterisation of chitosan oligomer-stearic acid (CSO-SA)

##### 2.1.4.1 Characterisation of chitosan oligomer-stearic acid using <sup>1</sup>H NMR

In order to confirm the presence of the fatty acid chain in the chitosan oligomer conjugate, samples were characterised using proton nuclear magnetic resonance spectrometer (NMR). The <sup>1</sup>H NMR spectra of CSO, CSO-SA, and SA were obtained by using an NMR Bruker Avance 500 spectrometer (Bruker Instruments, USA). 5 mg of each sample was diluted in 1 mL deuterium oxide (D<sub>2</sub>O) with the addition of one drop of acetic-d<sub>3</sub> acid-d to dissolve the product. Meanwhile,

stearic acid (5 mg) was dissolved in chloroform-d ( $\text{CDCl}_3$ ). The  $^1\text{H}$  NMR Bruker Avance 500 with 32 scans was run for all the samples, and the spectrum of each sample analysed.

#### **2.1.4.2 Characterisation of chitosan oligomer-stearic acid using Fourier Transform Infrared Spectroscopy (FTIR)**

Samples of CSO-SA, CSO and SA were analysed using FTIR. Approximately 5 - 10 mg of sample was pressed on the top of the pan and four scans were obtained. Samples were analysed from 660 to 4000  $\text{cm}^{-1}$  using a PerkinElmer Spectrum100 FTIR (PerkinElmer, UK). The spectra of CSO-SA, pure CSO and SA were then compared.

#### **2.1.4.3 Determination of amine groups substitution using the ninhydrin assay**

In order to measure the amount of chitosan conjugated with stearic acid, ninhydrin was used as a reagent to react with the primary and secondary amine group in the conjugated product (Curotto and Aros, 1993). The two most common calorimetric assays used for the primary amines determination are ninhydrin and trinitrobenzene sulfonic acid (TNBS) assays. Based on the previous study (Pearce et al., 1988), the ninhydrin assay has advantages compared to TNBS assay. For the TNBS assay, the chromophore appears to be an orange colour. However, in the ninhydrin assay, the chromophore which is called Ruhemann's purple is produced for all primary amines that react with ninhydrin and this chromophore is fully soluble under the conditions of that assay with no interference from yellow chromophores common in other products (Pearce et al., 1988). Also, the prepared buffer is sufficiently strong (4N sodium acetate at pH 5.5) so that the preliminary adjustment of the pH of the samples is not necessary (Moore and Stein, 1954).

For this study, 4M acetate buffer (pH 5.5) was used to maintain the conditions of the reaction. Generally, in this assay, the reagent changes colour from yellow to purple if there is a free amine group in the product after a certain time and at high temperature (Figure 2.2). Theoretically, in this study, when the chitosan oligomer

reacts with stearic acid, the amine groups are replaced with a fatty acid chain with a reduction in intensity of the purple colour.

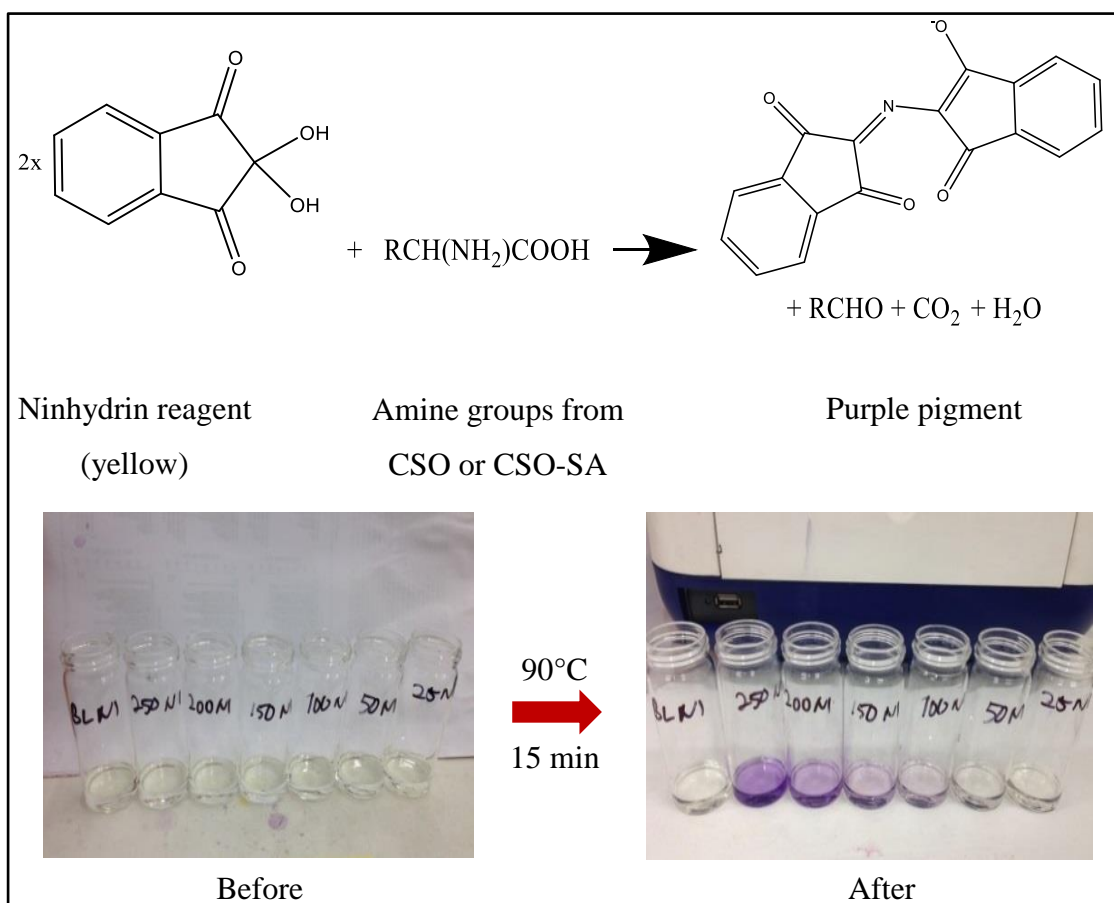


**Figure 2.2 Ninhydrin assay: Reaction of ninhydrin reagent with amine groups from CSO or CSO-SA or CSO-LA (colour of ninhydrin changes from light yellow (left) to purple (right))**

The percent of free amine groups present in the CSO-SA conjugate was determined using the ninhydrin assay by comparing the gradients of the slopes (absorbance versus concentration) produced for D-glucosamine, CSO and conjugated CSO. Serial dilution of glucosamine, CSO and CSO-SA (stock solution: 2000  $\mu\text{g/mL}$ ) were prepared in 0.2% acetic acid solution. The working solutions for CSO and CSO-SA were 100, 60, 40 and 20  $\mu\text{g/mL}$ . Ninhydrin solution was prepared by dissolving 0.35 g of ninhydrin in 100 mL ethanol. 4M acetate buffer was prepared by dissolving 32.82 g of sodium acetate anhydrous in 60 mL deionised water and 22.82 mL acetic acid made up to 100 mL with deionised water after complete dissolution.

The reaction was achieved by adding 0.5 mL of sample, 0.5 mL of 4M acetate buffer and 2 mL of ninhydrin solution into a 10 mL volumetric flask and heating at 90°C in a water bath with stirring for 15 min. 4M acetate buffer was used to maintain the reaction. After 15 min, the volumetric flask was taken out from the water bath and cooled down to room temperature. The solution was then made up to 10 mL with ethanol. The absorbance of samples was measured at 570 nm using an Agilent Cary 100 UV-Vis Spectroscopy (Agilent Technologies UK Ltd. Berkshire, UK). The amount of free amine groups in glucosamine, CSO and CSO-SA samples was determined by comparing the slopes using linear regression, where the absorbance (y) for each sample were plotted as a function of concentration (x).

### **2.1.5 Statistical analysis**

The % degree of substitution of all synthesised CSO-SA were analysed using Design Expert 6.0.8 Software (Stat-Ease, USA). A *p*-value of less than 0.05 was considered significant.

## **2.2 Conjugation of chitosan oligomer with lauric acid (CSO-LA)**

### **2.2.1 Introduction**

In order to determine the effect of chain length of the conjugated chitosan oligomer on the stability, mean particle size, and the proliferation of the hair follicle dermal papilla, lauric acid as a medium chain fatty acid was chosen for conjugation with chitosan oligomer. Lauric acid previously showed good inhibition of androgenic activity and also has an inhibitory effect on lymph node carcinoma of the prostate cancer (LNCaP) cells (Liu et al., 2009). As the melting point of lauric acid is relatively low (43.8°C) compared to stearic acid (69.3°C), formulating lauric acid into solid lipid nanoparticles or nanostructured lipid carriers system may be difficult. Liu and Wu, (2010) prepared lutein loaded-NLCs formulation with lauric acid as a solid lipid and found unstable NLCs formulation even at day 1. Due to that, by conjugating lauric acid with chitosan oligomer and acts as a coating material for NLCs, it would help to deliver lauric acid in the nanocarrier system to be delivered to

the skin. Having lauric acid conjugated with CSO may inhibit the  $5\alpha$ -reductase enzyme and promote hair growth. The conjugation between chitosan oligomer and lauric acid was performed using the methodology described in 2.1.3. The degree of substitution (%DS) was determined in order to calculate the amount of amine group substituted in the chitosan oligomer conjugated with lauric acid.

### **2.2.2 Synthesis and characterisation of chitosan oligomer-lauric acid (CSO-LA)**

The conjugation between chitosan oligomer and lauric acid was performed using the methodology described in Section 2.1.3. The amount of materials used in the conjugation between CSO and lauric acid was obtained from the optimised ratio from the previous conjugation; CSO (1 g) was conjugated with SA: EDC.HCl (0.5 g SA and 1.68 g EDC.HCl) for 6 hours. The characterisation of CSO-LA using  $^1\text{H}$ NMR, FTIR and the %DS was undertaken using the method described in Sections 2.1.4.1, 2.1.4.2 and 2.1.4.3, respectively.

## **2.3 Preparation and characterisation of selected CSO-SA or CSO-LA micelles**

CSO-SA or CSO-LA micelles were prepared by dissolving 5 mg/mL of CSO-SA into 0.2% v/v acetic acid in water. The sample was bath sonicated for an hour in order to dissolve completely. Samples were prepared in triplicate.

### **2.3.1 Measurement of particle size distribution of selected CSO-SA or CSO-LA micelles**

Dynamic light scattering (DLS) determines the mean size of particles (hydrodynamic diameter) undergoing Brownian motion and estimates the width of the distribution (polydispersity index). When a laser passes through the dispersion, the intensity of the scattered light fluctuates depending on the size of particles. The small particles diffuse faster which results in the intensity fluctuating more rapidly compared to the larger sizes in the dispersion. Hydrodynamic diameter is calculated from the translational diffusion coefficient using the Stokes-Einstein equation with

the assumption that all particles are spherical in shape, while polydispersity index (PDI) is the measurement of the heterogeneity of size distribution in a mixture.

Samples were analysed using dynamic light scattering (DLS) equipment (Zetasizer Nano ZS, Malvern Instruments, UK) for determination of the particle size distribution. 1 mL of the sample was pipetted directly into the zeta potential DTS1070 folded capillary cell (Malvern, UK) without dilution at 25°C. The size distribution of micelles was obtained as the hydrodynamic diameter ( $Z_{Ave}$ ) and polydispersity index (PDI). The measurement was performed in triplicate, and mean values were taken.

### **2.3.2 Measurement of zeta potential of selected CSO-SA or CSO-LA micelles**

In order to measure the surface charge of the micelles, zeta potential (ZP) was measured using the Zetasizer Nano ZS (Malvern Instruments, UK). This equipment uses electrophoretic light scattering technology to measure zeta potential, calculated from electrophoretic mobility using the Helmholtz-Smoluchowski equation by the Malvern data analysis software.

1 mL of the sample was pipetted directly into the zeta potential DTS1070 folded capillary cell (Malvern, UK) without dilution. The measurements were recorded at 25°C. The prepared formulation was analysed without further dilution, and the measurement was performed 3 times, and the average values were recorded.

### **2.3.3 Determination of micelles morphology by transmission electron microscope**

The morphological observation of 5 mg/mL of CSO-SA and CSO-LA micelles was determined using a transmission electron microscope (TEM; Philips/FEI CM120 Bio Twin, FEI Netherlands). Samples were placed on copper grid formvar/carbon support film 300 mesh (Agar Scientific, Stansted, Essex, UK), and excess droplets were blotted with filter paper. After a few seconds, a drop of 1% uranyl acetate was placed onto the copper grid for negative staining. The grid was air-dried at room temperature and observed using TEM.

### **2.3.4 Measurement of critical micelle concentration (CMC) using UV spectrophotometer of selected CSO-SA and CSO-LA**

In order to determine whether CSO-SA and CSO-LA coated nanoparticles exist as micelles or monomers in water, a study on CMC was conducted. CMC of final CSO-SA and CSO-LA were performed in order to determine the minimum concentration of product that can produce a micellar system. CMC was performed based on a previous method (Tanhaei et al., 2013) with slight modification. CMC is determined by a sudden change in the related physical properties upon micelle formation (Tanhaei et al., 2013). In this study, pyrene was used as a probe.

CSO-SA or CSO-LA micelles were diluted in a serial dilution concentration starting from 2.5 to 0.001 mg/mL in water. Pyrene stock solution was prepared by dissolving 40 mg pyrene in 1 mL acetone. The pyrene stock solution was further diluted by transferring 100  $\mu$ L to a 10 mL volumetric flask and making up to volume with acetone. 7  $\mu$ L of pyrene was pipetted into each serial dilution of samples. As pyrene is a hydrophobic probe, it will be incorporated into the hydrophobic area in the micellar system.

Pyrene in acetone was scanned from 200 – 800 nm using UV-Vis Spectrophotometer (Agilent Cary 100, UK). Blank and samples were transferred into a 96-well plate (Nunc, Wiesbaden, Germany) and the absorbance was read at 334 nm using microplate reader (SpectraMax®M2e, Molecular Devices, USA). The value of CMC was determined from the absorbance versus concentration of samples plotted graph. The inflection point of the absorbance versus concentration of the samples plot was taken as the CMC of the surfactant in the corresponding pyrene solutions (Tanhaei et al., 2013)

### **2.3.5 Statistical analysis**

Statistical analysis using Student t-test, with IBM SPSS 23 Statistic Data Editor Software (USA) was undertaken. A *p*-value of less than 0.05 was considered significant for all experiments.

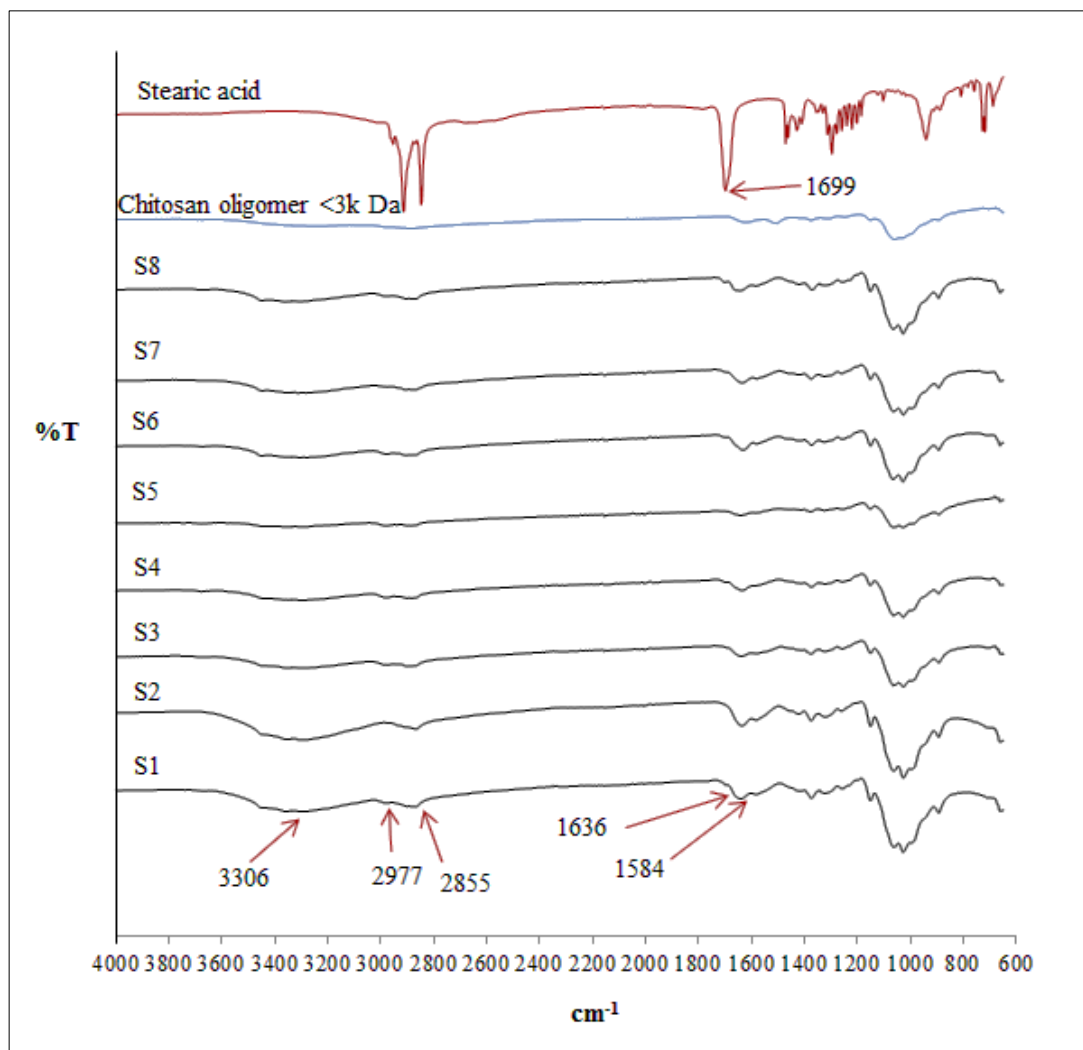
## 2.4 Results and discussion

### 2.4.1 Conjugation between chitosan oligomer and stearic acid (CSO-SA)

#### 2.4.1.1 <sup>1</sup>HNMR and FTIR of CSO-SA

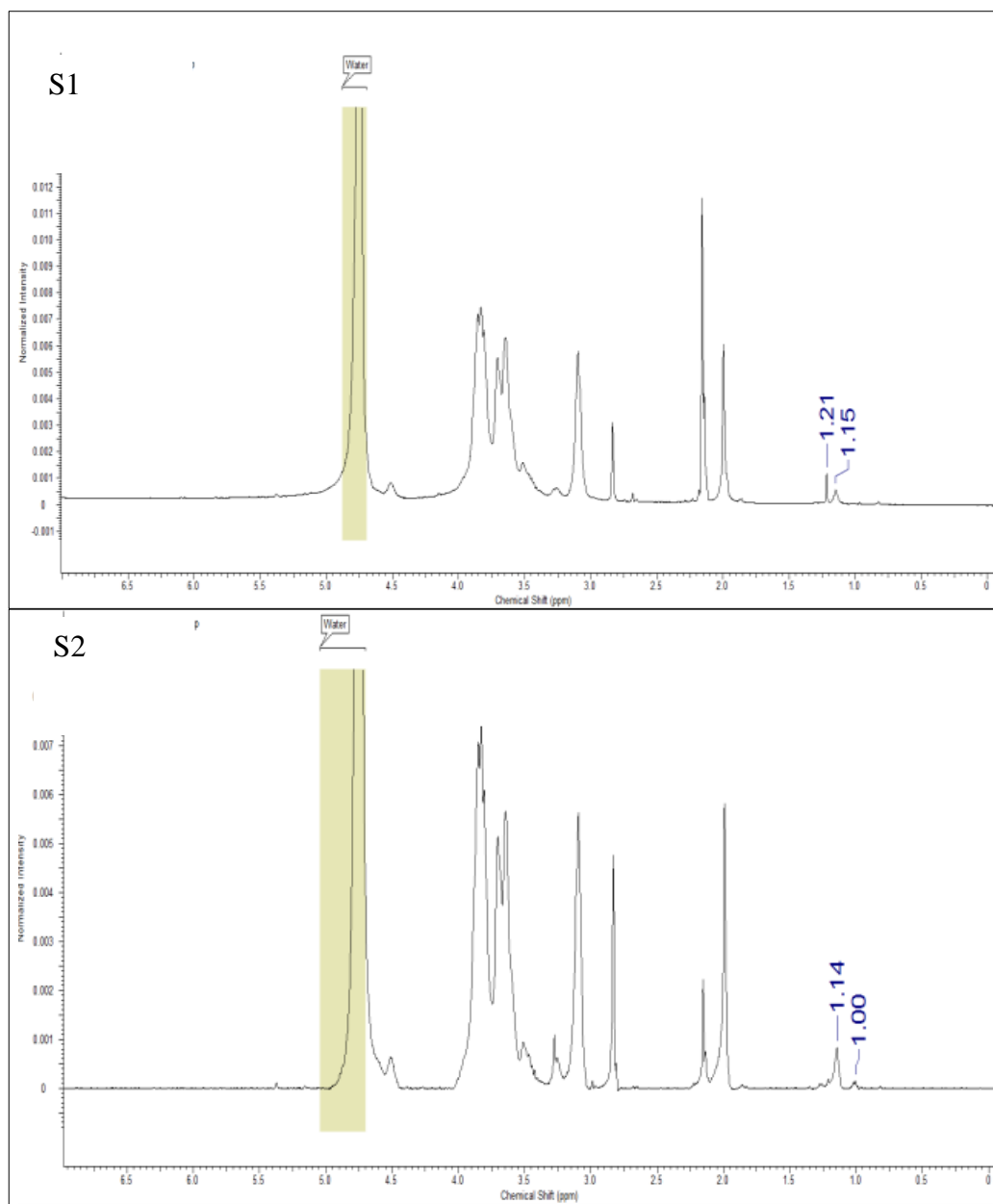
The formation of CSO-SA was confirmed using FTIR and <sup>1</sup>H NMR. Figure 2.3 shows the IR spectra of all samples. Compared to the spectra of raw materials (stearic acid and CSO), there were some changes in the IR spectrum of chitosan-stearic acid resulting from the binding between the stearic acid carboxylic group and the chitosan amine group. The IR spectra for CSO (without conjugation) showed absorption peaks at 1620 cm<sup>-1</sup> attributed to C=O stretching of the secondary amine (amide I band). The IR spectra of all eight products of the CSO-SA synthesis showed two peaks around 1636 and 1584 cm<sup>-1</sup> corresponding to the N-stearoyl (attributed to the C=O stretching (amide I band) and N-H bending vibrations (amide II band), respectively). The increase of the C-H absorption around 2977 and 2855 cm<sup>-1</sup> indicated the presence of the stearoyl chain. The broad peak at around 3306 cm<sup>-1</sup> represented the -OH group from the chitosan oligomer.

The other peak indicating the presence of carboxyl groups (-COOH) from stearic acid was shown around ~1699 cm<sup>-1</sup>. After conjugation of different amount of stearic acid to chitosan oligomer, the peak around 1699 cm<sup>-1</sup> was reduced which suggested that stearic acid had reacted with chitosan oligomer. Meanwhile, the presence of amide band was in agreement with a previous study (Zhao et al., 2014) where chitosan was conjugated with fatty acid (lauric acid) and produced N-lauroyl bond (amide I band). They found that, the -OH bond stretching attributed from chitosan appeared at 3430.6 cm<sup>-1</sup>. Meanwhile the stretching vibration of amide I band was found at 1642.9, 1641.1 and 1641.0 cm<sup>-1</sup> which were slightly shifted from our study.



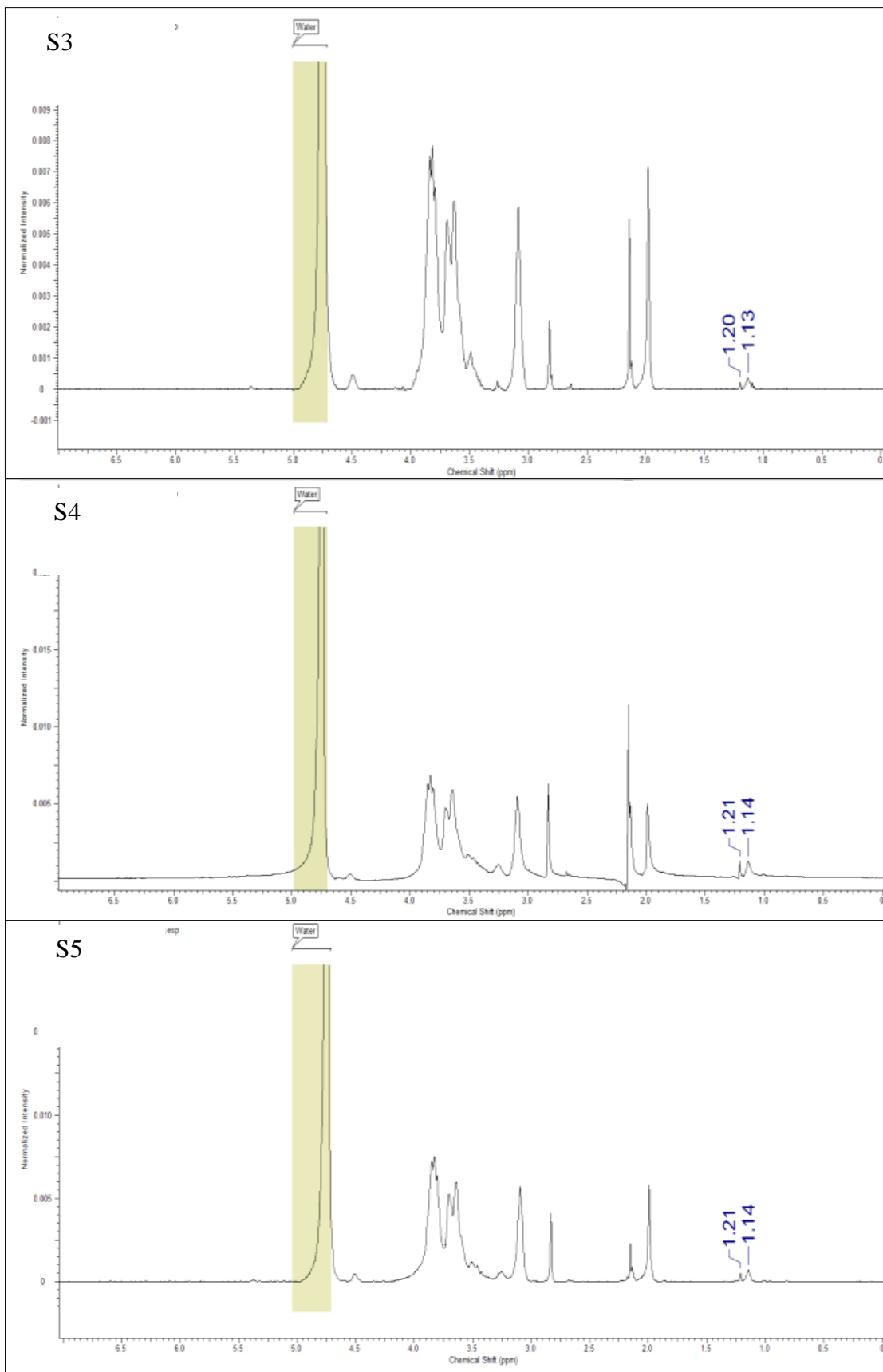
**Figure 2.3 FTIR spectra of chitosan oligomer-stearic acid from eight different condition of synthesis; varying ratio of SA:EDC.HCl/time of reaction (hours)/amount of stearic acid (g). S1 (1:5/6/0.5), S2 (1:10/6/0.5), S3 (1:5/24/0.5), S4 (1:10/24/0.5), S5 (1:5/6/1), S6 (1:10/6/1), S7 (1:5/24/1) and S8 (1:10/24/1.0)**

Figure 2.4 shows  $^1\text{H}$  NMR spectra for all conjugations. The chemical shifts represent the methyl and methylene hydrogen of the stearate group. The chemical shifts shown at 1.0 - 1.1 ppm represent protons from  $\text{CH}_3$  of stearic acid whereas the other peaks at 1.13 - 1.15 ppm corresponded to the protons of the  $\text{CH}_2$  group of the acyl chain. The remainder of the peaks shown are the hydrogen peaks from the chitosan oligomer.

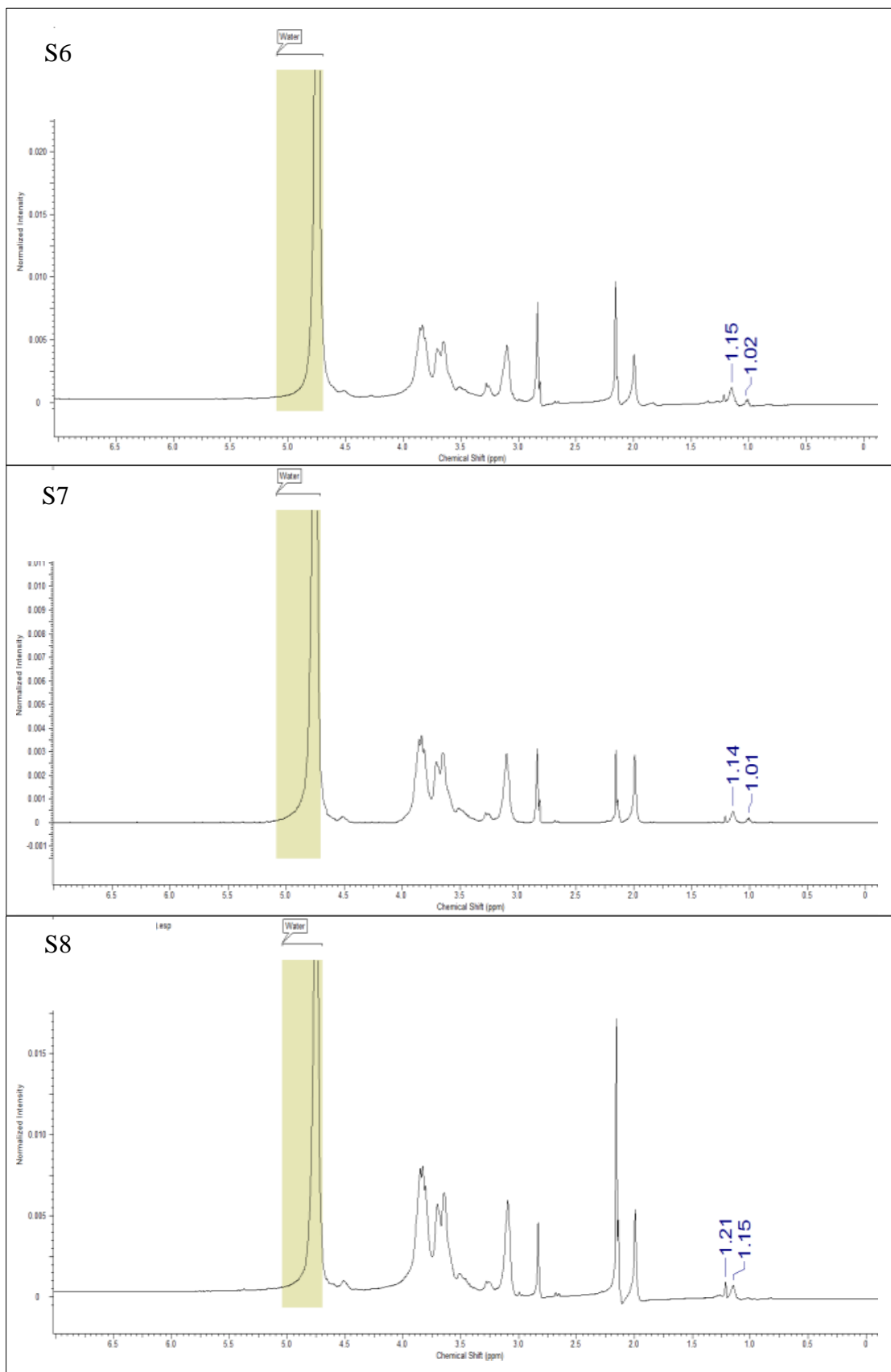


**Figure 2.4**  $^1\text{H}$  NMR spectra of chitosan oligomer-stearic acid from eight synthesis; varying ratio of SA: EDC.HCl/time of reaction (hours)/amount of stearic acid (g). S1 (1:5/6/0.5), S2 (1:10/6/0.5), S3 (1:5/24/0.5), S4 (1:10/24/0.5), S5 (1:5/6/1), S6 (1:10/6/1), S7 (1:5/24/1) and S8 (1:10/24/1.0)

(continued)



(continued)



These NMR results demonstrated that stearic acid was conjugated to the chitosan oligomer. This finding is in agreement with Xie et al. (2012) and Hu et al. (2009). However, both researchers used different molecular weight of CSO as a starting material. Xie et al. (2012) prepared CSO-SA from 18 kDa MW CSO and Hu et al. (2009) prepared CSO-SA with different molecular weights of chitosan (9.28 kDa and 18.0 kDa).

#### **2.4.1.2 Ninhydrin assay of D-glucosamine, CSO and different samples of CSO-SA**

A preliminary study of the ninhydrin assay was conducted on 96-well plate. Samples with different concentration were pipetted into a 96-well plate with buffer and ninhydrin solutions and placed in an oven (set up at 90°C) for 15 min. After 15 min, the absorbance was measured using microplate reader (SpectraMax®M2e, Molecular Devices, USA). The absorbance reading for all samples was not consistent due to uneven heating in the oven.

A further study of the ninhydrin assay was undertaken in the volumetric flasks. Different concentration of samples with acetate buffer and ninhydrin solutions were placed in 10 mL volumetric flasks at the same time in the water bath. The same problem occurred whereby the absorbance of the samples was found to be inconsistent and the graph of absorbance versus concentration of samples was not linear, due to uneven heating in the water bath.

Consequently, in subsequent experiments, only one volumetric flask at a time was placed in the water bath which was maintained at 90°C. This protocol gave a consistent reading of the absorbance even though it was time-consuming. These showed that, the temperature of reaction in this assay was really important and slight changes of temperature would affect the absorbance measurement.

The slopes for absorbance versus concentration were plotted and gradients calculated (Figure 2.5). The slope for chitosan oligomer (CSO) and D-glucosamine were 0.0126 and 0.0676, respectively (Figure 2.5). In Samples S1, S5, S6, and S7; the amount of free amine groups decreased due to the substitution of stearic acid. Samples S2, S4 and S8 showed low %DS.

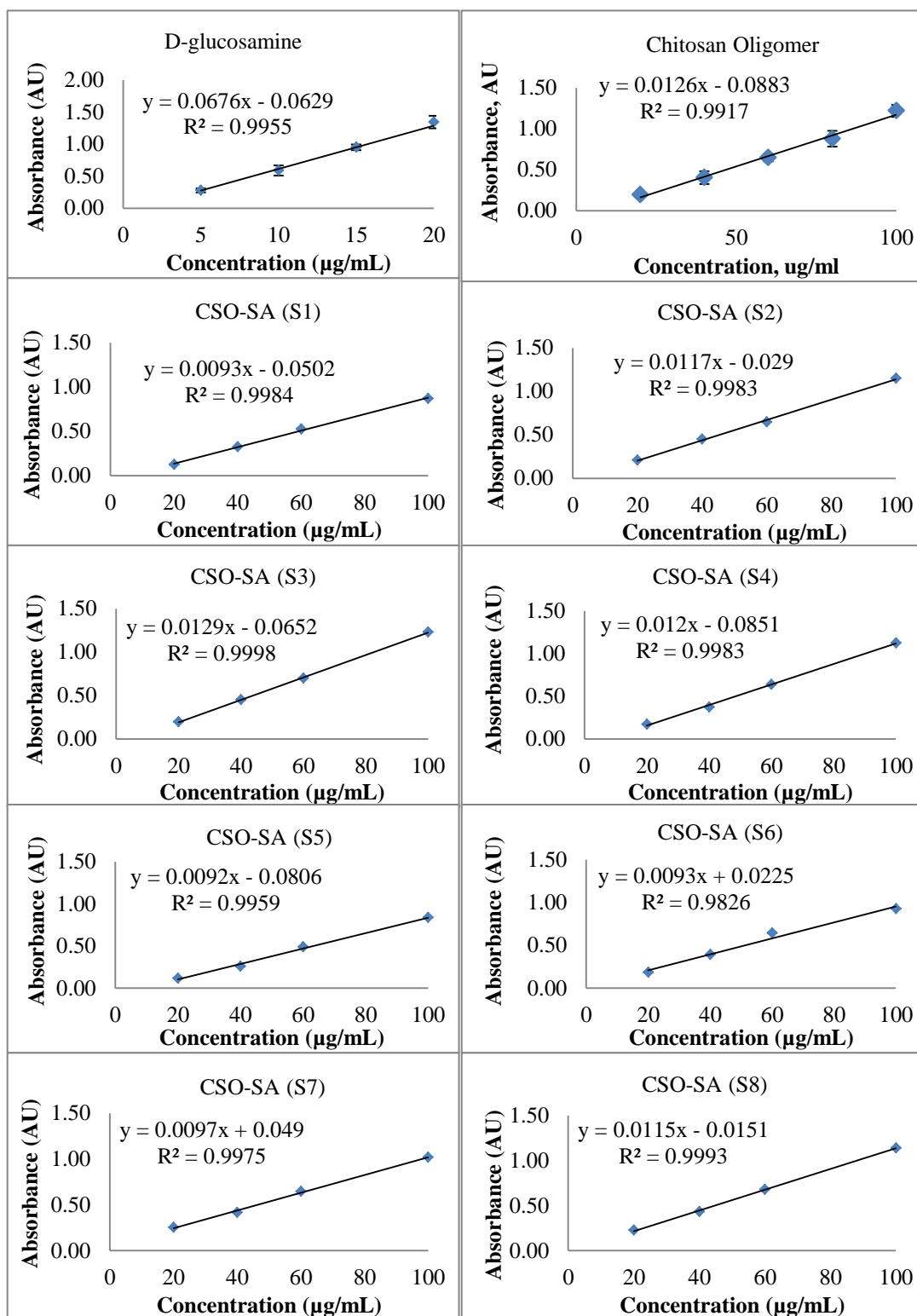


**Figure 2.5 Absorbance versus concentration from ninhydrin assay of D-glucosamine, CSO and different samples of CSO-SA (n=3, mean ± SD)**

By comparing the slope from D-glucosamine, CSO and CSO-SA; the %DS of the synthesised CSO-SA was calculated (Table 2.3). Sample S3 showed a negative value of %DS. This may possibly be due to the high temperature and prolonged reaction time combined with low amounts of materials (SA: EDC.HCl/Time/SA-1:5/24/0.5). By comparing the slope of CSO and D-glucosamine, CSO has approximately 81% of D-glucosamine and 19% of *N*-acetyl-D-glucosamine. These *N*-acetyl-D-glucosamine groups could be further deacetylated causing an increasing number of free amine groups in the final product.

A wide range of results has been reported in previous research on the amount of %DS. Xie et al. (2012) reported that %DS of stearic acid conjugated with chitosan was approximately 27% using a TNBS assay. They used 0.7 g of SA with EDC (SA: EDC; 1:10 ratio) conjugated with chitosan (MW 18 kDa). The reaction between SA and EDC was carried out for 30 min and the reaction between chitosan and SA: EDC solutions were kept for 6 hours.

Du et al. (2010) prepared different molecular weight chitosan oligomer with different amounts of SA at 1:10 ratio between SA and EDC. The reaction between chitosan and SA: EDC solutions (200 mL) were continued for 24 h. The %DS (TNBS assay) of conjugated chitosan oligomer with SA were found to be approximately 14% when they synthesised 1 g of CSO (MW = 3 kDa) with 25% SA. Increasing the amount of SA from 25 to 80% increased the %DS from 14 to 63%.

On the other study, Hu et al. (2009) prepared 0.825 g stearic acid with 5.5 g EDC (in 17 mL ethanol) and reacted with 0.5 g CSO (in 33 mL DI water). The reaction between SA and EDC was done at 80°C for 4 h, and the %DS was found to be approximately 6.5% using TNBS assay.

Yuan et al. (2010) synthesised chitosan with different amount of SA. 2 g of chitosan (5 kDa MW) was reacted with different amounts of SA (15%, 30% or 50% relating to the molar number of glucosamine unit in chitosan) with ratio between SA and EDC was 1:10 for 24 h. Increasing the amount of SA from 15 to 50% had increased the %DS from 4 to 40%.

**Table 2.3 Slope, percent of free amine groups and degree of substitution based on ninhydrin assay**

	Chitosan oligomer (CSO)	Chitosan conjugated with stearic acid (CSO-SA)							
		Sample							
		SA: EDC.HCl/time of reaction (hours)/ amount of stearic acid (mg)							
		S1	S2	S3	S4	S5	S6	S7	S8
		1:5/6/0.5	1:10/6/0.5	1:5/24/0.5	1:10/24/0.5	1:5/6/1	1:10/6/1	1:5/24/1	1:10/24/1
<b>Slope</b>	0.0126	0.0093	0.0117	0.0129	0.0012	0.0092	0.0093	0.0097	0.0115
<b>Free amine (%)</b>	81.4	86.2	82.7	80.9	82.3	86.4	86.2	85.6	83.0
<b>%DS</b>		6.0	1.64	-0.55	1.09	6.18	6.0	5.27	2.0

%DS – degree of substitution calculated by assuming the D-glucosamine slope has 100% amine groups, and the CSO and CSO-SA were then identified by comparing each slope (slope of D-glucosamine = 0.0676)

As seen for the above mentioned studies, the %DS for all synthesised products had different values. Variation in the amount of chitosan used with different molecular weight and volume of chitosan solutions, time of reaction between chitosan and EDC, reaction time between chitosan and SA.EDC.HCl and also the amount of SA and EDC used affect %DS. In this study, all the conjugated products produced low %DS, even though the reaction between SA and EDC.HCl was done for 2 h and continue for another 6 or 24 h with ratios of SA:EDC.HCl at 1:5 or 1:10.

In order to find the optimised CSO-SA synthesised product, factorial model was generated using ANOVA Design Expert 6.0.8 Software (State-Ease Inc, USA) (Table 2.4). This software indicated there was no significant difference ( $p>0.05$ ) on the model term with the factors used. Due to the similar values of %DS for samples S1, S5, S6, and S7; S1 (0.5 g stearic acid and the ratio 1:5 of SA: EDC.HCl was reacted for 6 h) will be used for subsequent experiments in order to reduce the time and the materials used.

**Table 2.4 Analysis of variance (ANOVA) for a 2<sup>3</sup> factorial design on degree of substitution (%DS)**

	Sum of squares	<i>df</i>	F-value	<i>p</i> -value
Model	38.67	3	4.28	0.0971
<i>A</i>	4.76	1	1.58	0.2773
<i>B</i>	18.03	1	5.98	0.0707
<i>C</i>	15.88	1	5.27	0.0834

A – Ratio of stearic acid with EDC. HCl, B –Time (hours), C – Amount of stearic acid (mg)

## 2.4.2 Conjugation between chitosan oligomer and lauric acid (CSO-LA)

### 2.4.2.1 $^1\text{H}$ NMR and FTIR of CSO-LA

In order to obtain a similar amount of conjugation of lauric acid with CSO, CSO-LA was synthesised based on the parameters used in the CSO-SA conjugation. Similar molar ratios between LA: EDC.HCl and SA: EDC.HCl was used in this section. The formation of CSO-LA was confirmed using FTIR and  $^1\text{H}$  NMR. Figure 2.6 shows the IR spectra of all samples. Compared to lauric acid alone and chitosan oligomer, there were some changes to the IR spectrum of chitosan-lauric acid resulting from the binding between the lauric acid carboxylic group and the chitosan amine group.

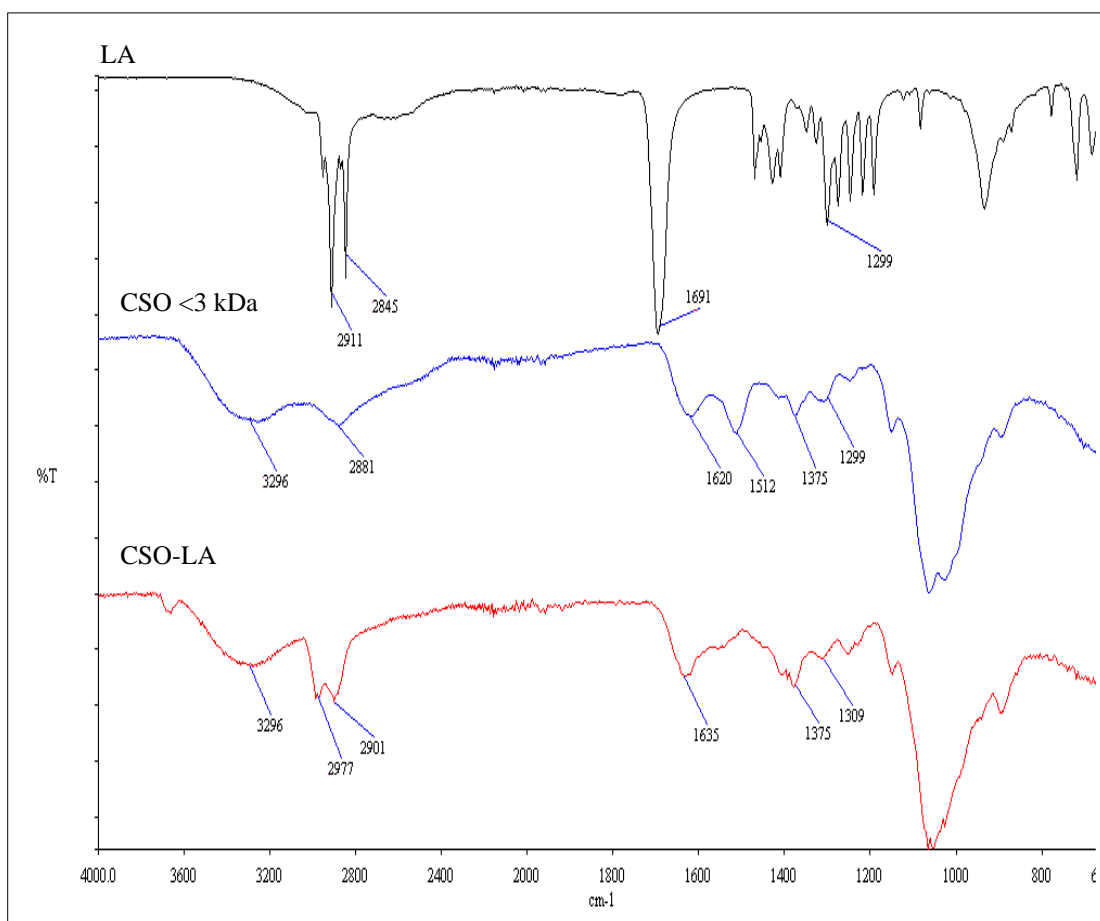


**Figure 2.6** FTIR spectra of lauric acid (LA), chitosan oligomer (CSO) and chitosan oligomer-lauric acid (CSO-LA) based on a parameter of ratio 1:5; LA: EDC.HCl, 6 h reaction time and 0.5 g – lauric acid

The IR spectra for CSO (without conjugation) showed absorption peaks 1620 attributed to C=O stretching of the secondary amine (amide I band). The IR spectra of CSO-LA showed shifted two peaks at around 1635 and 1529  $\text{cm}^{-1}$  corresponding to the N-lauroyl (amide I and II bands, respectively). The increase of the C-H absorption around 2977 and 2901  $\text{cm}^{-1}$  indicated the presence of the lauroyl chain. The broad peak at around 3296  $\text{cm}^{-1}$  represents the -OH group from the chitosan oligomer. The other peak indicating the presence of carboxyl groups (-COOH) from lauric acid is at  $\sim 1691 \text{ cm}^{-1}$ . After conjugation of lauric acid to chitosan oligomer, the peak around 1691  $\text{cm}^{-1}$  was reduced which suggests that lauric acid has reacted with chitosan oligomer. Based on the  $^1\text{H}$  NMR spectra (Figure 2.7), there were chemical shifts that represented the methyl and methylene hydrogen of the laurate group.

The chemical shifts shown at 0.85 ppm represent protons from  $\text{CH}_3$  of lauric acid whereas the peaks at 1.17 - 1.24 ppm correspond to the protons of the  $\text{CH}_2$  group of acyl chain. The rest of the peaks were hydrogen peaks from the chitosan oligomer. These results confirmed that lauric acid was successfully conjugated to the chitosan oligomer. These results are in agreement with Zhao et al. (2014), who successfully conjugated LA with CSO for surface functionalization of titanium to enhance osteoblast functions and inhibit bacteria adhesion.

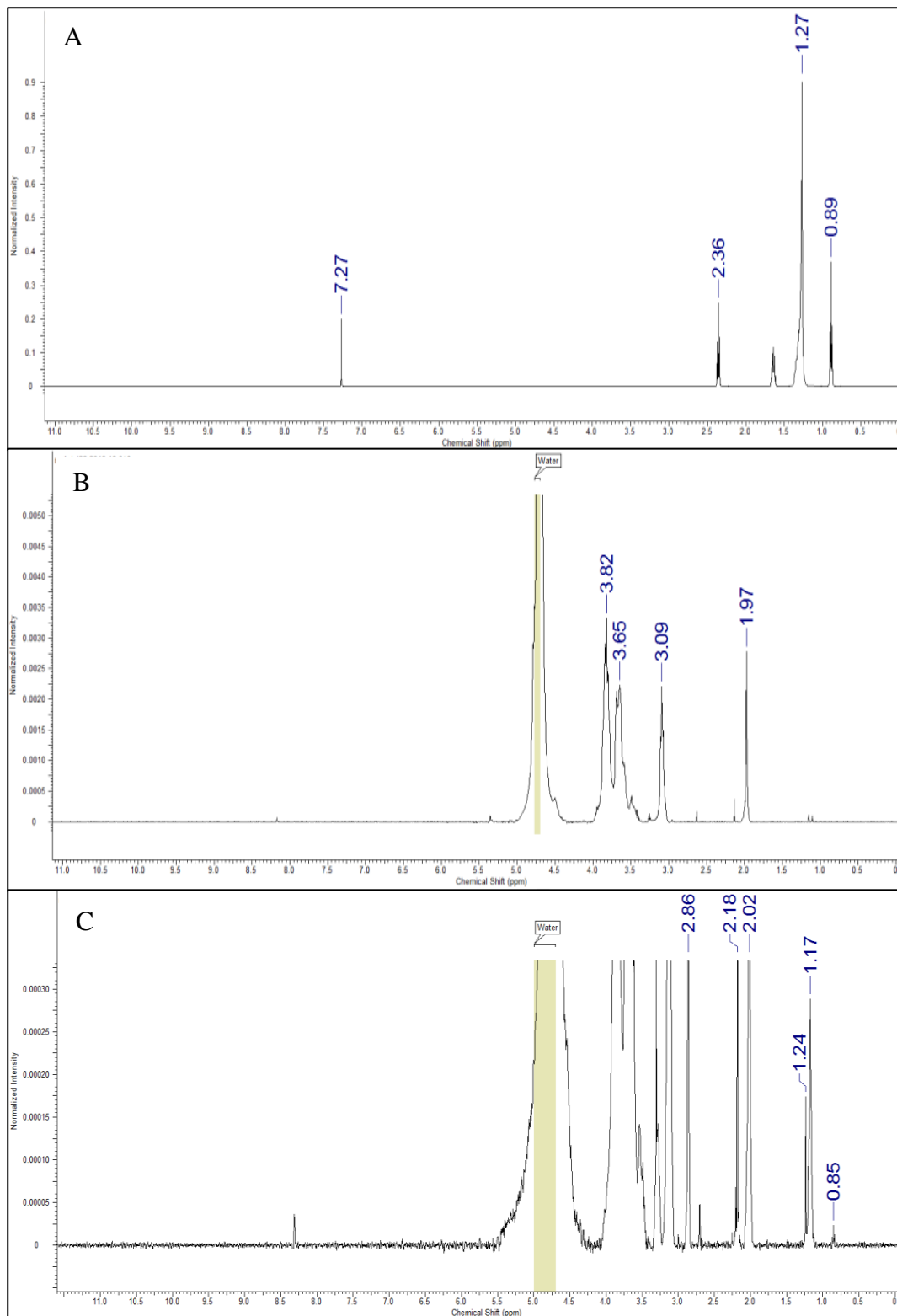


**Figure 2.7**  $^1\text{H}$  NMR spectra of lauric acid (A), chitosan oligomer (B) and CSO-LA (C) based on ratio LA: EDC.HCl/time of reaction (hours)/amount of lauric acid (g), 1:5/6/0.5)

### 2.4.2.2 Ninhydrin assay of D-glucosamine, CSO and CSO-LA

Based on the ninhydrin assay (Figure 2.8), the slopes for chitosan oligomer (CSO) was 0.0126, and 0.0165 for CSO-LA. By comparing the slopes from glucosamine, CSO and CSO-LA; the %DS of CSO-LA was found to be 6.2%.

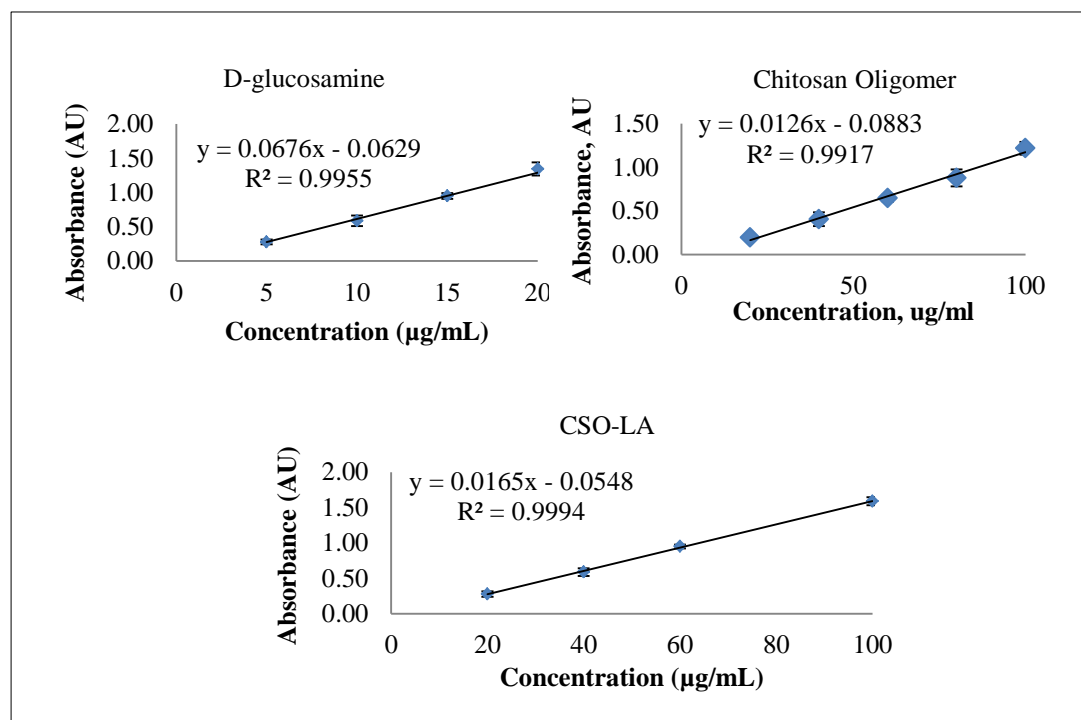


**Figure 2.8 Graph of absorbance versus concentration from ninhydrin assay of D-glucosamine, CSO and CSO-LA (n=3, mean  $\pm$  SD)**

The value for %DS of CSO-LA was close to that of CSO-SA (Section 2.4.1.2). This shows that, by using the same molar ratio of fatty acid: EDC.HCl, consistent values are produced with using different types of fatty acids.

Little research has been conducted on the preparation of CSO-LA. Zhao et al., (2014) synthesised LA with CSO, no information on the %DS was reported. However, based on  $^1\text{H}$ NMR and FTIR results, successfully grafting of lauric acid and CSO was claimed.

Lauric acid previously showed good inhibition of androgenic activity and also has an inhibitory effect on lymph node carcinoma of the prostate cancer (LNCaP)

cells (Liu et al., 2009). Due to that, by conjugating lauric acid with chitosan oligomer and acts as a coating material for NLCs, it would help to deliver lauric acid in the nanocarrier system to be delivered to the skin.

### 2.4.3 Size distribution, surface charge and morphology of CSO-SA and CSO-LA micelles

Table 2.5 shows the values for size distribution and surface charge of CSO-SA (S1) and CSO-LA. No measurement on hydrodynamic diameter of CSO-SA using Zetasizer Nano ZS were conducted as the mean size was greater than 1000 nm and PDI was 1.0.

**Table 2.5 Size distribution and surface charge of CSO-SA and CSO-LA micelles (n=3, mean  $\pm$  SD)**

Material	Hydrodynamic diameter (nm)	PDI	Zeta potential (mV)
CSO-SA (S1)	-	1.0	+41.7 $\pm$ 0.5
CSO-LA	220.3 $\pm$ 21.4	0.406 $\pm$ 0.013	+30.7 $\pm$ 3.2

The size, PDI and zeta potential value of the micelles were determined in acetic acid solution

In the DLS technique, the intensity is used to calculate the hydrodynamic diameter. However, if there are larger particles in the distribution (less than 1000 nm), the larger particle normally will dominate scattering compared to the smaller sized particles, resulting in a large reported value for hydrodynamic diameter and broader PDI. In this case of CSO-SA micelles, if the size of particles was larger than 1000 nm, particles would not undergo Brownian motion and data cannot accurately be translated to hydrodynamic diameter using Stoke-Einstein equation. Based on the cumulant fit analysis from DLS, this sample had predominantly larger particles.

However, for CSO-LA micelles in acetic acid solution (5 mg/mL), smaller size of micelles with  $220.3 \pm 21.4$  nm and PDI less than 0.5 were found. A smaller particle size compared to CSO-SA micelles was found probably due to the shorter chain of lauric acid (C<sub>12</sub>) attached to chitosan oligomer back bone compared to stearic acid (C<sub>18</sub>).

Both CSO conjugated micelles gave a positive zeta potential (Table 2.5). The surface charge of CSO-SA micelles was significantly higher than CSO-LA micelles at 5 mg/mL ( $p < 0.05$ ). Figure 2.9 shows the morphology of CSO-SA and CSO-LA micelles at 5 mg/mL in acetic acid solution. Both samples showed small size of particles, suggesting that CSO-SA and CSO-LA at this concentration appeared in micellar systems.

There is a suggestion that larger sizes measured from DLS instrument is due to the possibility of poorly dispersed material that occurred while preparing the micelles. As both products would not dissolve in any solvents and water, no appropriate method of preparing and controlling the size of the micelles have been undertaken, resulting in larger mean particle size and higher PDI.

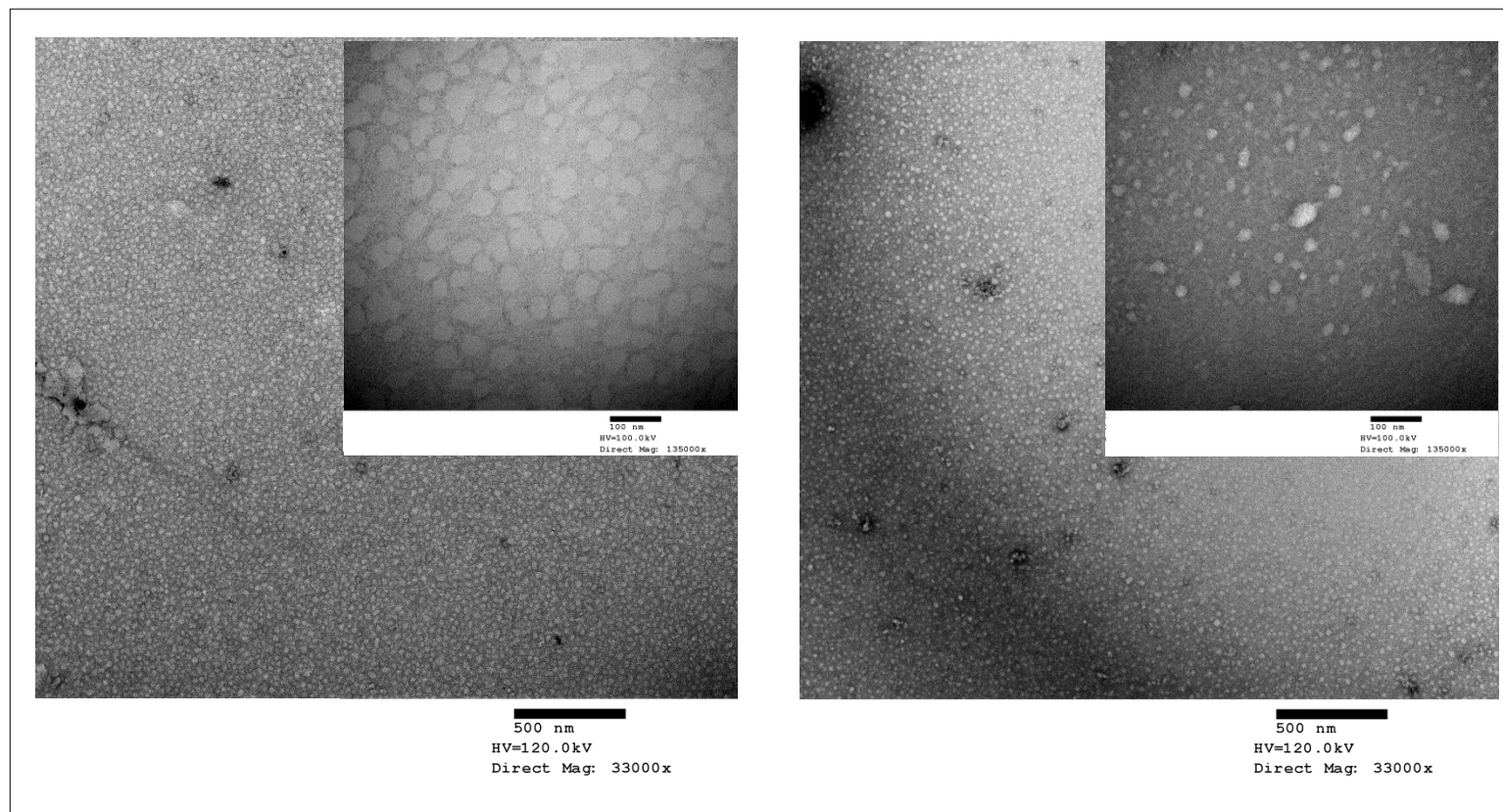


**Figure 2.9** Transmission electron micrographs of CSO-SA and CSO-LA micelles at 5 mg/mL in acetic acid solution

#### 2.4.4 Critical micelles concentration (CMC) of selected CSO-SA and CSO-LA

Due to the hydrophobic properties of fatty acid, stearic or lauric acid and hydrophilic properties of the backbone of chitosan in conjugated-chitosan oligomer, the synthesised CSO-SA and CSO-LA could self-aggregate and form micelles. Figure 2.11 shows the absorbance versus log concentration of CSO-SA and CSO-LA in 0.2% acetic acid solution.

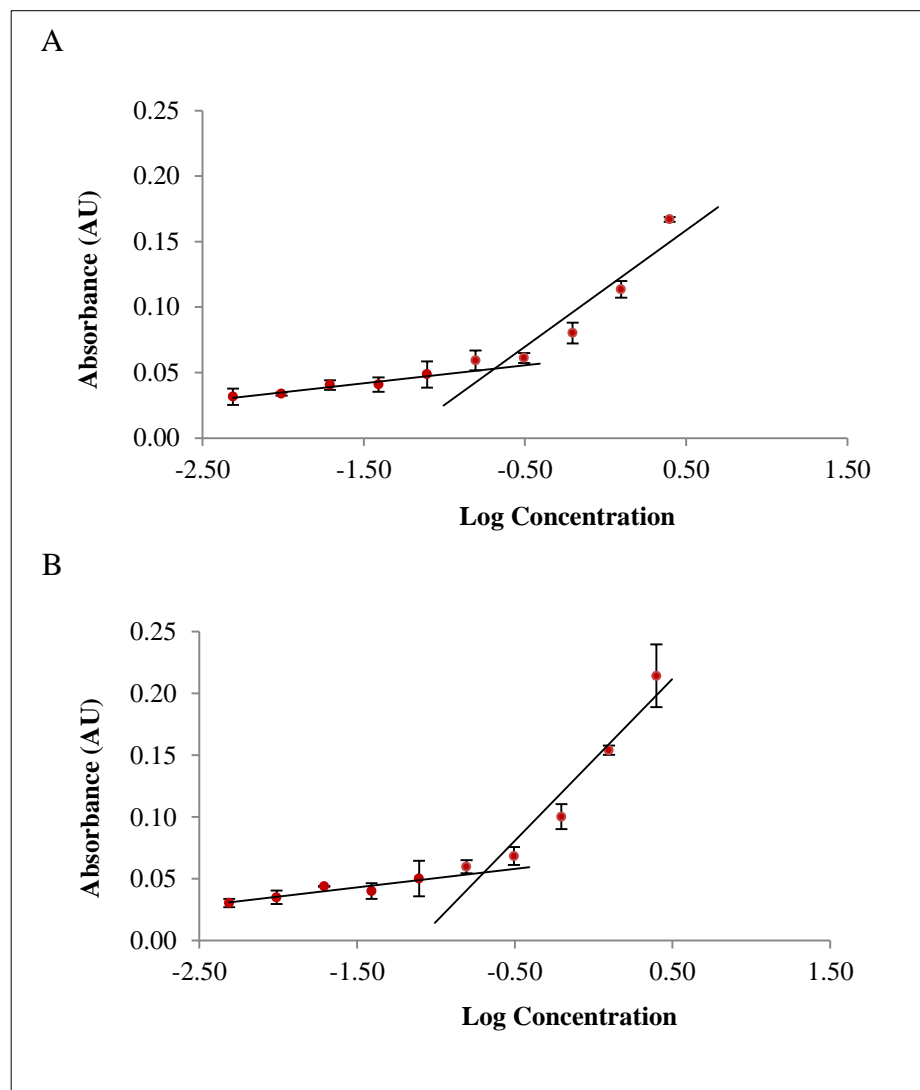


**Figure 2.10 Absorbance of pyrene versus logarithm of chitosan oligomer-stearic acid (CSO-SA) concentration (A) and chitosan oligomer-lauric acid (CSO-LA) concentration (B) (n=3, mean  $\pm$  SD)**

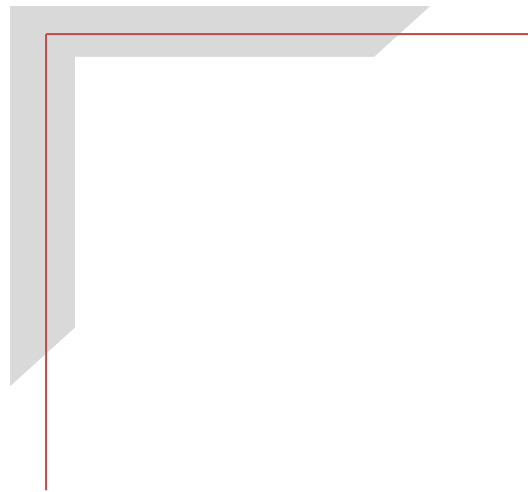
The starting concentration of CSO-SA or CSO-LA (5 mg/mL) of conjugated chitosan was prepared in 0.2% acetic acid solution and diluted with water to obtain serial dilution, to determine the CMC of CSO-SA and CSO-LA micelles. This value was used to predict either at that concentration, CSO-SA or CSO-LA appeared in monomers or micelles when used in the coating process of DST-NLCs. The measured CMC was found to be  $0.17 \pm 0.01$  mg/mL for both CSO-SA and CSO-LA, which indicated that CSO-SA and CSO-LA micelles had a self-assembling ability. The CMC for both samples was similar as indicated in previous sections that they produced similar values of %DS.

Both measured CMC values from this study were in agreement with the previous study (Hu et al., 2009). Hu et al. (2009) synthesised CSO-SA and the CMC of the micelles was 0.140 mg/mL with degree substitution of 6.47%. Previous research (Hu et al., 2009; Yuan et al., 2010), suggest increasing the %DS of CSO-SA produced a decrease in CMC; i.e., modifying the amounts of hydrophobic chain that attach to chitosan oligomer affect CMC values.

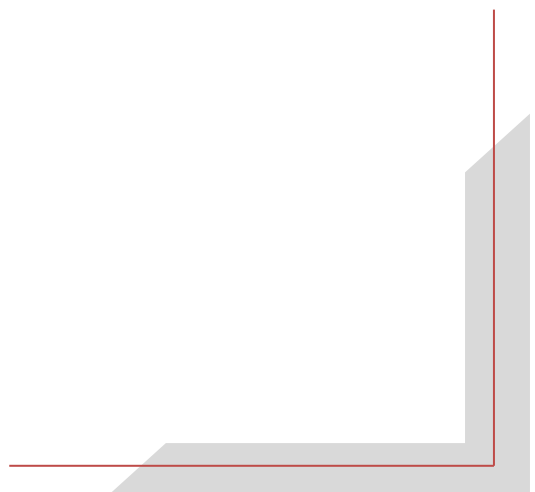
## 2.5 Conclusions

The aim of this chapter is to conjugate and characterise chitosan oligomer with stearic and lauric acid. It can be concluded that:

1. All conjugations between chitosan oligomer and stearic acid or lauric acid were successful based on the  $^1\text{H}$ NMR and FTIR spectra. For CSO-SA conjugation, due to the non-significant difference on the model on %DS from design of experiment, sample S1 was selected for further studies. S1 with 0.5 g stearic acid and the ratio of SA with 1:5 of SA: EDC.HCl was reacted for 6 h, in order to obtain the highest %DS value (6.0%) for this reaction. Product S1 was chosen as a coating material for the next chapter.
2. CSO-LA based on the optimal CSO-SA molar ratio was synthesized and characterized. Based on the ninhydrin results for both CSO-SA and CSO-LA, the degree of substitution was very similar (~6.0%). This showed that the synthesis was reproducible.
3. The CMC results for both optimised CSO-SA and CSO-LA were similar at 0.17 mg/mL.
4. The synthesised chitosan oligomer produced a positive charge which would be useful to be a coating material for nanoparticles for topical delivery as hair, skin and cell membrane are negatively-charged.



# **Chapter 3 Preparation of dutasteride-loaded nanostructured lipid carriers coated with chitosan oligomer-fatty acid**



### **3.1 Preparation and characterisation of dutasteride-loaded nanostructured lipid carrier coated with chitosan oligomer-stearic acid**

#### **3.1.1 Introduction**

This chapter describes the preparation and characterisation of dutasteride-loaded nanostructured lipid carrier coated with chitosan oligomer-stearic acid. The formulation was optimised using a design of experiments approach, and DST-NLCs were produced by the melt dispersion-ultrasonication method. The size distribution of particles, entrapment efficiency, and drug loading were measured as dependent variables whereas the independent variables were the amount of stearic acid, Lutrol® micro 68 and Phosal® 53 MCT. The content of drug was scaled-up in later experiments. In order to obtain positively-charged nanoparticles, the optimised dutasteride-loaded nanostructured lipid carrier formulations were coated with chitosan oligomer-stearic acid (CSO-SA). Only the optimised CSO-SA (described in Chapter 2) was chosen at this stage. The highest degree of substitution (%DS), namely formulation S1 was chosen to be used in this study.

#### **3.1.2 Method development and validation using reverse-phase high-performance liquid chromatography (RP-HPLC) assay for quantification of dutasteride**

##### **3.1.2.1 Materials**

Dutasteride was purchased from Carbosynth Ltd (UK). HPLC grade trifluoroacetic acid, methanol and water were purchased from Sigma-Aldrich Ltd (UK).

##### **3.1.2.2 Instrumentation**

As described in the British Pharmacopeia 2017 (British Pharmacopeia Commission, 2017), dutasteride was assayed using liquid chromatography using 40:60 v/v of water and acetonitrile as mobile phase and end-capped octadecylsilyl

silica gel column at 35°C (flow rate at 1 mL/min and the wavelength at 220 nm). The retention was 1.6 min.

In order to avoid interference from other components present in the nanoparticles preparation, namely lipid and surfactant, an optimal separation should be undertaken using a suitable column as a stationary phase. Preliminary studies on the maximum wavelength ( $\lambda_{\max}$ ) UV absorbance of dutasteride was undertaken. The prepared solutions of dutasteride in methanol were scanned for the  $\lambda_{\max}$  from 200 – 600 nm using a UV-Vis Spectrophotometer (Agilent Cary 100, UK) and found to be at 241 nm.

In this study, high-performance liquid chromatography (HPLC) with UV/Vis detector (Agilent 1100 Series, USA) at wavelength 241 nm was used to determine the content of dutasteride in the nanoparticle formulation. A Synergi™ 4  $\mu\text{m}$  Polar-RP 80 Å, 250 x 4.6 mm column (Phenomenex, Torrance, California) was selected as a stationary phase for the separation. This column has an ether-linked phenyl phase and is suitable for the separation of polar and aromatic compounds. As dutasteride has a phenyl group in its structure, this column can be useful for the separation of dutasteride from other components of the formulation. The quantitative determination of dutasteride was carried out using a mobile phase 70:30 (by volume) of acetonitrile and 0.1% v/v trifluoroacetic acid (TFA) in HPLC grade water. The injection volume was 30  $\mu\text{L}$  (Table 3.1).

### 3.1.2.3 Preparation of dutasteride standard solution

10 mg dutasteride was weighed accurately and transferred to a 10 mL volumetric flask. 5 mL methanol was added and sonicated to dissolve the drug. Methanol was added to volume and the flask was shaken to mix the solution well. The stock solution concentration of dutasteride was 1000  $\mu\text{g/mL}$ . Serial dilutions were prepared from the stock solution giving 1, 3, 5, 10, 25, 50, 70, 100  $\mu\text{g/mL}$  dutasteride.

**Table 3.1 HPLC chromatographic condition for determination of dutasteride**

Column:	Synergi™ 4 µm Polar-RP 80 Å, 250 x 4.6 mm
Mobile phase:	Acetonitrile and 0.1% TFA in HPLC grade water (70:30)
Wavelength:	241 nm
Flow rate:	1 mL/min
Injection volume:	30 µL
Run time:	15 minutes

#### 3.1.2.4 Retention time

In order to ensure there was no interference of the formulation components with dutasteride at the same wavelength, a preliminary analysis was undertaken by injecting a formulation with dutasteride and also blank formulation (formulation without dutasteride) into the HPLC system to determine the appropriate retention time.

#### 3.1.2.5 Method validation

Linearity, accuracy, specificity, precision, limit of detection (LOD) and limit of quantification (LOQ) were determined according to ICH Q2 guidelines for validation of analytical procedures (International Conference on Harmonisation, 1996).

##### 3.1.2.5.1 Linearity

For linearity measurement, serial dilutions of dutasteride at 1, 3, 5, 10, 25, 50, 70, 100 µg/mL of the stock solution were prepared. The solutions were sonicated and filtered through 0.22 µm PES membrane syringe filter (Millex®GP, Merck Millipore, UK) and transferred to the vials. 30 µL of each sample was injected onto the HPLC column. A calibration curve was prepared four times from fresh stock solutions. The standard curves were obtained by plotting peak area versus dutasteride concentration.

### 3.1.2.5.2 Accuracy

The accuracy of the method was determined by the recovery method (Equation 3.1), which expresses the closeness between the determined value and the reference value (International Conference on Harmonisation, 1996). The recovery was checked at 3, 5, 10, 25, 50, 70 and 100 µg/mL.

$$\text{Accuracy} = 100 - \left[ \frac{(\text{Reference value} - \text{measured value})}{\text{Reference value}} \times 100 \right] \quad \text{Equation 3-1}$$

### 3.1.2.5.3 Precision

The precision of an analytical procedure expresses the closeness of agreement between a series of measurements obtained from multiple sampling of the same homogeneous sample under the prescribed conditions (International Conference on Harmonisation, 1996). In this study, precision (calculated using Equation 3.2) was determined using two methods. One is determined under the same operating conditions over a short interval of time (intra-day), and another is determined on a different day (inter-day). The intra-day and inter-day precisions were determined at three different concentrations (8, 40 and 90 µg/mL). The repeatability study was done by using the chosen 40 µg/mL concentration and injecting it for 9 times to get the RSD (relative standard deviation).

$$\text{Precision (\%RSD)} = \frac{\text{Standard deviation}}{\text{Mean value}} \times 100 \quad \text{Equation 3-2}$$

where;

%RSD – percent relative standard deviation

### 3.1.2.5.4 Limit of detection (LOD) and limit of quantification (LOQ)

The detection limit (LOD) of an individual analytical procedure is the lowest amount of analyte in a sample which can be detected but not necessarily quantified as an accurate value; while the quantification limit (LOQ) of an individual analytical

procedure is the lowest amount of analyte in a sample which can be quantitatively determined with suitable precision and accuracy. The detection and quantification of limit can be determined using various methods. In this study, LOD and LOQ were determined using the equation (Equation 3-3 and Equation 3-4).

$$\text{LOD} = \frac{3.3 \sigma}{S} \quad \text{Equation 3-3}$$

$$\text{LOQ} = \frac{10\sigma}{S} \quad \text{Equation 3-4}$$

where:

$\sigma$  = the standard deviation of the response

$S$  = the slope of the calibration curve estimated from calibration curve

### 3.1.3 Preparation of dutasteride-loaded nanostructured lipid carriers (DST-NLCs)

#### 3.1.3.1 Materials

Stearic acid (n-octadecanoic acid) 98% and dutasteride (purity >98.0%) [(5a,17b)-N-[2,5-Bis(trifluoromethyl)phenyl]-3-oxo-4-azaandrost-1-ene-17-carboxamide] with molecular weight 528.53 were purchased from Tokyo Chemical Industry (TCI, UK). Chitosan oligomer (CSO) with molecular weight less than 3 kDa was obtained from Carbosynth Ltd (UK). Phosal® 53 MCT was a gift of Lipoid AG, Switzerland. Lutrol® micro 68 (Poloxamer 188) was obtained from BASF, (Germany). Ethanol (96% v/v analytical grade) was obtained from Sigma-Aldrich Company Ltd (UK). Deionised water (PURELAB Option, ELGA, UK) was obtained on site from a water system. Table 3.2 shows the description of main materials used in the nanoparticle preparation.

**Table 3.2 Description of main materials used in the nanoparticle preparation**

<b>Material</b>	<b>Group</b>	<b>Function</b>	<b>Phase</b>
<b>Dutasteride</b>	Drug	5 $\alpha$ -reductase inhibitor	Oil
<b>Stearic acid</b>	Fatty acid	Solid lipid	Oil
<b>Phosal® 53 MCT</b>	53% lecithin in caprylic/capric triglycerides, alcohol, glyceryl stearate, oleic acid and ascorbyl palmitate	Emulsifier + liquid lipid	Oil
<b>Lutrol® micro 68 (Poloxamer 188)</b>	Amphiphilic block copolymer with 1800 g/mol molecular mass of polyoxypropylene and 80% polyoxyethylene content	Emulsifier	Water

### 3.1.3.2 Preparation of DST-NLCs

DST-NLCs was prepared by the melt dispersion ultrasonication method (Patel et al., 2012; Uprit et al., 2013; Gomes et al., 2014). Dutasteride, stearic acid, and Phosal® 53 MCT were weighed into a glass vial (30 mL). Lutrol® micro 68 was added to another glass vial (30 mL) with water. Both glass vials were heated separately at 80-90° in a water bath. When the drug dissolved in the liquid lipid (using the micromagnetic bar to stir) and both vial contents reached the desired temperature, the aqueous solution was added to the oil phase solution. The mixture was homogenised using an IKA Ultra Turrax T25 (IKA-Werke GmbH & Co KG, Germany) at 19,000 rpm for 10 min. The hot solution was further processed using a probe-type sonicator (MSE Soniprep 150, MSE Ltd UK) at 18W, for 5 min. Procedures for DST-NLCs preparations and characterisation are summarised in Figure 3.1.

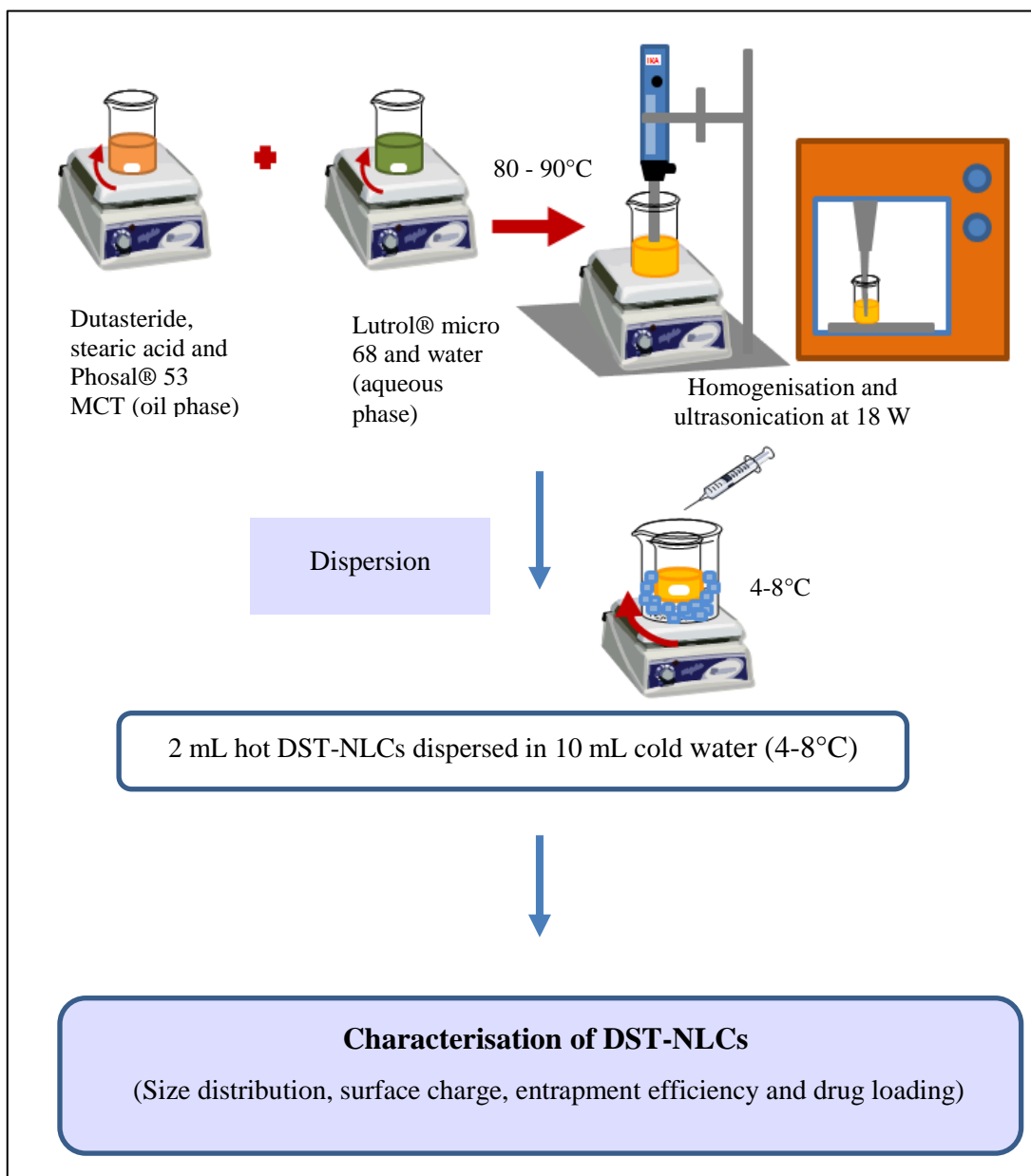


**Figure 3.1 Schematic diagram of preparation and characterisation of dutasteride-loaded nanostructured lipid carriers (DST-NLCs)**

2 mL of hot dispersion was syringed using a needle (25 gauges, 5/8th inch, BD Microlance™ 3, Becton Dickinson, Spain) into 10 mL of cold water (4-8°C) and stirred for 10 min. The final dispersion was stored at 4-8°C for 24 h before being characterised. The weight of dutasteride was maintained constant at 5 mg for all of the experiments, and 10 mL of water was used for all formulations. In order to proceed with this method, the formulation with the highest stearic acid, Lutrol® F68, and Phosal® 53 MCT content was chosen. Statistical analysis using Student t-test,

with IBM SPSS 23 Statistic Data Editor Software (USA) was undertaken. A *p*-value of less than 0.05 was considered significant for all experiments.

### 3.1.3.3 Experimental design of preparation of DST-NLCs using a 2<sup>3</sup> full factorial design

The amount of solid lipid and surfactant used to prepare DST-NLCs was varied to obtain the smallest mean particle size, smallest polydispersity index, and highest entrapment efficiency and drug loading. Dutasteride content was maintained at 5 mg in all formulations. This was achieved with a 2<sup>3</sup> full factorial design (Design Expert 6.0.8 Software; Stat-Ease, USA). The three factors evaluated were; the contents of stearic acid, Lutrol® F68 and Phosal® 53 MCT, tabulated in Table 3.3 with the value and coded number (-1 for the low level and +1 for the high level).

**Table 3.3 Value and coded units of a 2<sup>3</sup> full factorial design for preparation of DST-NLCs**

Independent Variables	Coded	Level	
		Low (-1)	High (+1)
Stearic acid (mg)	A	50	100
Lutrol® micro 68 (mg)	B	25	50
Phosal® 53 MCT (mg)	C	25	50

In this study, the design of experiments approach allows an understanding of the formulation parameters and permits the formulation to be optimised to achieve the smallest size (ideally ranging between 200-300 nm), smallest polydispersity index (<0.3) and the highest entrapment efficiency and drug loading. The experiments were conducted in triplicate in order to calculate the experimental error. The experimental design required in total 8 preparations (a total of 24 experiments were therefore conducted). Table 3.4 shows the actual and coded values for the lower and higher level. A factorial design was used in order to obtain maximum information such as the interaction between the factors without the need of a large

number of experiments (Dillen et al., 2004). It is also can predict the cause-effect relationship of the experiment. The experiment results were analysed using ANOVA from Design Expert 6.0.8 (Stat-Ease Inc, USA).

**Table 3.4 Design of experiments for formulation of dutasteride-loaded nanostructured lipid carrier (DST-NLCs) using 2<sup>3</sup> factorial design**

Formulation	Stearic acid (mg)	Lutrol® micro 68 (mg)	Phosal® 53 MCT (mg)
S1	50 (-1)	25 (-1)	25 (-1)
S2	100 (+1)	25 (-1)	25 (-1)
S3	50 (-1)	50 (+1)	25 (-1)
S4	100 (+1)	50 (+1)	25 (-1)
S5	50 (-1)	25 (-1)	50 (+1)
S6	100 (+1)	25 (-1)	50 (+1)
S7	50 (-1)	50 (+1)	50 (+1)
S8	100 (+1)	50 (+1)	50 (+1)

Number in bracket represents the coded value

#### 3.1.3.4 Preparation of scaled-up DST-NLCs

In this study, the optimised DST-NLCs preparation (Section 3.1.3.3) was chosen based on the statistical analysis. The formulation was scaled up from 100 mg to 300 mg of stearic acid to allow the use of the desired amount of dutasteride. Quantities of other materials (dutasteride, Phosal® 53 MCT and Lutrol® micro 68) were up-scaled employing the optimal ratio, with water kept constant at 10 mL Table 3.5). In order to compare the effect of size distribution with or without dutasteride, a blank formulation (NLCs without dutasteride) was prepared.

**Table 3.5 Before (x) and after scale-up (3x) contents of DST-NLCs**

<b>Formulation</b>	<b>Dutasteride (mg)</b>	<b>Stearic acid (mg)</b>	<b>Lutrol® micro 68 (mg)</b>	<b>Phosal® 53 MCT (mg)</b>
<b>x (with DST)</b>	5	100	50	25
<b>3x (with DST)</b>	15	300	150	75
<b>3x (without DST)</b>	0	300	150	75

### 3.1.3.5 Preparation of DST-NLCs coated with CSO-SA

CSO-SA (2.5, 5 or 10% w/w of solid lipid content) and CSO (5% w/w of solid lipid content) were dissolved in acidified water (0.2% acetic acid in deionised water). 250 µL of the solution was added using a syringe, into 5 mL of DST-NLCs with constant stirring for 10 min. Chitosan oligomer-SA S1 (from Chapter 2) was selected based on the ninhydrin assay. Particle size and zeta potential of resultant coated NLCs were determined. Differences in charge between the negatively-charged DST-NLCs and the positive charge of CSO-SA should allow the coating material to deposit on the outer surface of DST-NLCs. Different amounts of CSO-SA solutions (in acidified water) added into the DST-NLCs would be expected to increase the hydrodynamic diameter of DST-NLCs.

### 3.1.3.6 Characterisation of DST-NLCs

#### 3.1.3.6.1 Measurement of particle size distribution of DST-NLCs

Dynamic light scattering (DLS) size analysis techniques measure hydrodynamic quantities, usually the translational and/or rotational diffusion coefficients, which are then related to sizes and shapes via theoretical relations (Pecora, 2000). DLS determines the mean size of particles (hydrodynamic diameter) undergoing Brownian motion and estimates the width of the distribution (polydispersity index). When a laser passes through the dispersion, the intensity of the scattered light fluctuates depending on the size of particles. The small particles diffuse faster which results in the intensity fluctuating more rapidly compared to the

larger sizes in the dispersion. Hydrodynamic diameter is calculated from the translational diffusion coefficient using the Stokes-Einstein equation with the assumption that all particles are spherical in shape, while polydispersity index (PDI) is the measurement of the heterogeneity of size distribution in a mixture.

All formulations were analysed after 1 day using dynamic light scattering (DLS) equipment (Zetasizer Nano ZS, Malvern Instruments, UK) for determination of the particle size distribution. 1 mL of the sample was pipetted directly into the zeta potential DTS1070 folded capillary cell (Malvern, UK) without dilution at 25°C. The size distribution of nanoparticles was obtained as the hydrodynamic diameter ( $Z_{Ave}$ ) and polydispersity index (PDI). The prepared formulation was analysed, and the measurement was performed in triplicate, and mean values were taken.

#### **3.1.3.6.2 Measurement of zeta potential of DST-NLCs**

In order to measure the surface charge of the particles, zeta potential (ZP) was measured using the Zetasizer Nano ZS (Malvern Instruments, UK). This equipment uses electrophoretic light scattering technology to measure zeta potential, calculated from electrophoretic mobility using the Helmholtz-Smoluchowski equation by the Malvern data analysis software.

1 mL of the sample was pipetted directly into the zeta potential DTS1070 folded capillary cell (Malvern, UK) without dilution. The measurements were recorded at 25°C. The prepared formulation was analysed without further dilution, and the measurement was performed 3 times, and the average values were recorded.

#### **3.1.3.6.3 Determination of nanoparticle morphology by transmission electron microscope**

The morphology of the nanoparticles was determined using a transmission electron microscope (TEM; Philips/FEI CM120 Bio Twin, FEI Netherlands). Samples were placed on copper grid formvar/carbon support film 300 mesh (Agar Scientific, Stansted, Essex, UK), and excess droplets were blotted with filter paper. After a few seconds, a drop of 1% uranyl acetate was placed onto the copper grid for

negative staining. The grid was air-dried at room temperature and observed using TEM.

#### 3.1.3.6.4 Entrapment efficiency and drug loading measurement

Entrapment efficiency and drug loading for each preparation were calculated as described previously (Gu et al., 2011). Entrapment efficiency and drug loading were determined using Sephadex® gel G-50 (Sigma-Aldrich, UK) as a mini-column in a 5 mL syringe. Sephadex is a crosslinked dextran and used in the gel filtration (size-exclusion chromatography). This method was used in order to separate the untrapped and entrapped DST in the NLCs system due to their different sizes. The larger size of DST-NLCs will pass through the gel, and the smaller size of DST (the untrapped DST) will retain in the gel.

5 mL of the gel was packed in the syringe which was placed in the centrifuge tube (size 50 mL). In order to remove excess water, the tube was centrifuged at 1000 rpm for 10 s (angle rotor 19776-H, at 104 x g, brake no. 9) in a refrigerated centrifuge (Sigma Laborzentrifugen GmbH, Germany) at 20°C.

After removing the excess water, 0.5 mL of the DST-NLCs solution was pipetted in the middle of the column and separated through column chromatography at 1000 rpm for 5 min. The column was washed with 0.5 mL distilled water at 1000 rpm for another 5 min. The untrapped dutasteride was retained in the Sephadex G-50 gel. The collected sample which comprises dutasteride-entrapped in NLCs was diluted with ethanol in a 10 mL volumetric flask and sonicated for 10 minutes in order to dissolve the particles before being filtered using 0.22 µm PES membrane syringe filter (Millex®GP, Merck Millipore, UK). The solution was assayed using HPLC in order to determine the amount of entrapped dutasteride in the NLCs (as described in Section 3.1.2). The amount of entrapped dutasteride in the preparation ( $n_1$ ) and total ( $n_2$ ) were quantified by HPLC at 241 nm (Equation 3-5). Measurement was performed in replicate and the average values were recorded. Dutasteride loading was calculated using Equation 3-6.

$$\text{Entrapment efficiency (\%)} = \frac{n_1}{n_2} \times 100 \quad \text{Equation 3-5}$$

where;

$n_1$  = concentration of entrapped dutasteride in DST-NLCs

$n_2$  = total concentration of dutasteride in DST-NLCs

$$\text{Drug loading (\%)} = \frac{C_1}{C_0} \times 100 \quad \text{Equation 3-6}$$

where;

$C_1$  = total weight of entrapped dutasteride in DST-NLCs

$C_0$  = total weight of solid lipid, surfactant and dutasteride in DST-NLCs

#### 3.1.3.6.5 Physical stability study

The physical stability of DST-NLCs was investigated, exploring changes in the size distribution and surface charge with time. Each formulation was stored in a refrigerator 4-8°C and at 25°C (incubator). Particle size distribution and zeta potential were compared at day 1, 30, 60 and 180. Entrapment efficiency for DST-NLCs was determined over 180 days.

### 3.2 Preparation and characterisation of dutasteride-loaded nanostructured lipid carriers coated with chitosan oligomer-lauric acid

This section describes the preparation and characterisation of a dutasteride-loaded nanostructured lipid carrier coated with chitosan oligomer-lauric acid. Previous research (Liu et al., 2009) found that lauric acid has potent anti-androgenic activity compared to other free fatty acids. Chitosan oligomer was synthesised with lauric acid and used as a coating for DST-NLCs. DST-NLCs used in this section were prepared based on the optimised formulation from Section 3.1 and then coated with CSO-LA. The prepared formulations were then characterised for size distribution, zeta potential, morphology and stability as described in Sections 3.1.3.6.1, 3.1.3.6.2, 3.1.3.6.3, 3.1.3.6.4 and 3.1.3.6.5, respectively.

### **3.3 Thermal behaviour and viscosity of DST-NLCs, uncoated and coated with 5% CSO-SA and 5% CSO-LA**

#### **3.3.1 Freeze drying of DST-NLCs, uncoated and coated with 5% CSO-SA and 5% CSO-LA**

5 mL of DST-NLCs uncoated and coated with 5% CSO-SA or 5% CSO-LA samples was transferred into a 14 mL glass vial and closed with a Parafilm® (Merck Millipore, Ireland) and holes were applied using a syringe needle (25 gauges, 5/8th inch, BD Microlance™ 3, Becton Dickinson, Spain). Samples were kept frozen for an overnight at -20°C. Freeze drying process was conducted using a Savant MicroModulyo Freeze Dryer (Thermo Electron Corporation, UK) for 48 h without the addition of cryo-protectant. The freeze-dried formulations were stored in the desiccator prior to use.

#### **3.3.2 Determination of crystallinity using x-ray powder diffractometer (XRPD)**

In order to determine the crystallization behaviour between dutasteride and other materials used in the formulation, XRPD was employed. Freshly prepared nanoparticles, uncoated and coated with 5% CSO-SA and 5% CSO-LA were freeze dried. An X-ray diffractometer (Rigaku MiniFlex 600, Japan) equipped with a 600 W X-ray tube, a copper anode operating in reflectance mode at wavelength  $\lambda 1.5418 \text{ \AA}$ , with a voltage of 40kV and current 15 mA at room temperature, was used for diffraction studies. Samples of dutasteride alone, a physical mixture of dutasteride and formulation components (dutasteride, stearic acid, Phosal® 53 MCT, Lutrol® micro 68, CSO-SA/CSO-LA with similar ratio with DST-NLCs were mixed in the mortar using a pestle) and freeze-dried DST-NLCs/empty NLCs (uncoated and coated with 5% CSO-SA or 5% CSO-LA) were mounted to the horizontal axis to obtain a scanning range of 5 - 40°, a scanning rate of 5°(2 $\theta$ )/min and scan step 0.05°(2 $\theta$ )/min.

### **3.3.3 Determination of the thermal behaviour of formulations using differential scanning calorimetry (DSC)**

DSC measures the heat of a sample relative to a reference (Kodre et al., 2014). For instance, a solid sample melts to a liquid phase; more heat flows to the sample to produce the phase change, resulting in an absorption of heat by the samples, which is called endothermic. DSC analysis of dutasteride, stearic acid and physical mixture of all formulations was performed using a differential scanning calorimetry (Q2000 TA Instrument, USA). Calibrations for cell constant and enthalpy were performed with indium. Samples (~5 mg) were heated in aluminium pans under a dry nitrogen environment. TA aluminium pans and lids (Tzero, TA Instrument, USA) and heating rates of 10°C/min from 25 - 260°C were used in all experiments (Buanz et al., 2015). Data were analysed using the TA Instruments Universal Analysis 2000 software. Measurements were performed in triplicate, and the mean values were calculated.

### **3.3.4 Measurement of dynamic viscosity using a micro viscometer**

In order to determine the effect of coating on the viscosity of the formulations, dynamic viscosity measurement for all coated and uncoated NLCs was performed. Viscosity for all nanoparticle formulations was measured using an AMVn Automated Micro Viscometer (Anton Paar GmbH, Graz, Austria). AMVn is a falling ball viscometer that follows Hoppler's falling ball principle. It is a closed system that does not allow the liquids to contact air and measures the time for a rolling ball to pass through opaque or transparent liquids. The instrument was equilibrated to  $20 \pm 0.01$  °C for 30 min prior to use. Using a syringe, formulation was loaded carefully, without allowing any bubbles to enter, into a 1.6 mm capillary containing a metal ball. The viscosity for all samples was measured at different angles (50, 60 and 70°). In order to determine the effect of different temperatures on the measured viscosity, different temperatures were investigated; ambient temperature (20°C), human skin surface temperature 32°C and internal body temperature (37°C). The measurement was performed in triplicate and mean values taken.

### 3.4 Statistical analysis

All data were analysed either using t-test or one-way ANOVA and Tukey's post-hoc test, using IBM SPSS 23 Statistic Data Editor Software (USA), except data from the experimental design for the model interaction among materials used which were analysed using Design Expert 6.0.8 Software (Stat-Ease, USA). A *p*-value of less than 0.05 was considered significant.

### 3.5 Results and discussion

#### 3.5.1 Validation of RP-HPLC method for assay of dutasteride

Based on preliminary studies, mobile phase comprising acetonitrile and 0.1% v/v TFA in water, in the ratio of 70:30 (v/v) was selected. The retention time for dutasteride was 8.6 min. Figure 3.2 shows that there was no interference for the detection of dutasteride by other materials used in the formulation.

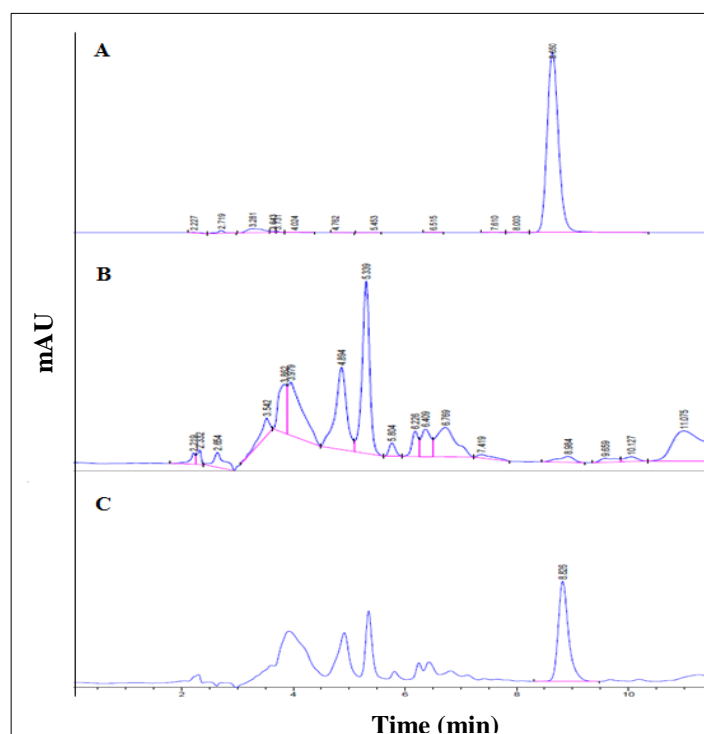


**Figure 3.2** Peak area versus time for the dutasteride solution (A), NLCs without dutasteride (B), NLCs with dutasteride (C)

For the linearity study, seven standard solutions of dutasteride were prepared; ranging from 3 to 100  $\mu\text{g/mL}$ . The plot of concentration versus peak area was linear (Figure 3.3), with a correlation coefficient of 1.0.

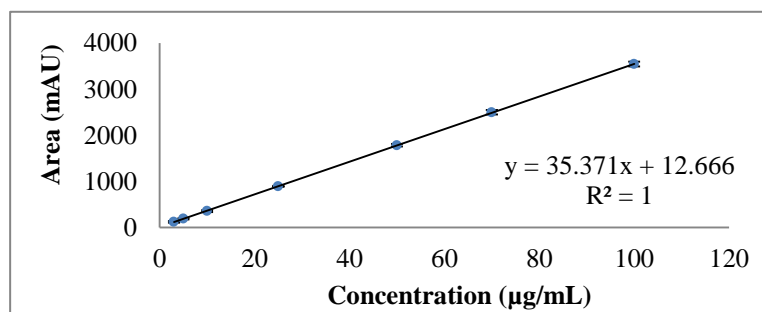


**Figure 3.3 Calibration curve of dutasteride; peak area versus concentration (n=4, mean  $\pm$  SD)**

As shown in Table 3.6, the linear regression data showed good linearity between 3 and 100  $\mu\text{g/mL}$ . LOD and LOQ were found to be 0.38 and 3  $\mu\text{g/mL}$ , respectively. The calculation of LOD and LOQ is shown in Appendix A1.

**Table 3.6 Regression characteristics and validation parameters of dutasteride using HPLC**

Parameters	Value
Linearity range ( $\mu\text{g/mL}$ )	3 - 100
Number of sample per curve	7
Correlation coefficient ( $R^2$ )	1.0
Slope (m)	35.371
Intercept (c)	12.666
<sup>a</sup> LOD ( $\mu\text{g/mL}$ )	0.34
<sup>b</sup> LOQ ( $\mu\text{g/mL}$ )	3.0
Accuracy (%)	97.3 – 104.4
Repeatability, %RSD at 40 $\mu\text{g/mL}$ (n=9)	1.27
Precision, % ( <sup>c</sup> RSD, n=3)	
Interday (n=3)	0.57 – 1.27
Intraday (n=3)	0.27 – 2.08

<sup>a</sup>LOD is limit of detection, <sup>b</sup>LOQ is limit of quantification and <sup>c</sup>RSD is relative standard deviation at 8, 40 and 90  $\mu\text{g/mL}$

The intra-day and inter-day precisions were determined at three different concentrations (8, 40 and 90 µg/mL). The RSD (%) for inter-day and intra-day precisions were 0.57 – 1.27% and 0.27 – 2.08%, respectively. The repeatability was calculated for nine injected samples (40 µg/mL), the RSD% of the measurement was found to be 1.27%.

### **3.5.2 Preparation and characterisation of dutasteride-loaded nanostructured lipid carrier coated with chitosan oligomer-stearic acid**

#### **3.5.2.1 Experimental design for preparation of DST-NLCs: hydrodynamic diameter and particle size distribution**

DST-NLCs were prepared based on the ratio of ingredients generated from the design of experiments (Design Expert 6.0.8, Stat-Ease Inc., USA). Each formulation was prepared three times. All of the formulations gave mean size of DST-NLCs with mean greater than 100 nm at day 1 and day 14 (Table 3.7). At day 1, all formulations had mean hydrodynamic diameter between 177 – 279 nm, in the desired range for skin delivery (Lademann et al., 2007; Mahe et al., 2009; Mittal et al., 2015). A large increase (2-fold) of size after 14 days storage at 4°C indicated the samples were unstable which is evident for formulation S3 and S7 where the size increased to more than 500 nm ( $p < 0.05$ ). Having the lowest amount of stearic acid (50 mg) and highest amount of Lutrol® micro 68 (50 mg), with 25 or 50 mg of Phosal® 53 MCT would not produce small particles ( $p > 0.05$ ). Usually, surfactant is used to emulsify and stabilise the formulation, however, having the highest amount of surfactant (50 mg Lutrol® micro 68) with stearic acid (50 mg) did not produce the small size of particles which can be seen for S7. This result shows that an optimum amount of surfactant should be used in the formulation.

**Table 3.7 Particle size distribution of DST-NLCs at day 1 and 14 stored at 4°C (n=3, mean ± SD)**

<b>Formulation</b>	<b>Stearic acid (mg)</b>	<b>Lutrol® micro 68 (mg)</b>	<b>Phosal® 53 MCT (mg)</b>	<b>Hydrodynamic diameter (nm) (day 1)</b>	<b>PDI (day 1)</b>	<b>Hydrodynamic diameter (nm) (day 14)</b>	<b>PDI (day 14)</b>
<b>S1</b>	50	25	25	211.5 ± 32.5	0.193 ± 0.019	259.1 ± 36.3	0.176 ± 0.027
<b>S2</b>	100	25	25	246.8 ± 40.5	0.176 ± 0.024	307.6 ± 6.1	0.193 ± 0.014
<b>S3</b>	50	50	25	278.6 ± 44.1	0.243 ± 0.013	528.9 ± 25.6	0.269 ± 0.049
<b>S4</b>	100	50	25	190.3 ± 12.5	0.101 ± 0.016	229.0 ± 16.3	0.124 ± 0.019
<b>S5</b>	50	25	50	274.4 ± 28.8	0.267 ± 0.029	356.8 ± 13.4	0.298 ± 0.035
<b>S6</b>	100	25	50	269.5 ± 22.9	0.225 ± 0.011	330.5 ± 17.2	0.243 ± 0.091
<b>S7</b>	50	50	50	221.2 ± 27.7	0.340 ± 0.039	527.0 ± 55.2	0.376 ± 0.025
<b>S8</b>	100	50	50	176.8 ± 27.2	0.150 ± 0.017	217.9 ± 23.6	0.180 ± 0.008

---

All formulations contain 5 mg of dutasteride

Formulation S4 and S8 produced the smallest mean sizes. There was no significant difference ( $p>0.05$ ) between S4 and S8, showing that within this ratio (100 mg stearic acid and 50 mg Lutrol® micro 68), the amount of Phosal® 53 MCT did not affect the size. The same was found in PDI results where there was no significant difference between S4 and S8 ( $p>0.05$ ). The experimental design was used in order to find the interaction among the materials used. The model of hydrodynamic diameter and polydispersity index was analysed using ANOVA from Design Expert 6.0.8 (Stat-Ease, USA) software. The main independent factors studied that might influence the model of hydrodynamic diameter and polydispersity index were the amounts of stearic acid (A), the amount of Lutrol® F68 (B) and the amount of Phosal® 53 MCT (C). Based on the design, 8 batches of formulation were prepared. At day 1, there was no significant difference in model term for the hydrodynamic diameter results ( $p>0.05$ ) which showed all particles had similar range and no interaction was found between the materials used. However, after 14 days (stored at 4-8°C), there was a significant difference in the model term for the hydrodynamic diameter (Table 3.8), and there was an interaction between the materials used.

Based on the model, stearic acid (A), and interaction between stearic acid (A) and Lutrol® micro 68 (B) showed a significant difference ( $p<0.05$ ) (Table 3.8). Even though Phosal® 53 MCT was used as a secondary emulsifier, different amount of Phosal® 53 MCT either 25 or 50 mg in NLCs preparation showed no significant difference on hydrodynamic diameter ( $p>0.05$ ). Stearic acid which was a major component in the system influenced the size of particles. When the highest amount of stearic acid (100 mg) was used, it needed more emulsifier to stabilize the nanoparticles. 25 mg of Lutrol® micro 68 produced a larger mean size of particles, suggesting that 25 mg of Lutrol® micro 68 was not sufficient to maintain the size of particles. When 25 mg or 50 mg of Phosal® 53 MCT was used in this formulation, stable nanoparticles with respect to mean size were obtained. The mathematical modelling between the independent variables (the amount of materials used in the DST-NLCs preparation) and dependent variables (hydrodynamic diameter) was obtained by the following equation (coded value at day 14):

$$\text{Hydrodynamic diameter (nm)} = 344.60 - 73.35*A + 31.10*B - 78.90*A*B$$

Equation 3-7

where;

*A* – Stearic acid

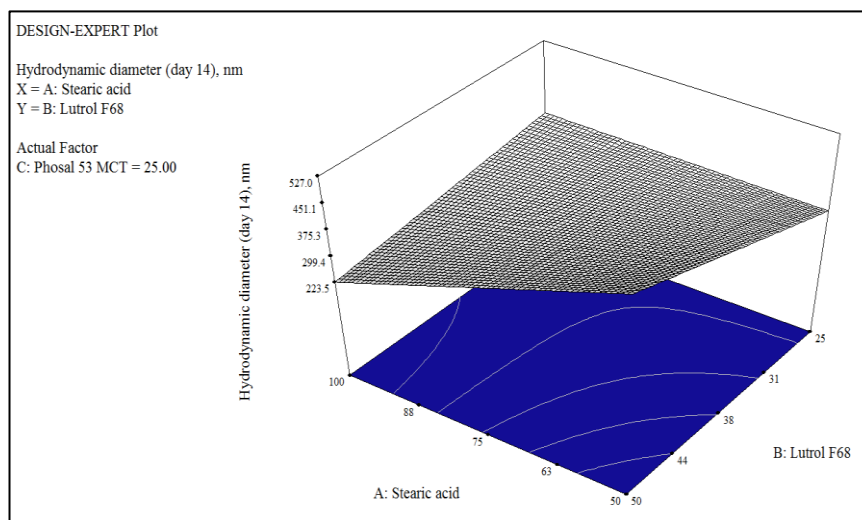
*B* – Lutrol® micro 68

**Table 3.8 Analysis of variance (ANOVA) for a 2<sup>3</sup> factorial design for hydrodynamic diameter at day 14 (storage at 4°C)**

	Sum of squares	<i>df</i>	<i>F</i> -value	<i>P</i> value
Model	99861.59	3	26.13	0.0043*
<i>A</i>	42748.88	1	33.56	0.0044*
<i>B</i>	7626.12	1	5.99	0.0707
<i>AB</i>	49486.58	1	38.85	0.0034*

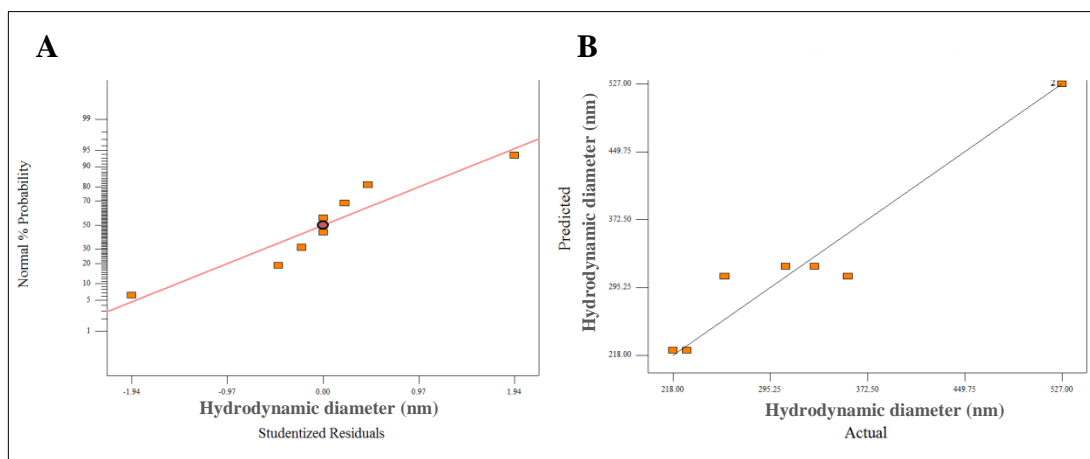
*A* – stearic acid, *B* – Lutrol® micro 68, \* Significance level  $p < 0.05$

Figure 3.4 shows the plot of interaction between stearic acid (*A*) and Lutrol® micro 68 (*B*) for the hydrodynamic diameter. Based on the graph (model), it was predicted that 100 mg stearic acid, 50 mg Lutrol® micro 68 and 25 or 50 mg Phosal® 53 MCT, the smallest mean size of particles with a hydrodynamic diameter of 223.5 nm would be produced. This is due to sufficient amount of the main surfactant, having the capability to stabilise and coat the whole of nanoparticles, resulting in the smaller size of particles.



**Figure 3.4 3D figure of interaction between stearic acid (A) and Lutrol® micro 68 (B) for hydrodynamic diameter at day 14**

Hydrophilic-lipophilic Balance (HLB) of surface active agents is one of the main criteria to be considered in order to develop a stable emulsion. The higher HLB value, the more water-soluble is the surfactant. In this case, Lutrol® F68 has high HLB value >24 and soy phosphatidylcholine (53% in Phosal® 53 MCT) has low HLB value (HLB 4). By using a mix of emulsifiers, the emulsion can be stabilised in terms of coalescence rate (Trotta et al., 2003). When all particles have adequate amount of stabiliser or emulsifier, smaller mean size was resulted. Figure 3.5A shows the normal percent probability versus studentized residuals on hydrodynamic diameter. All the error terms were normally distributed, as all of the points approximated to a straight line. Figure 3.5B shows the predicted versus actual value for hydrodynamic diameters. In order to accept the model term, the value of coefficient determination (R-squared) is considered. At day 14, hydrodynamic diameter 'R-squared' was 0.9515 while the Predicted R-squared was 0.8058. At the end of the model, this value was in reasonable agreement with the 'Adjustment R-squared' which was 0.9150.



**Figure 3.5** Normal percent probability versus studentized residuals (A) and predicted versus actual value for hydrodynamic diameter at day 14 (B)

The model for PDI showed significant difference ( $p < 0.05$ ) at day 14, indicating that the particle size distribution significantly increased with time (Table 3.9). Model A, C, AB, and AC were significantly different with respect to PDI. Compared to the hydrodynamic diameter result, Phosal® 53 MCT alone did not influence the measurement, however, for the PDI, it affected the measurement. When the same amount of stearic acid (50 or 100 mg) and Lutrol® micro 68 (25 or 50) were used, increasing the amount of Phosal® 53 MCT (25 or 50 mg) resulted in increased polydispersity index. This model also confirmed that the interaction between stearic acid and Lutrol® micro 68 and Phosal® 53 MCT affected the measured value.

**Table 3.9** Analysis of variance (ANOVA) for  $2^3$  factorial design for polydispersity index at day 14 (storage at 4°C)

	Sum of squares	df	F-value	p-value
Model	0.046	5	267.18	0.0037*
A	0.018	1	527.01	0.0019*
B	$1.805 \times 10^{-4}$	1	5.27	0.1486
C	0.014	1	412.03	0.0024*
AB	0.012	1	337.28	0.0030*
AC	$1.861 \times 10^{-3}$	1	54.32	0.0179*

A – stearic acid, B – Lutrol® micro 68, C – Phosal® 53 MCT, \* Significance level  $p < 0.05$

Figure 3.6 shows a 3D plot of the interaction between stearic acid (A) and Lutrol® micro F68 (B). 100 mg stearic acid, 50 mg Lutrol® micro 68 and 25 mg Phosal® 53 MCT would produce a narrow particle size distribution (PDI=0.125). When the amount of surfactant was increased, the size of particles reduced and a narrower particle size distribution was produced. Previous research found that an optimal amount of surfactant used in nanoparticle preparation decreased the size of particle (Prozorov et al., 1999). At a very low concentration of surfactant, aggregation is accelerated where the proportion of the particle surface that is coated is small. At a higher surfactant concentration, all the particles were coated, agglomeration reduced, and the particle size was reduced (Prozorov et al., 1999). However, if the surfactant concentration (in this case Phosal® 53 MCT) was increased excessively, it might produce a population of agglomerated particles having a larger size (due to the presence of liquid lipid in this surfactant, and an insufficient amount of Lutrol® micro 68) resulting in a higher PDI.

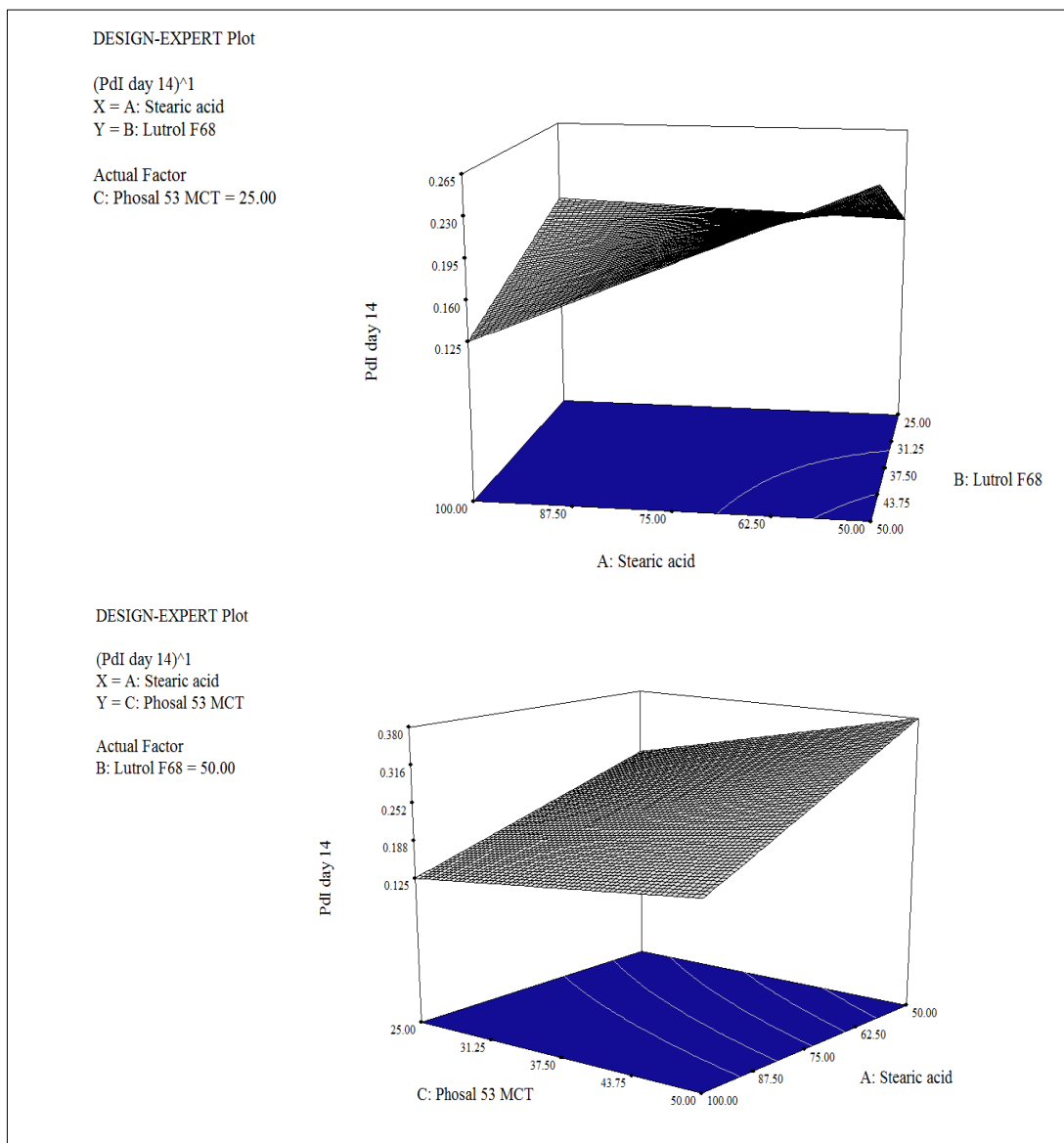


**Figure 3.6 3D plot of interaction between stearic acid (A) and Lutrol® micro 68 (B) (above), and stearic acid (A) and Phosal® 53 MCT (C) (bottom) for the polydispersity index at day 14.**

Figure 3.7A shows the normal percent probability versus studentized residuals for polydispersity index. All the error terms were normally distributed as all of the points approximated to a straight line. As shown in Figure 3.7B the ‘Predicted R-squared’ (0.9761) from the model was in reasonable agreement with the ‘Adjustment R-squared’ (0.9948). Equation 3-8 shows the model of the amount of materials used in the DST-NLCs preparation PDI at day 14 (in coded number).

$$\text{PDI at day 14} = 0.23 - 0.048*A + 4.750 \times 10^{-3}*B + 0.042*C - 0.038*A*B - 0.015*A*C$$

## Equation 3-8

where;

A – Stearic acid

B – Lutrol® micro 68

C – Phosal® 53 MCT

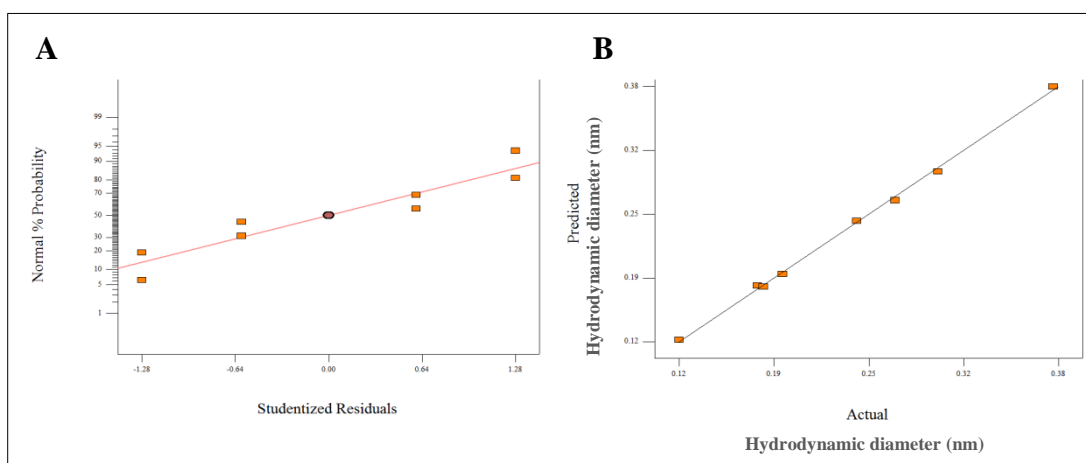


**Figure 3.7 Normal percent probability versus studentized residuals (A) and predicted versus actual value for polydispersity index at day 14 (B)**

### 3.5.2.1.1 Surface charge

Based on ANOVA analysis (Design Expert 6.0.8, Stat-Ease Inc. USA) on zeta potential values at day 14, there was no significant difference ( $p > 0.05$ ) on the model (Table 3.10). All particles had a surface charge of approximately -20 mV. Honary and Zahir (2013) reported that for a low molecular weight of stabilizers, zeta potential value at +/- 30 mV or more can give good stabilisation.

Saeb et al. (2014) prepared silver nanoparticles with strong and stable antimicrobial activity with highly negatively-charged particles. When the surface charge was low (zeta potential value near to 0), the particles aggregated and flocculated due to absence of repulsive forces which prevent agglomeration. This showed that surface charge values indicate the physical stability of nanoparticles,

where large negative or positive charge will tend to repel each other and no tendency to flocculate or aggregate (Saeb et al., 2014).

**Table 3.10 Analysis of variance (ANOVA) for a 2<sup>3</sup> factorial design for zeta potential at day 14**

	Sum of squares	df	F-value	p-value
Model	10.28	6	3.80	0.3739
A	1.84	1	4.07	0.2929
B	0.031	1	0.069	0.8362
C	2.17	1	4.81	0.2724
AB	2.46	1	5.44	0.2578
AC	1.25 x 10 <sup>-3</sup>	1	2.77 x 10 <sup>-3</sup>	0.9665
BC	3.78	1	8.38	0.2118

A – stearic acid, B – Lutrol® F68, C – Phosal® 53 MCT

However, comparison of the surface charge between day 1 and day 14 (Figure 3.8) showed an insignificant reduction ( $p > 0.05$ ) on the zeta potential values in Formulation S4, suggesting better stability compared to other formulations. Change in the surface charge is probably due to instability, such as aggregation. As aggregated particles have a lower surface area and reduction of surface charge compared to a single particle which has a higher surface area resulting in an increase of surface charge. This result showed that, the measurement of surface charge on different days could be a useful indicator to predict the physical stability of the nanoparticles.

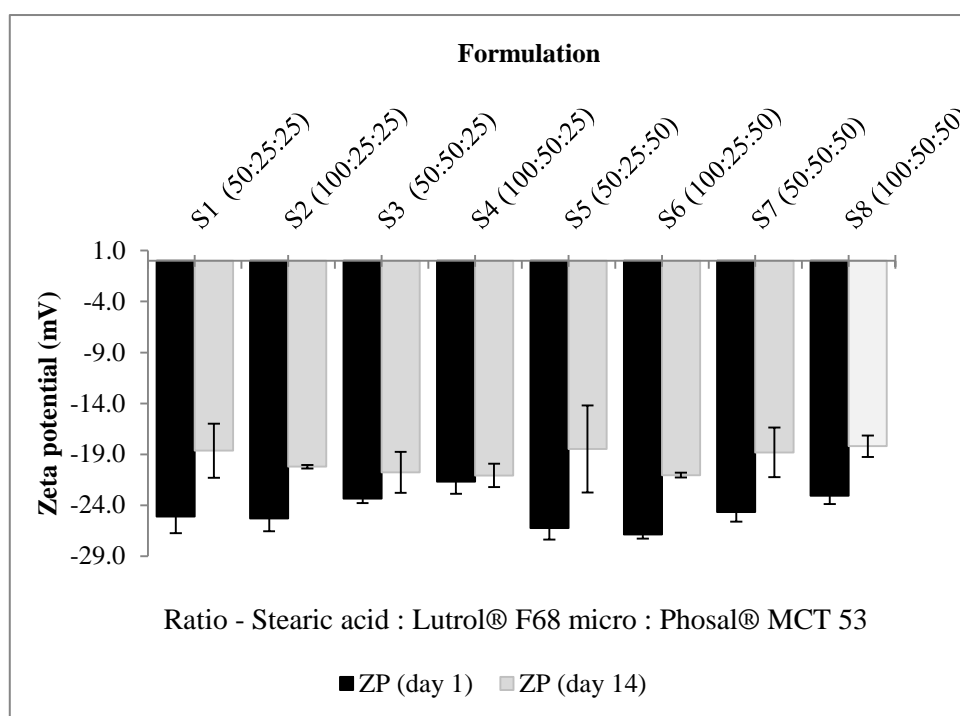


**Figure 3.8 Zeta potential measurement of DST-NLCs at day 1 and 14 stored at 4-8°C (n=3, mean  $\pm$  SD)**

### 3.5.2.1.2 Entrapment efficiency and drug loading

The relationship model of DST-NLCs between materials used and the entrapment efficiency and drug loading was analysed using an ANOVA analysis. The independent factors investigated that may affect entrapment efficiency and drug loading of DST-NLCs in these formulations were the amount of stearic acid (*A*), Lutrol® F68 (*B*) and Phosal® 53 MCT (*C*). The entrapment efficiency for the formulations investigated was between 63 and 98% (Table 3.11).

**Table 3.11 Entrapment efficiency and drug loading of DST-NLCs at day 1 (n=3, mean  $\pm$  SD)**

<b>Formulation</b>	<b>Stearic acid (mg)</b>	<b>Lutrol® micro 68 (mg)</b>	<b>Phosal® 53 MCT (mg)</b>	<b>EE (%)</b>	<b>DL (%)</b>
<b>S1</b>	50	25	25	79.6 $\pm$ 10.3	4.40 $\pm$ 0.58
<b>S2</b>	100	25	25	81.7 $\pm$ 20.3	3.31 $\pm$ 0.75
<b>S3</b>	50	50	25	63.2 $\pm$ 21.8	2.98 $\pm$ 0.61
<b>S4</b>	100	50	25	97.6 $\pm$ 2.4	3.27 $\pm$ 0.07
<b>S5</b>	50	25	50	80.0 $\pm$ 0.6	2.49 $\pm$ 0.65
<b>S6</b>	100	25	50	97.7 $\pm$ 1.2	3.09 $\pm$ 0.35
<b>S7</b>	50	50	50	64.8 $\pm$ 7.7	2.09 $\pm$ 0.32
<b>S8</b>	100	50	50	92.5 $\pm$ 5.6	2.66 $\pm$ 0.24

EE – entrapment efficiency, DL – drug loading

Table 3.12 shows ANOVA results for the entrapment efficiency at day 1. Based on the model, no interaction was found among the materials used for entrapment efficiency. Stearic acid (A) content was found to affect the entrapment efficiency. Figure 3.9 shows 100 mg stearic acid, 50 mg Lutrol® micro 68 and 25 or 50 mg Phosal® 53 MCT produced the highest entrapment efficiency (predicted from the design of experiment model = 95.1%). The amount of stearic acid had a significant effect on the entrapment efficiency ( $p < 0.05$ ). By increasing the amount of stearic acid from 50 to 100 mg, it was predicted that the entrapment efficiency increased from 64 to 95.1%, suggesting a higher amount of stearic acid was needed in order to load dutasteride in nanoparticle preparation.

At day 1, even though the mean size of particles were in a similar range (approximately 200 nm), some formulations produced lower entrapment efficiency. This may be due to insufficient amount of surfactant, resulting in lower entrapment of dutasteride. S4, S6, and S8 showed high entrapment, greater than 90% (Table 3.11). However, the hydrodynamic diameter for S6 after day 14 was greater than 300 nm, and therefore this formulation was not considered for the next set of experiments. Based on the results for entrapment efficiency and size, formulations S4 and S8 were carried forward for the next experiment.

At this stage, entrapment efficiency was considered to be important, but secondary factor to particle size. The main factor to be considered was the size of the particles which should be stable and within a certain range (200 – 300 nm). Entrapment efficiency can be modified based on the amount of drug added into the carriers. Once the optimal formulation based on the hydrodynamic diameter and PDI was identified, optimisation based on entrapment efficiency was undertaken later.

**Table 3.12 Analysis of variance (ANOVA) for a 2<sup>3</sup> factorial design for entrapment efficiency at day 1**

	Sum of squares	df	F-value	p-value
Model	1116.71	3	10.46	0.0230*
A	838.45	1	23.56	0.0083*
B	54.80	1	1.53	0.2832
AB	223.66	1	6.28	0.0663

A – stearic acid and B – Lutrol® F68, \* Significance level  $p < 0.05$

The mathematical modelling of DST-NLCs between the materials used (independent variables) and entrapment efficiency (dependent variables) was described by the following equation (coded value):

$$EE\% = 82.14 + 10.24*A - 2.61*B + 5.29*A*B \quad \text{Equation 3-9}$$

where;

A – stearic acid

B – Lutrol® micro 68

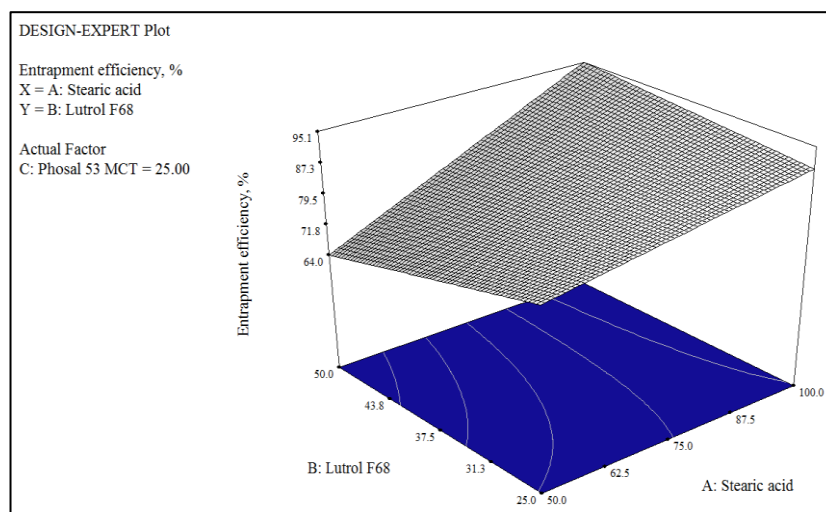


**Figure 3.9 3D plot of stearic acid (A) and Lutrol® micro 68 (B) for the entrapment efficiency (%)**

When drug loading was analysed using Design Expert ANOVA, there was no significant difference of the model between materials used and drug loading ( $p > 0.05$ ) (Table 3.13). Changing the amount of materials used did not produce any linear model, suggesting that the large standard deviation values of total drug loading resulted in no significant model being generated. At this stage, drug loading can be neglected as a main criterion, whereas the size distribution would be considered.

**Table 3.13 Analysis of variance (ANOVA) for a  $2^3$  factorial design on drug loading at day 1**

	Sum of squares	df	F-value	p-value
Model	3.03	5	4.07	0.2090
A	0.017	1	0.11	0.7670
B	0.66	1	4.40	0.1707
C	1.65	1	11.05	0.0798
AB	0.23	1	1.53	0.3419
AC	0.49	1	3.25	0.2130

A – stearic acid, B – Lutrol® F68, C – Phosal® 53 MCT

### 3.5.2.1.3 Hydrodynamic diameter, particle size distribution and entrapment efficiency for DST-NLCs: effect of scaled-up formulation

Based on the results of particle size distribution outlined in Section 3.5.2.1, only 1 formulation (Formulation S4) was chosen. Production quantities were scaled up 3 times (3x) with or without DST, using the same ratio of materials. Table 3.14 shows the mean hydrodynamic diameter, PDI and entrapment efficiency which were not significantly altered by scaling up ( $p>0.05$ ). The surface charge of scaled-up DST-NLCs and NLCs (without DST) was slightly lower ( $p<0.05$ ) than non-scaled-up DST-NLCs.

**Table 3.14 Hydrodynamic diameter, PDI and zeta potential of DST-NLCs after scaled-up (day 1) (n=3, mean  $\pm$  SD)**

Formulation	Hydrodynamic diameter (nm)	PDI	Zeta Potential (mV)	Entrapment efficiency (%)
<b>x (with DST)</b>	190.3 $\pm$ 12.5	0.101 $\pm$ 0.016	-22.0 $\pm$ 1.2	97.6 $\pm$ 2.4
<b>3x (with DST)</b>	178.6 $\pm$ 18.4	0.124 $\pm$ 0.025	-17.1 $\pm$ 0.9	96.6 $\pm$ 0.1
<b>3x (without DST)</b>	176.5 $\pm$ 1.9	0.117 $\pm$ 0.010	-17.8 $\pm$ 2.8	-

x - Refers to scale-up time, 15 mg dutasteride

### 3.5.2.1.4 Entrapment efficiency and drug loading of DST-NLCs: Optimisation of dutasteride content in scaled-up NLCs

The amount of dutasteride was optimised in order to determine the maximum dutasteride that could be loaded in the NLCs. 17.5 mg dutasteride (DST 17.5) was found to be the optimal content, giving highest entrapment efficiency (97.3  $\pm$  1.2%) as shown in Figure 3.10. No significant difference in the entrapment efficiency between 15 mg and 17.5 mg of dutasteride was observed ( $p>0.05$ ). When drug content was increased to 20 mg (DST 20), the entrapment efficiency decreased to

90.1 ± 1.1% ( $p < 0.05$ ), indicating the limitation of the amount of drug that can be loaded in this carrier system, as reported previously (Gaber et al., 2006). There was no significant difference ( $p > 0.05$ ) in drug loading (3.49 ± 0.10%) for 17.5 mg of dutasteride in the NLCs when the amount of drug was varied from 15 to 20 mg.

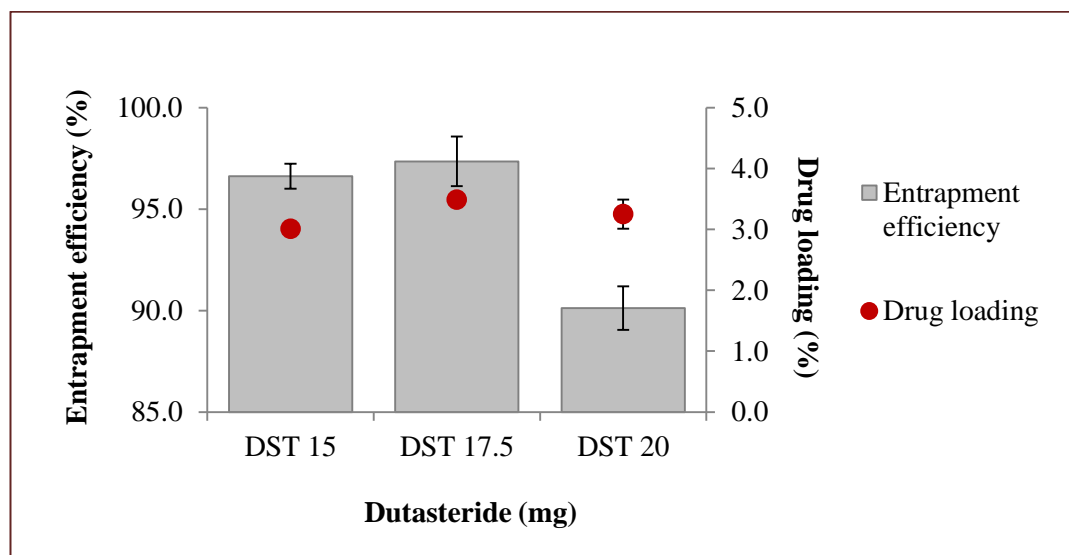


**Figure 3.10** Entrapment efficiency and drug loading of DST-NLCs with different amounts of dutasteride (15, 17.5 and 20 mg) (n=3, mean ±SD)

### 3.5.2.2 Size distribution and zeta potential of DST-NLCs before and after coating with CSO-SA and CSO

DST-NLCs were prepared and coated with different concentrations of CSO-SA (2.5, 5 and 10%) and 5% CSO as shown in Table 3.15. Based on statistical analysis, there was no significant increase in mean particle size for DST-NLCs ( $p > 0.05$ ) when coated with 2.5% CSO-SA and 5% CSO. Coating of DST-NLCs with 5 and 10% CSO-SA produced significant increases in mean size ( $p < 0.05$ ) compared to uncoated DST-NLCs. In term of the PDI, there was no significant difference ( $p > 0.05$ ) between uncoated DST-NLCs and those coated with different concentrations of CSO-SA preparations. All PDI measurements showed values less than 0.3 indicating the particles were in monodisperse nanoparticle populations (Tagalakis et al., 2015).

**Table 3.15 Size distribution and surface charge for DST-NLCs before and after coating with different concentrations of CSO-SA and CSO (n=3, mean  $\pm$  SD)**

Parameter	DST-NLCs	DST-NLCs 2.5% CSO-SA	DST-NLCs 5% CSO-SA	DST-NLCs 10% CSO-SA	DST-NLCs 5% CSO
Hydrodynamic diameter (nm)	187.6 $\pm$ 7.0	207.8 $\pm$ 10.5	220.1 $\pm$ 11.9	230.1 $\pm$ 8.2	208.4 $\pm$ 1.6
PDI	0.117 $\pm$ 0.008	0.124 $\pm$ 0.009	0.149 $\pm$ 0.024	0.147 $\pm$ 0.026	0.167 $\pm$ 0.025
Zeta potential (mV)	-18.3 $\pm$ 0.9	+23.2 $\pm$ 2.1	+26.0 $\pm$ 1.1	+30.0 $\pm$ 1.2	+21.7 $\pm$ 2.1

All preparations contain 17.5 mg dutasteride

The zeta potential values of DST-NLCs changed from negative to positive following coating ( $p < 0.05$ ), with CSO-SA or CSO adsorbed to negative charged DST-NLCs, producing positively-charged nanoparticles (Table 3.15). Zeta potential increased from +26.0 to +30.0 mV when concentration of CSO-SA was increased from 5% to 10% ( $p < 0.05$ ). The charge was higher for DST-NLCs coated with 5% CSO-SA than with 5% CSO ( $p < 0.05$ ). These findings indicated a strong interaction between DST-NLCs and CSO-SA, potentially stabilising the nanoparticles. This may result in part, from CSO-SA having some amphiphilic properties, as reported by Hu et al., (2009) who produced stable doxorubicin-loaded polymeric micelles with surface charge of +32 to +44 mV using a chitosan oligomer-stearic acid conjugate. It is likely that the highly positively-charged CSO-SA was bound electrostatically to the negatively-charged surface of DST-NLCs.

Previous studies (Fonte et al., 2011; Luo et al., 2011; Nair et al., 2012; Ridolfi et al., 2012; Kuo and Wang, 2013) have demonstrated the electrostatic interaction between positively-charged chitosan and negatively-charged nanoparticles. Generally, the colloidal system is stable if zeta potential value is higher than  $\pm 30$  mV (Xu et al., 2011).

### 3.5.2.2.1 Stability of DST-NLCs, uncoated and coated with CSO-SA and CSO

#### 3.5.2.2.1.1 Hydrodynamic diameter, PDI and surface charge

Physical stability tests are important in order to evaluate the quality of formulation over a certain period. Determination of particle size changes allows for verification of the time-dependent stability of particles regarding the tendency for aggregation and sedimentation (Gomes et al., 2014). Uncoated DST-NLCs and those coated with 2.5, 5 and 10% CSO-SA were stable at 4-8°C over a period of 180 days, with all measured mean particle sizes in the range approximately 200 nm to 250 nm.

DST-NLCs coated with 2.5, 5 and 10% CSO-SA had unchanged mean particle size and PDI ( $p>0.05$ ) when compared between day 1 and day 60 (Table 3.16). There was a significant difference in the mean particle size between day 1 and day 180 ( $p<0.05$ ). Though, between samples at day 180, there was no significant difference ( $p>0.05$ ). DST-NLCs coated with 5% CSO demonstrated physical instability, with aggregation even when stored at 4-8 and 25°C (day 30), possibly due to differences in the chemical structures of the CSO compared to CSO-SA, which has a hydrophobic chain absent in unconjugated CSO.

At day 30, DST-NLCs coated with 10% CSO-SA aggregated when stored at 25°C. Increasing the concentration of CSO-SA to 10% produced aggregation, possibly resulting from excess CSO-SA in the formulation, not associated with the NLC coating. In addition, when uncoated DST-NLCs and those coated with 2.5 and 5% CSO-SA were stored at 25°C, the mean particle size increased 2-fold at day 30 compared to samples stored at 4-8°C.

The data indicated NLCs coated with chitosan without conjugation were relatively unstable. Having the hydrophobic stearyl chain which produces amphiphilic properties in the chitosan-conjugate may enhance the stability of the nanoparticles when the CSO-SA (at an appropriate concentration) is employed as a coating material.

**Table 3.16 Size distribution and surface charge of DST-NLCs, uncoated and coated with CSO-SA or CSO (n=3, mean  $\pm$  SD)**

<b>Storage condition</b>	<b>DST-NLCs</b>	<b>DST-NLCs 2.5% CSO-SA</b>	<b>DST-NLCs 5% CSO-SA</b>	<b>DST-NLCs 10% CSO-SA</b>	<b>DST-NLCs 5% CSO</b>
<b>Day 1 (Initial)</b>					
Hydrodynamic diameter (nm)	187.6 $\pm$ 7.0	207.8 $\pm$ 10.5	220.1 $\pm$ 11.9	230.1 $\pm$ 8.2	208.4 $\pm$ 1.6
PDI	0.117 $\pm$ 0.008	0.124 $\pm$ 0.009	0.149 $\pm$ 0.024	0.147 $\pm$ 0.026	0.167 $\pm$ 0.025
Zeta potential (mV)	-18.3 $\pm$ 0.9	+23.2 $\pm$ 2.1	+26.0 $\pm$ 1.1	+30.0 $\pm$ 1.2	+21.7 $\pm$ 2.1
<b>Day 30 at 4-8°C</b>					
Hydrodynamic diameter (nm)	216.8 $\pm$ 6.0	226.3 $\pm$ 19.8	239.0 $\pm$ 24.3	241.9 $\pm$ 7.5	Aggregation
PDI	0.132 $\pm$ 0.017	0.162 $\pm$ 0.041	0.193 $\pm$ 0.064	0.213 $\pm$ 0.006	Aggregation
Zeta potential (mV)	-17.2 $\pm$ 2.6	+28.8 $\pm$ 3.6	+33.9 $\pm$ 1.8	+33.8 $\pm$ 1.8	Aggregation
<b>Day 30 at 25°C</b>					
Hydrodynamic diameter (nm)	435.3 $\pm$ 32.0	463.8 $\pm$ 34.5	443.6 $\pm$ 62.9	Aggregation	Aggregation
PDI	0.208 $\pm$ 0.036	0.280 $\pm$ 0.129	0.233 $\pm$ 0.032	Aggregation	Aggregation
Zeta potential (mV)	-17.0 $\pm$ 0.7	+21.6 $\pm$ 6.6	+24.0 $\pm$ 1.0	Aggregation	Aggregation

(Table 3.16 continued)

<b>Day 60 at 4-8°C</b>					
Hydrodynamic diameter (nm)	228.5 ± 6.8	234.5 ± 22.9	243.8.0 ± 18.8	259.8 ± 4.2	Aggregation
PDI	0.128 ± 0.004	0.164 ± 0.048	0.155 ± 0.025	0.215 ± 0.020	Aggregation
Zeta potential (mV)	-17.2 ± 2.6	+31.4 ± 2.4	+32.2 ± 10.4	+29.4 ± 5.6	Aggregation
<b>Day 60 at 25°C</b>					
Hydrodynamic diameter (nm)	435.3 ± 32.0	631.8 ± 149.8	578.2 ± 27.0	Aggregation	Aggregation
PDI	0.208 ± 0.036	0.229 ± 0.016	0.274 ± 0.113	Aggregation	Aggregation
Zeta potential (mV)	-18.9 ± 1.6	+20.0 ± 2.8	+20.0 ± 1.6	Aggregation	Aggregation
<b>Day 180 at 4-8°C</b>					
Hydrodynamic diameter (nm)	242.4 ± 8.6	241.1 ± 8.4	246.5 ± 5.8	275.4 ± 10.0	Aggregation
PDI	0.137 ± 0.026	0.147 ± 0.024	0.152 ± 0.008	0.248 ± 0.016	Aggregation
Zeta potential (mV)	-16.5 ± 0.9	+31.9 ± 1.9	+32.3 ± 2.0	+32.1 ± 1.1	Aggregation
<b>Day 180 at 25°C</b>					
Hydrodynamic diameter (nm)	Aggregation	Aggregation	Aggregation	Aggregation	Aggregation
PDI	Aggregation	Aggregation	Aggregation	Aggregation	Aggregation
Zeta potential (mV)	Aggregation	Aggregation	Aggregation	Aggregation	Aggregation

Chitosan undergoes gradual chain degradation followed by the destruction of functional groups which results in loss of physicochemical properties (Szymańska and Winnicka, 2015). Szymańska and Winnicka, (2015) reported that many studies have been conducted in order to increase the stability of chitosan-based system such as adding stabilizer (mannitol, sorbitol, glycerol) during storage, or cryoprotectant (mannitol, sucrose, trehalose) during freeze-drying process, adding metal ion in chitosan/hyaluronate complexes, blending with other non-ionic polymers and also chemical or physical crosslinking with chitosan. Fernandes et al., (2013) found that chitosan crosslinked with genipin influenced the swelling ability, mucoadhesiveness, and acidic stability of the prepared microparticles. Chemical crosslinking has shown to give higher stability, where it reduces the gelation process. The conjugation between chitosan backbone and the hydrophobic chain has increased the chitosan stability. The data in Table 3.16 shows that having a hydrophobic chain (stearic acid) attached to the CSO has made the conjugated CSO-SA more stable compared to unconjugated chitosan.

The size of particles (200 - 300 nm) showed an acceptable range for the topical delivery as in agreement with Mahe et al., (2009), where they found that particles of approximately 200 nm mean sizes applied to the skin were found around the hair follicles. Mittal et al., (2015) reported that particles with a size approximately 300 nm were found in the transfollicular region. These studies suggest to deliver the drug into the hair follicle regions, size of particles in the range of 200-300 nm is appropriate.

#### **3.5.2.2.1.2 Entrapment efficiency**

Due to the gelling properties of chitosan, the DST-NLCs coated with CSO-SA or CSO could not pass down the Sephadex gel, prohibiting measurement of the entrapment efficiency. Hence, entrapment efficiency was measured only for uncoated samples (DST-NLCs). Based on Figure 3.11, the entrapment efficiency was monitored for 6 months at 4-8°C. The results showed the entrapment efficiency was  $97.3 \pm 1.2\%$  on day 1 with no significant reduction ( $p > 0.05$ ) at day 180 ( $96.6 \pm 1.9\%$ ), indicating considerable stability.

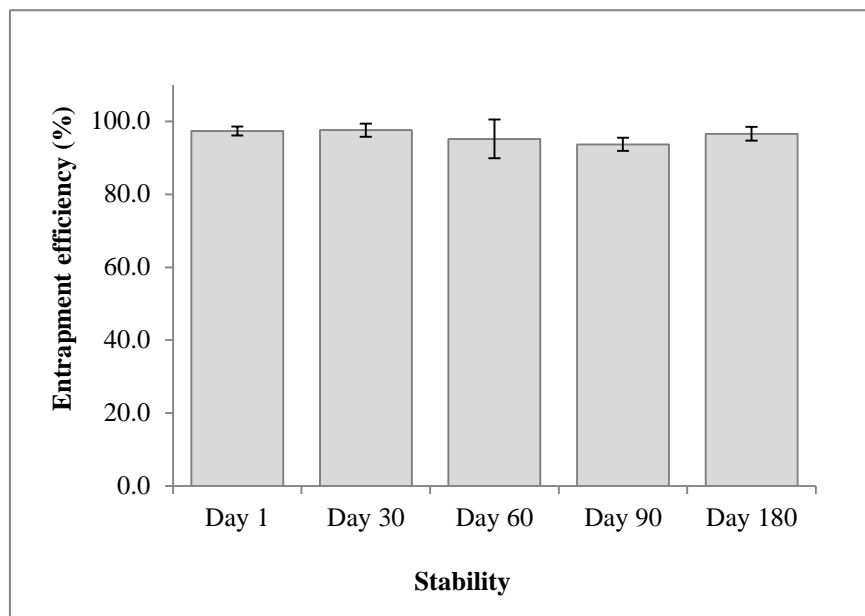


**Figure 3.11 Entrapment efficiency of DST-NLCs uncoated at day 1, 30, 60, 90 and 180 stored at 4-8°C (n=3, mean  $\pm$  SD)**

### 3.5.2.3 Morphology of uncoated and coated DST-NLCs

Figure 3.12 shows TEM of uncoated DST-NLCs and those coated with CSO/CSO-SA nanoparticles. All samples showed monodispersed nanoparticles, spherical in shape, in the size range approximately 200 to 250 nm, consistent with the dynamic light scattering characterisation.

Based on the figures, DST-NLCs coated with 5% CSO (Figure 3.12B) shows a denser layer of coating compared to DST-NLCs coated with 5% CSO-SA or 10% CSO-SA. Even though DST-NLCs coated with 5% CSO showed denser layer compared to those coated with 5% CSO-SA, however it did not help the stability of the samples after day 30 (Section 3.5.2.2.1). Smaller particles were present with the main larger DST-NLCs can be seen from Figure 3.12C and D, suggesting excess amounts of CSO-SA in the preparations. Absence of excess CSO can be seen for DST-NLCs coated with 5% CSO (Figure 3.12B), resulting all DST-NLCs particles have been fully coated with 5% CSO.

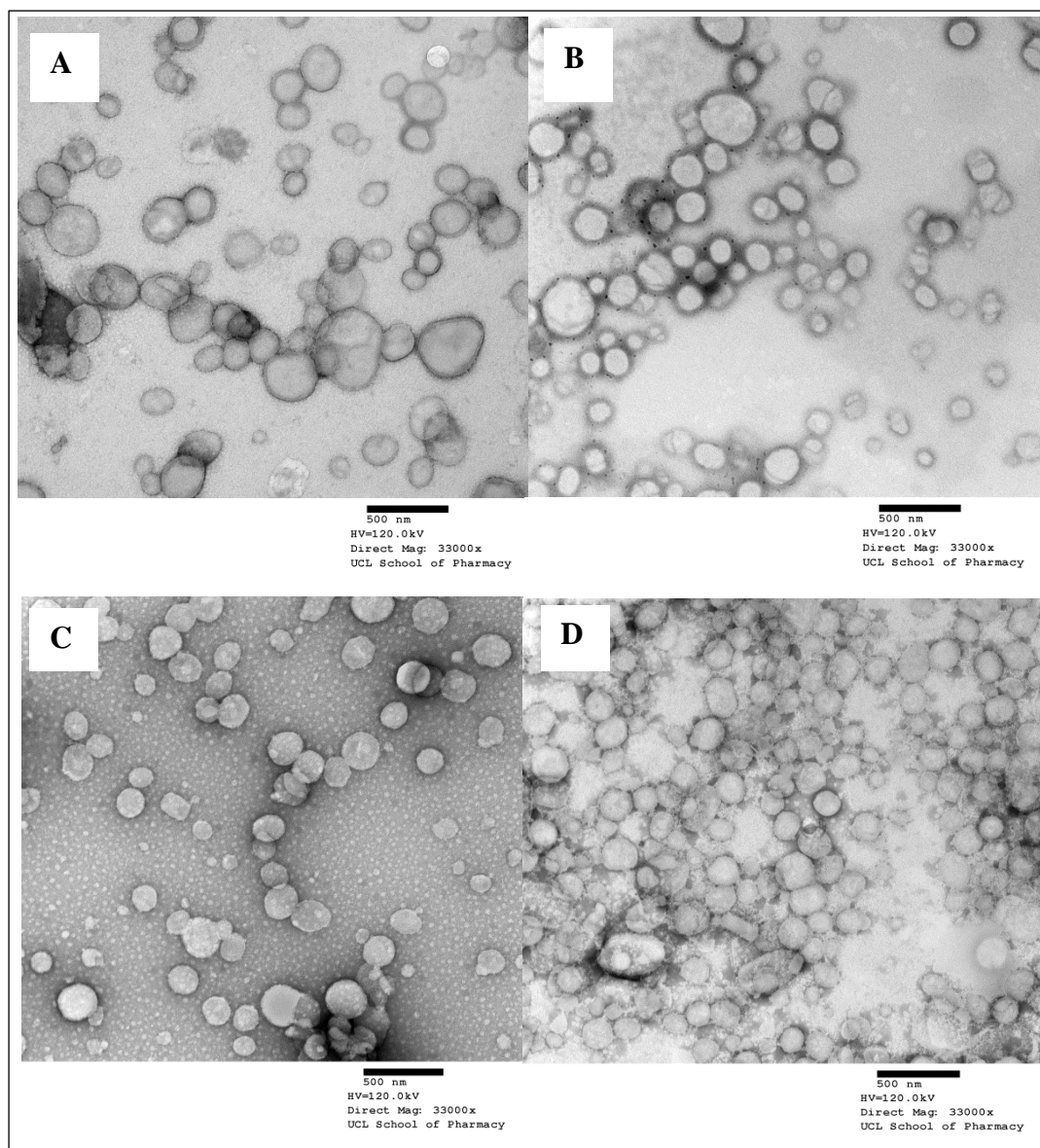


**Figure 3.12 TEM images of DST-NLCs, uncoated (A), coated with; 5% CSO (B), 5% CSO-SA (C) and 10% CSO-SA (D)**

A similar trend can be seen from Figure 3.12A for uncoated DST-NLCs, suggesting all surfactants (Lutrol® micro 68 and Phosal® 53 MCT) have been fully emulsified and stabilised the formulation, with no evident excess of surfactants. These results were in agreement with the CMC results of CSO-SA (Section 2.4.4) where 2.5% CSO-SA (0.12 mg/mL of CSO-SA in DST-NLCs preparations) existed as a monomer, meanwhile concentrations greater than CMC values: 5% CSO-SA (0.24 mg/mL of CSO-SA in DST-NLCs preparations) and 10% CSO-SA (0.48

mg/mL of CSO-SA in DST-NLCs preparations), resulted in micelles in preparation of DST-NLCs.

### 3.5.3 Preparation and characterisation of dutasteride-loaded nanostructured lipid carrier coated with chitosan oligomer-lauric acid

#### 3.5.3.1 Particle size distribution and zeta potential

DST-NLCs were prepared and coated with different concentrations of CSO-LA (2.5, 5 and 10% w/w of solid lipid) as shown in Table 3.17. Based on the statistical analysis, uncoated DST-NLCs produced a mean particle size of  $184.2 \pm 2.9$  nm, and no significant difference ( $p > 0.05$ ) was found with DST-NLCs coated with 2.5 and 5% of CSO-LA. Coating DST-NLCs with 10% CSO-LA produced a significant increase ( $p < 0.05$ ) in mean size, suggesting a thicker layer of coating existed on DST-NLCs.

**Table 3.17 Size distribution and surface charge for DST-NLCs before and after coating with different concentrations of CSO-LA (n=3, mean  $\pm$  SD)**

Storage condition	DST-NLCs	DST-NLCs 2.5% CSO-LA	DST-NLCs 5% CSO-LA	DST-NLCs 10% CSO-LA
Hydrodynamic diameter (nm)	$184.2 \pm 2.9$	$183.8 \pm 1.3$	$188.4 \pm 2.2$	$199.5 \pm 3.3$
PDI	$0.118 \pm 0.016$	$0.115 \pm 0.015$	$0.124 \pm 0.011$	$0.118 \pm 0.009$
Zeta potential (mV)	$-18.0 \pm 2.3$	$+19.9 \pm 2.6$	$+24.8 \pm 2.1$	$+29.2 \pm 2.0$

All preparations contain 17.5 mg dutasteride

In terms of PDI, there was no significant difference ( $p > 0.05$ ) between uncoated DST-NLCs and those coated with different concentrations of CSO-LA. All

PDI measurements were less than 0.3, indicating monodisperse nanoparticle populations (Tagalakis et al., 2015).

For the surface charge, a similar trend was found as for coating with CSO-SA, with DST-NLCs coated with different concentration of CSO-LA resulted in a significant change of zeta potential values from negative ( $-18.0 \pm 2.3$  mV) to more than +20 mV of charge ( $p < 0.05$ ). Significant increases ( $p < 0.05$ ) in surface charge were found when the amount of CSO-LA increased from 2.5 to 5.0 and 10%. Zhao et al. (2014) prepared chitosan conjugated with lauric acid, though no measurement of surface charge was reported. As chitosan normally is positively-charged, they found that surface modification of titanium substrate with chitosan-lauric acid was deposited onto an implant surface and improved the biological functions of osteoblasts, and at the same time reduced bacterial infection. In the *in vitro* tests, they have confirmed that the cell adhesion, cell viability, intracellular alkaline phosphatase activity and mineralization capacity of osteoblasts were significantly improved when cultured onto chitosan-lauric acid surface functionalized titanium substrates (Zhao et al., 2014), suggesting the positive charge of the chitosan improved the biocompatibility and addition of lauric acid improved antibacterial activity.

### **3.5.3.2 Stability of DST-NLCs, uncoated and coated with CSO-LA**

#### **3.5.3.2.1 Hydrodynamic diameter, PDI and surface charge**

Section 3.5.2.2.1 describes how the particles produced in this study were not stable when stored at room temperature, thus the stability of uncoated and DST-NLCs coated with CSO-LA was determined at 4-8°C. DST-NLCs uncoated and coated with different concentrations of CSO-LA had significantly different mean particles size at day 1 and day 180 ( $p < 0.05$ ) (Table 3.18). DST-NLCs coated with 5% CSO-LA were stable with respect to mean size from day 30 to day 180 ( $p > 0.05$ ).

**Table 3.18 Size distribution and surface charge of DST-NLCs, uncoated and coated with CSO-LA at day 1, 30, 60 and 180 stored at 4-8°C (n=3, mean ± SD)**

<b>Storage condition</b>	<b>DST-NLCs</b>	<b>DST-NLCs 2.5% CSO-LA</b>	<b>DST-NLCs 5% CSO-LA</b>	<b>DST-NLCs 10% CSO-LA</b>
<b>Day 1 (Initial)</b>				
Hydrodynamic diameter (nm)	184.2 ± 2.9	183.8 ± 1.3	188.4 ± 2.2	199.5 ± 3.3
PDI	0.118 ± 0.016	0.115 ± 0.015	0.124 ± 0.011	0.118 ± 0.009
Zeta potential (mV)	-18.0 ± 2.3	+19.9 ± 2.6	+24.8 ± 2.1	+29.2 ± 2.0
<b>Day 30 at 4-8°C</b>				
Hydrodynamic diameter (nm)	221.7 ± 3.4	217.5 ± 7.8	228.7 ± 14.1	252.0 ± 4.4
PDI	0.137 ± 0.017	0.131 ± 0.003	0.143 ± 0.054	0.196 ± 0.018
Zeta potential (mV)	-18.1 ± 1.9	+28.7 ± 3.4	+32.2 ± 1.6	+32.6 ± 1.6
<b>Day 60 at 4-8°C</b>				
Hydrodynamic diameter (nm)	235.1 ± 4.8	230.2 ± 9.5	237.0 ± 7.0	275.3 ± 18.9
PDI	0.132 ± 0.015	0.131 ± 0.017	0.130 ± 0.009	0.198 ± 0.021
Zeta potential (mV)	-18.2 ± 0.5	+27.5 ± 3.1	+31.9 ± 5.0	+33.3 ± 2.7
<b>Day 180 at 4-8°C</b>				
Hydrodynamic diameter (nm)	265.3 ± 7.8	251.7 ± 10.0	249.4 ± 7.1	283.8 ± 12.0
PDI	0.149 ± 0.015	0.130 ± 0.024	0.130 ± 0.024	0.197 ± 0.030
Zeta potential (mV)	-15.8 ± 1.0	+25.6 ± 6.2	+31.4 ± 6.0	+31.2 ± 3.0

DST-NLCs coated with 2.5 and 10% CSO-LA produced an insignificant difference ( $p > 0.05$ ) of mean size from day 30 to day 60 and significant increase ( $p < 0.05$ ) at day 180, suggesting the formulation of CSO-LA in the preparation resulted in gelation. Having the hydrophobic chain (lauroyl chain) in the chitosan-conjugate could enhance the stability of the nanoparticles when the CSO-LA (at an appropriate concentration) was employed as a coating material. In this case, coating DST-NLCs with 5% CSO-SA showed the highest stability where there was no significant difference ( $p > 0.05$ ) in the hydrodynamic diameter when compared between day 30 to day 60 and day 180.

In terms of PDI value, there was no significant difference ( $p > 0.05$ ) between day 1 to day 180 for all formulations except DST-NLCs coated with the highest concentration (10% CSO-LA) produced significant increase ( $p < 0.05$ ) from day 1 to day 30, 60 and 180. This result showed that there was a limitation of the amount of coating materials should be added in the nanoparticles formulation in order to control the PDI of the samples. Having the highest concentration of CSO-LA (10%) produced a larger size with a higher PDI value due to an excess amount of CSO-LA in the preparation.

The zeta potential of uncoated DST-NLCs was changed from negative to positive charge ( $p < 0.05$ ), coated with CSO-LA (Table 3.18). Zeta potential values increased when the concentration of CSO-LA increased ( $p < 0.05$ ). These findings indicated a good interaction between DST-NLCs and CSO-LA. These results were similar to the previous section (3.5.2.2). Increasing concentration of CSO-LA added into DST-NLCs showed an increment of the surface charge; suggesting a presence of a thicker coating on DST-NLCs.

### 3.5.3.3 Morphology of uncoated and coated DST-NLCs

TEMs of the uncoated DST-NLCs and those coated with CSO-LA showed monodispersed spherical nanoparticles in the size range approximately 200 to 250 nm, consistent with the dynamic light scattering results (Figure 3.13).

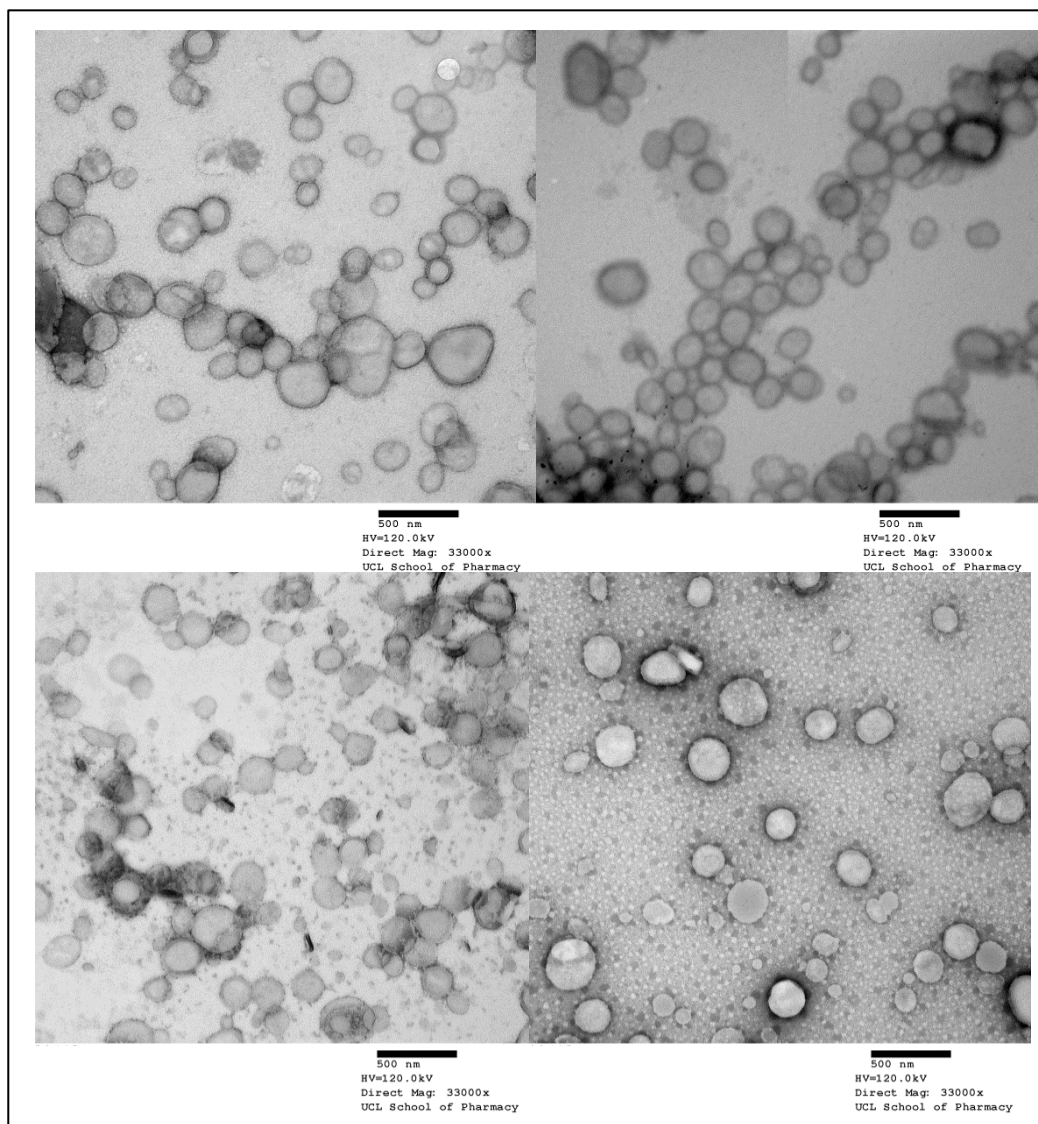


**Figure 3.13 TEM images of DST-NLCs, uncoated (A), coated with; 2.5% CSO-LA (B), 5% CSO-LA (C) and 10% CSO-LA (D)**

Coating with 5 and 10% CSO-LA showed a similar TEM image to the observation for DST-NLCs coated with CSO-SA (Section 3.5.2.3), where the smaller particles were present with the main larger particles (Figure 3.13C and D). At 5 and 10% CSO-LA concentrations, CSO-LA was present in a micellar system; resulting due to concentration was higher than CMC value of CSO-LA (Section 2.4.4). There were no small particles present for coating with 2.5% CSO-LA, suggesting this concentration was lower than the CMC value, resulting CSO-LA present in a monomer (Figure 3.13B).

#### 3.5.3.4 XRPD of DST-NLCs, uncoated and coated with 5% CSO-SA, 5% CSO-LA and physical mixture of formulation components

XRPD was performed to characterise the crystallinity of the formulations. The X-ray diffraction pattern of lyophilised DST-NLCs either uncoated or coated with CSO-SA or CSO-LA as well as the physical mixture of the ingredients used and also the pure stearic acid, Lutrol® micro 68 and combination of stearic acid and Phosal® 53 MCT are shown in Figure 3.14.

The XRPD diffractogram of dutasteride shows a number of sharp diffraction peaks at  $2\theta$  of 15.6, 17.9, 19.7, 20.6, 21.6 and 22.9, indicating the crystalline nature of dutasteride (Figure 3.14). However, when dutasteride was formulated into NLCs either coated or uncoated with CSO-SA or CSO-LA, the crystallinity of the drug reduced with evidence of amorphous structure. There was only a broad diffraction peak at  $2\theta$  of 6.6 and 21.5 which came from the stearic acid as the main ingredient used in the formulation. By comparing pure stearic acid with DST in NLCs system, either coated or uncoated with CSO-SA or CSO-LA, the peak intensities were weaker, indicating the degree of crystallinity of stearic acid in the NLCs system was reduced. This result agrees with similar research where the degree of crystallinity of monocaprates was reduced when formulated in SLNs and NLCs (Lin et al., 2007). Coating DST-NLCs with 5% CSO-SA or 5% CSO-LA produced no difference in the XRPD diffractogram.

The physical mixture (dutasteride, stearic acid, Phosal® 53 MCT, Lutrol® micro 68, either with or without 5% CSO-SA/5% CSO-LA was homogeneously mixed using pestle and mortar), gave sharp diffraction peaks at  $2\theta$  of 6.65, 21.5 and 24.2 which came from the stearic acid. There were also broad peaks at  $2\theta$  of 23.2 which came from Lutrol® micro 68. Hence, when dutasteride is loaded into NLCs, either coated or without coated, the degree of the crystallinity of dutasteride is reduced, and there is evidence of the amorphicity, and dutasteride appears homogeneously dispersed in the NLC system.

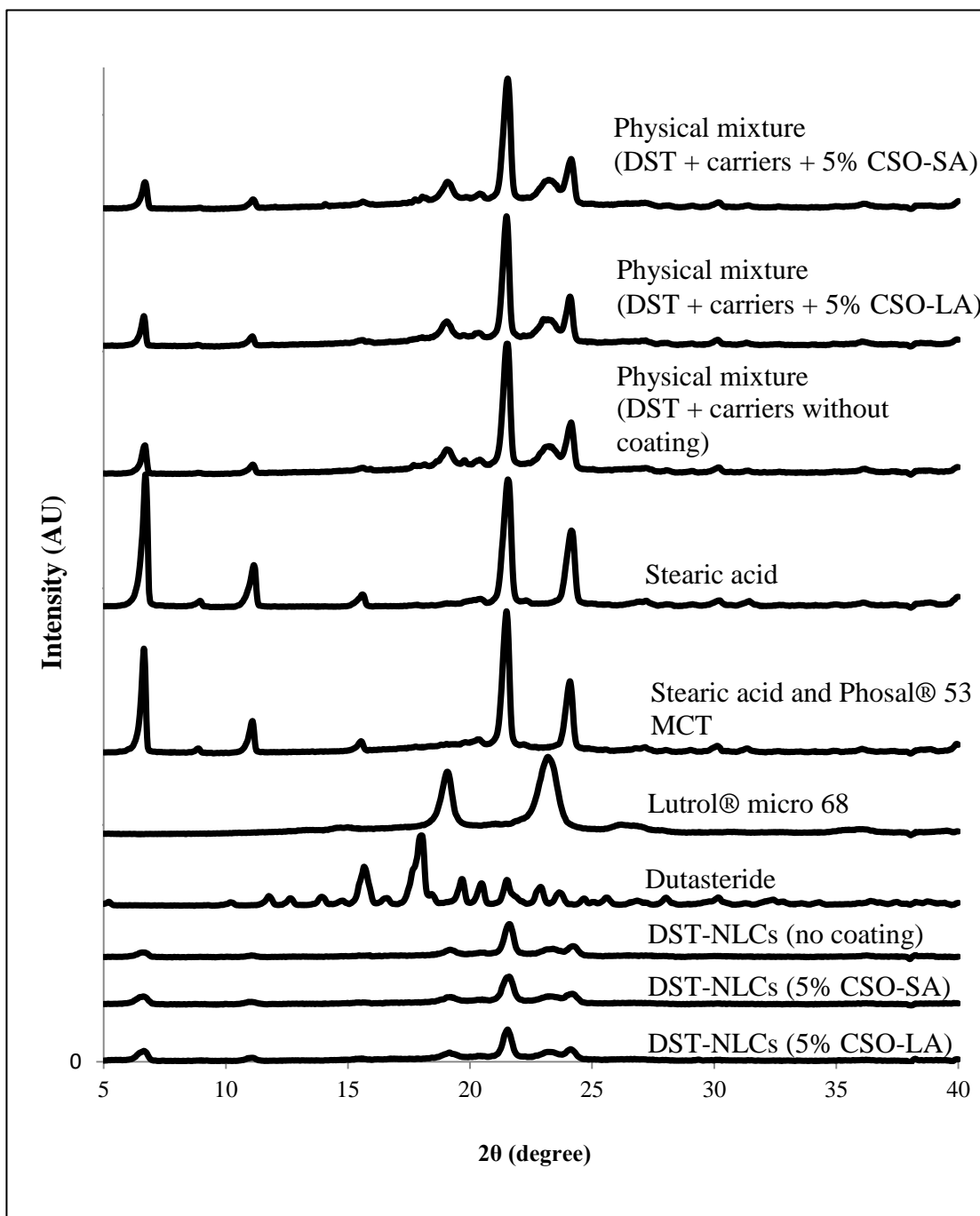


**Figure 3.14** X-ray diffractograms of dutasteride, physical mixture and freeze-dried formulations DST-NLCs uncoated and coated with CSO-SA and CSO (carriers: stearic acid, Phosal® 53 MCT, Lutrol® micro 68)

### 3.5.3.5 DSC of DST-NLCs, uncoated and coated with 5% CSO-SA, 5% CSO-LA and physical mixture of formulations components

Figure 3.15 shows DSC thermograms for dutasteride alone, stearic acid, Lutrol® micro 68, freeze-dried DST-NLCs, uncoated and coated with 5% CSO-SA or 5% CSO-LA, and physical mixtures of bulk materials with and without CSO-SA or CSO-LA. In this study, all samples show endothermic peaks. Dutasteride has a sharp endothermic peak at 249.97°C, corresponding to the melting point of dutasteride (GlaxoSmithKline Inc., 2013). This demonstrated the crystalline nature of the drug, in agreement with XRPD data (Section 3.5.3.4). Stearic acid, used as the main ingredient of NLCs also showed a sharp endothermic peak at 69.09°C which showed that it was in the crystalline state, in agreement with the literature (Inoue et al., 2004).

The physical mixture of dutasteride, stearic acid, Phosal® 53 MCT and Lutrol® micro 68 (without coating) produced no endothermic peak for dutasteride. Medium chain triglyceride in the Phosal® 53 MCT as a liquid lipid acts as a solvent for dutasteride. The endothermic peaks for stearic acid melting in the physical mixture with or without 5% CSO-SA or 5% CSO-LA were 68.5, 67.9 and 68.6°C, respectively.

A similar result was found for freeze-dried DST-NLCs uncoated and coated with 5% CSO-SA or 5% CSO-LA, where no endothermic peak of dutasteride was observed as it is likely that dutasteride dissolved in the lipid carriers. However, the endothermic peaks for stearic acid were shifted to 66.3, 66.1 and 66.0°C for the freeze-dried DST-NLCs uncoated and coated with 5% CSO-SA and 5% CSO-LA. Endothermic peaks for freeze-dried DST-NLCs uncoated were sharper compared to those coated with 5% CSO-SA or CSO-LA, which produced broader peaks. These results suggest that the presence of chitosan was in agreement with a previous study (El-Hefian et al., 2011). El-Hefian et al., (2011) reported that decreasing the ratio of chitosan/PVA produced broader peak and shifted the peak to a lower temperature.

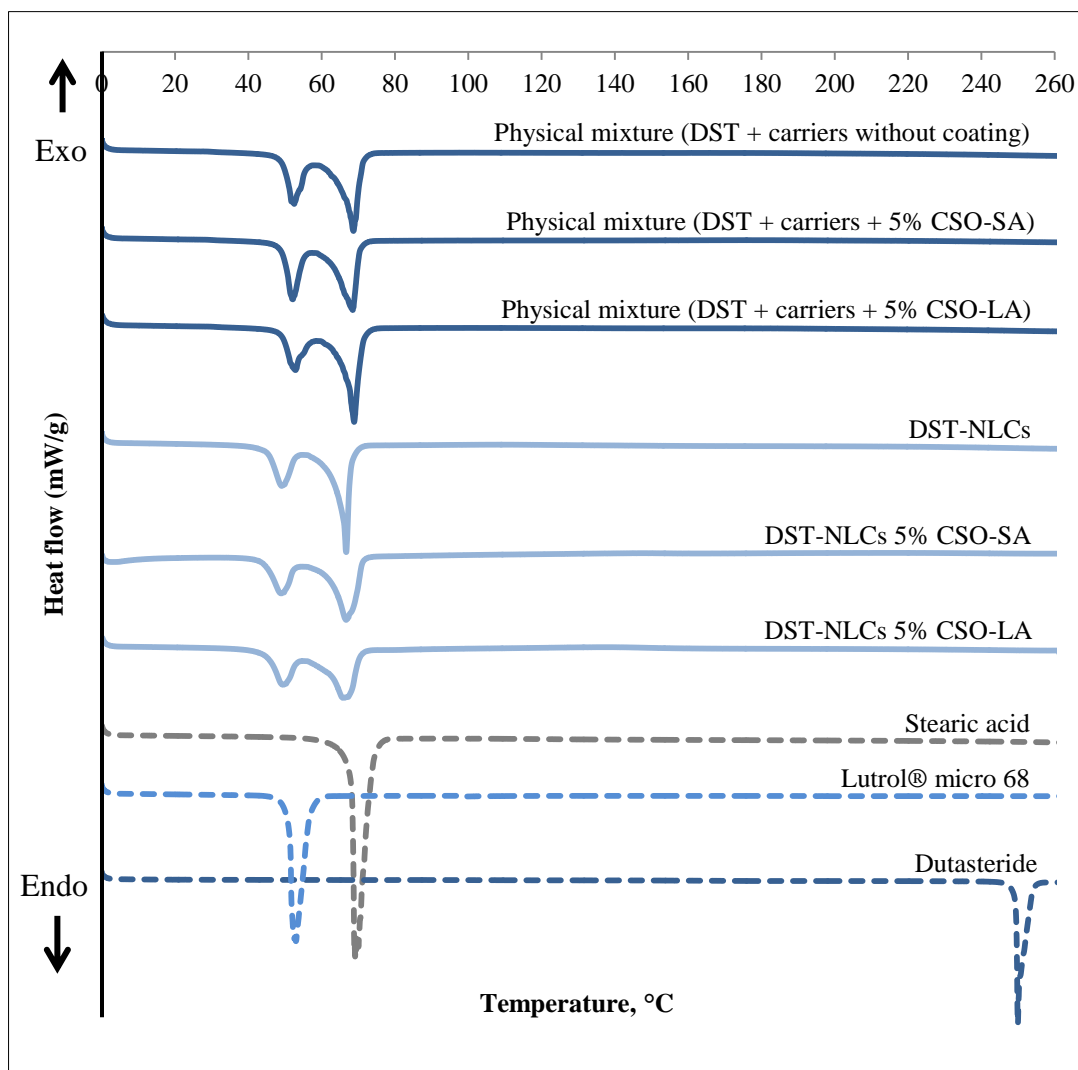


**Figure 3.15 DSC thermograms of dutasteride, physical mixture and freeze-dried formulations DST-NLCs uncoated and coated with CSO-SA and CSO (carriers: stearic acid, Phosal® 53 MCT, Lutrol® micro 68)**

The absence of an endothermic peak of drug melting in the nanoparticles formulation suggests that drug was in the amorphous state as in agreement with Lin et al. (2007). It can be concluded that dutasteride was in the amorphous phase and homogeneously dispersed in the NLCs, either coated or uncoated with 5% CSO-SA or 5% CSO-LA. These less crystallinity structure (due to the combination of solid lipid and liquid lipid in the NLCs system) suggests a sustained dutasteride release to the skin which is suitable for the topical application as described in the previous study (Pardeike et al., 2009). It is suggested that a sustained drug release is suitable

for drugs that are irritating at high concentrations or for drugs that need to be applied for long duration.

### 3.5.3.6 Viscosity of DST-NLCs uncoated and coated with 5% CSO-SA and 5% CSO-LA

As shown in Table 3.19, the dynamic viscosity of DST-NLCs uncoated with 5% CSO-SA or % CSO-LA at an angle of 70° was 1.088 mPa.s at 20°C. There was no significant difference ( $p>0.05$ ) when the angle of the capillary was decreased from 70° to 60° and 50°. However, when the temperature was increased from 20°C to 32°C and 37°C at a 70° angle, the viscosity of the sample significantly reduced ( $p<0.05$ ).

**Table 3.19 Viscosity of DST-NLCs uncoated and coated with CSO-SA or CSO-LA at different temperature and angles (n=3, mean ± SD)**

Temperature	Dynamic viscosity at different angles, mPa.s		
	70°	60°	50°
<u>DST NLCs</u>			
20°C	1.088 ± 0.025	1.092 ± 0.030	1.095 ± 0.035
32°C	0.856 ± 0.027	0.858 ± 0.029	0.860 ± 0.033
37°C	0.785 ± 0.031	0.787 ± 0.034	0.792 ± 0.042
<u>DST NLCs 5% CSO-SA</u>			
20°C	1.160 ± 0.012	1.160 ± 0.011	1.161 ± 0.011
32°C	0.881 ± 0.016	0.880 ± 0.015	0.879 ± 0.014
37°C	0.787 ± 0.014	0.785 ± 0.013	0.783 ± 0.014
<u>DST NLCs 5% CSO-LA</u>			
20°C	1.156 ± 0.028	1.149 ± 0.018	1.145 ± 0.013
32°C	0.878 ± 0.007	0.877 ± 0.006	0.878 ± 0.002
37°C	0.797 ± 0.004	0.795 ± 0.003	0.794 ± 0.002

The dynamic viscosity for DST-NLCs coated with 5% CSO-SA at an angle 70° (at 20°C) was significantly greater ( $p < 0.05$ ) than for the uncoated DST-NLCs. Similar results as with DST-NLCs were found, with no significant difference ( $p > 0.05$ ) when the angle was decreased to 60° and 50°. When the temperature was increased to 32°C and 37°C, the viscosity was found to reduce significantly ( $p < 0.05$ ).

Similarly with DST-NLCs, coating with 5% CSO-LA, increased viscosity of the formulation to 1.156 mPa.s (70° angle at 20°C). No significant difference ( $p > 0.05$ ) was found when the angle was decreased to 60° and 50°. Similarly increasing the temperature to 32° and 37°, reduced viscosity ( $p < 0.05$ ). By increasing the temperature, the molecules move faster and reduced the viscosity (Al-Shammari et al., 2011).

Usually, colloidal suspensions do not follow the Newtonian behaviour which has a linear relationship between shear stress and shear rate (Bergenholtz et al., 2002). Based on these results, for coated and uncoated DST-NLCs, changing the angle of flow did not change the dynamic viscosity. These results indicate the formulations were acting as Newtonian fluids, suggesting the nanoparticles prepared were too dilute. As chitosan is used as a natural thickener for topical or oral applications, adding chitosan in the formulation increased the viscosity of the products, suggesting a better retention of drug on the skin and a reduction of drug in the receptor chamber, which could reduce the systemic side effects as reported from the previous study (Siqueira et al., 2011). The research was performed on the abdominal porcine skin using Franz diffusion cell and found benzophenone-3 loaded chitosan-coated polymeric nanoparticles has lower amount of drug was found in the receptor compartment compared to control formulation and uncoated nanoparticles.

### 3.6 Conclusions

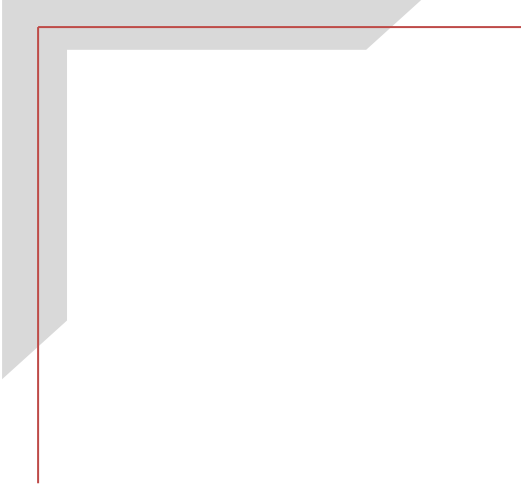
The aim of this chapter is to prepare dutasteride-loaded nanostructured lipid carriers (DST-NLCs), coated with chitosan oligomer conjugated with stearic acid, and lauric acid. Based on the results, it can be concluded that:

1. Formulation S4 (100 mg stearic acid, 50 mg Lutrol® micro 68, 25 mg Phosal® 53 MCT and 5 mg dutasteride) was selected based on the ANOVA analysis from

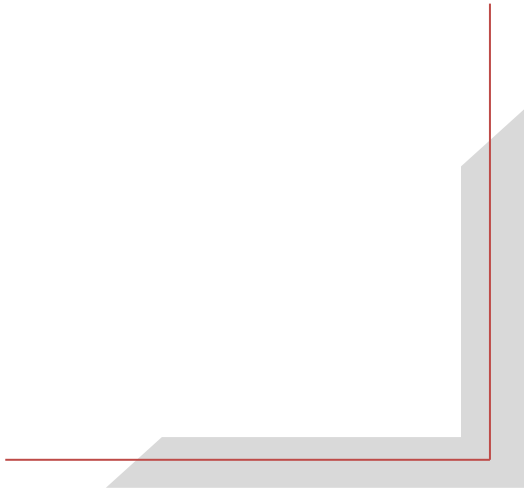
the design of experiments for size distribution at day 14, which predicted the smallest hydrodynamic diameter 231 nm and narrow particle size distribution 0.125 at day 14. At this ratio, the entrapment efficiency was predicted to give 95.1% at day 1.

2. Using this ratio of components, production has been successfully scaled-up to 300 mg of stearic acid content in order to increase the amount of dutasteride that can be incorporated from 0.083 mg/mL to 0.29 mg/mL. No significant difference ( $p>0.05$ ) in the hydrodynamic diameter, PDI and entrapment efficiency was found on scale up. The hydrodynamic diameter, PDI, zeta potential entrapment efficiency and drug loading were 187.6 nm, 0.117, -18.3 mV, 97.3 % and 3.49%, respectively.
3. The entrapment efficiency of DST-NLCs (17.5 mg DST) was  $97.3 \pm 1.2\%$ , and these nanoparticles were stable for up to 180 days at 4-8°C.
4. There was a significant increase ( $p<0.05$ ) in the size of DST-NLCs coated with 5 and 10% CSO-SA and 10% CSO-LA. The zeta potential values of DST-NLCs and those coated with CSO-SA and CSO-LA significantly increased ( $p<0.05$ ) from negative to positive charge which strengthened the evidence of coating.
5. Based on the physical stability study, DST-NLCs uncoated and coated with CSO-SA or CSO-LA were only stable up to 6 months when stored at 4-8°C where all the mean particles sizes were in the range of 250 – 300 nm but not at 25°C (only for DST-NLCS coated with CSO-LA). DST-NLCs coated with CSO without conjugation showed aggregation even at day 30 when stored at both storage conditions.
6. 5% CSO-SA or CSO-LA was chosen as the optimal coating concentration to stabilise the DST-NLCs, where at this concentration which was higher than CMC value, CSO-SA or CSO-LA exist in the micellar system, as in agreement from TEM images.
7. Based on the XRPD and DSC diffractograms, the degree of the crystallinity of dutasteride in NLCs was reduced, and there was evidence of amorphicity of dutasteride and homogeneously dispersion in the NLCs.
8. Values for the viscosity of DST-NLCs formulation either coated or uncoated with 5% CSO-SA or 5% CSO-LA did not change with changes of angles of measurement. These results suggest the formulations were acting as Newtonian fluids, as the sample was too dilute. Increasing the temperature from 20°C to

32°C and 37°C, significantly reduced the viscosity, whilst adding chitosan conjugated in the formulation increased the viscosity ( $p < 0.05$ ) of the products.



# **Chapter 4 *In vitro* characterisation of nanostructured lipid carrier formulations**



## 4.1 Introduction

The first section of this chapter describes *in vitro* release and permeation studies of formulations described in Chapter 3 either uncoated or coated with CSO-SA, CSO-LA or CSO. An *in vitro* release study was conducted in order to determine the rate of release of drugs from the nanoparticles systems. Additionally, *in vitro* permeation studies were conducted to quantify the amount of drug present in the skin and potential systemic exposure following application of the formulations. In order to mimic topical application of the formulation, both *in vitro* release and permeation studies were performed using a vertical Franz diffusion cell (PermeGear, USA).

The second section of this chapter describes *in vitro* studies of cytotoxicity on hair follicle dermal papilla cells and skin irritation studies using 3D reconstructed human epidermis (3D RHE). In order to determine the maximum non-toxic concentration (EC90) of unencapsulated and encapsulated dutasteride-loaded NLCs, MTT assays on normal hair follicle dermal papilla cells were undertaken. Then, skin irritation study was further conducted in order to determine the irritant possibility of the formulation. Both experiments used cells and tissues from the normal human primary cell rather than immortalised cells.

The third section of this chapter describes the preparation and characterisation of Cou-6-loaded nanostructured lipid carrier coated with chitosan oligomer-fatty acid. Cou-6 was chosen as a dye in this formulation, since the absence of fluorescing properties for dutasteride ( $\lambda_{\max} = 421$  nm), meant the drug itself could not visualise by fluorescence microscopy. In order to determine the location of nanoparticles in the hair follicle dermal papilla cells (cell uptake study) or pig ear skin (permeation study), NLCs loaded with Cou-6 uncoated and coated with 5% CSO-SA and 5% CSO-LA were prepared. This dye is highly fluorescent and is hydrophobic (Log P = 6.06), compared to dutasteride hydrophobicity (Log P = 5.09), and is a useful model. In order to standardise the exposure of the formulation on the cells and on the pigskin, the same amount of stearic acid, Phosal® 53 MCT, and Lutrol® micro 68 were used. The amount of Cou-6 was optimised and coated with different types of coating materials (5% CSO-SA and 5% CSO-LA) and experiments repeated.

## 4.2 Materials and methods

### 4.2.1 Materials

Stearic acid (n-octadecanoic acid) 98% and minoxidil were purchased from Tokyo Chemical Industry (TCI, UK). Dutasteride (purity >98.0%) [(5 $\alpha$ ,17 $\beta$ )-N-[2,5-bis(trifluoromethyl)phenyl]-3-oxo-4-azaandrost-1-ene-17-carboxamide] and chitosan oligomer (CSO) with molecular weight less than 3 kDa were obtained from Carbosynth Ltd (UK). Phosal® 53 MCT was a gift of Lipoid AG (Switzerland). Lutrol® micro 68 (Poloxamer 188) was obtained from BASF (Germany). Ethanol (96% v/v analytical grade), Cou-6, trifluoroacetic acid, Sephadex G-50 and amphotericin B were obtained from Sigma-Aldrich Company Ltd (UK). Hair follicle dermal papilla cells (passage 2 - cells were taken from a 78-year old man from the occipital area) and growth medium were obtained from Promo-Cell, Germany. Penicillin/streptomycin and PBS pH 7.4 were purchased from Gibco-BRL, USA. Deionised water (PURELAB Option, ELGA, UK) was obtained on site from a water system.

### 4.2.2 *In vitro* release and permeation studies of DST from solution, DST-NLCs, uncoated and coated with CSO-SA, CSO-LA, and CSO

#### 4.2.2.1 Preliminary study of receptor media and types of membrane for release study

Due to the limited solubility of dutasteride in PBS (pH 7.4), preliminary experiments to inform the selection of a suitable dissolution media were performed using 20% ethanol and 2% sodium dodecyl sulphate (SDS). A solubility study of dutasteride in DST-NLCs was undertaken by pipetting 200  $\mu$ L of DST-NLCs (0.29 mg/mL as theoretical solubility) into 10 mL of different types of media which was stirred at ambient temperature ( $\sim$ 20°C) in a glass vial for 30 min. Next, the sample was diluted in ethanol and filtered using a 0.22  $\mu$ m PES membrane syringe filter (Millex®GP, Merck Millipore, UK) before being injected into the HPLC system.

Selection of the membrane for the release study was conducted based on different types of membrane used in previous studies; using a dialysis membranes with molecular weight cut-off 1 kDa and 14 kDa (Spectrum Laboratories, USA) or 0.45  $\mu\text{m}$  nitrocellulose membrane (Merck Millipore, Ireland) (Madheswaran et al., 2013; 2015).

#### **4.2.2.2 *In vitro* release of DST from solution, DST-NLCs, uncoated and coated with CSO-SA, CSO-LA and CSO**

*In vitro* release was studied using a Franz diffusion cell (PermeGear, USA). A 0.45  $\mu\text{m}$  nitrocellulose membrane (MF<sup>TM</sup> Membrane Filters, Merck Millipore, Ireland) was mounted on the Franz diffusion cell (surface area = 0.64  $\text{cm}^2$ ), maintained at  $37 \pm 1^\circ\text{C}$  and stirred using a magnetic stirrer (600 rpm), with receptor chamber filled with 5 mL of PBS pH 7.4 with addition of ethanol or SDS. DST-NLCs, with or without CSO conjugated or non-conjugated, and dutasteride in 70% ethanol as control (250  $\mu\text{L}$ ), were pipetted in the donor chamber and sampling (200  $\mu\text{L}$ ) was performed at 0, 0.25, 0.5, 1, 2, 3, 6, 8, 12, 24, 30 and 36 h from the receptor chamber. Sample was replaced with 200  $\mu\text{L}$  of temperature-equilibrated fresh buffer. Samples were injected into the HPLC to determine drug release using the assay described in Section 3.1.2.

#### **4.2.2.3 Preliminary study of types of membrane for permeation study**

Different types of membrane were studied for the permeation studies from synthetic and animal sources; a) synthetic membrane (Strat-M®, transdermal diffusion membrane from Millipore which comprised different layers of membrane mimicking the layers of the epidermis and dermis) and b) a full thickness pig ear skin. Strat-M® and pig ear skin were selected based on previous reports (Jacobi et al., 2007; Şenyiğit et al., 2010; Raber et al., 2014; Uchida et al., 2015). 250  $\mu\text{L}$  of DST-NLCs was pipetted in the donor chamber and sampling (200  $\mu\text{L}$ ) was performed at 0, 0.25, 0.5, 1, 2, 3, 6, 8, 12, 24, 30, 36 and 48 h, with 200  $\mu\text{L}$  of temperature-equilibrated fresh buffer was added to the receptor chamber after sampling.

#### 4.2.2.4 *In vitro* permeation of DST from solution, DST-NLCs, uncoated and coated with CSO-SA, CSO-LA and CSO

An *in vitro* percutaneous absorption or permeation study of the developed formulations was conducted to quantify the amount of drug localised in the skin and potential systemic exposure as described by The Organisation for Economic Co-operation and Development (OECD, 2004). In order to mimic topical application of the formulation, *in vitro* permeation was performed using a vertical Franz diffusion cell (PermeGear, USA). Pig ears were obtained from a local slaughterhouse (Farnborough, UK) from a freshly slaughtered pig (used for food consumption). The ears were washed with deionised water and hairs were trimmed carefully with scissors. The pig ear skin (Figure 4.1) was excised using a scalpel and forceps, and the subcutaneous tissue was removed. The average thickness of the skin was ~0.5 mm. The skin was cut and frozen (-20°C) for future use. The diffusion surface area of the Franz cell was 0.64 cm<sup>2</sup>. The receptor chamber was filled with 5 mL of PBS (pH 7.4) with 2% SDS and 0.02% sodium azide and maintained at 37 ± 1°C whilst being stirred using a magnetic stirrer (600 rpm). This methodology assured that the skin surface facing the donor chamber was maintained at 32 ± 0.1°C during the entire experiment (Verkhovskiy et al., 2015).

The skin was mounted between the donor and receptor chambers and allowed to equilibrate for 1 h. 250 µL of DST-NLCs formulation, with or without chitosan, was pipetted into the donor chamber. 200 µL samples were withdrawn at 0, 0.25, 0.5, 1, 2, 3, 6, 8, 12, 24, 30, 36 and 48 h, and 200 µL of temperature equilibrated fresh buffer added to the receptor chamber. Nanoparticle formulations were compared to ethanolic solutions of dutasteride (0.29 mg/mL in 70% v/v ethanol).

After 48 h, the left sample in the donor chamber was collected and dissolved in 2 mL ethanol. Then, the skin was removed from the Franz cell, and the stratum corneum was removed using a tape stripping method with slight modification (Tsai et al., 1991). The skin patch was mounted on a board and a piece of adhesive tape (Scotch Magic Tape, 810,3M, USA), 1.5 cm wide and about 3 cm long, was used to strip the skin. The tape was of sufficient size to cover the full area of the skin which was in contact with the formulation.

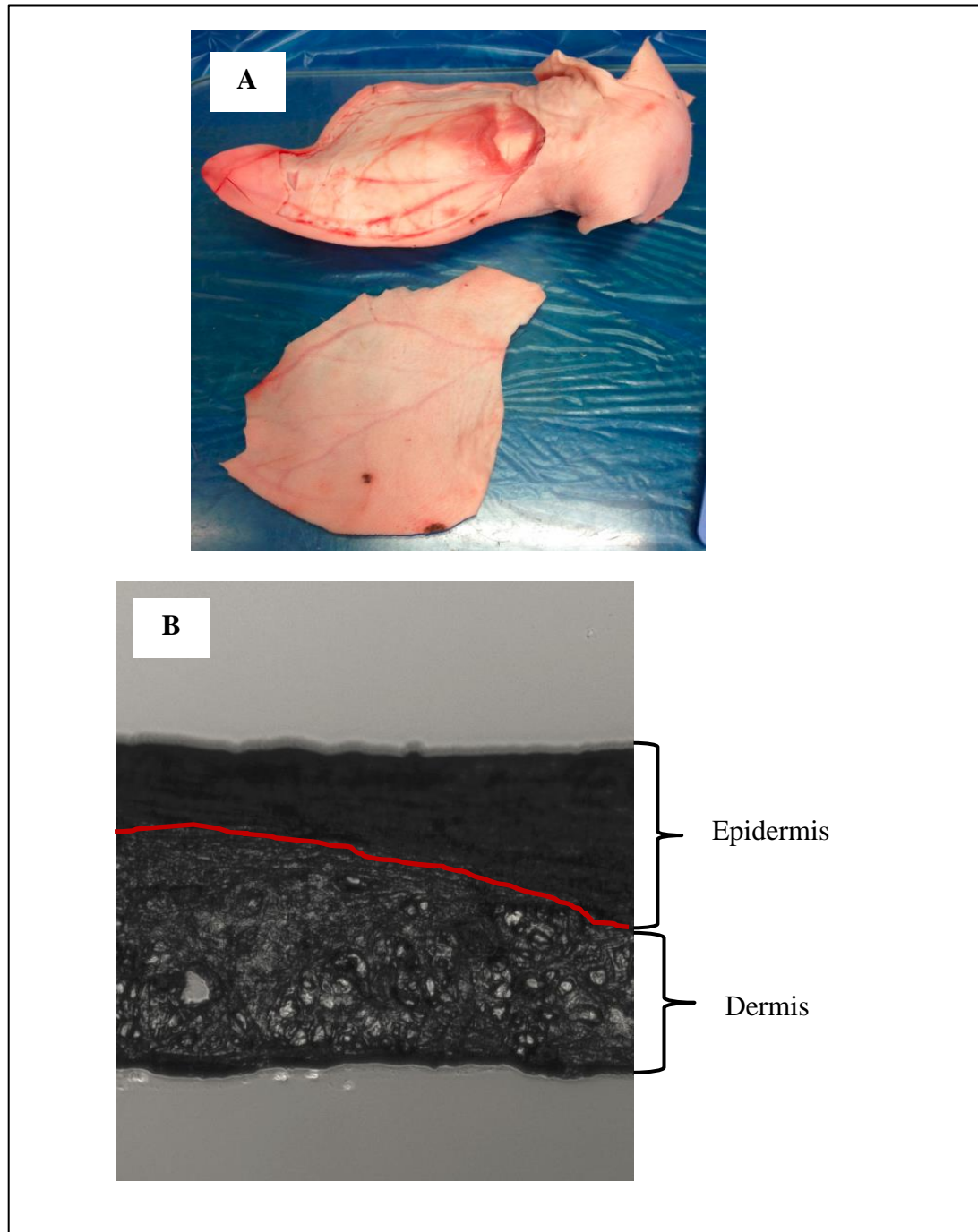


**Figure 4.1 Pig ear skin used for the permeation studies (A) and visualised using a light microscope after being cryotomed at 50  $\mu\text{m}$  thickness (B)**

The stripping procedure was conducted 10 times, and the tapes were transferred into a small vial with the addition of 1 mL of ethanol and bath sonicated for 1 h. Meanwhile, the epidermis/dermis was chopped into small pieces using a

scalpel and stirred for 24 h with 0.5 mL ethanol and further bath sonicated for 1 h. The solutions were filtered using a 0.22  $\mu\text{m}$  PES membrane syringe filter (Millex®GP, Merck Millipore, Ireland) into an insert before injection into the HPLC for quantification of the drug which permeated in the skin. Figure 4.2 shows the in-house set-up of Franz diffusion cells modified from Verkhovskiy et al. (2015). The large shallow water bath was filled with deionised water to the level of the circulation port of Franz cell.

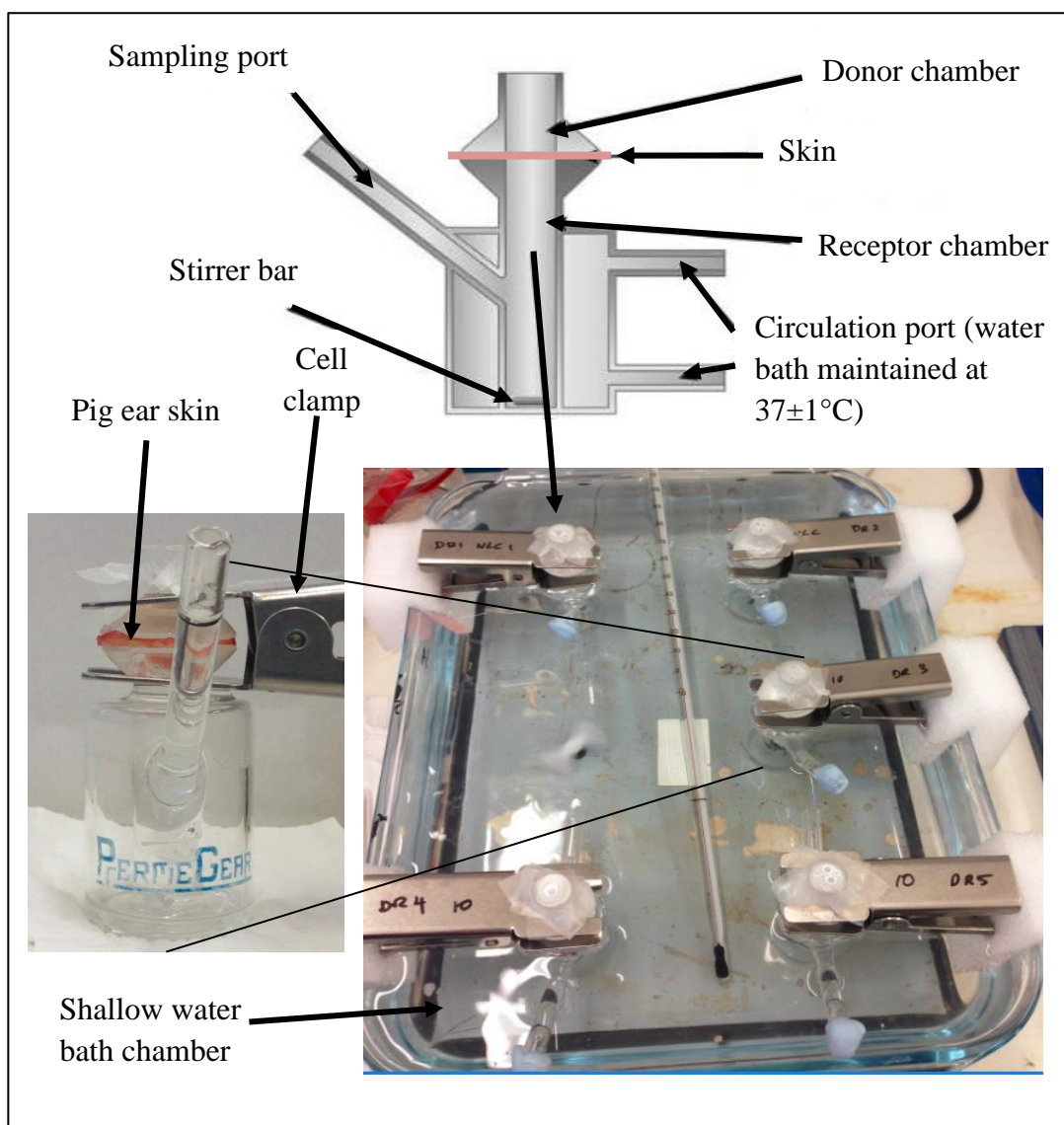


**Figure 4.2** In-house set-up of Franz diffusion cells for permeation study (modified from Verkhovskiy et al., 2015)

The shallow water bath chamber was set-up on a multi-hot plate and stirrer, with a magnetic stirring bar and thermometer. The temperature was set at  $37 \pm 1^\circ\text{C}$ . During the study, deionised water (pre-warmed at  $37 \pm 1^\circ\text{C}$ ) was added periodically to the water bath chamber to replace that lost by evaporation. The pig ear skin was mounted, and a cell clamp was used to hold both donor and receptor chambers in place. After pipetting the sample into the donor chamber, the open donor chamber and sampling port were covered with Parafilm® (Merck Millipore, Ireland) in order to prevent the evaporation.

The total quantity of the drug ( $Q$ ) that diffused to the receptor compartment in time period ( $t$ ) during the steady state and the flux at steady state,  $J_{ss}$  [ $\mu\text{g}/(\text{cm}^2\text{h})$ ], were calculated by Fick's first law using the linear portion of the correlation between the accumulated quantity of drug that diffused through the skin by unit area and time, and the permeation coefficient ( $K_p$ ) was obtained from the relation between the flux and the initial concentration of drug added to the donor compartment as shown in Equations 4-1 and 4-2 (Grams, 2005; Caon et al., 2014). All the experiments were performed 4 times and mean values calculated.

$$J_{ss} = \frac{1}{A} \times \frac{dQ}{dt} \quad \text{Equation 4-1}$$

$$K_p = \frac{J_{ss}}{C_d} \quad \text{Equation 4-2}$$

where:

$J_{ss}$  = flux at steady state,  $\mu\text{g}/\text{cm}^2/\text{h}$

$Q$  = mass of drug diffused to the receptor compartment,  $\mu\text{g}$

$A$  = surface area,  $\text{cm}^2$

$t$  = time, h

$K_p$  = permeation coefficient,  $\text{cm}/\text{h}$

$C_d$  = initial concentration of drug added to the donor compartment,  $\mu\text{g}/\text{cm}^3$

### 4.2.3 *In vitro* proliferation and cytotoxicity of DST-NLCs/empty NLCs, uncoated and coated with 5%CSO-SA and 5% CSO-LA

#### 4.2.3.1 Proliferation and cytotoxicity study

For the *in vitro* study of cytotoxicity, human hair follicle dermal papilla cells (HFDPCs) (Promo-Cell, Germany) were used (Figure 4.3A). The hair follicle dermal papilla cells were isolated from a Caucasian adult man aged 78-years old from an occipital area. The certificate of analysis of human follicle dermal papilla cells is shown in Appendix C. Figure 4.3B shows the cells at a higher magnification (cells with coumarin-6 dye). The cells were grown in HFDPCs growth medium (Promo-Cell, Germany), with 100 IU/mL penicillin/streptomycin (Gibco-BRL, MD) and 2.5 µg/mL amphotericin B (Sigma-Aldrich, UK) in a humidified 95% atmosphere with  $5 \pm 1\%$  CO<sub>2</sub> at  $37 \pm 1^\circ\text{C}$ . Cultured HFDPCs from passage 4-6 were seeded ( $3.75 \times 10^4$  per mL) into 96-well plates (Nunc, Wiesbaden, Germany) and grown to a confluence of 60–70% for 24 h.

The MTT assay is a colourimetric assay using the tetrazolium salt thiazolyl blue for detection of cell viability, cytotoxicity and proliferation (Mosmann, 1983). Many MTT studies have been improved in order to increase their accuracy (Denizot and Lang, 1986; Gerlier and Thomasset, 1986; Hunt and Mchale, 2005). This assay detects only living cells and the colour generated is dependent on the number of living cells present (Mosmann, 1983).

In order to determine the proliferation and cytotoxicity of the cells, a 3-(4, 5-dimethylthiazol-2-yl)-2, 5-diphenyl tetrazolium bromide (MTT) assay was performed. For this study, optimisation of the methodology for cell proliferation/cytotoxicity was conducted whereby different cell densities ( $7.5 \times 10^4$  cell per mL and  $3.75 \times 10^4$  cell per mL) and duration of MTT assay (3 or 5 days) were investigated. Dutasteride in dimethyl sulfoxide (DMSO) was used in this study.

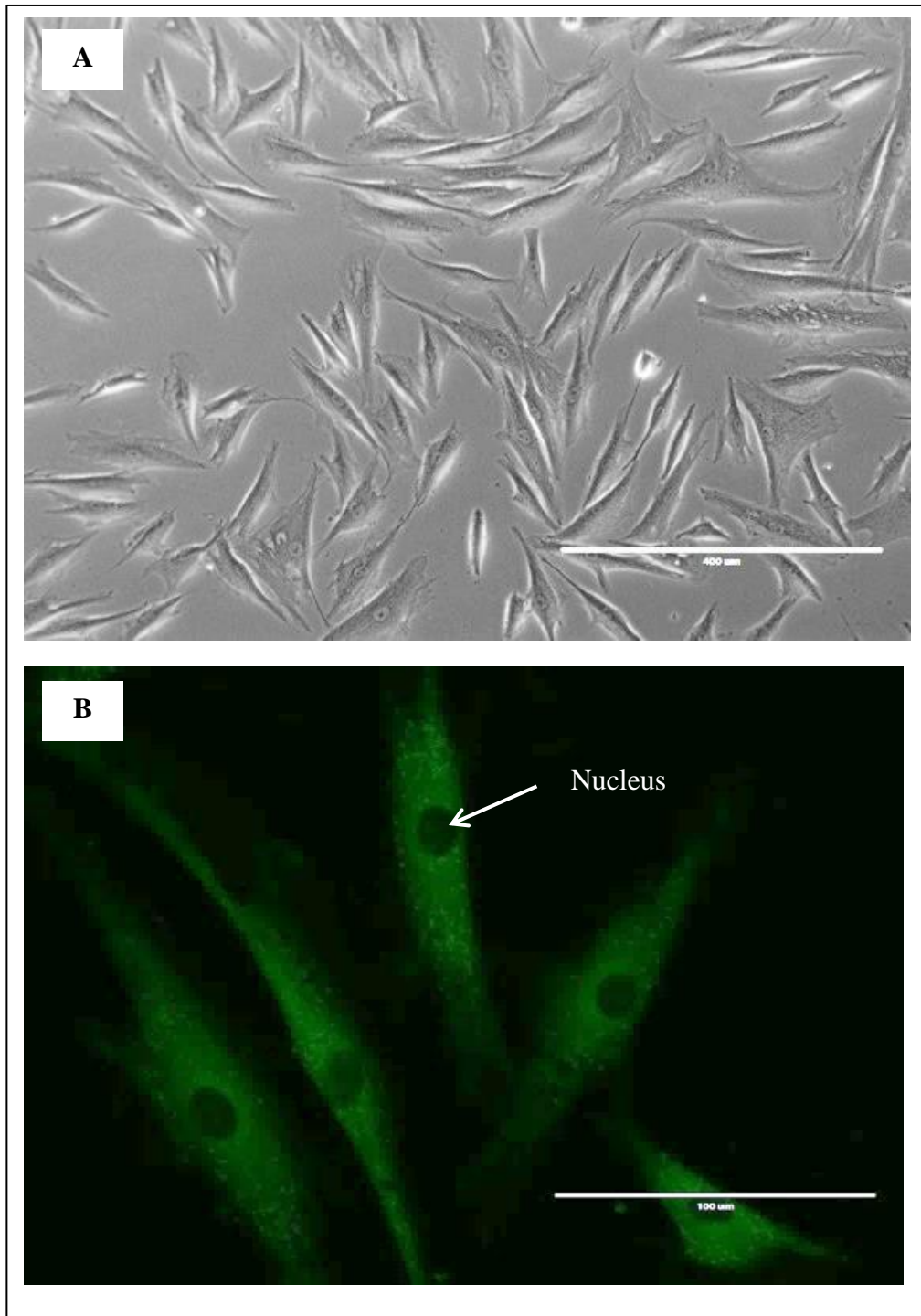


**Figure 4.3** Hair follicle dermal papilla cells (A) and cells with coumarin-6 dye (B)

Figure 4.4 shows the reaction underpinning the MTT assay. MTT solutions were added into the wells containing cells at a certain time point, and the living cells converted MTT (yellow) to MTT formazan producing a purple colour (absorbance at

570 nm). In this study, the MTT assay was performed for 4 hours after 5 days of the treatment time point.

For the treatment, the cell was treated with dutasteride alone (1.6 - 100  $\mu\text{M}$ ), and with dutasteride incorporated into nanoparticles, either uncoated or coated with 5% CSO-SA or 5% CSO-LA (3.125 - 100  $\mu\text{M}$ ). Empty NLCs uncoated and coated with 5% CSO-SA or 5% CSO-LA (at the same concentration as DST-NLCs uncoated and coated with 5% CSO-SA or 5% CSO-LA) were investigated in the same manner in order to study the cytotoxicity of the carrier without dutasteride. As a positive control, cells were treated with minoxidil (100  $\mu\text{M}$ ). After 5 days of treatment, the media were removed.

Stearic acid and lauric acid alone in DMSO were also tested on the cells in order to study the proliferation effect. Different concentration of stearic acid and lauric acid in DMSO (200 – 6.25  $\mu\text{M}$ ) were tested on cells at a density at  $3.75 \times 10^4$  cell per mL and left for 5 days.

On the day of the MTT assay, 5 mg/mL of MTT was dissolved in PBS pH 7.4, vortexed and filtered using a 0.22  $\mu\text{m}$  PES membrane syringe filter (Millex®GP, Merck Millipore, UK) and further diluted into fresh media to obtain a final concentration of MTT of 0.5 mg/mL. The MTT solutions were added into each well, and the plates were incubated for 4 h at  $37 \pm 1^\circ\text{C}$ ,  $5 \pm 1\%$   $\text{CO}_2$ . The supernatant was then removed, and 100  $\mu\text{L}$  of DMSO was added to dissolve the MTT formazan products.

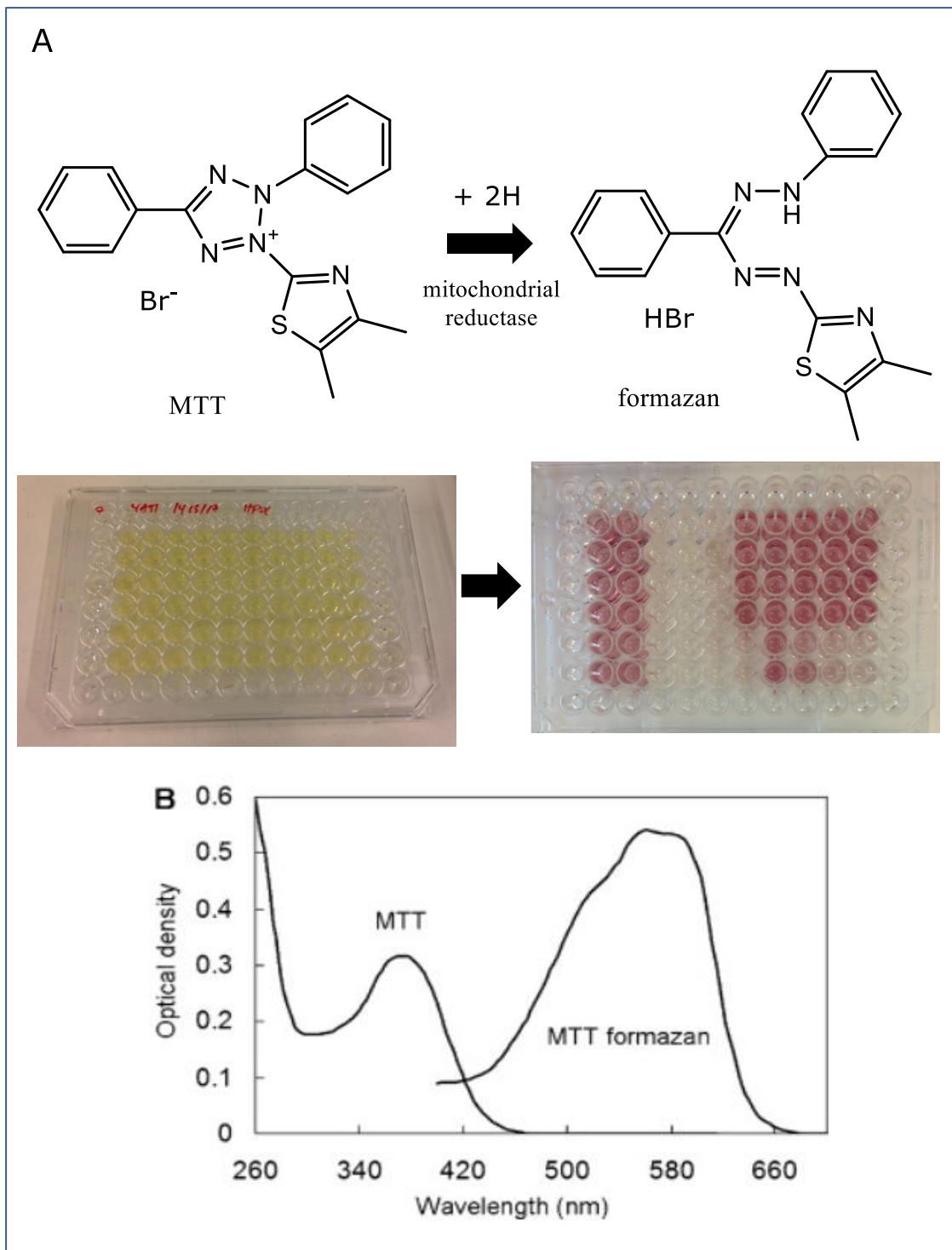


**Figure 4.4** Chemical structure of MTT and MTT formazan (A) and absorption spectra of MTT in water and MTT formazan in sunflower oil (modified from Stockert et al., 2012)

Absorbance was measured spectrophotometrically at 570 nm using a microplate reader (SpectraMax®M2e, Molecular Devices, USA). The 50% inhibitory dose values ( $IC_{50}$ ) was defined as the concentration of formulation or drug inhibiting 50% of the cells, and the maximum non-toxic concentration (MNTC),  $EC_{90}$  was defined as the concentration of formulation or drug inhibiting 10% of the cells. These were calculated by regression analysis of the dose-response curves generated using OriginPro 9.1 Software (USA). Results were calculated as percentages of untreated controls in four cultures, with values expressed as means  $\pm$  SD.

#### **4.2.4 *In vitro* skin irritation study using EpiDerm™ SIT 3D reconstructed human epidermis (RHE)**

The skin irritation study was conducted in order to identify formulations that may be cutaneous irritants. Currently, there are two types of skin irritation studies, with the test compound either tested on animals (*in vivo*) or cells/tissue (*in vitro*). *In vivo* skin irritation studies are generally performed on rabbits (Draize rabbit test) as described in OECD TG 404 (OECD, 2002). The albino rabbits are exposed to test substances and left for 4 h. At the end of the exposure period, the test substances should be removed using water. All animals are then examined for signs of erythema and oedema, and the responses scored at 60 min, and then at 24, 48 and 72 hours after patch removal.

In order to meet the 3R (Replacement, Reduction and Refinement) requirements regarding animal studies, several human-derived tissues have been produced and validated especially for cosmetic and pharmaceutical applications. In March 2009, the European Commission banned animal testing on any finished cosmetic product or ingredients, and in March 2013 they prohibited the marketing and sale of finished cosmetic products or ingredients tested on the animal (Fischer, 2015). Hence, an *in vitro* skin irritation studies on human-derived tissue has been used widely and is considered the best alternative to *in vivo* studies for cosmetic and pharmaceutical products. Currently, all the validated protocols follow OECD 439 Guidelines (OECD, 2015). Currently, there are number of tissues are commercially available such as EpiDerm™ SIT (MatTek, Slovak Republic), EpiSkin™ SM (SkinEthic, France), SkinEthic™ RHE (SkinEthic, France) and LabCyte EPI-

MODEL 24 SIT (Japan Tissue Engineering Co, Japan) for *in vitro* skin irritation studies.

In this study, EpiDerm™ SIT tissues were used (Figure 4.5), following the supplier's protocol (MatTek *In vitro* Life Science Laboratories, Slovakia) (Figure 4.6). EpiDerm™ SIT (3D Reconstructed Human Epidermal model) is a multi-layered highly differentiated tissue model consisting of normal, human-derived keratinocytes. The % cell viability was measured by comparing the negative control (Dulbecco's phosphate-buffered saline, DPBS) with the test formulations. The tissues were transferred from agarose to assay medium on receipt, incubated ( $37 \pm 1^\circ\text{C}$ ,  $5 \pm 1\%$   $\text{CO}_2$ , 95 % RH) for  $60 \pm 5$  min and transferred into fresh pre-warmed assay medium and incubated for another  $18 \pm 3$  h (Kandárová et al., 2009).

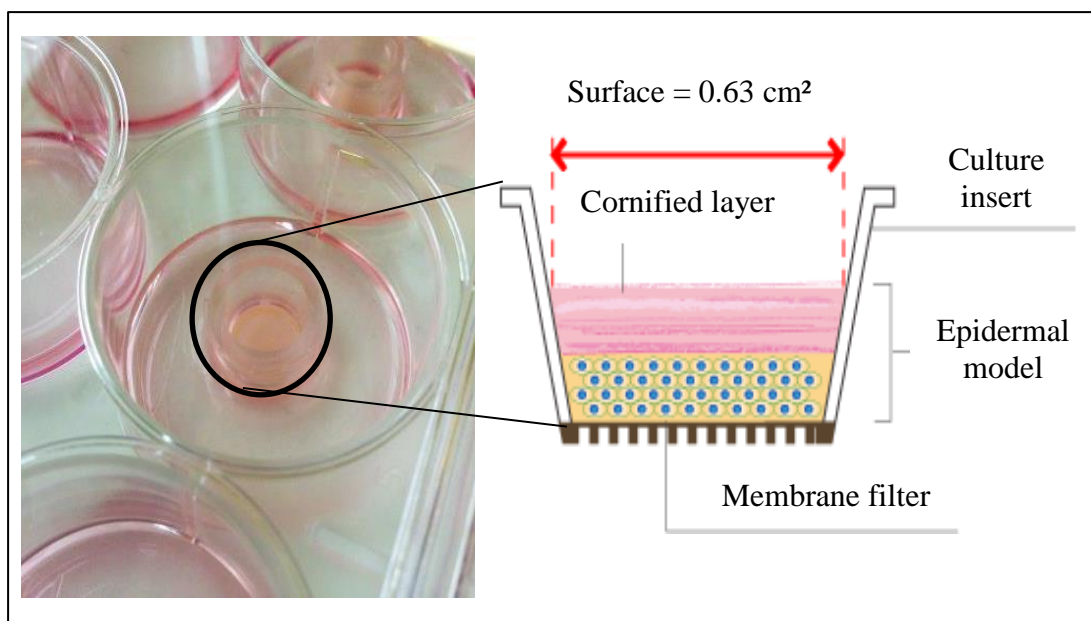


**Figure 4.5 EpiDerm™ SIT (EPI-200) tissues in the medium for skin irritancy testing**

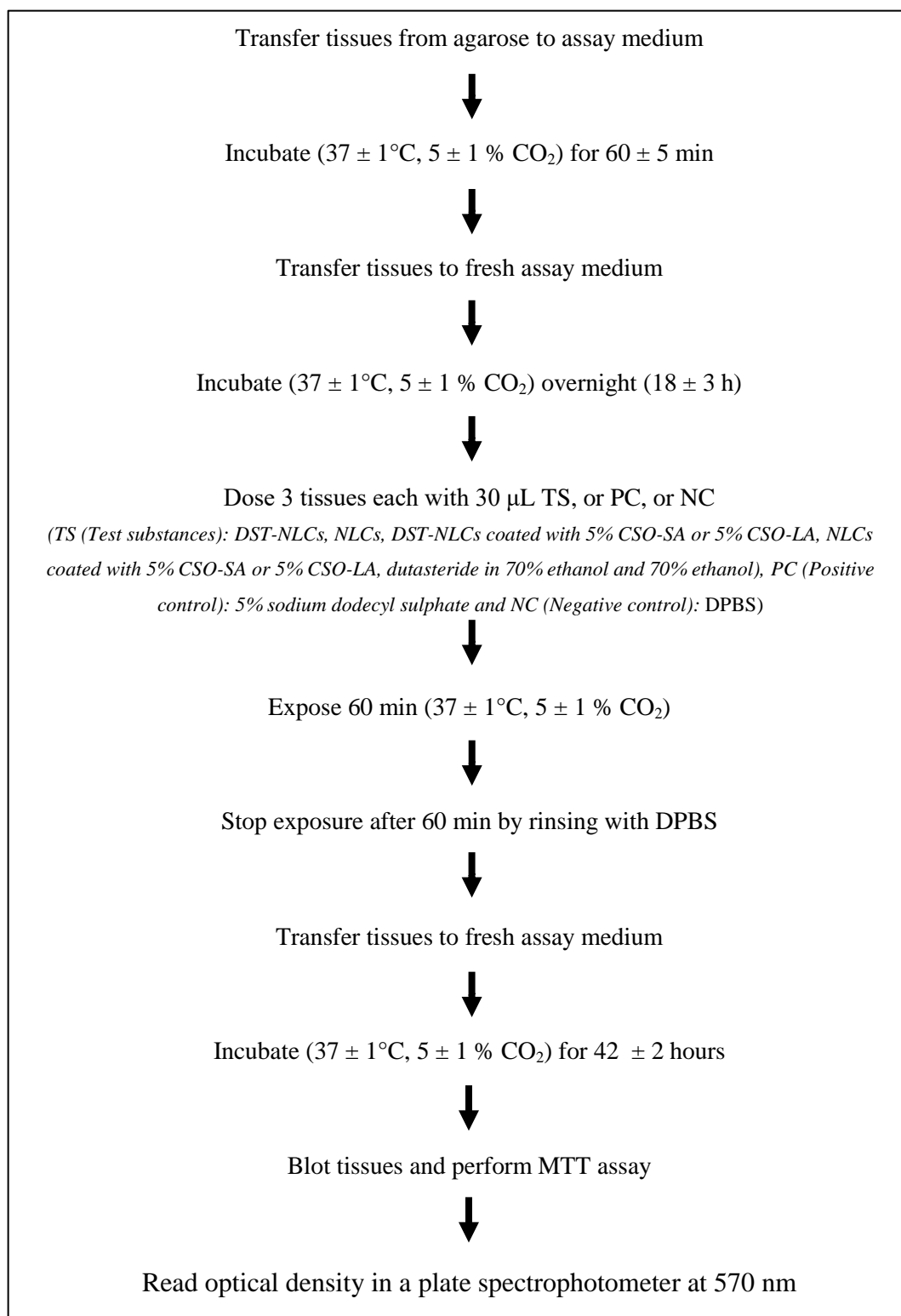


**Figure 4.6 Protocol of skin irritation studies using 3D reconstructed human epidermis skin**

Tissues were dosed with 30  $\mu$ L of test substances (TS: DST-NLCs, NLCs, DST-NLCs coated with 5% CSO-SA or 5% CSO-LA, NLCs coated with 5% CSO-SA or 5% CSO-LA, dutasteride in 70% ethanol and 70% ethanol), positive control (PC: 5% sodium dodecyl sulphate, SDS) and NC: negative control (DPBS). Tissues were exposed to the formulations for 60 min, and then rinsed with DPBS 15 times and transferred into fresh assay medium and incubated for  $42 \pm 2$  h. Tissues were blotted, and the MTT assay was performed. MTT kit containing MTT solutions and isopropanol were supplied by MatTek *In vitro* Life Science Laboratories (Slovak Republic). Formazan products from the cells were extracted using isopropanol for 24 h and read at 570 nm using microplate reader (SpectraMax®M2e, Molecular Devices, USA). Based on the EU and GHS classification (R38/Category 2), an irritant is predicted if the mean relative tissue viability of three individual tissues exposed to the test substance is reduced below 50% of the mean viability of the negative controls (OECD, 2015) as shown in Table 4.1.

**Table 4.1 Interpretation of results of skin irritation study (OECD, 2015)**

<i>In vitro</i> result	<i>In vivo</i> prediction
Mean tissue viability $\leq 50\%$	Irritant (I), (R38 or GHS Category 2)
Mean tissue viability $\geq 50\%$	Non-irritant (NI)

#### 4.2.5 Formulation of coumarin-6 loaded NLCs, uncoated and coated with 5% CSO-SA and 5% CSO-LA

##### 4.2.5.1 Method development and validation of coumarin-6 assay using reverse-phase high-performance liquid chromatography (RP-HPLC)

In this section, coumarin-6 (Cou-6), a fluorescence dye, was chosen as a model compound to be incorporated into the NLCs in order to observe cell and skin uptake, due to the absence of fluorescing properties of dutasteride. The quantitative and qualitative of the composition of others materials in the NLC formulations was

maintained constant. The entrapment efficiency and drug loading of this dye were optimised, requiring development of a reverse phase high-performance liquid chromatography (RP-HPLC) analytical method to determine the amount of Cou-6 in the formulations. In this chapter, a simple, accurate, linear and precise assay for determination of coumarin-6 in the formulation was developed, using reverse phase HPLC with a UV detector.

#### 4.2.5.1.1 Experimental

#### 4.2.5.1.2 Instrumentation and method validation

High-performance liquid chromatography (HPLC) with UV/Vis detector (Agilent 1100 Series, USA) was used to determine the content of Cou-6 in the nanoparticle formulation. A similar mobile phase and stationary phase were used as for dutasteride, except the wavelength for detection of Cou-6 was 466 nm (Table 4.2). Linearity, accuracy, specificity, precision and system suitability, limit of detection (LOD) and limit of quantification (LOQ) were determined according to ICH guidelines for validation of analytical procedures (International Conference on Harmonisation, 1996) as described in Section 3.1.2.

**Table 4.2 HPLC chromatographic condition for determination of Cou-6**

Column:	Synergi™ 4 µm Polar-RP 80 Å, 250 x 4.6 mm
Mobile phase:	Acetonitrile and 0.1% TFA in HPLC grade water (70:30)
Wavelength:	466 nm
Flow rate:	1 mL/min
Injection volume:	30 µL
Run time:	15 min

#### 4.2.5.1.3 Preparation of Cou-6 standard solution

25 mg Cou-6 was weighed accurately and transferred to a 25 mL volumetric flask. Ethanol was added and sonicated to dissolve the dye. Ethanol was added to make up to volume, and the flask was shaken to mix the solution well. The stock solution concentration of Cou-6 was 1000 µg/mL. Serial dilutions were prepared from the stock solution giving 0.5, 1, 2.5, 5, 7.5, 10 and 12.5 µg/mL Cou-6 solutions.

#### 4.2.6 Preparation of Cou-6 loaded NLCs, uncoated and coated with 5% CSO-SA and 5% CSO-LA

Cou-6 loaded nanostructured lipid carriers (Cou-6-NLCs) were prepared based on the method described in Section 3.1.3.2. The weight of Cou-6 was varied from 0.2 to 1.0 mg. Cou-6, 300 mg of stearic acid, 75 mg of Phosal® 53 MCT, 150 mg of Lutrol® micro 68 and 10 mL of water were used. Table 4.3 shows the formulation of the Cou-6-NLCs. Cou-6-NLCs coated with 5% CSO-SA or 5% CSO-LA were prepared following the method described in Section 3.1.3.5. 250 µL of the solution (5 mg/mL of CSO-SA or CSO-LA in 0.2% acetic acid solution) was added, using a syringe, into 5 mL of Cou-6-NLCs with constant stirring for 10 min.

**Table 4.3 Formulation of Cou-6-loaded nanostructured lipid carrier (Cou-6-NLCs)**

<b>Materials</b>	<b>Amount</b>
Stearic acid	300 mg
Phosal® 53 MCT	75 mg
Lutrol® micro 68	150 mg
Cou-6	0.2 – 1.0 mg

#### **4.2.6.1 Characterisation of Cou-6-NLCs, uncoated and coated with 5% CSO-SA or 5% CSO-LA**

Characterisation of the nanoparticles for size distribution and surface charge using Zetasizer ZS were followed the previous method (3.1.3.6.1 and 3.1.3.6.2).

Entrapment efficiency and drug loading were performed as described in the previous section (3.1.3.6.4) except the collected sample after centrifuge was diluted with ethanol in a 5 mL volumetric flask in order to achieve Cou-6 content above LOQ values.

#### **4.2.6.2 Skin and cell uptake studies of Cou-6 in NLCs, uncoated and coated with 5% CSO-SA or 5% CSO-LA and in ethanol**

##### **4.2.6.2.1 Skin uptake study of Cou-6**

The optimised formulation of Cou-6 in NLCs was used in this experiment, and a comparable amount of free Cou-6 (3.3 µg/mL) was dissolved in 70% ethanol as a control. The set-up of the Franz diffusion cells was similar to that for the permeation study (Section 4.2.2.4). The pig ear skin was mounted in Franz diffusion cells and Cou-6-NLCs formulation uncoated and coated with 5% CSO-SA or 5% CSO-LA (250 µL) was pipetted to the donor chamber. At 6, 12 and 24 h, the pig ear skin was removed from the Franz cells and cut into smaller sizes. The skin was left frozen in the Leica CM1850 cryostat (Leica Microsystems, Wetzlar, Germany) (-30°C) before being mounted into the cryostat chuck using OCT (optimum cutting temperature) compound (VWR International, UK). The skin was cryotomed at a thickness of 50 µm using a Leica CM1850 cryostat at -30°C, and skin slices directly transferred to microscope adhesion slides and visualised using an inverted fluorescence microscope (EVOS® FL Imaging System, Life Technologies, USA) with a DAPI LED light cube without removing the stratum corneum.

#### 4.2.6.2.2 Cell uptake studies of Cou-6

For the cell uptake study, in order to ensure the concentration of Cou-6 loaded NLCs would not kill the cells, 25  $\mu\text{M}$  of NLCs (comparable with empty DST-NLCs) as described in Section 4.2.3.2 were used on the hair follicle dermal papilla cells. 1 mL of cells at a density of  $3.75 \times 10^4$  cells/mL were transferred into each 12-well plate (Nunc, Wiesbaden, Germany) and left for 24 h. On the treatment day, 25  $\mu\text{M}$  of uncoated NLCs containing Cou-6, COU-6-NLCs coated with 5% CSO-SA or 5% CSO-LA, and Cou-6 in ethanol were transferred into the 12-well plate. The final concentration of ethanol in the media was maintained at 0.1% in order to avoid cell death. At 1, 3, 6 and 12 h, the media was removed and washed with PBS (pH 7.4) before being visualised using an inverted fluorescence microscope (EVOS® FL Imaging System, Life Technologies, USA) with a DAPI LED light cube at 10X magnification.

### 4.3 Statistical analysis

All data were analysed using either a t-test or one-way ANOVA and Tukey's post-hoc test, using IBM SPSS 23 Statistic Data Editor Software (USA). A *p*-value of less than 0.05 was considered significant for all experiments.

## 4.4 Results and discussion

### 4.4.1 *In vitro* release of DST from solutions, NLCs, uncoated and coated with CSO-SA or CSO

#### 4.4.1.1 Preliminary study of receptor media and types of membrane

Based on previous reports (Xie et al., 2014; Madheswaran et al., 2015), ethanol or sodium dodecyl sulphate was added into the media. In this study, 20% ethanol or 2% SDS were added to PBS (pH 7.4). With 20% ethanol in PBS pH 7.4, only  $0.024 \pm 0.024$  mg/mL of dutasteride dissolved, a higher solubility of drug was

found with 2% SDS ( $0.252 \pm 0.013$  mg/mL). Based on these findings, 2% SDS in PBS pH 7.4 was selected as the receptor medium for future experiments.

Different types of membrane were also screened in order to identify a suitable membrane for this study. Dialysis membranes (1 kDa and 14 kDa MW cut-off), and 0.45  $\mu$ m cellulose membrane were studied. Unfortunately, though the pore size of the dialysis membranes used was larger than the molecular weight of dutasteride (528 g/mol), no drug was detected in the receptor medium using either sizes of dialysis membranes, suggesting an interaction may have occurred between dutasteride and the dialysis membranes. The 0.45  $\mu$ m cellulose membrane permitted detection of dutasteride in the receptor chamber. Consequently, 0.45  $\mu$ m cellulose membrane was used for the release study.

#### **4.4.1.2 *In vitro* release of DST from solution, DST-NLCs, uncoated and coated with CSO-SA, CSO-LA and CSO**

Figure 4.7 shows dutasteride release profile from DST-NLCs uncoated and coated with CSO-SA, CSO-LA and CSO, and release from a solution in 70% ethanol. All nanoparticles formulations produced a measurable release profile at 1, 2, 3, 6 h. However, as the detected amounts were lower than LOQ for the HPLC assay, all values at these time points have not been plotted. All nanoparticle preparations showed rapid release over the first 12 h, with uncoated DST-NLCs exhibiting faster release ( $82.6 \pm 6.0\%$ ) at 24 h than all other formulations ( $p < 0.05$ ). DST-NLCs coated with 5% and 10% CSO-SA had slower drug release due to the presence of the polymer in the outer regions of the particles. The same trend was found for DST-NLCs coated with 5 and 10% CSO-LA, which also had a slower release. Similar findings have been reported on chitosan coating delaying the release of dutasteride compared to uncoated liquid crystalline nanoparticles (Madheswaran et al., 2015). Though, the mean size of DST-NLCs coated with CSO-SA was significantly different ( $p < 0.05$ ) compared to CSO-LA, the release profile did not differ.

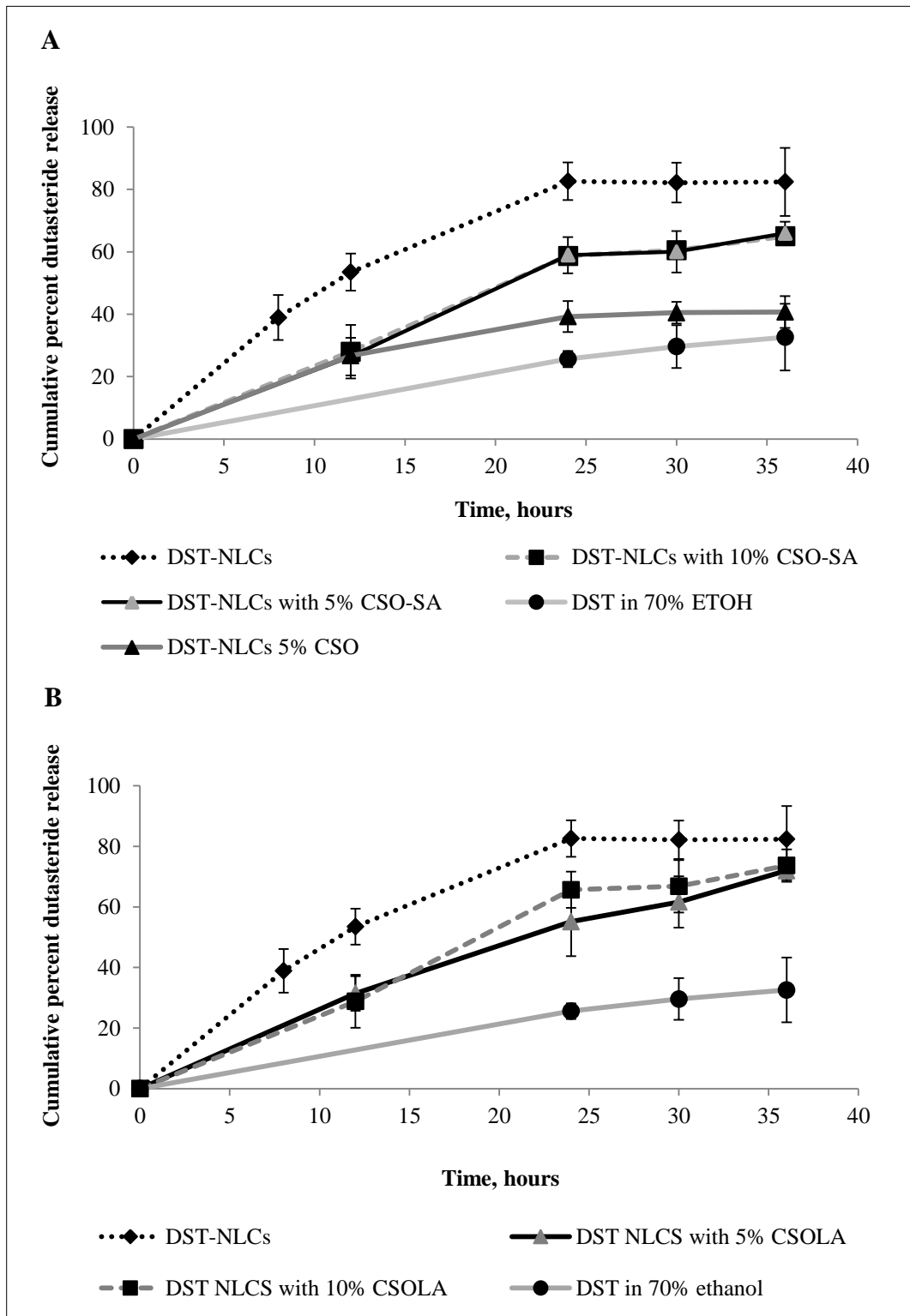


**Figure 4.7** Dutasteride release from different DST-NLC formulations and control (dutasteride in ethanol) (n=3, mean ± SD)

There was no significant difference ( $p>0.05$ ) between DST-NLCs coated with 5 and 10% of CSO-SA, and 5.0 and 10% CSO-LA, all formulations having approximately 26% and 66% drug release at 12 h and 36 h, respectively. Coating DST-NLCs with 5% CSO-SA or CSO-LA may represent the maximum coating of nanoparticles, additional CSO-SA or CSO-LA does not contribute to further retardation of drug release. This result showed that DST-NLCs were successfully coated with CSO-SA and CSO-LA, with a consequent reduction in release rate.

Dutasteride in 70% ethanol (as a control) showed only  $32.6 \pm 10.7\%$  release at 36 h into the receptor medium. This was due to the limited solubility of dutasteride in the receptor media. This result was similar to that described previously whereby dutasteride and finasteride (slightly soluble in water) were released more slowly from an ethanolic solution than from a nanocarrier formulation (Madheswaran et al., 2015).

There was no significant difference ( $p>0.05$ ) in drug release at 36 h between DST-NLCs coated with 5% CSO (no conjugation) and control. DST-NLCs coated with 5% CSO (without conjugation) showed a significantly slower release ( $p<0.05$ ) compared to DST-NLCs coated with CSO-SA and CSO-LA, with  $40.7 \pm 5.1\%$  of drug release at 36 h, suggesting a possibility of unstable formulation and limited solubility of dutasteride in the receptor medium.

Dutasteride in the nanoparticles coated with CSO-SA gave a sustained release of the drug into the receptor chamber, which may be useful for topical or transfollicular delivery. Moreover, when the nanoparticle formulations are applied to the balding scalp area and massaged for a certain time, particles may travel deeper in the transfollicular region from where they may release the drug slowly (Lademann et al., 2007). As a result, this would help to reduce the frequency of usage by the patient.

#### **4.4.2 *In vitro* permeation study of DST from solution, DST-NLCs, uncoated and coated with CSO-SA, CSO-LA and CSO**

*In vitro* permeation studies were performed in order to study the permeation profile of DST-NLCs coated with CSO-SA, CSO-LA and CSO. Different types of

membrane were studied in order to identify the suitable membrane for the permeation study.

Tables 4.4 and 4.5 show permeation parameters of dutasteride from different formulations using Strat® membrane and pig ear skin, respectively. There was a significant difference ( $p < 0.05$ ) for the percent dutasteride permeated between both membranes used. Drug permeation of DST-NLCs was almost 5-fold higher in the Strat-M® membrane compared to pig ear skin over 48 h. At 36 h, some drug was detected in the receptor media from the Strat® membrane. The flux and permeation coefficient using Strat-M® membrane were found to be  $0.646 \mu\text{g}/\text{cm}^2/\text{h}$  and  $0.065 \text{ cm}/\text{h}$ , respectively. No flux or permeation coefficient was calculated for the pig ear skin as no permeation of dutasteride was detected in the receptor chamber after 48 h.

**Table 4.4 Permeation parameters of DST from DST-NLCs using Strat-M® membrane after 48 h (n=4, mean  $\pm$  SD)**

Parameter	Value
DST in the membrane ( $\mu\text{g}$ )	$26.81 \pm 1.66$
Dutasteride permeated (%)	$38.59 \pm 1.81$
Flux, $J_{ss}$ ( $\mu\text{g}/\text{cm}^2/\text{h}$ )	$0.646 \pm 0.028$
Permeation coefficient, $K_p$ , (cm/h)	$0.065 \pm 0.003$
Amount of dutasteride in the membrane per area ( $\mu\text{g}/\text{cm}^2$ )	$41.66 \pm 1.96$
Drug recovery (%)	$81.0 \pm 2.5$

**Table 4.5 Permeation parameters of DST from solution, DST-NLCs, uncoated and coated with CSO-SA, CSO-LA and CSO using pig ear skin after 48 h (n=4, mean  $\pm$  SD)**

<b>Parameter</b>	<b>DST-NLCs</b>	<b>DST-NLCs 5% CSO-SA</b>	<b>DST-NLCs 10% CSO-SA</b>	<b>DST-NLCs 5% CSO-LA</b>	<b>DST-NLCs 10% CSO-LA</b>	<b>DST-NLCs 5% CSO</b>	<b>DST in 70% ETOH</b>
DST in the skin, $\mu\text{g}$	$4.96 \pm 1.36$	$1.80 \pm 0.26$	$1.71 \pm 0.22$	$2.01 \pm 0.22$	$1.84 \pm 0.18$	$1.34 \pm 0.41$	$8.03 \pm 1.27$
% dutasteride permeated	$7.02 \pm 1.93$	$2.91 \pm 0.42$	$2.81 \pm 0.37$	$3.45 \pm 0.37$	$3.01 \pm 0.31$	$2.16 \pm 0.66$	$14.05 \pm 2.05$
Flux ( $J_{ss}$ ), $\mu\text{g}/\text{cm}^2/\text{h}$	N/D	N/D	N/D	N/D	N/D	N/D	N/D
Permeation coefficient ( $K_p$ ), $\text{cm}/\text{h}$	N/D	N/D	N/D	N/D	N/D	N/D	N/D
Amount of dutasteride in the skin per area, $\mu\text{g}/\text{cm}^2$	$6.09 \pm 1.09$	$2.82 \pm 0.40$	$2.70 \pm 0.35$	$3.16 \pm 0.34$	$2.89 \pm 0.28$	$2.11 \pm 0.64$	$12.62 \pm 1.72$
% recovery	$93.2 \pm 2.1$	$88.5 \pm 11.4$	$85.1 \pm 4.0$	$93.1 \pm 1.10$	$116.1 \pm 27.8$	$93.0 \pm 2.9$	$71.2 \pm 10.2$

N/D – non-detectable

The permeation parameters of nanoparticles for pig ear skin and synthetic membrane showed different results which likely due to their difference in structural properties. Uchida et al. (2015) found that the diffusion and partition parameters of certain drugs using Strat® membrane were similar to human and hairless rat skin. However, in their research, the Log P (Log partition octanol/water) was limited between -0.12 to 3.5 at pH 7.4 and the molecular weight of the compound was in a range 152 to 289 g/mol. In contrast with this study, the log P and the molecular weight of dutasteride were high. These characteristics may limit the permeation of drug to the skin and produce different results with pig ear skin.

The follicular structure of pig ear skin is very similar to that of human skin, whereby the infundibula extend deep in the dermis, as in humans (Jacobi et al., 2007). Permeation studies of DST-NLCs, uncoated and coated with CSO-SA, CSO-LA and CSO were conducted using pig ear skin (Table 4.5).

In this study, for all formulations using pig ear skin, no dutasteride was detectable by HPLC in the receptor chamber (LOQ = 3 µg/mL) after 48 h. Hence, considering the amount of dutasteride present in the skin, the highest permeation in the skin ( $12.62 \pm 1.72$  µg/cm<sup>2</sup>) was found from the control (ethanol solution). There was a significant difference ( $p < 0.05$ ) of dutasteride in the skin from ethanol and the nanoparticle formulations. This result was in agreement with the previous research, in that ethanol acts as a penetration enhancer in topical products (Williams and Barry, 2004). They found that, for an ethanol-water co-solvent vehicle, ethanol appears to be concentration dependent, where increasing the amount of ethanol produced dehydration of the biological membrane, thus reducing the permeation across the tissue. Additionally, permeation of ethanol into the stratum corneum can alter the solubility properties of the tissue, resulting in an improvement for drug partitioning into the membrane (Megrab et al., 1995). In this study, 70% ethanol was used and showed higher permeation compared to nanoparticle formulations.

There was a significantly higher ( $p < 0.05$ ) amount of dutasteride in the skin per area for DST-NLCs ( $6.09$  µg/cm<sup>2</sup>) compared to DST-NLCs coated with 5% CSO-SA ( $2.82$  µg/cm<sup>2</sup>), 10% CSO-SA ( $2.70$  µg/cm<sup>2</sup>), 5% CSO-LA ( $3.16$  µg/cm<sup>2</sup>) and 10% CSO-LA ( $2.89$  µg/cm<sup>2</sup>) and 5% CSO ( $2.11$  µg/cm<sup>2</sup>). There was no

significant difference ( $p>0.05$ ) of amount of dutasteride in the skin per area between 5% and 10% of CSO-SA/CSO-LA.

This result was in agreement with previous research (Siqueira et al., 2011). They found that benzophenone-3 was found less in the dermis and epidermis from chitosan coated polymeric nanocapsules of benzophenone-3 compared to those uncoated with chitosan. Firstly, the results can be explained due to different surface charge between chitosan and the skin. As described from the previous research where nanocapsules coated with chitosan increased the retention in the superficial layers of the epithelium (Campos et al., 2003). Secondly, it is due to bioadhesive characteristics of chitosan (Rinaudo, 2006) which limit the penetration of drug to the skin. Thirdly, different viscosities of DST-NLCs, uncoated and coated with CSO-SA or CSO (Section 3.5.3.6) may prevent the nanoparticles penetrating deeper into the skin.

Further experiments, such as *in vivo* studies, are required to confirm and further explore these observed formulation effects on skin permeation. During clinical use, dutasteride will be applied on the scalp, where the surface area will be much larger than the membrane used in this *in vitro* study. Moreover, massaging the scalp will increase the total amount of the drug in the skin; previous research has shown that massage resulted in deeper penetration of nanoparticles in the follicular hair region (Lademann et al., 2007). The small size of these DST-NLCs uncoated and coated with CSO-SA or CSO-LA (200 - 250 nm) will ensure deep penetration into the hair follicle duct (Lademann et al., 2007), whilst the different sizes of nanoparticles may affect the penetration depth (Patzelt et al., 2011). Particles in the size range used in this study would be predicted to penetrate the upper part of the follicle of terminal hair, and would likely penetrate deeper in the vellus hair follicles, especially on the balding site, where the hair is short, thin and fine. Application of ethanol-based formulations produces adverse reactions such as scalp dryness, irritation, burning and contact dermatitis (Lachenmeier, 2008), which can be overcome through nanoparticle formulations.

### 4.4.3 Optimisation of methodology for cytotoxicity studies

#### 4.4.3.1 Effect of different cell density on MTT assays

The cell proliferation study using MTT assay was optimised in terms cell density. Dutasteride alone in DMSO was used for this initial experiment. Based on a previous study (Han et al., 2004),  $7.5 \times 10^4$  cells per mL was initially selected. Then, the cell density was reduced by half,  $3.75 \times 10^4$  cells per mL and the results were compared. Cells at different densities were treated with dutasteride in DMSO and left for 5 days.

After 5 days of treatment, there was no significant difference ( $p > 0.05$ ) in cell viability at the highest concentration (100  $\mu$ M) between both cell densities due to the effect of cell death (Figure 4.8).

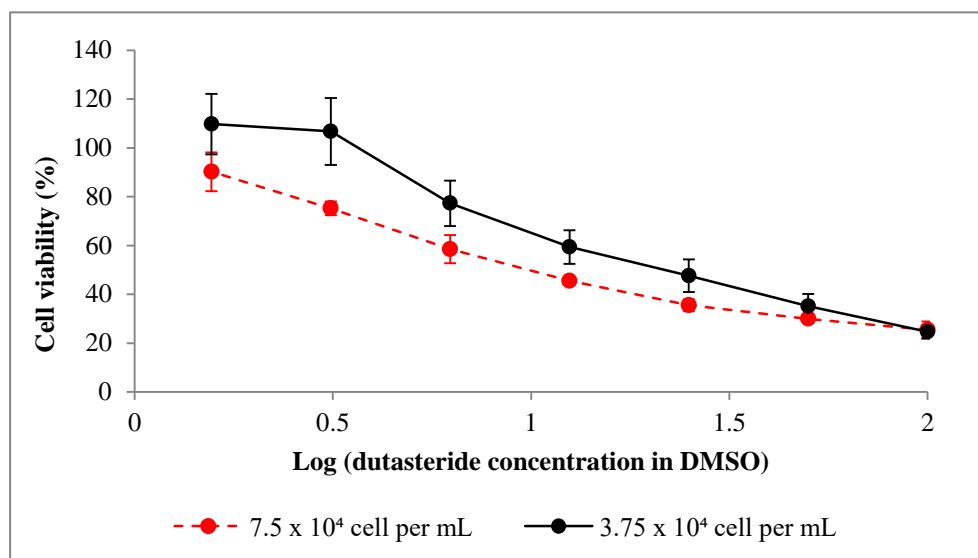


**Figure 4.8 Percentage cell viability for different cell densities of dutasteride in DMSO after 5 days (n=4, mean  $\pm$  SD)**

The highest proliferation observed was only  $90 \pm 7.9\%$  at 1.56  $\mu$ M for the  $7.5 \times 10^4$  cells per mL. At  $3.75 \times 10^4$  cells per mL, cell proliferation increased to approximately  $110 \pm 12.4\%$  at the same concentration. However, there was a

significant difference ( $p < 0.05$ ) in cell viabilities between both cell densities at lower concentrations (1.56 – 50  $\mu\text{M}$ ), suggesting that after 5 days of treatment, when the higher cell density was used, insufficient nutrients for the cells and accumulation of metabolic by-products, resulted in cell death, as previously reported (Butler, 2005). Based on these data, the cell density of  $3.75 \times 10^4$  cells per mL ( $7.5 \times 10^3$  cells per well) was selected for subsequent studies.

#### 4.4.3.2 Effect of different experimental durations on the MTT assay

To establish the optimum duration of the experiment, different durations of treatment were studied. In previous research, most MTT assays for hair growth compounds were conducted for 2 to 5 days of treatment (Han et al., 2004; Jo et al., 2013; Choi et al., 2015; Park et al., 2016). As this experiment was undertaken to study cell proliferation after treatment, a longer duration would be appropriate. In this study, the cells were treated with different concentrations of dutasteride in DMSO for 3 or 5 days. The results showed there was no significant difference ( $p > 0.05$ ) in cell viability between day 3 and 5 (Figure 4.9). The longer duration of the MTT assay (5 days) was chosen for all studies.

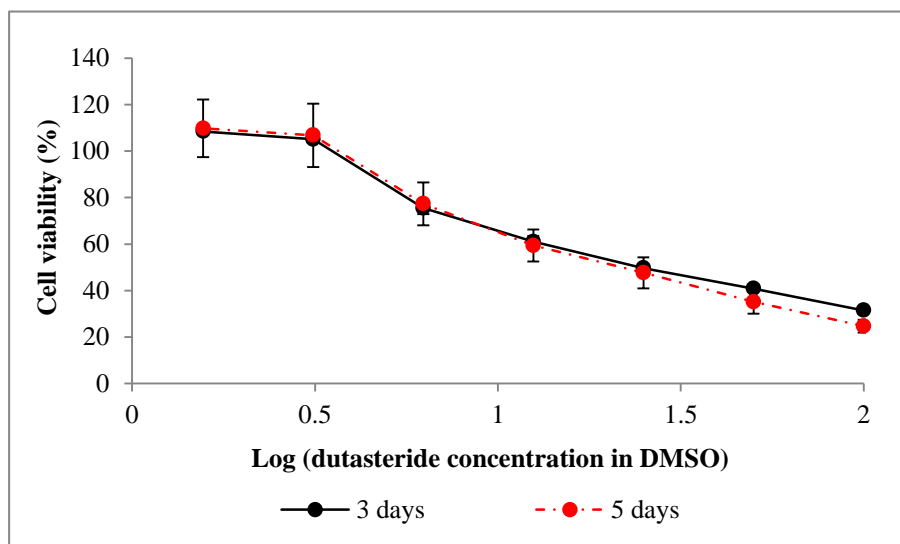


**Figure 4.9 Cell viability study of dutasteride alone in DMSO at different days (n=4, mean  $\pm$  SD)**

#### 4.4.4 *In vitro* cytotoxicity study of DST-NLCs, uncoated and coated with 5% CSO-SA and 5% CSO-LA

Figure 4-10 shows cytotoxicity profiles of dutasteride (in DMSO), empty nanoparticles, uncoated and coated with 5% CSO-SA or 5% CSO-LA and also DST-NLCs, uncoated and coated with 5% CSO-SA and 5% CSO-LA. After 5 days of treatment with various concentrations of dutasteride (alone) and nanoparticles, there was a significant difference ( $p < 0.05$ ) in the cytotoxicity values ( $IC_{50}$ ) between dutasteride in DMSO and nanoparticles.

Dutasteride alone showed cytotoxicity at a very low concentration ( $IC_{50} = 10.4 \pm 1.82 \mu\text{M}$ ). Values of  $IC_{50}$  for DST-NLCs, uncoated and coated with 5% CSO-SA or 5% CSO-LA (Figure 4-11B) were much higher, being  $58.1 \pm 13.0 \mu\text{M}$ ,  $59.3 \pm 13.1 \mu\text{M}$  and  $58.9 \pm 14.8 \mu\text{M}$ , respectively. However, NLCs alone (without dutasteride) uncoated and coated with 5% CSO-SA or 5% CSO-LA also showed cytotoxicity ( $IC_{50}$ ),  $58.1 \pm 13.0 \mu\text{M}$ ,  $59.0 \pm 14.6 \mu\text{M}$  and  $56.2 \pm 12.6 \mu\text{M}$ , respectively in a dose-dependent manner. No significant difference in  $IC_{50}$  was found between DST-NLCs and NLCs ( $p > 0.05$ ).

The maximum non-toxic concentration (MNTC,  $EC_{90}$ ) is defined as the concentration of a formulation or drug inhibiting 10% of the cells.  $EC_{90}$  for dutasteride in DMSO ( $2.1 \pm 0.2 \mu\text{M}$ ) was significantly lower ( $p < 0.05$ ) than dutasteride in nanoparticles and empty nanoparticles. There was no significant difference ( $p > 0.05$ ) in  $EC_{90}$  between uncoated DST-NLCs and those coated with 5% CSO-SA or 5% CSO-LA. The  $EC_{90}$  for DST-NLCs uncoated and coated with 5% CSO-SA or 5% CSO-LA was  $38.1 \pm 13.1 \mu\text{M}$ ,  $53.6 \pm 8.3 \mu\text{M}$  and  $39.3 \pm 11.5 \mu\text{M}$ , respectively. The  $EC_{90}$  for NLCs uncoated and coated with 5% CSO-SA or 5% CSO-LA was  $42.3 \pm 12.4 \mu\text{M}$ ,  $49.4 \pm 6.0 \mu\text{M}$  and  $39.3 \pm 11.5 \mu\text{M}$ , respectively. Similar results were found, with no significant difference ( $p > 0.05$ ) in  $EC_{90}$  between NLCs uncoated and coated with 5% CSO-SA or 5% CSO-LA.

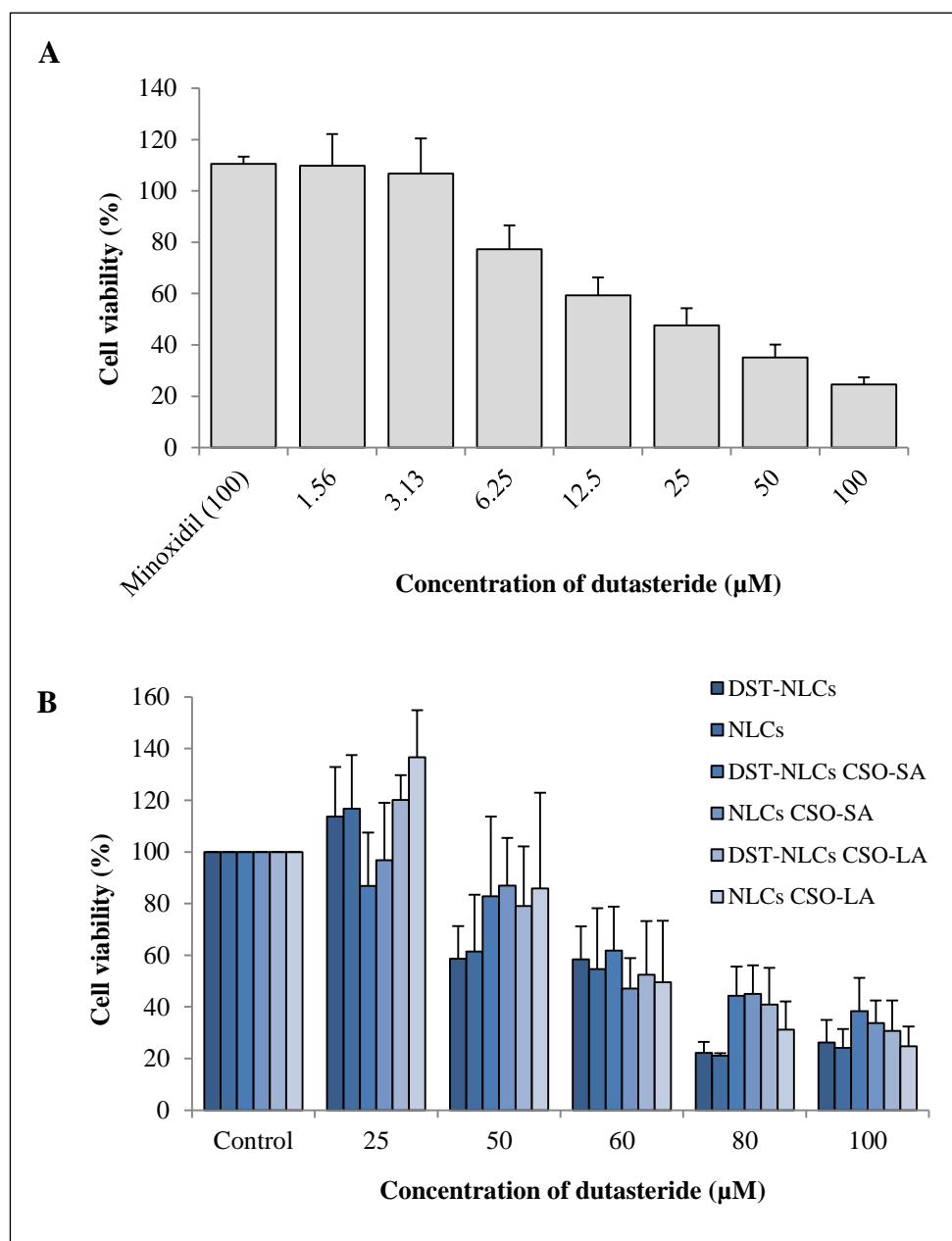


**Figure 4.10** Cytotoxicity of dutasteride alone (A), empty NLCs uncoated and coated with 5% CSO-SA and 5% CSO-LA and DST-NLCs uncoated and coated with 5%CSO-SA and 5%CSO-LA (B) on hair follicle dermal papilla cells (n=4, mean  $\pm$  SD)

Based on these findings, dutasteride in the nanoparticles, either coated with 5% CSO-SA or 5% CSO-LA could be applied at a higher concentration compared to the dutasteride without nanoparticles. This shows that when dutasteride was delivered in the nanoparticles, it increased the EC<sub>90</sub> more than 20-fold. This finding

is supported by the release study (Section 4.2.2) showing a slow release of the drug from the nanocarrier system, which would potentially reduce the toxicity on the cells. When dutasteride was formulated in a nanoparticle formulation, the drug was released slowly allowing a longer period for the drug to interact with the cells and exert its activity, and at the same time preventing the cells being killed immediately.

At 25  $\mu\text{M}$  dutasteride, some of the nanoparticles formulations showed cell proliferation, especially the DST-NLCs and NLCs (empty) coated with 5% CSO-LA which exhibited the highest proliferation of  $120.2 \pm 9.5\%$  and  $136.6 \pm 18.3\%$ , respectively. DST-NLCs and NLCs coated with 5% CSO-SA showed least cell proliferation,  $86.8 \pm 20.6\%$  and  $96.7 \pm 22.3\%$ , respectively.

It should be noted that NLCs (empty nanoparticles) coated with 5% CSO-LA proliferated the hair follicle dermal papilla cells at 25  $\mu\text{M}$  (comparable with the formulation containing dutasteride). As stearic acid is a main ingredient in the nanoparticle preparation, a combination of nanoparticles with 5% CSO-LA may enhance the proliferation of the cell. These findings are in agreement with previous research (Liang and Liao, 1992; Liu et al., 2009), showing that lauric acid had potent  $5\alpha$ -reductase inhibition activity and inhibited proliferation of lymph-node carcinoma cells.

These findings suggest that combination of dutasteride with the carrier and coated with 5% CSO-LA at 25  $\mu\text{M}$  can promote the proliferation of human follicles dermal papilla cells.

#### **4.4.4.1 Effect of stearic acid and lauric acid on cell proliferation**

In order to study whether the observed proliferation of the cells in Section 4.4.4 was due to the presence of stearic and lauric acids, both were dissolved separately in DMSO (200 – 6.25  $\mu\text{M}$  in a final concentration in media). Stearic acid (carbon chain,  $\text{C}_{18}$ ) was selected in this study as it was a major component used in the preparation of NLCs. Lauric acid (carbon chain  $\text{C}_{12}$ ) was used in the conjugation of chitosan oligomer which then used for coating. Due to the limited solubility of stearic acid in DMSO, the highest concentration of fatty acids studied was 200  $\mu\text{M}$  (in final concentration).

Figure 4.11 shows the results of the proliferation study using stearic and lauric acid. Stearic and lauric acid show no cytotoxicity on human follicle dermal papilla cells even at the highest concentration (200  $\mu\text{M}$ ). There was no significant difference ( $p>0.05$ ) between these two fatty acids on cell proliferation at all concentrations tested. Both fatty acids at the highest concentration (200  $\mu\text{M}$ ) showed the highest proliferation;  $122.7 \pm 13\%$  for lauric acid and  $115.6 \pm 6.6\%$  for stearic acid.

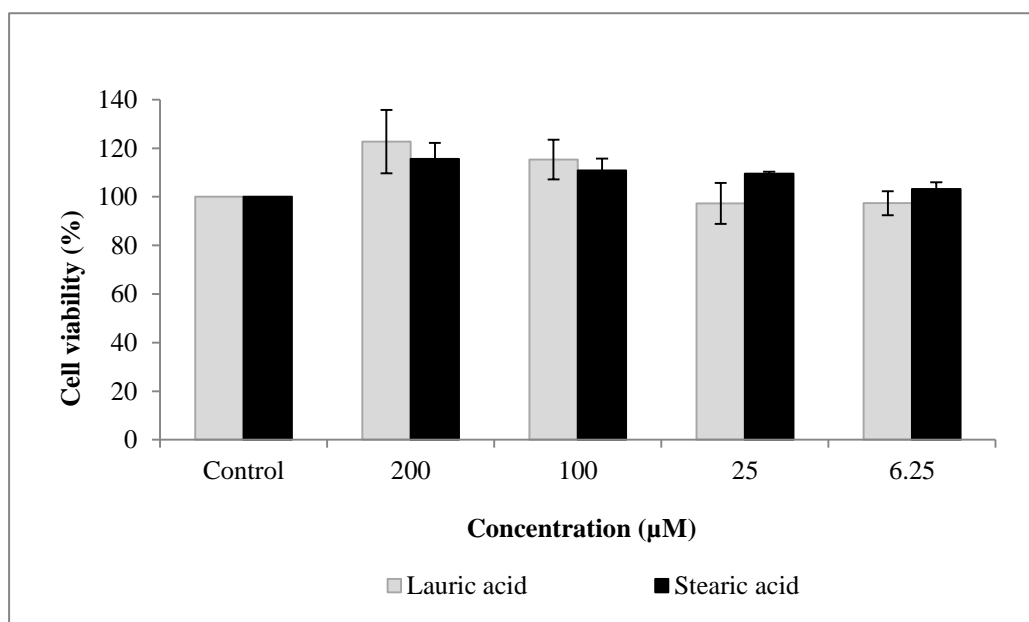


**Figure 4.11** Cell proliferation study of lauric and stearic acids on hair follicle dermal papilla cells (n=4, mean  $\pm$  SD)

This result showed that lauric acid promoted cell proliferation, probably by inhibiting the  $5\alpha$ -reductase enzyme. This result is in agreement with Liu et al. (2009), who found that the unsaturated fatty acid, oleic acid and the saturated fatty acid, lauric acid had a potent effect on the inhibition of the  $5\alpha$ -reductase enzyme. Raynaud et al. (2002) have also reported that free fatty acids (oleic and lauric), the main compounds in a lipido-sterolic extract of *Serenoa repens* (LSESr, Permixon®) inhibit type I and II  $5\alpha$ -reductase activity.

It has been reported previously that stearic acid has very low  $5\alpha$ -reductase activity (Liu et al., 2009), so the result of cell proliferation observed may be due to

the higher concentration has been used in this study. By combining stearic acid and dutasteride in the NLCs system, followed by coating with CSO-SA or CSO-LA, suggesting to enhance the growth of the hair follicle dermal papilla cells. These results showed that NLCs are a promising carrier for delivery of dutasteride to the transfollicular area.

#### **4.4.5 Evaluation of *in vitro* skin irritation using 3D Reconstructed Human Epidermis (RHE)**

In order to explore the potential irritancy of the drug and the NLCs formulations, skin irritation on the 3D reconstructed human epidermis (EpiDerm™ RHE) was investigated using the manufacturer's validated protocol. Using this model, cell viability less than 50% indicates the potential irritancy of ingredients, classified as a GHS Category 2. Figure 4.12A shows the colour of MTT formazan from cells treated with different formulations after MTT assay, as strong purple indicates higher cell viability. All formulations showed no irritancy with the mean cell viability greater than 50% (Figure 4.12B). There was a significant difference ( $p < 0.05$ ) between the positive control (with 5% sodium dodecyl sulphate, produced 7% cell viability) which showed irritancy compared to the negative control (DPBS) and all the formulations. There was no significant difference ( $p > 0.05$ ) in the percent cell viability between the nanoparticles uncoated and coated (with 5% CSO-SA and 5% CSO-LA) formulations and with the negative control (DPBS).

The percent cell viability for 70% ETOH and 0.29% dutasteride in 70% ETOH was significantly decreased ( $p < 0.05$ ) compared to the negative control (DPBS), being  $78.7 \pm 7.3\%$  and  $87.6 \pm 4.7\%$ , respectively. There was no significant difference ( $p > 0.05$ ) in cell viability between 70% ETOH and 0.29% dutasteride in 70% ETOH. Previous research has found that ethanol at a concentration greater than 60% produced irritancy on the EpiDerm™ Skin Model (Genno et al., 1998). Golla et al. (2009) developed a skin irritation quantitative structure-property relationship model using rabbit Draize test data and found that ethanol was an irritant. Typical adverse effects of dryness, erythema and desquamation were found when ethanol, propylene glycol, water-based solutions of minoxidil were repeatedly applied to the skin (Padois et al., 2011). Minoxidil-loaded SLNs produced no irritancy/corrosive

while the commercial products (5% minoxidil in ethanol-propylene glycol and water based) exhibited corrosive potential (Padois et al., 2011).

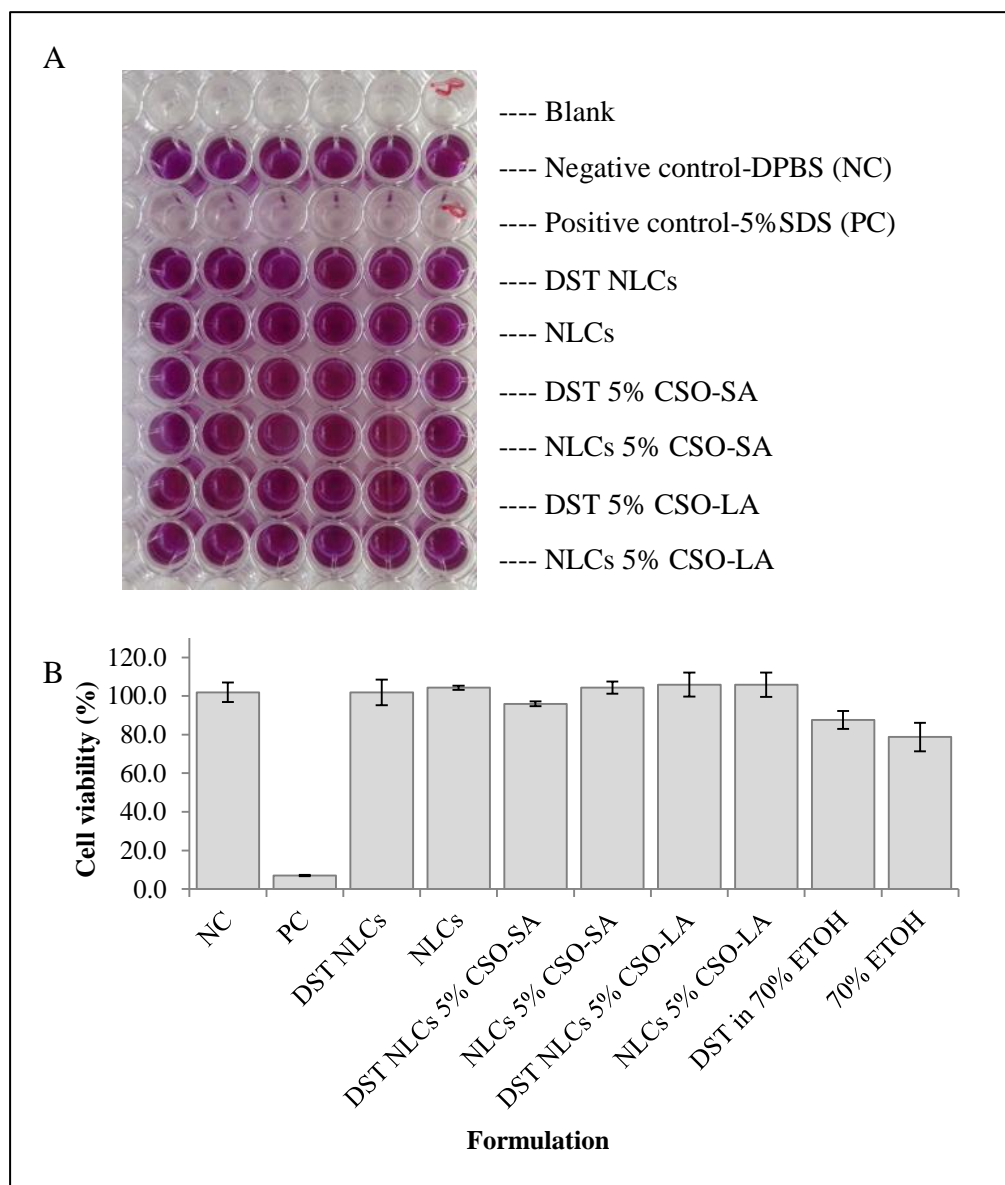


**Figure 4.12** Skin irritation results for different formulations on 3D reconstructed human epidermis (RHE) (n=3, mean  $\pm$  SD)

By comparing the cell viability results of DST-NLCs and DST in 70% ethanol (at the same concentration of dutasteride), there was a significant difference ( $p < 0.05$ ). DST-NLCs, uncoated or coated and those without DST showed no irritation (greater than 96% cell viability), indicating no irritancy effect on the skin.

Dutasteride is categorised as R38, Skin irritation 2 (Fluorochem, 2012), suggesting that delivering dutasteride in the nanoparticles (water being the continuous phase in nanoparticle preparations) to the skin promoted higher cell viability, and lower toxicity compared to ethanol.

Previous studies found that delivering drugs in nanoparticles decreased and/or eliminated skin irritation (Shah et al., 2007; Mandawgade and Patravale, 2008). Shah et al. (2007) prepared tretinoin in SLNs and found that such a formulation was significantly less irritating ( $p < 0.05$ ) to the rabbit skin than a marketed tretinoin cream. Castro et al. (2009) prepared retinoic acid-loaded SLNs and found reduced skin irritation compared to a retinoic acid-based cream, using a female rhino mouse model. These findings showed that drug-loaded nanoparticles protect the skin from direct contact with the drug, allowing the drug to gradually present to the skin and reducing skin irritation.

#### **4.4.6 Method development and validation of a coumarin-6 assay using RP-HPLC**

A similar mobile phase and HPLC set-up developed for dutasteride (Section 3.1.2) were used for the assay of Cou-6, except the wavelength of detection was 466 nm. The retention time for Cou-6 was 9.2 minutes. Due to the comparable hydrophobicity characteristics of the two compounds (Log P dutasteride = 5.09 and Log P Cou-6 = 6.06), their retention times were close. Figure 4.13 shows there was no interference in the detection between Cou-6 and the other materials used in the formulation.

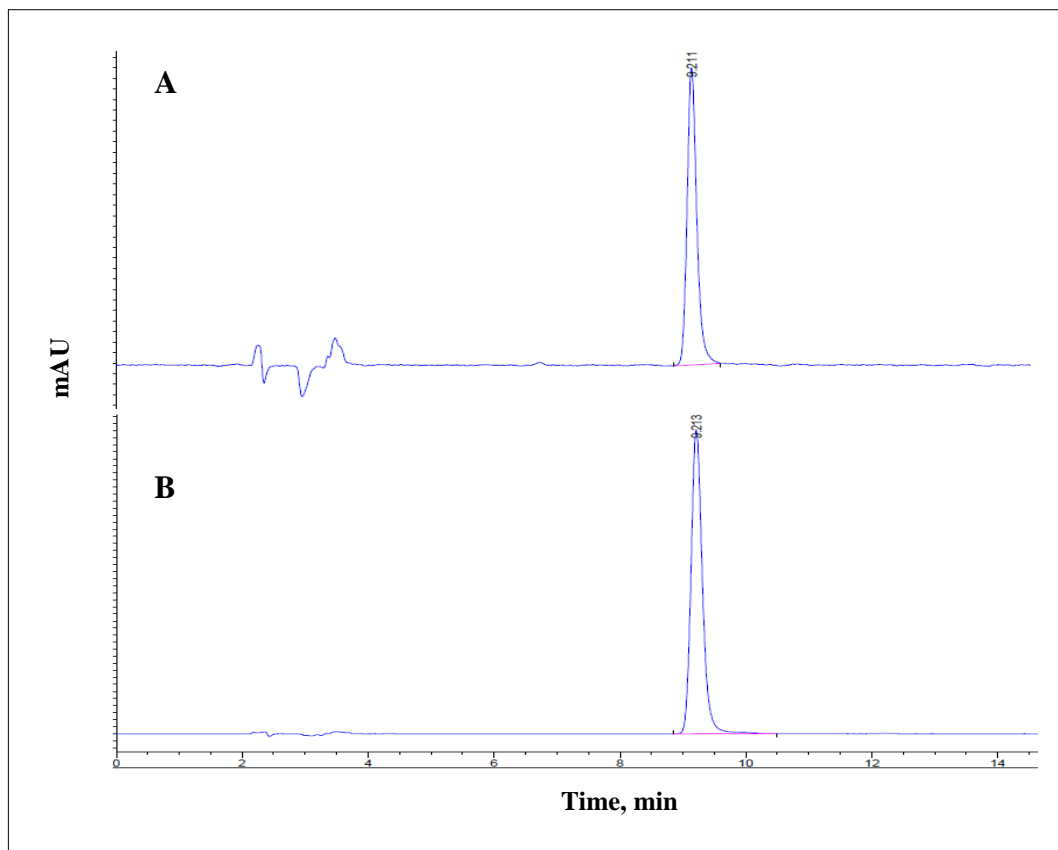


**Figure 4.13 Peak area versus time for the NLCs with Cou-6 (A) and Cou-6 in ethanol, 10  $\mu\text{g}/\text{mL}$  (B)**

The graph of concentration versus peak area was plotted and (Figure 4.14); the regression data showed a linear relationship between 0.25 and 12.5  $\mu\text{g}/\text{mL}$ . Table 4.6 shows the regression characteristics and validation parameters of Cou-6. LOD and LOQ were 0.06 and 0.25  $\mu\text{g}/\text{mL}$ , respectively. The calculation of LOD and LOQ is shown in Appendix A2. The intraday and interday precisions were determined at three different concentrations (1.5, 6.0 and 11.0  $\mu\text{g}/\text{mL}$ ). The RSD (%) for interday and intraday was 0.24 – 3.20% and 1.79 – 4.20% respectively. The repeatability was calculated by injecting nine samples (6.0  $\mu\text{g}/\text{mL}$ ) and determining the RSD%; this was 1.78%.

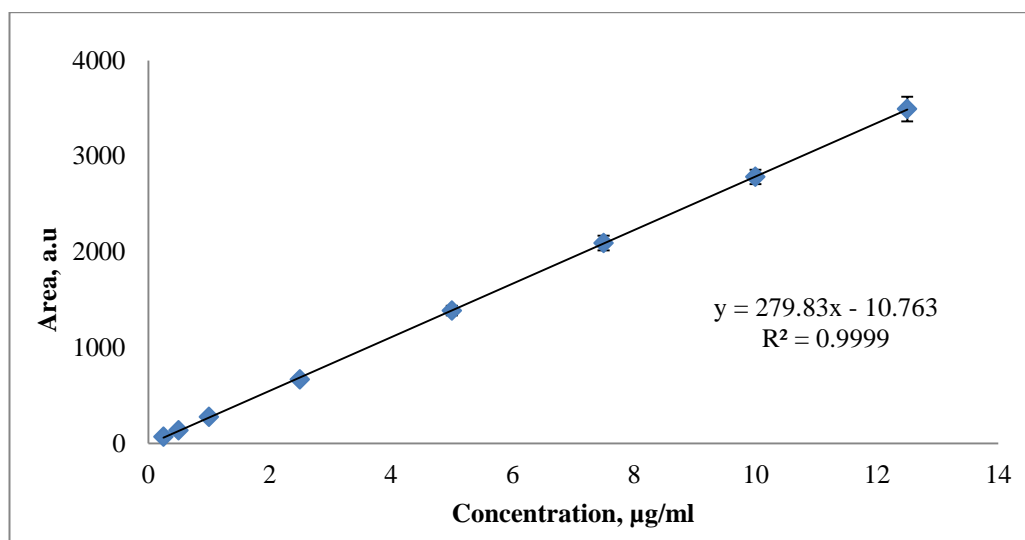


**Figure 4.14** Calibration curve of Cou-6, peak area versus concentration (n=4, mean  $\pm$  SD)

**Table 4.6** Regression characteristics and validation parameters of Cou-6

Parameters	Values
Linearity range ( $\mu\text{g/mL}$ )	0.25 – 12.5
Number of samples per curve	8
Correlation coefficient ( $r^2$ )	0.9999
Regression equation ( $y = mx + c$ )	
Slope (m)	279.83
Intercept (c)	-10.763
<sup>a</sup> LOD ( $\mu\text{g/mL}$ )	0.06
<sup>b</sup> LOQ ( $\mu\text{g/mL}$ )	0.25
Accuracy (%)	97.3 – 113.2
Repeatability, %RSD at 6 $\mu\text{g/mL}$ (n=9)	1.78
Precision, % ( <sup>c</sup> RSD, n=3)	
Interday (n=3)	0.24 – 3.20
Intraday (n=3)	1.79 – 4.20

<sup>a</sup>LOD is limit of detection, <sup>b</sup>LOQ is limit of quantification and <sup>c</sup>RSD is relative standard deviation at 1.5, 6.0 and 11.0  $\mu\text{g/mL}$

The data for validation of the Cou-6 assay met the acceptance criteria from the ICH Q2 Guideline. The method developed for assay of Cou-6 was found to be sensitive, precise, accurate and simple. Hence, this RP-HPLC method could be used for routine analysis, and for determining entrapment efficiency and drug loading for the formulation containing Cou-6.

#### 4.4.7 Characterisation of Cou-6-loaded NLCs, uncoated and coated with 5% CSO-SA or 5% CSO-LA

##### 4.4.7.1 Effect of Cou-6 content on size distribution, entrapment efficiency and drug loading

Increasing the amount of the Cou-6 dye from 0.2 (3.33  $\mu\text{g/mL}$ ) to 1 mg (16.67  $\mu\text{g/mL}$ ) in a total of 300 mg stearic acid, 150 mg Lutrol® micro 68 and 75 mg Phosal® 53 MCT in NLCs produced no significant change ( $p>0.05$ ) in the hydrodynamic diameter and polydispersity index compared to DST-NLCs as described in Section 3.5.2.1.3 (Figure 4.15). Mean size ranged from 193 to 201 nm and PDI from 0.119 to 0.143.

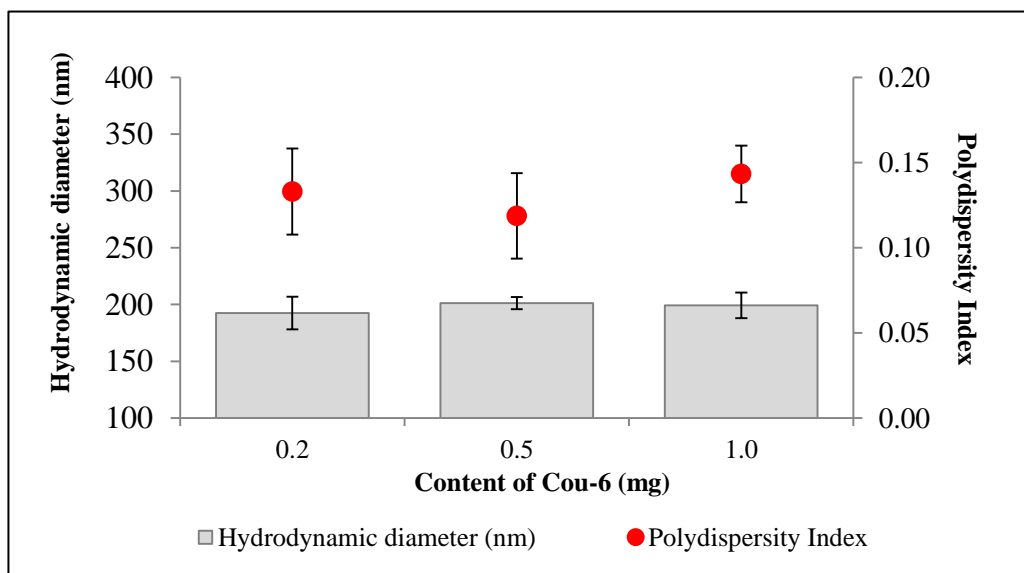


**Figure 4.15** Hydrodynamic diameter and polydispersity index for Cou-6-NLCs for different contents of Cou-6 (n=3, mean  $\pm$  SD)

In terms of the entrapment efficiency, 0.2 mg Cou-6 was incorporated in the NLCs rather than 0.1 mg (1.67  $\mu\text{g}/\text{mL}$ ), as the lower amount could be quantified accurately (lower than LOQ) by HPLC. The entrapment efficiency of Cou-6-loaded NLCs significantly decreased ( $p < 0.05$ ) from 0.2 mg to 1 mg (Figure 4.16). The loading efficiency was low ( $0.05 \pm 0.01\%$ ) compared to dutasteride ( $3.49 \pm 0.10\%$ ) as described in Section 3.5.2.1.4, showing that the carrier formulations had a limited loading of Cou-6 compared to dutasteride. These findings may be due to the limited solubility of Cou-6 in the oil-based carrier (stearic acid), which limits the amount of dye encapsulated in the NLCs. Sobhani et al., (2015) reported that solubility of the drug in oil for the preparation of nanoemulsion was very important in order to maintain the drug solubilisation in nanoemulsion.

The encapsulation efficiency of Cou-6 in NLCs can be increased by increasing the amount of carrier. The current formulation comprised of 300 mg of stearic acid, 150 mg of Lutrol® micro 68 and 75 mg of Phosal® MCT 53. However, in this study, a similar amount of carriers were employed as for dutasteride in order to minimise the cytotoxicity effect on hair follicle dermal papilla cells.

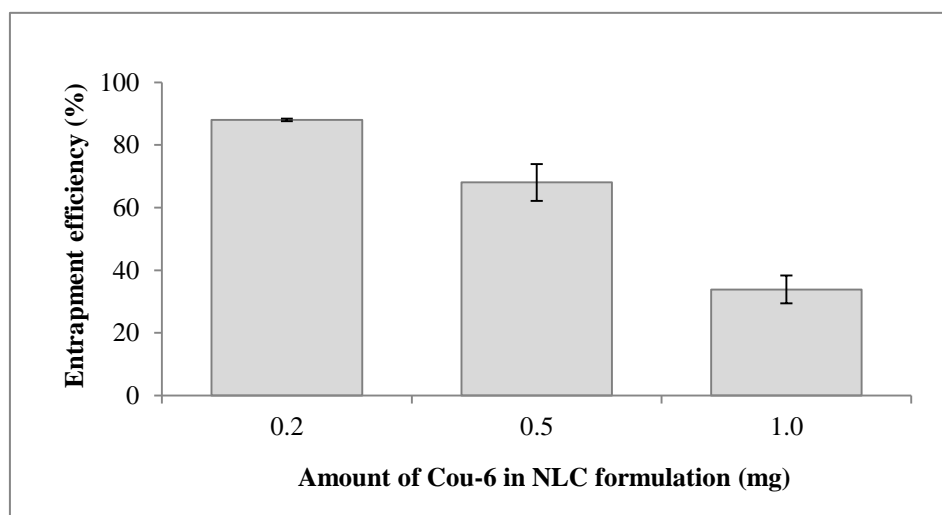


**Figure 4.16** Entrapment efficiency for Cou-6 loaded NLCs (n=3, mean  $\pm$  SD)

#### 4.4.7.2 Effect of coating of Cou-6-NLCs with 5% CSO-SA or 5% CSO-LA on mean particle size and zeta potential

Figure 4.17 shows the effect of coating Cou-6-NLCs, with 5% CSO-SA and 5% CSO-LA on hydrodynamic diameter and surface charge. The mean size of Cou-6-NLCs ( $192.4 \pm 14.4$  nm) did not significantly increase ( $p > 0.05$ ) when coated with either chitosan conjugates. Particle surface charge increased ( $p < 0.05$ ), changing from negative to positive on coating from  $-16.8 \pm 0.7$  mV uncoated to  $+24.4 \pm 1.2$  and  $27.7 \pm 0.6$  mV when coated with 5% CSO-SA and 5% CSO-LA, respectively. Hydrodynamic diameter and zeta potential results in Cou-6-NLCs uncoated or coated with 5% CSO-SA or 5% CSO-LA were not significantly difference ( $p > 0.05$ ) with those uncoated DST-NLCs or coated with 5% CSO-SA or 5% CSO-LA as described in Sections 3.5.2.2 and 3.5.3.1. These findings indicate Cou-6 was appropriate as a model for dutasteride for uptake studies of NLCs formulations.

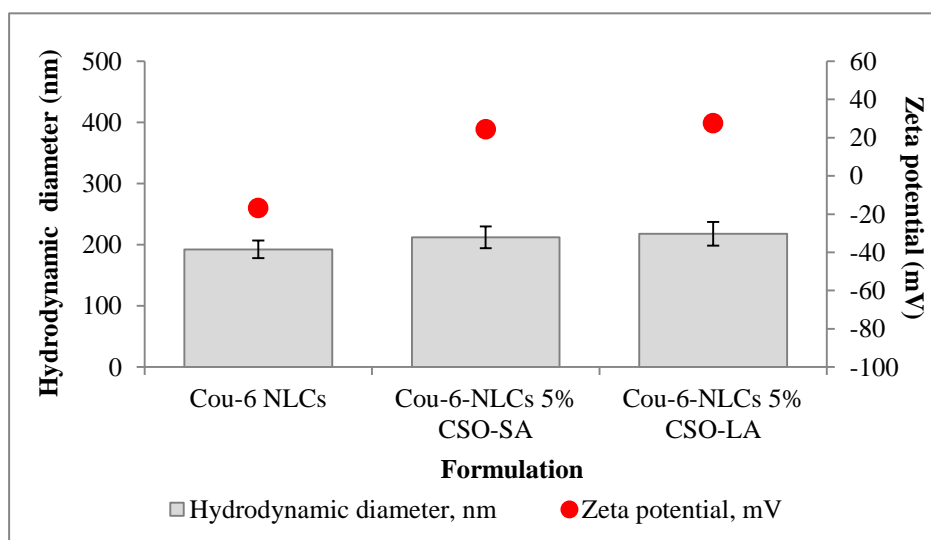


**Figure 4.17** Hydrodynamic diameter and polydispersity index for Cou-6-NLCs, uncoated and coated with 5% CSO-SA and 5% CSO-LA ( $n=3$ , mean  $\pm$  SD)

#### 4.4.8 Skin uptake of Cou-6 in solution and Cou-6-loaded NLCs, uncoated and coated with 5% CSO-SA and 5% CSO-LA

Figure 4.18 shows the skin uptake of Cou-6 from NLCs and in ethanol at different times.

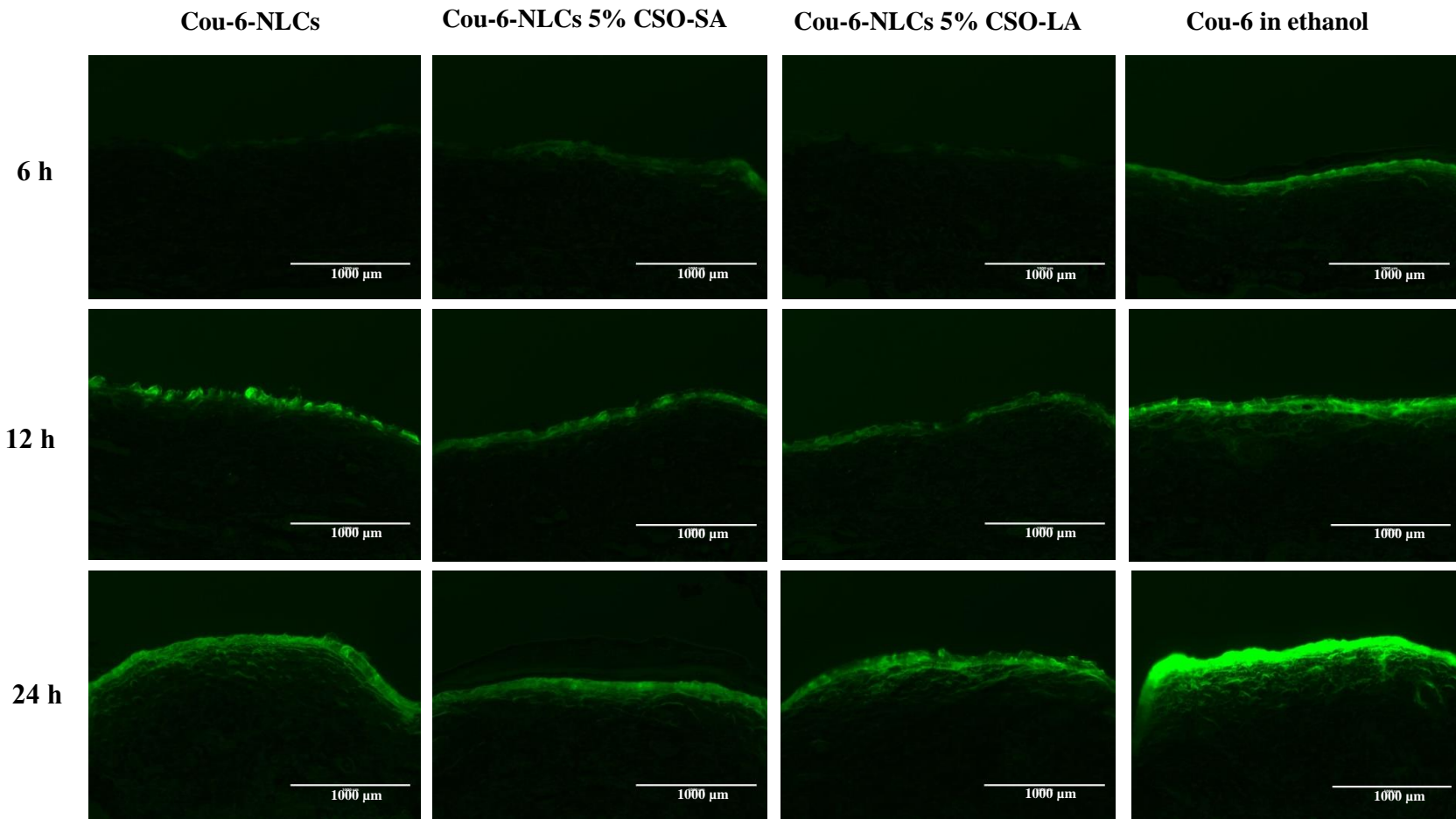


**Figure 4.18** Skin uptake of Cou-6 in full thickness pig ear skin (cryostat was set at 50  $\mu\text{M}$  thickness) from Cou-6-loaded NLCs, uncoated and coated with 5% CSO-SA and 5% CSO-LA and Cou-6 in solution

No quantification of the dye could be obtained from the skin due to the limited amount of Cou-6 which could be included in the formulations, resulting in concentrations lower than the LOQ of the assay.

All formulations showed skin uptake in a time-dependent manner in the upper layer of the skin, with greater uptake at 12 and 24 h than at 6 h especially in the upper region of the skin. The dye was also observed in the deeper layer of the skin. At 6 h, less intensity of fluorescent dye could be seen in the skin from Cou-6-NLCs uncoated and coated with 5% CSO-SA or 5% CSO-LA, suggesting the slow release of the dye from the NLCs at the beginning of the experiment, and the intensity of the colour increased as a longer time of dye exposed to the skin.

Cou-6 in ethanolic solution showed the highest intensity compared to the nanoparticle formulations, due to direct contact of the dye with the skin even at 6 h. This finding agrees with the previous permeation study, in which dutasteride in ethanol showed the highest permeation (Section 4.4.2).

In this study, the mean particle size of the NLCs was approximately 200 – 250 nm (Section 4.4.7.2) which is in agreement with Lin et al. (2013). They prepared diphencyprone-loaded NLCs, having a hydrodynamic diameter approximately 208 to 265 nm. This size range produced localization of NLCs in follicles and intercellular lipids of stratum corneum, following *in vivo* percutaneous absorption after 6 h.

Another study investigated nanoparticle deposition in mammalian skin and found nanoparticles in mean size of 20 – 200 nm could not penetrate beyond the superficial layers of the barrier (Campbell et al., 2012). This result proved that nanoparticles could not penetrate the skin barrier, but it is useful as skin surface reservoirs in order to control the drug release over time (Campbell et al., 2012). Patlolla et al., (2010) also reported that nanoparticles do not cross the skin but possibly permeate into stratum corneum and release the drug in a controlled manner into the upper epidermis.

However, nanoparticles have a tendency to diffuse and accumulate in the hair follicles (Fang et al., 2014). An earlier study demonstrated that nanoparticles with size 320 nm showed high drug accumulation in the transfollicular region after the massage, and were retained for up to 10 days in the hair follicle (Lademann et al.,

2007). In this study, massaging was not applied, and the intensity of Cou-6 can only be seen mostly in the upper layer of the skin. If massaging was applied, the nanoparticles may go to the transfollicular region and stay longer in the hair follicles. However, no transfollicular region could be seen in these skin samples.

#### **4.4.9 Cell uptake of Cou-6 in solution and Cou-6-loaded NLCs, uncoated and coated with 5% CSO-SA and 5% CSO-LA**

Figure 4.19 shows the uptake of Cou-6 in ethanolic solutions and NLCs uncoated and coated with 5% CSO-SA and 5% CSO-LA in the hair follicle dermal papilla cells at different times. Due to the limited amount of Cou-6 taken up by the cells; no quantification of the dye would be conducted using HPLC or UV spectrophotometer (lower than LOQ). There was a similar trend for cell uptake and the skin uptake (Section 4.4.8), with Cou-6 in all formulations being taken up in a time-dependent manner. There was no apparent difference in the intensity of the fluorescence dye within cells either in solution or nanoparticle formulations. The intensity for all formulations was highest at the longest time point. This result shows Cou-6 was successfully taken by the cells. As the Log P of Cou-6 and dutasteride were close, Cou-6 can be considered a good model for studying cell uptake of these NLCs systems.

This is supported by Rivolta et al. (2011) who prepared Cou-6 loaded SLNs and demonstrated alveolar epithelial cells took up the Cou-6 loaded SLNs. No specific co-localization in the cells was found with the dye. Similar finding was reported for Cou-6 loaded SLNs treated for A549 lung cancer cells (Zhang et al., 2013), with increasing amounts of Cou-6 were taken up by cells with increased concentration and time. From these findings, Cou-6 loaded NLCs either uncoated or coated can be used as a model dye that represents dutasteride-loaded NLCs for uptake study as both have close similar characteristic of the nanoparticles (size distribution and surface charge) were not significantly different.

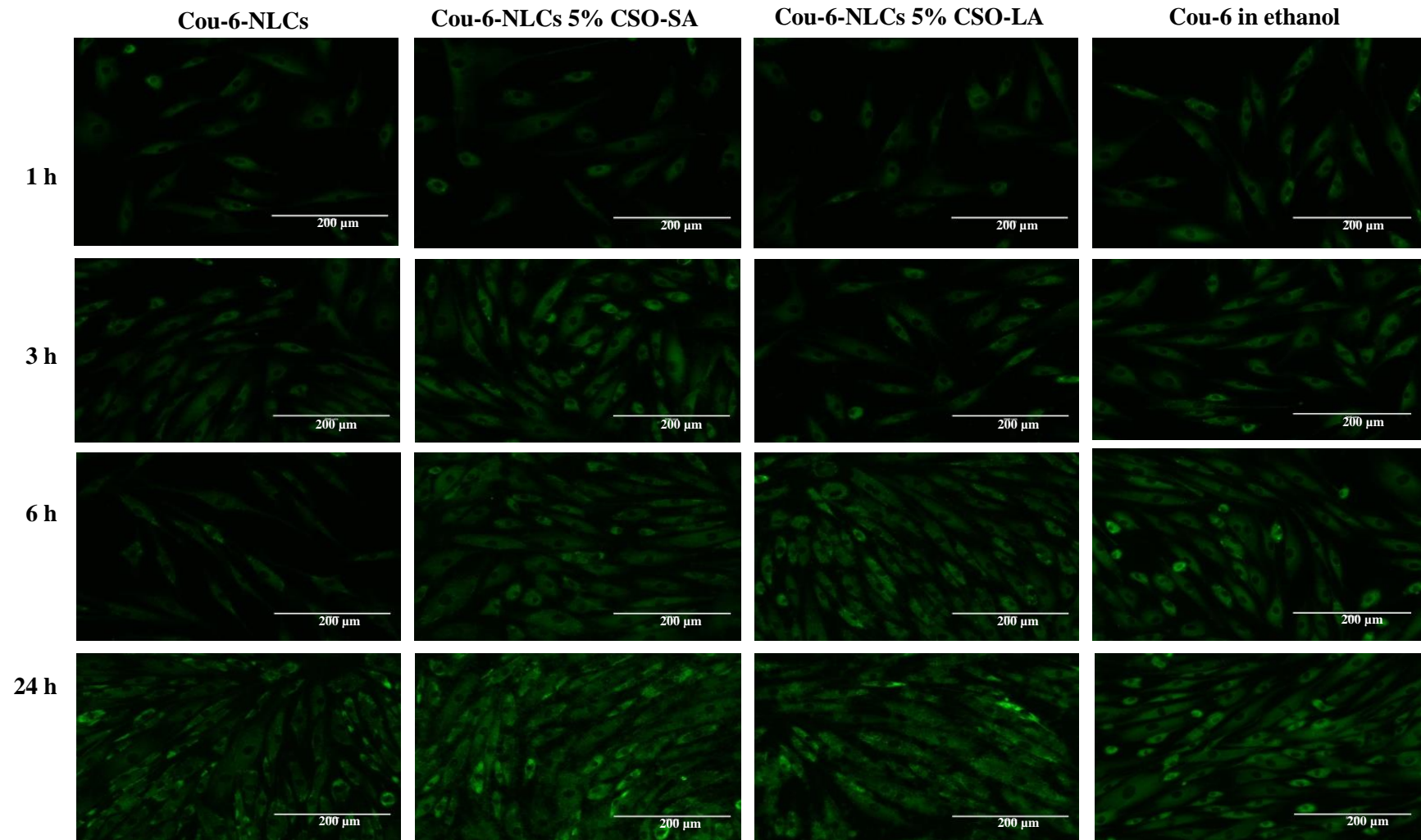


**Figure 4.19 Cell uptake study of Cou-6 in hair follicle dermal papilla cells from Cou-6-loaded NLCs, uncoated and coated with 5% CSO-SA and 5% CSO-LA and Cou-6 in solution**

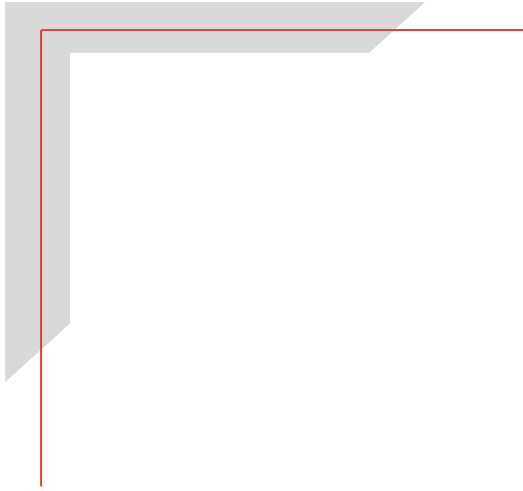
## 4.5 Conclusions

This chapter aims to characterise the release and permeation, cytotoxicity and irritation, skin and uptake using Cou-6 as a model dye, of DST-NLCs, uncoated and coated with 5% CSO-SA and 5% CSO-LA. Based on the results, it can be concluded that:

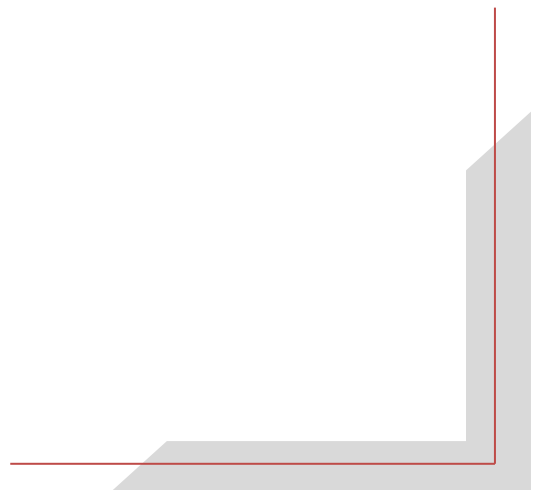
1. DST-NLCs without coating showed a higher release over 24 h. DST-NLCs coated with CSO-SA and CSO-LA had a lower drug release at 12, 24 and 30 h. Increasing the concentration of CSO-SA or CSO-LA had no significant impact on the release parameters. 5% CSO-SA and 5% CSO-LA were found to be the optimal coating concentration for the DST-NLCs.
2. For all formulations, no dutasteride was detectable by HPLC in the receptor chamber after 48 h of the permeation studies, suggesting no systemic exposure from these formulations in clinical studies. The highest permeation in the skin was found from ethanol-based solutions, then from DST-NLCs uncoated and coated with CSO-SA or CSO-LA.
3. Dutasteride alone showed an  $IC_{50}$  of 10.4  $\mu$ M for cytotoxicity. Values for DST-NLCs, uncoated and coated with 5% CSO-SA or 5% CSO-LA were higher approximately by 5-fold. Empty NLCs for both uncoated and coated with 5% CSO-SA or 5% CSO-LA showed cytotoxicity in a dose-dependent manner. The maximum non-toxic concentration ( $EC_{90}$ ) for dutasteride in the nanoparticles increased by more than 20-fold compared to dutasteride in DMSO.
4. For *in vitro* skin irritation study on the 3D Reconstructed Human Epidermis (RHE), all formulations with or without dutasteride either coated or uncoated with 5% CSO-SA or 5% CSO-LA showed no irritancy with a mean cell viability greater than 50%. The positive control (5% sodium dodecyl sulphate) gave the lowest cell viability.
5. Cou-6 was chosen as a model compound with properties similar to dutasteride and loaded with NLCs for the uptake study. In terms of mean hydrodynamic diameter, polydispersity index and surface charge, no significant differences were found between the formulations (0.2 mg Cou-6 in 300 mg stearic acid,

150 mg Lutrol® micro 68 and Phosal® 53 MCT) either coated or uncoated with 5% CSO-SA or 5% CSO-LA when compared to DST-NLCs, coated or uncoated with 5% CSO-SA or 5% CSO-LA. The entrapment efficiency and drug loading of Cou-6-NLCs were 88.0% and 0.05%, respectively.

6. All formulations showed skin uptake in a time-dependent manner where at 6 h, less dye was taken up compared to 12 and 24 h especially in the upper region of the skin. The dye could also be seen in the deeper layer of the skin. Cou-6 in ethanol showed the highest intensity compared to the nanoparticle formulations, due to direct contact of the dye on the skin surface, whereas nanoparticles either coated or uncoated with 5% CSO-SA or 5% CSO-LA showed less intensity.
7. A similar trend between the cell and skin uptake was found, where Cou-6 in all formulations was taken up in a time-dependent manner. No specific co-localization in the cells was found from the dye. The intensity for all formulations was highest at the longest time point. No difference regarding the intensity of the fluorescent dye either in solutions or nanoparticles formulations was found. This result showed Cou-6 was successfully taken up by the cells.



## **Chapter 5 General discussion and future work**



## 5.1 Summary

The skin is the largest organ in humans with a surface area of 1.8 - 2.0 m<sup>2</sup> (Uchechi et al., 2014). The skin has advantages for topical/transdermal delivery of drug to the targeted area by local delivery. It is suggested that by delivering drug topically directly on the scalp area, smaller amounts of drugs may be required to produce a therapeutic effect at the specific targeted site (Zhang et al., 2013) compared to oral delivery. However, drug permeation through the skin is usually limited by the stratum corneum (Uchechi et al., 2014). For effective delivery of drug to the skin, drug must partition from the formulation into the stratum corneum, and then diffuse within the stratum corneum, and partition to local tissues including epidermis, dermis, subcutis and appendages for topical delivery, and/or into epidermis, dermis and bloodstream for effective transdermal delivery (Kandavilli et al., 2010).

Both topical and transdermal delivery provides convenient, and pain-free self-administration for patients, thus makes this delivery route particularly popular. In the case of hair loss treatment, which requires a long duration of treatment, this is also likely to enhance patient adherence. For some drugs that produce systemic adverse effects, limiting the penetration of drug to the systemic area, achieved by engineering an appropriate carrier for the drug, such as nanoparticle (including nanospheres, solid lipid nanoparticles, micelles and micellar-like nanoparticles, liposomes and nanoemulsions), is an appropriate strategy for topical delivery (Zhang et al., 2013).

In this project, a topical/dermal or transfollicular delivery system for dutasteride was designed and characterised. The general aim of this project was to prepare and characterise dutasteride-loaded nanostructured lipid carrier (DST-NLCs) coated with chitosan oligomer conjugated with stearic acid, or lauric acid for dermal delivery in order to increase the stability of nanoparticles, enhance local drug delivery, sustained drug release and reduce cytotoxicity. Dutasteride, which has both Type I and Type II 5 $\alpha$ -reductase inhibitory activity was chosen as an anti-androgenic drug. Stearic acid, which is one of the main ingredients in the DST-NLCs preparation used in this project, also acts as a less potent 5 $\alpha$ -reductase inhibitor.

The hypothesis of this project was, that modifying the surface of DST-NLCs with chitosan conjugated with different types of fatty acids will enhance the stability of nanoparticle, delivery and safety of dutasteride therapy. Encapsulating dutasteride in the lipid nanoparticle system for dermal application and incorporation of fatty acid as a carrier may provide a synergistic effect between drug and the carrier with respect to the anti-androgenic activity, due to the presence of the fatty acid, promoting cell growth, especially with lauric acid which has higher 5 $\alpha$ -reductase inhibitory activity than stearic acid (Liu et al., 2009). At the same time, having positively-charged nanoparticles for topical delivery, due to coating with chitosan oligomer-stearic or lauric acid, should produce slower drug release and retention at the targeted area, especially the hair follicles, reducing systemic effects and cytotoxicity on the hair follicle dermal papilla cells.

In **Chapter 2**, the conjugation between chitosan oligomer and different types of fatty acids and characterisation of the conjugates was described. The synthesised product was used as a coating material for the next experimental chapter. Chitosan oligomer was conjugated with stearic acid (SA) or lauric acid (LA) in order to produce amphiphilic chitosan, with stearic or lauric acid (attached to chitosan oligomer backbone) being the hydrophobic region, and the chitosan oligomer backbone being the hydrophilic region. The synthesised products used as coating materials were suggested as likely to increase the physical stability of nanoparticle formulations. All conjugations between chitosan oligomer and stearic acid or lauric acid were successful, based on <sup>1</sup>HNMR, FTIR and ninhydrin assays. In the optimisation of CSO-SA synthesis, sample S1 (0.5 g stearic acid; SA: EDC.HCl 1:5 reacted for 6 h) was selected. CSO-LA was also produced using the previously optimised CSO-SA reaction parameters. The degree of substitution of CSO-SA and CSO-LA was very similar (~6%). The critical micelle concentration values for both CSO-SA and CSO-LA were 0.17 mg/mL.

**Chapter 3**, describes the main body of experimental work in this thesis, specifically describes the preparation and characterisation of DST-NLCs coated with CSO-SA or CSO-LA. The formulations were produced by the melt dispersion-ultrasonication method. The optimisation of DST-NLCs was achieved using a design of experiments approach, whereby the size distribution of particles, entrapment efficiency and drug loading were measured as dependent variables whereas the

independent variables were the amount of stearic acid, Lutrol® micro 68 and Phosal® 53 MCT. To obtain positively-charged nanoparticles, the optimised negatively-charged DST-NLCs were coated with positively-charged CSO-SA or CSO-LA using a physical adsorption method.

The ratio of contents with 100 mg stearic acid, 50 mg Lutrol® micro 68, 25 mg Phosal® 53 MCT and 5 mg dutasteride gave the optimal physical properties; the smallest hydrodynamic diameter and narrowest particle size distribution. The formulation was scaled-up 3 times in order to increase the amount of dutasteride incorporated from 0.083 mg/mL to 0.29 mg/mL. The hydrodynamic diameter of DST-NLCs was increased with 5% CSO-SA, but not significantly increased when coated with 5% CSO-LA. Based on TEM micrographs, the uncoated DST-NLCs and those coated with CSO-SA or CSO-LA were spherical and in the size range, approximately 200 to 250 nm, comparable to the size measured by DLS.

The surface charge changed from negative to positive charge for DST-NLCs when coated with CSO-SA and CSO-LA, showing that the particles were successfully coated. Increasing the amount of CSO-SA or CSO-LA in the DST-NLCs formulation, further increased the positive charge.

The DST-NLCs were very stable at 4-8°C, with no significant difference ( $p > 0.05$ ) in entrapment efficiency from day 1 to day 180 (~97%). The mean hydrodynamic diameter was in the range 200 to 250 nm when stored at 4-8°C for DST-NLCs, either uncoated or coated with CSO-SA or CSO-LA up to 6 months. These are acceptable particle size for the topical delivery; Mahe et al., (2009) found the particles of approximately 200 nm mean size applied to the skin were found around the hair follicles. Mittal et al., 2015 also reported that particles with a size of approximately 300 nm were found in the transfollicular region following topical application.

When DST-NLCs were coated with 5% CSO (no conjugation), the NLCs were not stable and aggregated by day 30 at 4 – 8°C. All DST-NLCs formulations either uncoated or coated with CSO-SA or CSO were not stable when stored at 25°C; the mean size and PDI increased by 2-fold, with some formulation showing aggregation.

Dutasteride showed crystalline peaks in XRPD spectra and a sharp peak with DSC at 249.2°C corresponding to the drug melting temperature. The degree of crystallinity of dutasteride in the NLC systems was reduced, suggesting that dutasteride was present in an amorphous structure and homogeneously dispersed in the NLCs, whether the NLCs were uncoated or coated with 5% CSO-SA or 5% CSO-LA. These less crystallinity structure due to the combination of solid lipid and liquid lipid in the NLCs system, suggesting to produce a sustained dutasteride release to the skin which is suitable for the topical application as described in the previous study (Pardeike et al., 2009). Pardeike et al., (2009) reported that sustained drug release is important for drugs that are irritating at high concentrations or delivering drug for a long duration.

In **Chapter 4**, the *in vitro* characterisation of the optimised formulation of DST nanoparticles is described. *In vitro* release study was performed in order to compare the release of dutasteride from DST-NLCs, uncoated or coated with different percentages of CSO-SA and CSO-LA in PBS pH 7.4 solutions (with 2% SDS) to that of the control (DST in 70% ethanol), and also to confirm the presence of coating materials around the nanoparticles. DST-NLCs without coating showed the highest release of ~82% after 24 h. DST-NLCs coated with CSO-SA and CSO-LA showed slower drug release at 24 h (approximately 60 - 66%). By increasing the concentration of CSO-SA or CSO-LA from 5% to 10%, there was no significant difference in the release rate. These results indicate the successful presentation of coating materials on the surface of DST-NLCs.

An *in vitro* permeation study using full thickness pig ear skin was conducted in order to quantify the potential systemic exposure. After 48 h, no dutasteride was detectable by HPLC in the receptor chamber of Franz diffusion cells for all formulations, suggesting no systemic exposure of dutasteride from these formulations. The amount of dutasteride present in the skin from uncoated DST-NLCs was 2-fold higher than from those coated with 5% CSO-SA or 5% CSO-LA. The highest permeation in the skin was found from dutasteride in 70% ethanol which was in agreement with the previous research, in that ethanol acts as a penetration enhancer in topical products (Williams and Barry, 2004). Megrab et al. (1995) found for ethanol: water co-solvent vehicle, the effect of ethanol appears to be concentration-dependent, where increasing the amount of ethanol produced

dehydration of the biological membrane, thus reduce the permeation across the tissue. Additionally, permeation of ethanol into the stratum corneum can alter the solubility properties of the tissue, resulting in an improvement for drug partitioning into the membrane.

*In vitro* cytotoxicity was studied in order to determine the cytotoxic and proliferation effects of various concentrations of dutasteride alone and dutasteride in the nanoparticles either uncoated or coated with 5% CSO-SA or 5% CSO-LA. The same nanoparticles formulation (empty NLCs) was also tested in order to investigate whether the carrier itself potentially promoted cell proliferation. Dutasteride alone showed cytotoxicity ( $IC_{50}$ ) at very low concentration ( $\sim 10.4 \mu\text{M}$ ). Values of  $IC_{50}$  for DST-NLCs, uncoated and coated with 5% CSO-SA or 5% CSO-LA were up to 5-fold higher. NLCs alone (empty NLCs) uncoated and coated with 5% CSO-SA or 5% CSO-LA showed cytotoxicity in a dose-dependent manner. The maximum non-toxic concentration ( $EC_{90}$ ) for DST-NLCs either uncoated or coated with 5% CSO-SA or 5% CSO-LA was increased up to 20-fold compared to dutasteride alone. This was due to the slow release of drug from nanoparticle formulations, whereby the drug was released slowly allowing a longer period for the drug to interact with the cells and exert its activity, preventing the cells being killed immediately.

The irritation caused by the developed formulations was studied using 3D Reconstructed Human Epidermis. All formulations (DST-NLCs and empty NLCs) either uncoated or coated with 5% CSO-SA or 5% CSO-LA and dutasteride in 70% ethanol showed no irritancy (the mean cell viabilities were greater than 50%), with less cell viability for dutasteride in 70% ethanol. These results were due to water being the continuous phase in nanoparticle preparations, and slow dutasteride release from nanoparticle formulation, preventing the skin being irritated.

For skin and cell uptake studies, Cou-6 was used as a model fluorescent dye with similar properties to dutasteride. Cou-6-NLCs were prepared and optimised. In term of the hydrodynamic diameter and polydispersity index, no significant differences ( $p > 0.05$ ) were found for all formulations either coated or uncoated with 5% CSO-SA or 5% CSO-LA when compared to DST-NLCs. The maximum entrapment efficiency was found to be  $\sim 88\%$ .

Based on the skin uptake studies of Cou-6 in ethanol, or Cou-6-NLCs, uncoated and coated with 5% CSO-SA or 5% CSO-LA, all formulations showed fluorescent intensity within the skin in a time-dependent manner. The intensity for all formulations was highest in the upper skin layer at the longest time point. For cell uptake of Cou-6 in ethanol or Cou-6-NLCs, uncoated and coated with 5% CSO-SA or 5% CSO-LA, no specific localisation of dye was found with the cells. This result suggests that Cou-6 was successfully prepared and used as a model dye in the NLCs for both uptake studies, though it is not possible to state that the NLCs were located preferentially in the hair follicles.

## **5.2 General conclusions**

The main aim of this study has been achieved. DST-NLCs coated with CSO-SA or CSO-LA were successfully formulated and characterised; NLCs were stable and showed enhanced local drug delivery, reduced systemic exposure, slower drug release and reduced cytotoxicity.

The optimisation of the formulation vitally important in order to develop good, safe, effective and stable dosage forms. These can be undertaken by designing and optimise the formulation using different types of carrier, different methods of preparation and also varying the amount of excipients to be used in the preparation. In this study, optimisation was achieved using quality by design (QbD) principles, using a Design of Experiments software. This software could predict the cause-and-effect in the optimisation of the formulation. As described in Chapter 3, DoE was applied to optimise the carrier formulation, using a full-factorial design approach in order to optimise critical quality attributes; small mean particles size, narrow PDI and a stable formulation. DoE reduced the number of experiments or formulations prepared in order to achieve the target, by varying the different independent variables (factors) at the same time, as compared to traditional approaches where one-factor-at-a time experiment are employed. This approach produced a mathematical model of the response (dependent variables) from the factors used and predicted some interaction between the factors used.

The lipid nanoparticles coated with CSO-SA or CSO-LA engineered in this research could be used to deliver other hair growth therapeutic molecules for topical application. Having positively-charged nanoparticles from conjugated-CSO, produced higher stability of nanoparticles compared to non-conjugated CSO. Nanoparticles prepared in water as the continuous phase, showed higher cell viability on the 3D reconstructed human epidermis, suggesting these NLCs were a better carrier to be used compared to ethanol. Moreover, delivering 5 $\alpha$ -reductase inhibitor molecules in the nanocarriers reduced the cytotoxicity on the hair follicle dermal papilla cells. Lipid nanoparticles coated with chitosan could reduce the systemic exposure by limiting drug permeation as described in the permeation result, where DST-NLCs coated with CSO, CSO-SA or CSO-LA produced half of drug permeation compared to DST-NLCs.

The selection of a potent 5 $\alpha$ -reductase inhibitor compound to be conjugated with chitosan oligomer used as a coating material could enhance the hair follicle dermal papilla cell proliferation, suggesting it could enhance the synergistic activity with dutasteride. As revealed in the proliferation study of DST-NLCs coated with CSO-LA, these carriers gave better cell proliferation compared to DST-NLCs coated with CSO-SA.

In this study, empty NLCs coated with CSO-LA also showed an interesting result, producing cell proliferation with no irritancy on the 3D reconstructed human epidermis, suggesting that this formulation could be used for women, for whom dutasteride is not indicated. Stearic acid is the main ingredient in the nanoparticle preparation, and lauric acid (CSO conjugated with CSO-LA) could promote cell proliferation as described in the previous literature (Liu et al., 2009), lauric acid is more potent reductase inhibitor. Stearic and lauric acid can be found abundantly in the palm and coconut oils, and thus these oils are widely used as traditional remedies for hair loss treatment in tropical countries (Rele and Mohile, 1999; Gopala Krishna et al., 2010; DebMandal and Mandal, 2011; Kumar et al., 2012). This result showed that this empty nanoparticle formulation, when combined with CSO-LA, gave promising results as a therapy for hair growth.

Delivering dutasteride with the other therapeutic agents could also enhance the hair growth. Kandavilli et al., (2010) have filed a patent of topical compositions

comprising a combination of different types of 5-alpha reductase inhibitors, which one is dutasteride. Rafi and Katz, (2011) conducted an efficacy study on 15 male patients of a new formulation (topically applied of NuH® Hair containing dutasteride, finasteride and minoxidil; formulation and method of production undisclosed) applied daily in combination with administration of oral finasteride. Topical 5% minoxidil foam, and/or topical ketoconazole applied to the scalp, produced the most significant improvement in hair counts and overall appearance compared to the NuH® Hair product combined with two or fewer other interventions to treat androgenic alopecia. Thus, these combinations showed promising results. However, additional safety studies should be conducted. Based on this literature, co-delivering dutasteride with other hair growth promoter compounds in the nanoparticles described in this thesis could produce enhanced results, giving slow drug release, reduced cytotoxicity and potentially synergistic hair proliferation effects.

Clinical studies have shown that dutasteride is useful for treating androgenic alopecia when taken orally or applied topically. However, currently no dutasteride-based topical products have been approved in US or EU for the hair loss treatment. From a patient perspective, such a product would be beneficial to regrow the hair to be applied to the scalp at a reduced frequency. Hopefully, in a relevance short time, it is anticipated that a dutasteride-based topical product could be marketed and commercialised, and be one of several treatment options for the androgenic alopecia patients.

The findings of this study thus support the hypothesis that, by modifying the surface of NLCs with CSO-SA or CSO-LA, the stability of nanoparticles is enhanced, drug retention in the skin due to positively-charged nanoparticles is achieved with slow drug release, reducing toxicity and irritation. Figure 5.1 shows the overall schematic diagram of preparation of lipid nanoparticles for topical delivery of hair growth therapeutic molecules, based on the work presented in this thesis and the potential for future formulation development.

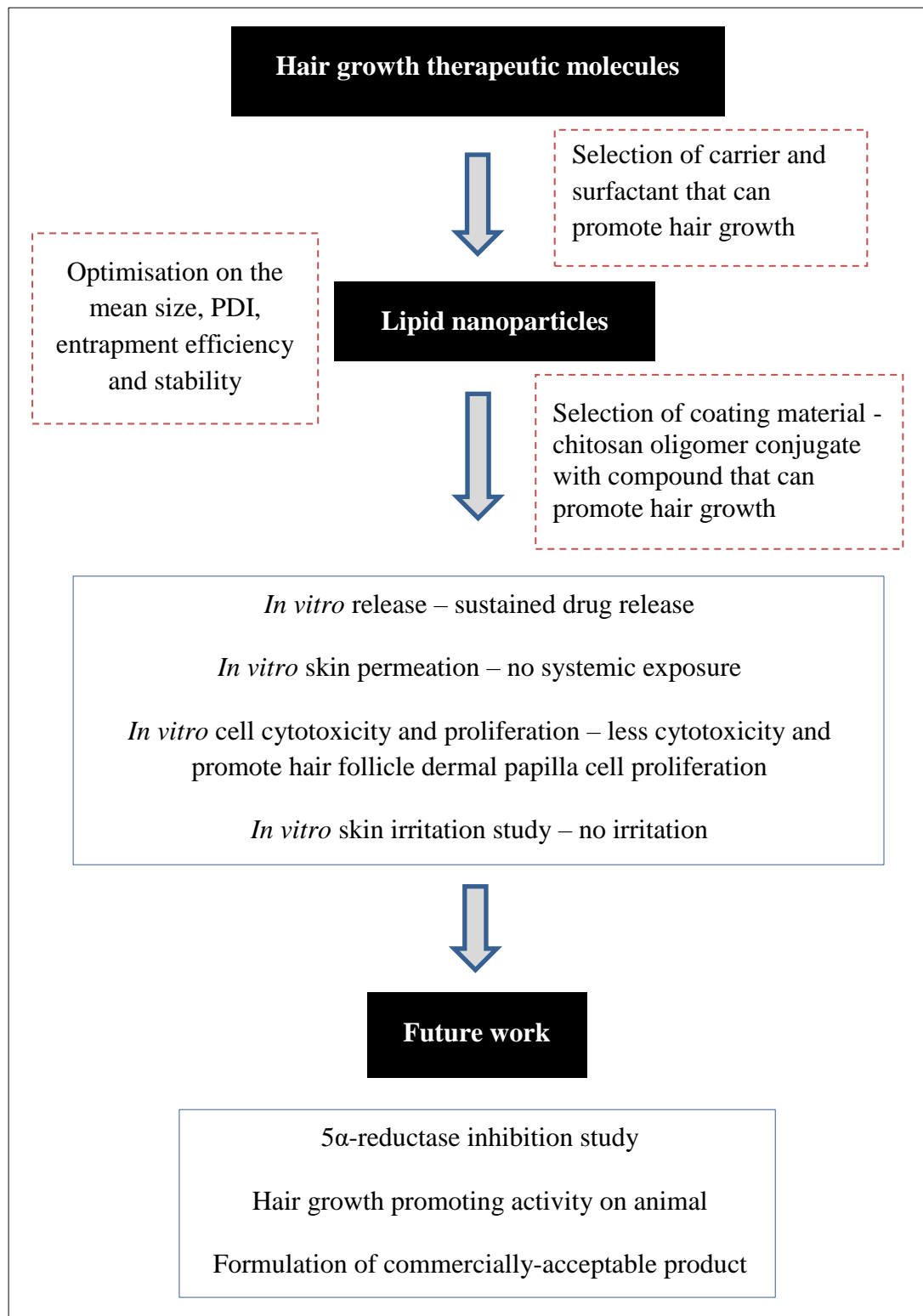


**Figure 5.1 Schematic diagram of preparation of lipid nanoparticles for topical delivery of hair growth therapeutic molecules and potential future work**

### 5.3 Future work

There are three main experimental studies to be considered for the future:

- a. Study of the reductase inhibition activity of DST-NLCs, uncoated and coated with CSO-SA or CSO-LA, using rat microsomal suspension
- b. Study of the hair growth promoting activity using an animal model (*in vivo*) of DST-NLCs, uncoated and coated with CSO-SA or CSO-LA
- c. Formulation development for a commercially-acceptable product

The cytotoxicity study described in this thesis has demonstrated that delivering dutasteride in the NLC system reduced cell cytotoxicity. As dutasteride is claimed to block the intracellular conversion of testosterone to DHT by  $5\alpha$ -reductase particularly for men, incorporating dutasteride in the nanoparticles (with a carrier itself also potentially inhibits  $5\alpha$ -reductase), enhance the inhibition of reductase enzyme activity. Study of the reductase inhibition activity of dutasteride with nanocarriers should therefore be undertaken, and this will give an idea of how the cell proliferation activity of the nanoparticles formulations has been achieved. This work should be undertaken using rat microsomal suspension from the liver as described previously (Kumar et al., 2011). DST-NLCs or empty NLCs, uncoated and coated with CSO-SA or CSO-LA will be reacted with the supernatants from the homogenated-liver with the addition of testosterone.  $5\alpha$ -reductase inhibition activity can be calculated, with finasteride used as a standard enzyme inhibitor (Kumar et al., 2011). The results will be expressed as finasteride equivalent  $5\alpha$ -reductase inhibitory activity value (units of mg finasteride equivalent per 1 g sample).

The second aspect of future work will be a study of hair growth promoting activity using an animal model. Based on the current characterisation and efficacy results, nanoparticle formulations showed good properties in term of drug sustained release, no systemic exposure, lower cytotoxicity, good stability, no skin irritation and promising results for skin and cell uptake and potential commercialisation. Therefore, the efficacy study on the mice of hair growth promoting activity should be performed using DST-NLCs and also the empty NLCs coated CSO-SA or CSO-LA. The study could be conducted as described in the previous literature (Park et al.,

2016). Different groups of male C57BL/6 mice will be used. The hair on the dorsal skin will be removed and randomly divided into different groups and treated with different types of formulation once a day for 3 weeks (2% minoxidil for positive control, negative control (DI water), DST-NLCs, empty NLCs, DST-NLCs coated with CSO-LA, and empty NLCs coated with CSO-LA). The lengths of 30 randomly plucked hairs will be measured at 19 day after topical application for each group, and histological study on the skin will be conducted in order to visualise the appearance of hair follicles.

The final aspect that needs consideration is the development of the formulation to yield a more patient-acceptable formulation and ultimately a commercially-acceptable product. Currently, DST-NLCs, uncoated and coated with CSO-SA or CSO-LA formulations are dispersed in water, which yields a low viscosity product. To enhance the formulation and aid dose delivery, it is proposed to deliver this nanoparticle dispersion either deliver as a liquid, in unmodified form (using a dropper) or it can be formulated into a semi-solid dosage form, such as foam, an emulsion (i.e. lotion) or hydrogel. The current formulation has low viscosity, and the formulation could run over the scalp, though such lotions are an established dosage form for application to the scalp. A preservative would be required to prevent microbial growth. Secondly, these nanoparticles dispersion could be delivered in a foam type. The latest foaming technology uses compressed air or nitrogen in polyethylene terephthalate (PET) packaging, this is potentially easier to use and at the same time more environmentally friendly, avoiding harmful emissions (typically propane or butane) from aerosol-based foam. Alternatively, a finished product based on these NLCs could be prepared by mixing this nanoparticle dispersion with an emulsion, formulating in an emulsion or adding a thickener such as Carbopol® polymer to form a hydrogel. Optimisation on the type of carrier should be performed as NLCs having chitosan (CSO-SA or CSO-LA) may affect the properties of the gel, the product formulating these NLCs into an emulsion or hydrogel carrier, the product would potentially easier to use by patient, having non-greasy properties, retarding flow of the formulations, and permitting easy distribution of small amounts of formulations evenly on the scalp. However, the physical stability of the NLCs, drug release and permeation profiles may be changed, and additional characterisation of nanoparticles and the complete formulation would be required.

# References

- Adolphe, C. and Wainwright, B. (2005) Pathways to improving skin regeneration, *Expert Reviews in Molecular Medicine*, 7(20), 1–14.
- Ahmed, E. M. (2015) Hydrogel: Preparation, characterization, and applications: A review, *Journal of Advanced Research*, 6(2), 105–121.
- Akbarzadeh, A., Rezaei-Sadabady, R., Davaran, S., Joo, S. W., Zarghami, N., Hanifehpour, Y., Samiei, M., Kouhi, M. and Nejati-Koshki, K. (2013) Liposome: classification, preparation, and applications, *Nanoscale Research Letters*, 8(102), 1–9.
- Akhtar, N., Rehman, M., Khan, H., Rasool, F., Saeed, T. and Murtaz, G. (2011) Penetration enhancing effect of polysorbate 20 and 80 on the in vitro percutaneous absorption of L-ascorbic acid, *Tropical Journal of Pharmaceutical Research*, 10(3), 281–288.
- Al-Shammari, B., Al-Fariss, T., Al-Sewailm, F. and Elleithy, R. (2011) The effect of polymer concentration and temperature on the rheological behavior of metallocene linear low density polyethylene (mLLDPE) solutions, *Journal of King Saud University - Engineering Sciences*, 23, 9–14.
- Aljuffali, I. A., Sung, C. T., Shen, F.-M., Huang, C.-T. and Fang, J.-Y. (2014) Squarticles as a lipid nanocarrier for delivering diphencyprone and minoxidil to hair follicles and human dermal papilla cells., *The AAPS Journal*, 16(1), 140–150.
- Ansari, N. H., Anis, E., Firdaus, S. F. S., Wahab, S. and Mishra, M. F. A. N. (2013) Synthesis of dutasteride loaded nanoemulsion, *International Journal of Scientific Research*, 2(11), 85–87.
- Attama, A. A., Momoh, M. A. and Builders, P. F. (2012) Chapter 5: Nanoparticulate drug delivery systems : A revolution in dosage form design and development, in Sezer, A. D. (ed.) *Recent Advances in Novel Drug Carrier Systems*. InTech Publisher, 107–140.
- Bala, I., Hariharan, S. and Kumar, M. N. V. R. (2004) PLGA nanoparticles in drug delivery: the state of the art., *Critical Reviews in Therapeutic Drug Carrier Systems*, 21(5), 387–422.
- Bartosova, L. and Bajgar, J. (2012) Transdermal drug delivery in vitro using diffusion cells, *Current Medicinal Chemistry*, 19, 4671–4677.
- Beloqui, A., Solinís, M. Á., Rodríguez-Gascón, A., Almeida, A. J. and Préat, V. (2016) Nanostructured lipid carriers: Promising drug delivery systems for future clinics, *Nanomed. Nanotechnology Biology and Medicine*, 12(1), 143–161.
- Bensouilah, J. and Buck, P. (2006) Skin Structure and Function, in Bensouilah, J. and Buck, P. (eds) *Aromadermatology: Aromatherapy in the Treatment and Care of*

Common Skin Conditions. Oxford: Radcliffe Publishing, 1–11.

- Bergenholtz, J., Brady, J. F. and Vicic, M. (2002) The non-Newtonian rheology of dilute colloidal suspensions, *Journal of Fluid Mechanics*, 456, 239–275.
- Bhaskar, K., Anbu, J., Ravichandiran, V., Venkateswarlu, V. and Rao, Y. (2009) Lipid nanoparticles for transdermal delivery of flurbiprofen: Formulation, in vitro, ex vivo and in vivo studies, *Lipids in Health and Disease*, 8(6), 1–15.
- Bhatia, G., Zhou, Y. and Banga, A. K. (2013) Adapalene microemulsion for transfollicular drug delivery, *Journal of Pharmaceutical Sciences*, 102(8), 2622–2631.
- Bhushan, B. (2010) Biophysics of Human Hair: Structural, Nanomechanical, and Nanotribological Studies, in Bhushan, B. (ed.) *Biophysics of Human Hair: Biological and Medical Physics*, Biomedical Engineering. Berlin, Heidelberg: Springer-Verlag, 1–19.
- Borges, V. R. de A., Simon, A., Sena, A. R. C., Cabral, L. M. and de Sousa, V. P. (2013) Nanoemulsion containing dapsona for topical administration: A study of in vitro release and epidermal permeation, *International Journal of Nanomedicine*, 8, 535–544.
- Bouchemal, K., Briançon, S., Perrier, E. and Fessi, H. (2004) Nano-emulsion formulation using spontaneous emulsification: Solvent, oil and surfactant optimisation, *International Journal of Pharmaceutics*, 280(1–2), 241–251.
- British Pharmacopoeia Commission (2017) *British Pharmacopoeia: Monograph A-I*. (Volume I). London: TSO.
- Brownlee, K. K., Moore, A. W. and Hackney, A. C. (2005) Relationship between circulating cortisol and testosterone: Influence of physical exercise, *Journal of Sports Science and Medicine*, 4(1), 76–83.
- Buanz, A., Prior, T. J., Burley, J. C., Raimi-Abraham, B. T., Telford, R., Hart, M., Seaton, C. C., Davies, P. J., Scowen, I. J., Gaisford, S. and Williams, G. R. (2015) Thermal behavior of benzoic acid/isonicotinamide binary cocrystals, *Crystal Growth & Design*, 15(7), 3249–3256.
- Butler, M. (2005) Animal cell cultures: Recent achievements and perspectives in the production of biopharmaceuticals, *Applied Microbiology and Biotechnology*, 68(3), 283–291.
- Campbell, C. S. J., Contreras-rojas, L. R., Delgado-charro, M. B. and Guy, R. H. (2012) Objective assessment of nanoparticle disposition in mammalian skin after topical exposure, *Journal of Controlled Release*, 162, 201–207.
- Campos, A. M. De, Sanchez, A., Gref, R., Calvo, P. and Alonso, M. J. (2003) The effect of a PEG versus a chitosan coating on the interaction of drug colloidal carriers with the ocular mucosa, *European Journal of Pharmaceutical Sciences*, 20, 73–81.

- Caon, T., Cucco, L., Granada, A., Piazzon, M., Antonio, M., Silva, S., Maria, C., Simões, O., Borsali, R. and Soldi, V. (2014) Chitosan-decorated polystyrene-b-poly (acrylic acid) polymersomes as novel carriers for topical delivery of finasteride, *European Journal of Pharmaceutical Sciences*, 52, 165–172.
- Castleberry, S. A., Quadir, M. A., Sharkh, M. A., Shopsowitz, K. E. and Hammond, P. T. (2017) Polymer conjugated retinoids for controlled transdermal delivery, *Journal of Controlled Release*, 262, 1–9.
- Castro, G. A., Luíza, A., Coelho, L. R., Oliveira, C. A., Mahecha, G. A. B., Oréface, R. L. and Ferreira, L. A. M. (2009) Formation of ion pairing as an alternative to improve encapsulation and stability and to reduce skin irritation of retinoic acid loaded in solid lipid nanoparticles, *International Journal of Pharmaceutics*, 381, 77–83.
- Cevc, G., Gebauer, D., Stieber, J., Schätzlein, A. and Blume, G. (1998) Ultraflexible vesicles, transfersomes, have an extremely low pore penetration resistance and transport therapeutic amounts of insulin across the intact mammalian skin, *Biochimica et Biophysica Acta - Biomembranes*, 1368(2), 201–215.
- Chan, J. M., Valencia, P. M., Zhang, L., Langer, R. and Farokhzad, O. C. (2010) Polymeric Nanoparticles for Drug Delivery, in Grobmyer, S. R. and Moudgil, B. M. (eds) *Cancer Nanotechnology: Methods and Protocols*. New York: Humana Press, 163–175.
- Cheung, R. C. F., Ng, T. B., Wong, J. H. and Chan, W. Y. (2015) Chitosan: An update on potential biomedical and pharmaceutical applications, *Marine Drugs*, 13(8), 5156–5186.
- Choi, S., Moon, J., Jeon, B., Jeon, Y., Yoon, B. and Lim, C. (2015) Hair growth promoting potential of phospholipids purified from porcine lung tissues, *Biomolecules & Therapeutics*, 23(2), 174–179.
- Choo, G.-H., Park, S.-J., Hwang, S.-J. and Kim, M.-S. (2013) Formulation and in vivo evaluation of a self- microemulsifying drug delivery system of dutasteride, *Drug Research*, 63(4), 203–209.
- Curotto, E. and Aros, F. (1993) Quantitative determination of chitosan and the percentage of free amine groups, *Analytical Biochemistry*, (211), 240–241.
- DebMandal, M. and Mandal, S. (2011) Coconut (*Cocos nucifera* L.: Arecaceae): in health promotion and disease prevention., *Asian Pacific Journal of Tropical Medicine*, 4(3), 241–247.
- Denizot, F. and Lang, R. (1986) Rapid colorimetric assay for cell growth and survival, *Journal of Immunological Methods*, 89(2), 271–277.
- Dillen, K., Vandervoort, J., Van Den Mooter, G., Verheyden, L. and Ludwig, A. (2004) Factorial design, physicochemical characterisation and activity of ciprofloxacin-PLGA nanoparticles, *International Journal of Pharmaceutics*, 275, 171–187.

- Doktorovova, S., Shegokar, R., Rakovsky, E., Gonzalez-Mira, E., Lopes, C. M., Silva, A. M., Martins-Lopes, P., Muller, R. H. and Souto, E. B. (2011) Cationic solid lipid nanoparticles (cSLN): Structure, stability and DNA binding capacity correlation studies., *International Journal of Pharmaceutics*, 420(2), 341–349.
- Dragojevic, S., Ryu, J. S. and Raucher, D. (2015) Polymer-based prodrugs: Improving tumour targeting and the solubility of small molecule drugs in cancer therapy, *Molecules*, 20(12), 21750–21769.
- Du, Y.-Z., Lu, P., Zhou, J.-P., Yuan, H. and Hu, F.-Q. (2010) Stearic acid grafted chitosan oligosaccharide micelle as a promising vector for gene delivery system: factors affecting the complexation., *International Journal of Pharmaceutics*, 391, 260–266.
- El-Hefian, E. A., Nasef, M. M. and Yahaya, A. H. (2011) Preparation and characterization of chitosan/poly (vinyl alcohol) blended films: Mechanical, thermal and surface investigations, *E-Journal of Chemistry*, 8(1), 91–96.
- Elmowafy, M., Samy, A., Abdelaziz E., A., Shalaby, K., Salama, A., A. Raslan, M. and A. Abdelgawadd, M. (2017) Polymeric nanoparticles based topical gel of poorly soluble drug: Formulation, ex-vivo and in vivo evaluation, *Beni-Suef University Journal of Basic and Applied Sciences*, (Article in press).
- Escobar-Chávez, J. J., Rodríguez-cruz, I. M., Domínguez-delgado, C. L., Díaz-torres, R., Revilla-vázquez, A. L. and Aléncaster, N. C. (2012) Nanocarrier systems for transdermal drug delivery, in Sezer, A. D. (ed.) *Recent Advances in Novel Drug Carrier Systems*. InTech Publisher, 201–240.
- Esposito, E., Zanella, C., Cortesi, R., Menegatti, E. and Nastruzzi, C. (1998) Influence of liposomal formulation parameters on the in vitro absorption of methyl nicotinate, *International Journal of Pharmaceutics*, 172(1–2), 255–260.
- Eun, H. C., Kwon, O. S., Yeon, J. H., Shin, H. S., Kim, B. Y., Ro, B. I., Cho, H. K., Sim, W. Y., Lew, B. L., Lee, W.-S., Park, H. Y., Hong, S. P. and Ji, J. H. (2010) Efficacy, safety, and tolerability of dutasteride 0.5 mg once daily in male patients with male pattern hair loss: a randomized, double-blind, placebo-controlled, phase III study., *Journal of the American Academy of Dermatology*.
- Euromonitor International (2013) *The Divergent Worlds of Hair Care: Global Strategies For Growth*.
- European Commission (2009) Regulation (EC) on cosmetic products. *Official Journal of the European Union*.
- Fang, C., Li, Y. and Fang, J. (2014) Delivery and targeting of nanoparticles into hair follicles, *Therapeutic Delivery*, 5, 991–1006.
- Fernandes, M., Gonçalves, I. C., Nardecchia, S., Amaral, I. F., Barbosa, M. A. and Martins, M. C. L. (2013) Modulation of stability and mucoadhesive properties of chitosan microspheres for therapeutic gastric application, *International Journal of Pharmaceutics*, 454(1), 116–124.

- Finnin, B. C. and Morgan, T. M. (1999) Transdermal penetration enhancers: Applications, limitations, and potential, *Journal of Pharmaceutical Sciences*, 88(10), 955–958.
- Fischer, K. (2015) Animal Testing and Marketing Bans of the EU Cosmetics Legislation, *European Journal of Risk Regulation*, 6(4), 613–621.
- Fluorochem (2012) Safety data sheet - Dutasteride. [http://www.fluorochem.co.uk/System/DownloadSDS?fileName=\(en-GB\)079399\\_1.00.pdf](http://www.fluorochem.co.uk/System/DownloadSDS?fileName=(en-GB)079399_1.00.pdf).
- Fonte, P., Nogueira, T., Gehm, C., Ferreira, D. and Sarmiento, B. (2011) Chitosan-coated solid lipid nanoparticles enhance the oral absorption of insulin, *Drug Delivery and Translational Research*, 1(4), 299–308.
- Gaber, N. N., Darwis, Y., Kok-Khiang, P. and Tze Fung Tan, Y. (2006) Characterization of polymeric micelles for pulmonary delivery of beclomethasone dipropionate, *Journal of Nanoscience and Nanotechnology*, 6(9–10), 3095–3101.
- Gasco, M. R. (1993) Method for producing solid lipid microspheres having a narrow size distribution. Italy: US Patent No. 5250236.
- Gelfuso, G. M., Gratieri, T., Simão, P. S., de Freitas, L. A. P. and Lopez, R. F. V. (2011) Chitosan microparticles for sustaining the topical delivery of minoxidil sulphate., *Journal of Microencapsulation*, 28(7), 650–658.
- Genno, M., Yamamoto, R., Kojima, H., Konishi, H. and Klausner, M. (1998) Evaluation of a new alternative to primary Draize skin irritation testing using the EpiDerm™ skin model, *Alternative Animal Testing Experiment*, 5, 195–200.
- Gerlier, D. and Thomasset, N. (1986) Use of MTT colorimetric assay to measure cell activation, *Journal of Immunological Methods*, 94(1–2), 57–63.
- GlaxoSmithKline Inc. (2013) Product monograph-AVODART®. Ontario. Available at: <https://ca.gsk.com/media/588688/avodart.pdf>.
- Godin, B. and Touitou, E. (2007) Transdermal skin delivery: Predictions for humans from in vivo, ex vivo and animal models, *Advanced Drug Delivery Reviews*, 59, 1152–1161.
- Golla, S., Madihally, S., Jr., R. L. R. and Gasem, K. A. M. (2009) Quantitative structure–property relationships modeling of skin irritation, *Toxicology in Vitro*, 23(1), 176–184.
- Gomes, M. J., Martins, S., Ferreira, D., Segundo, M. a and Reis, S. (2014) Lipid nanoparticles for topical and transdermal application for alopecia treatment: development, physicochemical characterization, and in vitro release and penetration studies., *International Journal of Nanomedicine*, 9, 1231–1242.
- Gopala Krishna, A. G., Raj, G., Bhatnagar, A. S., Prasanth Kumar, P. K. and

- Chandrashekar, P. (2010) Coconut oil: Chemistry, production and its applications - A Review, *Indian Coconut Journal*, 15–27.
- Grams, Y. Y. (2005) Influence of molecular properties and delivery system design on the transfollicular transport across the skin. Leiden University.
- Gu, X., Zhang, W., Liu, J., Shaw, J. P., Shen, Y., Xu, Y., Lu, H. and Wu, Z. (2011) Preparation and characterization of a lovastatin-loaded protein-free nanostructured lipid carrier resembling high-density lipoprotein and evaluation of its targeting to foam cells., *AAPS PharmSciTech*, 12(4), 1200–1208.
- Guterres, S. S., Alves, M. P. and Pohlmann, A. R. (2007) Polymeric nanoparticles, nanospheres and nanocapsules, for cutaneous applications, *Drug Target Insights*, 2, 147–157.
- Han, J. H., Kwon, O. S., Chung, J. H., Cho, K. H., Eun, H. C. and Kim, K. H. (2004) Effect of minoxidil on proliferation and apoptosis in dermal papilla cells of human hair follicle., *Journal of Dermatological Science*, 34, 91–98.
- Harcha, W. G., Mart, B., Tsai, T.-F., Katsuoka, K., Kawashima, M., RyojiTsuboi, Barnes, A., Ferron-Brady, G. and Chetty, D. (2014) A randomized , active- and placebo-controlled study of the efficacy and safety of different doses of dutasteride versus placebo and finasteride in the treatment of male subjects with androgenetic alopecia, *Journal of the American Academy of Dermatology*, 70(3), 489–498.
- Hibberts, N., Howell, A. and Randall, V. (1998) Balding hair follicle dermal papilla cells contain higher levels of androgen receptors than those from non-balding scalp., *The Journal of Endocrinology*, 156(1), 59–65.
- Hoare, T. R. and Kohane, D. S. (2008) Hydrogels in drug delivery: Progress and challenges, *Polymer*, 49(8), 1993–2007.
- Hommoss, A. (2008) Nanostructured Lipid Carriers (NLC) in dermal and personal care formulations. Free University of Berlin.
- Honary, S. and Zahir, F. (2013) Effect of zeta potential on the properties of nano-drug delivery systems - A Review (Part 2), *Tropical Journal of Pharmaceutical Research*, 12(2), 265–273.
- Hu, F.-Q., Liu, L.-N., Du, Y.-Z. and Yuan, H. (2009) Synthesis and antitumour activity of doxorubicin conjugated stearic acid-g-chitosan oligosaccharide polymeric micelles., *Biomaterials*, 30(36), 6955–6963.
- Hunt, N. and Mchale, S. (2005) Clinical review: The psychological impact of alopecia, *British Medical Journal*, 331, 951–953.
- Hussain, A., Samad, A., Singh, S. K., Ahsan, M. N., Haque, M. W., Faruk, A. and Ahmed, F. J. (2016) Nanoemulsion gel-based topical delivery of an antifungal drug: in vitro activity and in vivo evaluation, *Drug Delivery*, 23(2), 642–657.
- Ibrahim, K. A., El-Eswed, B. I., Abu-Sbeih, K. A., Arafat, T. A., Al Omari, M. M.

- H., Darras, F. H. and Badwan, A. A. (2016) Preparation of chito-oligomers by hydrolysis of chitosan in the presence of zeolite as adsorbent, *Marine Drugs*, 14(8), 1–13.
- Inoue, T., Hisatsugu, Y., Yamamoto, R. and Suzuki, M. (2004) Solid-liquid phase behavior of binary fatty acid mixtures: 1. Oleic acid/stearic acid and oleic acid/behenic acid mixtures, *Chemistry and Physics of Lipids*, 127(2), 143–152.
- International Conference on Harmonisation (1996) ICH harmonised tripartite guideline : Validation of analytical procedures: Text and methodology Q2(R1). Geneva.
- Iqbal, N., Vitorino, C. and Taylor, K. M. G. (2017) How can lipid nanocarriers improve transdermal delivery of olanzapine?, *Pharmaceutical Development and Technology*, 22(4), 587–596.
- Jacobi, U., Kaiser, M., Toll, R., Mangelsdorf, S., Audring, H., Otberg, N., Sterry, W. and Lademann, J. (2007) Porcine ear skin: an in vitro model for human skin., *Skin Research and Technology*, 13(1), 19–24.
- Janssen, M., Mihov, G., Welting, T., Thies, J. and Emans, P. (2014) Drugs and polymers for delivery systems in OA joints: Clinical needs and opportunities, *Polymers*, 6, 799–819.
- Jenning, V., Gysler, A., Schäfer-Korting, M. and Gohla, S. H. (2000) Vitamin A loaded solid lipid nanoparticles for topical use: Occlusive properties and drug targeting to the upper skin., *European Journal of Pharmaceutics and Biopharmaceutics*, 49, 211–218.
- Jeon, Y.-J. and Kim, S.-K. (2002) Antitumour activity of chitosan oligosaccharides produced in ultrafiltration membrane reactor system, *Journal of Microbiology and Biotechnology*, 12(3), 503–507.
- Jo, S. J., Choi, S.-J., Yoon, S.-Y., Lee, J. Y., Park, W.-S., Park, P.-J., Kim, K. H., Eun, H. C. and Kwon, O. (2013) Valproic acid promotes human hair growth in in vitro culture model., *Journal of Dermatological Science*, 72(1), 16–24.
- Kandárová, H., Hayden, P., Klausner, M., Kubilus, J. and Sheasgreen, J. (2009) An in vitro skin irritation test (SIT) using the EpiDerm Reconstructed Human Epidermal (RHE) model, *Journal of Visualized Experiments*, 29(July), 1–6.
- Kandavilli, S., Nalamothu, V. and Pandya, V. (2010) Topical compositions comprising 5-alpha reductase inhibitors. United State: US Patent US 2010/0048598 A1.
- Kang, Y. O., Jung, J. Y., Cho, D., Kwon, O. H., Cheon, J. Y. and Park, W. H. (2016) Antimicrobial silver chloride nanoparticles stabilized with chitosan oligomer for the healing of burns, *Materials*, 9(215), 1–10.
- Kaufman, K. D. (2002) Androgens and alopecia, *Molecular and Cellular Endocrinology*, 198, 89–95.

- Khandpur, S., Suman, M. and Reddy, B. S. (2002) Comparative efficacy of various treatment regimens for androgenetic alopecia in men., *The Journal of Dermatology*, 29, 489–98.
- Kim, M. S. (2013) Influence of hydrophilic additives on the supersaturation and bioavailability of dutasteride-loaded hydroxypropyl- $\beta$ -cyclodextrin nanostructures, *International Journal of Nanomedicine*, 8, 2029–2039.
- Kim, M. S., Ha, E. S., Choo, G. H. and Baek, I. H. (2015) Preparation and in vivo evaluation of a dutasteride-loaded solid-supersaturatable self-microemulsifying drug delivery system, *International Journal of Molecular Sciences*, 16(5), 10821–10833.
- Kodre, K., Attarde, S., Yendhe, P., Patil, R. and Barge, V. (2014) Differential scanning calorimetry: A review, *Research and Reviews: Journal of Pharmaceutical Analysis*, 3(3), 11–22.
- Kong, M., Chen, X. G., Kweon, D. K. and Park, H. J. (2011) Investigations on skin permeation of hyaluronic acid based nanoemulsion as transdermal carrier, *Carbohydrate Polymers*, 86(2), 837–843.
- Kreindler, T. G. (1987) Topical minoxidil in early androgenetic alopecia, *Journal of American Academy Dermatology*, 16(3 Pt 2), 718–724.
- Kumar, N., Rungseevijitprapa, W., Narkkhong, N.-A., Suttajit, M. and Chaiyasut, C. (2012) 5 $\alpha$ -reductase inhibition and hair growth promotion of some Thai plants traditionally used for hair treatment., *Journal of Ethnopharmacology*, 139(3), 765–771.
- Kumar, T., Chaiyasut, C., Rungseevijitprapa, W. and Suttajit, M. (2011) Screening of steroid 5 $\alpha$ -reductase inhibitory activity and total phenolic content of Thai plants, *Journal of Medicinal Plants Research*, 5(7), 1265–1271.
- Kuo, Y.-C. and Wang, C.-C. (2013) Cationic solid lipid nanoparticles with cholesterol-mediated surface layer for transporting saquinavir to the brain, *Biotechnology Progress*, (1), 1–9.
- Lachenmeier, D. W. (2008) Safety evaluation of topical applications of ethanol on the skin and inside the oral cavity, *Journal of Occupational Medicine Safety*, 16, 1–16.
- Lademann, J., Richter, H., Teichmann, A., Otberg, N., Blume-Peytavi, U., Luengo, J., Weiss, B., Schaefer, U. F., Lehr, C.-M., Wepf, R. and Sterry, W. (2007) Nanoparticles - An efficient carrier for drug delivery into the hair follicles., *European Journal of Pharmaceutics and Biopharmaceutics*, 66, 159–164.
- Lai, F., Logu, A. De, Zaru, M., Müller, R. H. and Fadda, A. M. (2007) SLN as a topical delivery system for *Artemisia arborescens* essential oil : In vitro antiviral activity and skin permeation study, *International Journal of Nanomedicine*, 2(3), 419–426.
- Larson, N. and Ghandeharia, H. (2012) Polymeric conjugates for drug delivery,

Chemistry and Materials, 24(5), 1–33.

- Lee, C.-M., Jang, D., Kim, J., Cheong, S.-J., Kim, E.-M., Jeong, M.-H., Kim, S.-H., Kim, D. W., Lim, S. T., Sohn, M.-H., Jeong, Y. Y. and Jeong, H.-J. (2011) Oleyl-chitosan nanoparticles based on a dual probe for optical/MR imaging in vivo., *Bioconjugate Chemistry*, 22, 186–192.
- Lembo, D. and Cavalli, R. (2010) Nanoparticulate delivery systems for antiviral drugs, *Antiviral Chemistry and Chemotherapy*, 21, 53–70.
- Li, J., Wang, X., Zhang, T., Wang, C., Huang, Z., Luo, X. and Deng, Y. (2015) A review on phospholipids and their main applications in drug delivery systems, *Asian Journal of Pharmaceutical Sciences*, 10, 81–98.
- Li, Q., Du, Y.-Z., Yuan, H., Zhang, X.-G., Miao, J., Cui, F.-D. and Hu, F.-Q. (2010) Synthesis of lamivudine stearate and antiviral activity of stearic acid-g-chitosan oligosaccharide polymeric micelles delivery system, *European Journal of Pharmaceutical Sciences*, 41(3–4), 498–507.
- Liang, T. and Liao, S. (1992) Inhibition of steroid 5 alpha-reductase by specific aliphatic unsaturated fatty acids., *Biochemical Journal*, 285, 557–562.
- Lin, X., Li, X., Zheng, L., Yu, L., Zhang, Q. and Liu, W. (2007) Preparation and characterization of monocaprato nanostructured lipid carriers, *Colloids and Surfaces A: Physicochemical and Engineering Aspects*, 311(1–3), 106–111.
- Lin, Y., Al-suwayeh, S. A., Leu, Y., Shen, F. and Fang, J. (2013) Squalene-containing nanostructured lipid carriers promote percutaneous absorption and hair follicle targeting of diphenacyprone for treating alopecia areata, *Pharmaceutical Research*, 30, 435–446.
- Liu, C. H. and Wu, C. T. (2010) Optimization of nanostructured lipid carriers for lutein delivery, *Colloids and Surfaces A: Physicochemical and Engineering Aspects*, 353(2–3), 149–156.
- Liu, J., Hu, W., Chen, H., Ni, Q., Xu, H. and Yang, X. (2007) Isotretinoin-loaded solid lipid nanoparticles with skin targeting for topical delivery., *International Journal of Pharmaceutics*, 328, 191–195.
- Liu, J., Shimizu, K. and Kondo, R. (2009) Anti-androgenic activity of fatty acids, *Chemistry & Biodiversity*, 6, 503–512.
- Luo, Q., Zhao, J., Zhang, X. and Pan, W. (2011) Nanostructured lipid carrier (NLC) coated with Chitosan Oligosaccharides and its potential use in ocular drug delivery system, *International Journal of Pharmaceutics*, 403(1–2), 185–191.
- MacNeil, S. (2007) Progress and opportunities for tissue-engineered skin., *Nature*, 445, 874–880.
- Madheswaran, T., Baskaran, R., Sundaramoorthy, P. and Yoo, B. K. (2015) Enhanced skin permeation of 5 $\alpha$ -reductase inhibitors entrapped into surface-modified liquid crystalline nanoparticles, *Archives of Pharmacal Research*, 38,

- Madheswaran, T., Baskaran, R., Thapa, R. K., Rhyu, J. Y., Choi, H. Y., Kim, J. O., Yong, C. S. and Yoo, B. K. (2013) Design and in vitro evaluation of finasteride-loaded liquid crystalline nanoparticles for topical delivery, *AAPS PharmSciTech*, 14(1), 45–52.
- Mahe, B., Vogt, A., Liard, C., Duffy, D., Abadie, V., Bonduelle, O., Boissonnas, A., Sterry, W., Verrier, B., Blume-Peytavi, U. and Combadiere, B. (2009) Nanoparticle-based targeting of vaccine compounds to skin antigen-presenting cells by hair follicles and their transport in mice., *The Journal of Investigative Dermatology*, 129(5), 1156–1164.
- Mandawgade, S. D. and Patravale, V. B. (2008) Development of SLNs from natural lipids: Application to topical delivery of tretinoin, *International Journal of Pharmaceutics*, 363, 132–138.
- Martins, S., Sarmiento, B., Ferreira, D. C. and Souto, E. B. (2007) Lipid-based colloidal carriers for peptide and protein delivery - Liposomes versus lipid nanoparticles, *International Journal of Nanomedicine*, 2(4), 595–607.
- Matos, B. N., Reis, T. A., Gratieri, T. and Gelfuso, G. M. (2015) Chitosan nanoparticles for targeting and sustaining minoxidil sulphate delivery to hair follicles, *International Journal of Biological Macromolecules*, 75, 225–229.
- Megrab, N. A., Williams, A. C. and Barry, B. W. (1995) Oestradiol permeation across human skin, silastic and snake skin membranes: The effects of ethanol/water co-solvent systems, *International Journal of Pharmaceutics*, 116(1), 101–112.
- Merchant, Z., Taylor, K. M. G., Stapleton, P., Razak, S. A., Kunda, N., Alfagih, I., Sheikh, K., Saleem, I. Y. and Somavarapu, S. (2014) Engineering hydrophobically modified chitosan for enhancing the dispersion of respirable microparticles of levofloxacin, *European Journal of Pharmaceutics and Biopharmaceutics*, 88(3), 816–829.
- Messenger, G. and Rundegren, J. (2004) Minoxidil: Mechanisms of action on hair growth, *British Journal of Dermatology*, 150, 186–194.
- Mittal, A., Schulze, K., Ebsen, T., Weissmann, S., Hansen, S., Guzmán, C. A. and Lehr, C.-M. (2015) Inverse micellar sugar glass (IMSG) nanoparticles for transfollicular vaccination, *Journal of Controlled Release*, 206, 140–152.
- Montenegro, L., Lai, F., Offerta, A., Sarpietro, M. G., Micicché, L., Maccioni, A. M., Valenti, D. and Fadda, A. M. (2016) From nanoemulsions to nanostructured lipid carriers: A relevant development in dermal delivery of drugs and cosmetics, *Journal of Drug Delivery Science and Technology*, 32, 100–112.
- Moore, S. and Stein, W. H. . (1954) A modified ninhydrin reagent for the photometric determination of amino acids and related compounds, *The Journal of Biological Chemistry*, 211, 907–913.

- Mosmann, T. (1983) Rapid colorimetric assay for cellular growth and survival: application to proliferation and cytotoxicity assay, *Journal Immunological Methods*, 65(1–2), 55–63.
- Motwani, M., Rhein, L. and Zatz, J. (2004) Deposition of salicylic acid into hamster sebaceous, *Journal of Cosmetic Science*, 55(6), 519–531.
- Müller, R. H., Jenning, V., Mader, K. and Lippacher, A. (2014) Lipid particles on the basis of mixtures of liquid and solid lipids and method for producing same. Germany: US 8663692 B1.
- Müller, R. H., Mäder, K. and Gohla, S. (2000) Solid lipid nanoparticles (SLN) for controlled drug delivery - A review of the state of the art, *European Journal of Pharmaceutics and Biopharmaceutics*, 50, 161–177.
- Müller, R. H., Petersen, R. D., Hommoss, A. and Pardeike, J. (2007) Nanostructured lipid carriers (NLC) in cosmetic dermal products, *Advanced Drug Delivery Reviews*, 59(6), 522–530.
- Müller, R. H., Radtke, M. and Wissing, S. A. (2002) Solid lipid nanoparticles (SLN) and nanostructured lipid carriers (NLC) in cosmetic and dermatological preparations, *Advanced Drug Delivery Review*, 54(1), 131–155.
- Naguib, Y. W., Rodriguez, B. L., Li, X., Hursting, S. D., Williams, R. O. and Cui, Z. (2014) Solid lipid nanoparticle formulations of docetaxel prepared with high melting point triglycerides: in vitro and in vivo evaluation., *Molecular Pharmaceutics*, 11, 1239–1249.
- Nair, R., Kumar, A. C. K., Priya, V. K., Yadav, C. M. and Raju, P. Y. (2012) Formulation and evaluation of chitosan solid lipid nanoparticles of carbamazepine., *Lipids in Health and Disease*, 11(72), 1–8.
- Nam, K. S., Kim, M. K. and Shon, Y. H. (2007a) Chemopreventive effect of chitosan oligosaccharide against colon carcinogenesis, *Journal of Microbiology and Biotechnology*, 17(9), 1546–1549.
- Nam, K. S., Kim, M. K. and Shon, Y. H. (2007b) Inhibition of proinflammatory cytokine-induced invasiveness of HT-29 cells by chitosan oligosaccharide, *Journal of Microbiology and Biotechnology*, 17(12), 2042–2045.
- No, H. K., Park, N. Y., Lee, S. H. and Meyers, S. P. (2002) Antibacterial activities of chitosans and chitosan oligomers with different molecular weights, *Journal of Food Science*, 67(4), 1511–1514.
- Noor, N. M., Abd. Aziz, A., Sarmidi, M. R. and Abd. Aziz, R. (2013) The effect of virgin coconut oil loaded solid lipid particles (VCO-SLPs) on skin hydration and skin elasticity, *Jurnal Teknologi*, 62, 39–43.
- OECD (2002) OECD TG 404: Acute dermal irritation/corrosion. Paris.
- OECD (2004) OECD 428: Guideline for the testing of chemicals (Skin Absorption : In vitro Method). Paris.

- OECD (2015) OECD 439: In vitro skin irritation : Reconstructed human epidermis test method. Paris.
- Ogunsola, O. a., Kraeling, M. E., Zhong, S., Pochan, D. J., Bronaugh, R. L. and Raghavan, S. R. (2012) Structural analysis of “flexible” liposome formulations: new insights into the skin-penetrating ability of soft nanostructures, *Soft Matter*, 8, 10226–10232.
- Olsen, E., Hordinsky, M., Whiting, D., Stough, D., Hobbs, S., Ellis, M. L., Wilson, T. and Rittmaster, R. S. (2006) The importance of dual 5 $\alpha$ -reductase inhibition in the treatment of male pattern hair loss: Results of a randomized placebo-controlled study of dutasteride versus finasteride, *Journal of the American Academy of Dermatology*, 55(6), 1014–1023.
- Özcan, I., Azizogl, E., Senyigit, T., Mine, O. and Ozgen, O. (2013) Enhanced dermal delivery of diflucortolone valerate using lecithin/chitosan nanoparticles : In vitro and in vivo evaluations, *International Journal of Nanomedicine*, 8, 461–475.
- Padois, K., Cantiéni, C., Bertholle, V., Bardel, C., Pirot, F. and Falson, F. (2011) Solid lipid nanoparticles suspension versus commercial solutions for dermal delivery of minoxidil., *International Journal of Pharmaceutics*, 416, 300–304.
- Pandey, R. and Khuller, G. K. (2005) Solid lipid particle-based inhalable sustained drug delivery system against experimental tuberculosis., *Tuberculosis*, 85(4), 227–234.
- Pappas, A. (2009) Epidermal surface lipids, *Dermato-Endocrinology*, 1(2), 72–76.
- Pardeike, J., Hommoss, A. and Müller, R. H. (2009) Lipid nanoparticles (SLN, NLC) in cosmetic and pharmaceutical dermal products., *International Journal of Pharmaceutics*, 366, 170–184.
- Park, S., Erdogan, S., Hwang, D., Hwang, S., Han, E. H. and Lim, Y.-H. (2016) Bee venom promotes hair growth in association with inhibiting 5 $\alpha$ -reductase expression, *Biological and Pharmaceutical Bulletin*, 39(6), 1060–1068.
- Park, S. J., Choo, G. H., Hwang, S. J. and Kim, M. S. (2013) Quality by design: Screening of critical variables and formulation optimization of Eudragit E nanoparticles containing dutasteride, *Archives of Pharmacal Research*, 36, 593–601.
- Pasut, G. and Veronese, F. M. (2007) Polymer-drug conjugation, recent achievements and general strategies, *Progress in Polymer Science*, 32, 933–961.
- Patel, D., Dasgupta, S., Dey, S., Ramani, Y. R., Ray, S. and Mazumder, B. (2012) Nanostructured lipid carriers (NLC)-based gel for the topical delivery of aceclofenac: Preparation, characterization, and in vivo evaluation, *Scientia Pharmaceutica*, 80, 749–764.
- Pathan, I. B. and Setty, M. C. (2009) Chemical penetration enhancers for transdermal drug delivery systems, *Tropical Journal of Pharmaceutical Research*, 8(2), 173–179.

- Patzelt, A. and Lademann, J. (2013) Drug delivery to hair follicles, *Expert Opinion on Drug Delivery*, 10(6), 787–797.
- Patzelt, A., Richter, H., Knorr, F., Schäfer, U., Lehr, C., Dähne, L., Sterry, W. and Lademan, J. (2011) Selective follicular targeting by modification of the particle sizes, *Journal of Controlled Release*, 150(1), 45–48.
- Paudel, K. S., Milewski, M., Swadley, C. L., Brogden, N. K., Ghosh, P. and Audra L Stinchcomb (2010) Challenges and opportunities in dermal/transdermal delivery, *Therapeutic Delivery*, 1(1), 109–131.
- Pearce, K. N., Karahalios, D. and Friedman, M. (1988) Ninhydrin assay for proteolysis in ripening cheese, *Journal of Food Science*, 53(2), 432–435.
- Pecora, R. (2000) Dynamic light scattering measurement of nanometer particles in liquids, *Journal of Nanoparticle Research*, 2, 123–131.
- Du Plessis, J., Ramachandran, C., Weiner, N. and Muller, D. G. (1994) The influence of particle size of liposomes on the deposition of drug into skin, *International Journal of Pharmaceutics*, 103, 277–282.
- Prozorov, T., Kataby, G., Prozorov, R. and Gedanken, a. (1999) Effect of surfactant concentration on the size of coated ferromagnetic nanoparticles, *Thin Solid Films*, 340, 189–193.
- Raber, a. S., Mittal, A., Schäfer, J., Bakowsky, U., Reichrath, J., Vogt, T., Schaefer, U. F., Hansen, S. and Lehr, C. M. (2014) Quantification of nanoparticle uptake into hair follicles in pig ear and human forearm, *Journal of Controlled Release*, 179(1), 25–32.
- Rafi, A. W. and Katz, R. M. (2011) Pilot study of 15 patients receiving a new treatment regimen for androgenic alopecia: The effects of atopy on AGA, *International Scholarly Research Network Dermatology*, 1–11.
- Randall, V. A. (2008) Androgens and hair growth, *Dermatologic Therapy*, 21, 314–328.
- Randall, V. A. (2010) Molecular Basis of Androgenetic Alopecia, in Trüeb, R. M. and Tobin, D. J. (eds) *Aging Hair*. Berlin, Heidelberg: Springer-Verlag, 9–24.
- Randall, V. A. and Botchkareva, N. I. (2008) The biology of hair growth, in Ahluwalia, G. S. (ed.) *Cosmetic Application of Laser and Light-Based Systems*. 1st edn. William Andrew Inc., 3–35.
- Randall, V. A., Thornton, M. J., Hamada, K., Redfern, C. P. F., Nutbrown, M., Ebling, F. J. G. and Messenger, A. G. (1991) Androgens and the hair follicle: Cultured human dermal papilla cells as a model system, *Annals New York Academy of Sciences*, 642, 355–375.
- Raynaud, J. P., Cousse, H. and Martin, P. M. (2002) Inhibition of type 1 and type 2 5alpha-reductase activity by free fatty acids, active ingredients of Permixon., *The Journal of Steroid Biochemistry and Molecular Biology*, 82(2–3), 233–239.

- Rele, A. S. and Mohile, R. B. (1999) Effect of coconut oil on prevention of hair damage. Part I, *Journal of Cosmetic Science*, 50, 327–339.
- Ridolfi, D. M., Marcato, P. D., Justo, G. Z., Cordi, L., Machado, D. and Durán, N. (2012) Chitosan-solid lipid nanoparticles as carriers for topical delivery of tretinoin., *Colloids and surfaces. B, Biointerfaces*, 93, 36–40.
- Rinaudo, M. (2006) Chitin and chitosan: Properties and applications, *Progress in Polymer Science*, 31(7), 603–632.
- Ringsdorf, H. (1975) Structure and properties of pharmacologically active polymers, *Journal of Polymer Science: Polymer Symposia*, 51(1), 135–153.
- Rivolta, I., Panariti, A., Lettiero, B., Sesana, S., Gasco, P., Gasco, M. R., Masserini, M. and Miserocchi, G. (2011) Cellular uptake of coumarin-6 as a model drug loaded in solid lipid nanoparticle, *Journal of Physiology and Pharmacology*, 62(1), 45–53.
- Robbins, C. R. (2012) Chemical composition of different hair types, in Robbins, C. R. (ed.) *Chemical and Physical Behavior of Human Hair*. 5th edn. Berlin Heidelberg: Springer-Verlag, 105–176.
- Russell, D. W. and Wilson, J. D. (1994) Steroid 5 $\alpha$ -Reductase: Two genes/two enzymes, *Annual Review Biochemistry*, 63, 25–61.
- Saeb, A. T. M., Alshammari, A. S., Al-Brahim, H. and Al-Rubeaan, K. A. (2014) Production of silver nanoparticles with strong and stable antimicrobial activity against highly pathogenic and multidrug resistant bacteria, *Scientific World Journal*, 2014.
- Sajid, M., Sarfaraz, M., Alam, N. and Raza, M. (2014) Preparation, characterization and stability study of dutasteride loaded nanoemulsion for treatment of benign prostatic hypertrophy, *Iranian Journal of Pharmaceutical Research*, 13(4), 1125–1140.
- Sato, T., Tadokoro, T., Sonoda, T., Asada, Y., Itami, S. and Takayasu, S. (1999) Minoxidil increases 17 $\beta$ -hydroxysteroid dehydrogenase and 5 $\alpha$ -reductase activity of cultured human dermal papilla cells from balding scalp, *Journal of Dermatological Science*, 19(2), 123–125.
- Schaefer, H. and Redelmeier, T. E. (2001) Skin penetration, in Rycroft, R. J. G., Menne, T., Prosch, P. J., and Lepoittevin, J.-P. (eds) *Textbook of Contact Dermatitis*. 3rd edn. Berlin, Heidelberg: Springer-Verlag, 209–226.
- Şenyiğit, T., Sonvico, F., Barbieri, S., Özer, Ö., Santi, P. and Colombo, P. (2010) Lecithin/chitosan nanoparticles of clobetasol-17-propionate capable of accumulation in pig skin, *Journal of Controlled Release*, 142(3), 368–373.
- Shah, K. A., Date, A. A., Joshi, M. D. and Patravale, V. B. (2007) Solid lipid nanoparticles (SLN) of tretinoin: Potential in topical delivery., *International Journal of Pharmaceutics*, 345(1–2), 163–171.

- Shaji, J. and Varkey, D. (2012) Recent advances in physical approaches for transdermal penetration enhancement, *Current Drug Therapy*, 7(3), 184–197.
- Sharma, P., Jain, D., Maithani, M., Mishra, S. K., Khare, P., Jain, V. and Singh, R. (2011) Development and characterization of dutasteride bearing liposomal systems for topical use., *Current Drug Discovery Technologies*, 8(2), 136–145.
- Sica, D. (2004) Minoxidil: an underused vasodilator for resistant or severe hypertension, *Journal of Clinical Hypertension*, 6(5), 283–287.
- Silva, A. C., Santos, D., Ferreira, D. C. and Souto, E. B. (2009) Minoxidil-loaded nanostructured lipid carriers (NLC): Characterization and rheological behaviour of topical formulations, *Pharmazie*, 64(3), 177–182.
- Singh, P., Sihorkar, V., Jaitely, V., Kanaujia, P. and Vyas, S. P. (2000) Pilosebaceous unit : Anatomical considerations and drug delivery opportunities, *Indian Journal of Pharmacology*, 32, 269–281.
- Sintov, A. C. and Shapiro, L. (2004) New microemulsion vehicle facilitates percutaneous penetration in vitro and cutaneous drug bioavailability in vivo., *Journal of Controlled Release*, 95(2), 173–183.
- Siqueira, N. M., Conti, R. V., Paese, K., Beck, R. C. R., Pohlmann, A. R. and Guterres, S. S. (2011) Innovative sunscreen formulation based on benzophenone-3-loaded chitosan-coated polymeric nanocapsules, *Skin Pharmacology and Physiology*, 24, 166–174.
- Sobhani, H., Tarighi, P., Ostad, S. N., Shafaati, A., Nafissi-Varcheh, N. and Aboofazeli, R. (2015) Formulation development and toxicity assessment of triacetin mediated nanoemulsions as novel delivery systems for rapamycin, *Iranian Journal of Pharmaceutical Research*, 14, 3–21.
- Sogias, I. A., Khutoryanskiy, V. V. and Williams, A. C. (2010) Exploring the factors affecting the solubility of chitosan in water, *Macromolecular Chemistry and Physics*, 211(4), 426–433.
- Stockert, J. C., Blázquez-Castro, A., Cañete, M., Horobin, R. W. and Villanueva, Á. (2012) MTT assay for cell viability: Intracellular localization of the formazan product is in lipid droplets, *Acta Histochemica*, 114(8), 785–796.
- Stough, D. (2007) Dutasteride improves male pattern hair loss in a randomized study in identical twins, *Journal of Cosmetic Dermatology*, 6(1), 9–13.
- Sun, T., Zhou, D., Xie, J. and Mao, F. (2007) Preparation of chitosan oligomers and their antioxidant activity, *European Food Research and Technology*, 225, 451–456.
- Szymańska, E. and Winnicka, K. (2015) Stability of chitosan - A challenge for pharmaceutical and biomedical applications, *Marine Drugs*, 13(4), 1819–1846.
- Tagalakis, A. D., Castellaro, S., Zhou, H., Bienemann, A., Munye, M. M., McCarthy, D., White, E. A. and Hart, S. L. (2015) A method for concentrating lipid peptide

DNA and siRNA nanocomplexes that retains their structure and transfection efficiency, *International Journal of Nanomedicine*, 10, 2673–2683.

Tanhaei, B., Saghatoleslami, N., Chenar, M. P., Ayati, A., Hesampour, M. and Mänttari, M. (2013) Experimental study of CMC evaluation in single and mixed surfactant systems, using the UV-Vis spectroscopic method, *Journal of Surfactants and Detergents*, 16(3), 357–362.

Thakur, R., Batheja, P. and Kaushik, D. (2008) Structural and biochemical changes in aging skin and their impact on skin permeability barrier, in Dayan, N. (ed.) *Skin Aging Handbook: An Integrated Approach to Biochemistry and Product Development*. USA: William Andrew Inc., 55–90.

Tiwari, B. D., Shikare, O. N. and Sontakke, A. M. (2014) Bioequivalence Study: Overview, *Journal of Pharmaceutical & Scientific Innovation*, 3(5), 421–424.

Tolgyesi, E., Coble, D. W., Fang, F. S. and Kairinen, E. O. (1983) A comparative study of beard and scalp hair, *Journal of the Society of Cosmetic Chemists*, 34, 361–382.

Trivedi, R. and Kompella, U. B. (2010) Nanomicellar formulations for sustained drug delivery: strategies and underlying principles, *Nanomedicine*, 5(3), 485–505.

Trommer, H. and Neubert, R. H. H. (2006) Overcoming the stratum corneum: The modulation of skin penetration, *Skin Pharmacology and Physiology*, 19, 106–121.

Trotta, M., Debernardi, F. and Caputo, O. (2003) Preparation of solid lipid nanoparticles by a solvent emulsification–diffusion technique, *International Journal of Pharmaceutics*, 257(1–2), 153–160.

Tsai, J., Cappel, M. J., Weiner, N. D., Flynn, G. L. and Ferry, J. (1991) Solvent effects on the harvesting of stratum corneum from hairless mouse skin through adhesive tape stripping in vitro, *International Journal of Pharmaceutics*, 68, 127–133.

Uchechi, O., Ogbonna, J. D. N. and Attama, A. A. (2014) Nanoparticles for dermal and transdermal drug delivery, in Sezer, A. D. (ed.) *Nanotechnology and Nanomaterials: Application of Nanotechnology in Drug Delivery*. InTech Publisher, 193–235.

Uchegbu, I. F., Carlos, M., Mckay, C., Hou, X. and Schätzlein, A. G. (2014) Chitosan amphiphiles provide new drug delivery opportunities, *Polymer International*, 63(7), 1145–1153.

Uchida, T., Kadhum, W. R., Kanai, S., Todo, H., Oshizaka, T. and Sugibayashi, K. (2015) Prediction of skin permeation by chemical compounds using the artificial membrane, Strat-M<sup>TM</sup>, *European Journal of Pharmaceutical Sciences*, 67, 113–118.

United Nations (2013) Globally harmonized system of classification and labelling of

chemicals (GHS). Fifth rev. New York and Geneva: United Nation.

- Uprit, S., Kumar Sahu, R., Roy, A. and Pare, A. (2013) Preparation and characterization of minoxidil loaded nanostructured lipid carrier gel for effective treatment of alopecia., *Saudi Pharmaceutical Journal*. King Saud University, 21(4), 379–385.
- Verkhovskiy, A. Y., Atochin, D. N., Udintsev, S. N., Tverdokhlebov, S. I. and Anfinogenova, Y. (2015) Transdermal delivery of xenon from lipophilic solution and water, *Dermatology Aspects*, 3(2), 1–6.
- Vijayan, V., Srinivasa Rao, D., Jayachandran, E. and Anburaj, J. (2010) Preparation and characterization of anti diabetic drug loaded solid lipid nanoparticles, *Journal of Innovative Trends in Pharmaceutical Sciences*, 1(8), 320–328.
- Wang, R., Li, L., Wang, B., Zhang, T. and Sun, L. (2012) FK506-loaded solid lipid nanoparticles: Preparation, characterization and in vitro transdermal drug delivery, *African Journal of Pharmacy and Pharmacology*, 6(12), 904–913.
- Williams, A. C. (2018) Part 5: Dosage form design and manufacture: Topical and transdermal drug delivery, in Aulton, M. E. and Taylor, K. M. G. (eds) *Aulton's Pharmaceutics: The Design and Manufacture of Medicines*. 5th edn. Churchill Livingstone Elsevier, 715–757.
- Williams, A. C. and Barry, B. W. (2004) Penetration enhancers, *Advanced Drug Delivery Review*, 56, 603–618.
- Wissing, S. A. and Müller, R. H. (2002) The influence of the crystallinity of lipid nanoparticles on their occlusive properties, *International Journal of Pharmaceutics*, 242, 377–379.
- Wissing, S. A. and Müller, R. H. (2003) The influence of solid lipid nanoparticles on skin hydration and viscoelasticity - In vivo study, *European Journal of Pharmaceutics and Biopharmaceutics*, 56(1), 67–72.
- Xie, X., Yang, Y., Chi, Q., Li, Z., Zhang, H., Li, Y. and Yang, Y. (2014) Controlled release of dutasteride from biodegradable microspheres: In vitro and in vivo studies, *PLoS ONE*, 9(12), 1–23.
- Xie, Y.-T., Du, Y.-Z., Yuan, H. and Hu, F.-Q. (2012) Brain-targeting study of stearic acid-grafted chitosan micelle drug-delivery system, *International Journal of Nanomedicine*, 7, 3235–3244.
- Xu, Y., Qin, Y., Palchoudhury, S. and Bao, Y. (2011) Water-soluble iron oxide nanoparticles with high stability and selective surface functionality., *Langmuir: The ACS Journal of Surfaces and Colloids*, 27, 8990–8997.
- Yassa, M., Saliou, M., De Rycke, Y., Hemery, C., Henni, M., Bachaud, J. M., Thiounn, N., Cosset, J. M. and Giraud, P. (2011) Male pattern baldness and the risk of prostate cancer., *Annals of Oncology*, 22(8), 1824–1827.
- Yildirim-Aksoy, M. and Beck, B. H. (2017) Antimicrobial activity of chitosan and a

chitosan oligomer against bacterial pathogens of warmwater fish, *Journal of Applied Microbiology*, 122, 1570–1578.

Yuan, H., Lu, L., Du, Y. and Hu, F. (2010) Stearic acid-g-chitosan polymeric micelle for oral drug delivery: In vitro transport and in vivo absorption, *Molecular Pharmaceutics*, 8(1), 225–238.

Zhang, D., Tan, T. and Gao, L. (2006) Preparation of oridonin-loaded solid lipid nanoparticles and studies on them in vitro and in vivo, *Nanotechnology*, 17(23), 5821–5828.

Zhang, Y., Zhang, Z., Jiang, T., Lv, H. and Zhou, J. (2013) Cell uptake of paclitaxel solid lipid nanoparticles modified by cell-penetrating peptides in A549 cells, *Pharmazie*, 68, 47–53.

Zhang, Z., Tsai, P.-C., Ramezanli, T. and Michniak-Kohn, B. B. (2013) Polymeric nanoparticles-based topical delivery systems for the treatment of dermatological diseases, *Wiley Interdiscip Rev Nanomed Nanobiotechnol*, 5(3), 205–218.

Zhao, L., Hu, Y., Xu, D. and Cai, K. (2014) Surface functionalization of titanium substrates with chitosan-lauric acid conjugate to enhance osteoblasts functions and inhibit bacteria adhesion., *Colloids and Surfaces B: Biointerfaces*, 119, 115–125.

# Appendix A

## 1. Calculation of the LOD and LOQ from the regression analysis using Microsoft Excel software for dutasteride

Nominal conc. (x)	AUC				Ave (y)	Cal. abs (Yi)
	1	2	3	4		
1	55.8	36.5	58.9	59.9	52.8	48.0
3	131.5	101.2	134.4	126.5	123.4	118.8
5	194.7	179.3	205.0	184.5	190.9	189.5
10	379.4	351.2	327.7	369.4	356.9	366.4
25	906.5	898.1	876.9	897.7	894.8	896.9
50	1817.5	1795	1762.5	1762.3	1784.3	1781.2
70	2561.5	2452.1	2473.1	2505.1	2498.0	2488.6
100	3595.0	3498.6	3500.1	3578.2	3543.0	3549

Cal – calculation from the equation

Result for regression analysis (from 3 – 100 µg/mL)

	<i>Coefficients</i>	<i>Std Error</i>	<i>t Stat</i>	<i>P-value</i>	<i>Lower 95%</i>	<i>Upper 95%</i>	<i>Lower 95.0%</i>	<i>Upper 95.0%</i>
Intercept	12.67	4.034	3.140	0.026	2.297	23.036	2.297	23.036
Variable 1	35.37	0.079	446.595	0.000	35.167	35.575	35.167	35.575

Equation from the regression analysis

$$\text{LOD} = 3.3\sigma/\text{slope} = (3.3 \times 4.034)/35.37 = 0.38 \mu\text{g/mL}$$

$$\text{LOQ} = 10\sigma/\text{slope} = (10 \times 4.034)/35.37 = 1.14 \sim 3 \mu\text{g/mL}$$

**Therefore the LOD and LOQ were 0.38 and 3 µg/mL, respectively.**

**2. Calculation of the LOD and LOQ from the regression analysis using Microsoft Excel software for coumarin-6**

Nominal conc. (x)	AUC				Ave (y)	Cal. abs (Yi)
	1	2	3	4		
0.25	19.8	77	66.4	69.9	64.7	59.2
0.5	39.6	137.8	129.4	139.5	133.1	129.2
1.0	82.0	294.9	266.1	277.6	280.6	269.1
2.5	194.5	707.7	672.6	677.4	653.5	688.8
5.0	390.4	1454.4	1350.4	1364.1	1443.1	1388.4
7.5	600.8	2209.3	2044	2052.1	2180.6	2088.0
10.0	897.1	2951.2	2716.7	2769.5	2862.8	2787.5
12.5	1088.2	3761.1	3368	3486	3624.1	3487.1

Cal – calculation from the equation

Result for regression analysis (from 0.25 – 12.5 µg/mL)

	<i>Coefficients</i>	<i>Std Error</i>	<i>t Stat</i>	<i>P-value</i>	<i>Lower 95%</i>	<i>Upper 95%</i>	<i>Lower 95.0%</i>	<i>Upper 95.0%</i>
Intercept	-10.76	5.464	-1.969	0.096	-24.13	2.608	-24.133	2.608
Variable 1	279.83	0.832	336.32	4.66 x 10 <sup>-14</sup>	277.798	281.870	277.798	281.870

Equation from the regression analysis

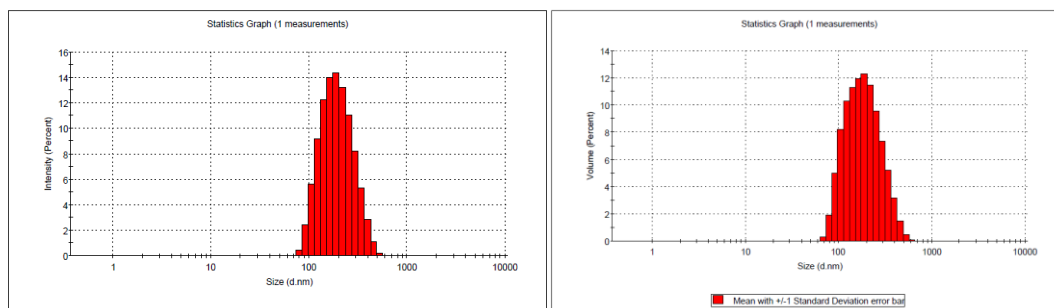
$$\text{LOD} = 3.3\sigma/\text{slope} = (3.3 \times 5.464)/279.83 = 0.064 \text{ } \mu\text{g/mL}$$

$$\text{LOQ} = 10\sigma/\text{slope} = (10 \times 5.464)/279.83 = 0.2 \sim 0.25 \text{ } \mu\text{g/mL}$$

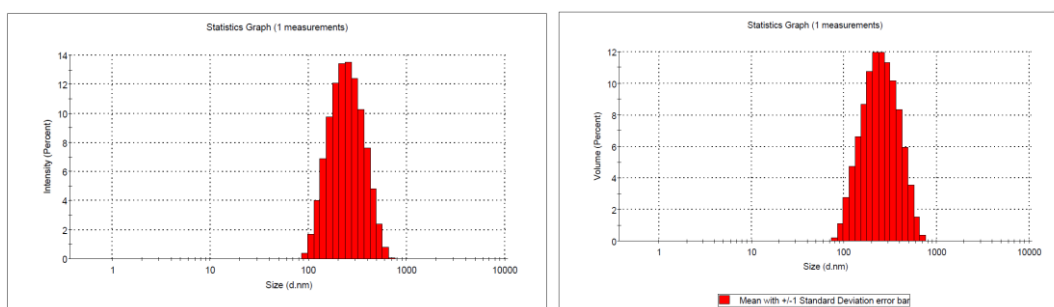
**Therefore the LOD and LOQ were 0.06 and 0.25 µg/mL, respectively.**

# Appendix B

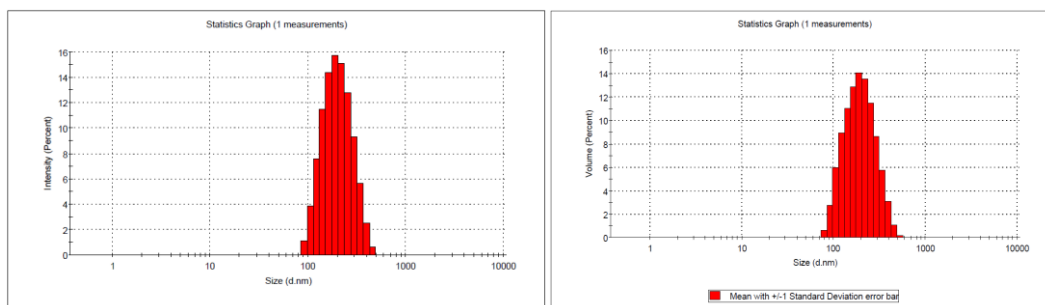
Graph of intensity and volume versus size (nm) for scaled-up DST-NLCs measured by dynamic light scattering



## 1. DST-NLCs (uncoated)



## 2. DST-NLCs coated with 5% CSO-SA



## 3. DST-NLCs coated with 5% CSO-LA

# Appendix C

## Certificate of Analysis

PromoCell

Human Follicle Dermal Papilla Cells (HFDPc)

### Description

Product Name	HFDPc-c / HFDPc-p
Order Number	C-12071 / C-12072
Lot Number	403Z030.5
Donor Age / Sex / Race	78 / male / caucasian
Tissue / Localization / Hair Color	skin / occipital / grey
Number of Viable Cells	600.000
Freezing Medium	Cryo-SFM (Order No.: C-29910)
QC Evaluation Medium	Follicle Dermal Papilla Cell Growth Medium (Order No.: C-28501)
Stage of Culture	HFDPc-c: thawing and seeding results in passage 2 (3 <sup>rd</sup> culture) HFDPc-p: shipped in passage 2 (3 <sup>rd</sup> culture)

### Viability & Growth Characteristics

Parameter	Test Method*	Result
Viability	Automated Viability Test	94 %
Population Doubling (PD) Time in Log Phase	Growth Promotion Test	25.9 h / PD
Population Doublings	Growth Promotion Test	> 10 PD*

### Phenotypic Characterization (tested within the first two passages)

Parameter	Test Method*	Result
Alkaline Phosphatase	Immunohistochemical Staining	positive

### Test for microbiological contaminants and infectious viruses

Parameter	Test Method	Result
Bacteria, Fungi	Sterility Test	negative
Mycoplasma Genus, M. Pulmonis	PCR	negative
HIV-1, HIV-2	PCR	negative
HBV, HCV	PCR	negative
HTLV-1, HTLV-2	PCR	negative

\* Using PromoCell's standardized culture system and procedures. The stated values may vary under customer culture conditions.

The tissue used by PromoCell for the isolation of human cell cultures is derived from donors who have signed an informed consent form, which outlines in detail the purpose of the donation and the procedure for processing the tissue ([www.promocell.com/ethics](http://www.promocell.com/ethics)).



*Corina Neumer*

Corina Neumer  
Head of Quality Control

Date: Nov 07, 2016

FOR IN VITRO RESEARCH USE ONLY. NOT FOR DIAGNOSTIC OR THERAPEUTIC PROCEDURES.

PromoCell GmbH  
Sickingenstr. 63 / 65  
69126 Heidelberg  
Germany

North America  
Deutschland  
France  
United Kingdom  
Other Countries

1 - 866 - 251 - 2860 (toll free)  
0800 - 776 66 23 (gebührenfrei)  
0800 90 93 32 (ligne verte)  
0800 - 96 03 33 (toll free)  
+49 6221 - 649 34 0

Email: [info@promocell.com](mailto:info@promocell.com)  
[www.promocell.com](http://www.promocell.com)

03/2015

# Publications and Presentations

## Published manuscript

Noor, N.M., Sheikh, K., Somavarapu, S., Taylor, K.M.G, 2017. Preparation and Characterization of Dutasteride-loaded Nanostructured Lipid Carriers coated with Stearic Acid-Chitosan Oligomer for Topical Delivery. *Eur. J. Pharm. Biopharm.* 117, 372–384.

European Journal of Pharmaceutics and Biopharmaceutics 117 (2017) 372–384



Research paper

## Preparation and characterization of dutasteride-loaded nanostructured lipid carriers coated with stearic acid-chitosan oligomer for topical delivery



Norhayati Mohamed Noor<sup>a,b,\*</sup>, Khalid Sheikh<sup>a</sup>, Satyanarayana Somavarapu<sup>a</sup>, Kevin M.G. Taylor<sup>a,\*</sup>

<sup>a</sup> Department of Pharmaceutics, UCL School of Pharmacy, 29-39 Brunswick Square, London WC1N 1AX, United Kingdom  
<sup>b</sup> Institute of Bioproduct Development (N22), Universiti Teknologi Malaysia, 81310 UTM Johor Bahru, Johor, Malaysia

### ARTICLE INFO

#### Article history:

Received 26 April 2016  
Revised 10 November 2016  
Accepted in revised form 11 April 2017  
Available online 12 April 2017

#### Keywords:

Alopecia  
Chitosan conjugation  
Dutasteride  
Nanostructured lipid carriers  
Topical delivery

### ABSTRACT

Dutasteride, used for treating benign prostate hyperplasia (BPH), promotes hair growth. To enhance delivery to the hair follicles and reduce systemic effects, in this study dutasteride has been formulated for topical application, in a nanostructured lipid carrier (NLC) coated with chitosan oligomer-stearic acid (CSO-SA). CSO-SA has been successfully synthesized, as confirmed using <sup>1</sup>H NMR and FTIR. Formulation of dutasteride-loaded nanostructured lipid carriers (DST-NLCs) was optimized using a 2<sup>3</sup> full factorial design. This formulation was coated with different concentrations of stearic acid-chitosan solution. Coating DST-NLCs with 5% SA-CSO increased mean size from 187.6 ± 7.0 nm to 220.1 ± 11.9 nm, and modified surface charge, with zeta potentials being -18.3 ± 0.9 mV and +25.8 ± 1.1 mV for uncoated and coated DST-NLCs respectively. Transmission electron microscopy showed all formulations comprised approximately spherical particles. DST-NLCs, coated and uncoated with CSO-SA, exhibited particle size stability over 60 days, when stored at 4–8 °C. However, NLCs coated with CSO (without conjugation) showed aggregation when stored at 4–8 °C after 30 days. The measured particle size for all formulations stored at 25 °C suggested aggregation, which was greatest for DST-NLCs coated with 10% CSO-SA and 5% CSO. All nanoparticle formulations exhibited rapid release in an *in vitro* release study, with uncoated NLCs exhibiting the fastest release rate. Using a Franz diffusion cell, no dutasteride permeated through pig ear skin after 48 h, such that it was not detected in the receptor chamber for all samples. The amount of dutasteride in the skin was significantly different (*p* < 0.05) for DST-NLCs (6.09 ± 1.09 µg/cm<sup>2</sup>) without coating and those coated with 5% CSO-SA (2.82 ± 0.40 µg/cm<sup>2</sup>), 10% CSO-SA (2.70 ± 0.35 µg/cm<sup>2</sup>) and CSO (2.11 ± 0.64 µg/cm<sup>2</sup>). There was a significant difference (*p* < 0.05) in the cytotoxicity (IC<sub>50</sub>) between dutasteride alone and in the nanoparticles. DST-NLCs coated and uncoated with CSO-SA increased the maximum non-toxic concentration by 20-fold compared to dutasteride alone. These studies indicate that a stearic acid-chitosan conjugate was successfully prepared, and modified the surface charge of DST-NLCs from negative to positive. These stable, less cytotoxic, positively-charged dutasteride-loaded nanostructured lipid carriers, with stearic acid-chitosan oligomer conjugate, are appropriate for topical delivery and have potential for promotion of hair growth.

© 2017 Published by Elsevier B.V.

### **Published Poster Presentations**

Poster presentation: AAPS Annual Meeting and Exposition, 25 October 2015, Orlando, USA (Title: Topical Delivery of Dutasteride by Stearic Acid-Chitosan Coated Nanostructured Lipid Carriers)

Poster presentation: APS PharmSci 2016, University of Strathclyde, Scotland, 5<sup>th</sup> September 2016 -7<sup>th</sup> September 2016, Poster presentation - Transfollicular Delivery of Dutasteride-Nanostructured Lipid Carriers Coated with Stearic Acid-Chitosan Oligomer

### **Internal UCL Presentations**

PhD Research Day, UCL School of Pharmacy, 15<sup>th</sup> April 2016, Poster presentation - Preparation and Characterization of Dutasteride-Nanostructured Lipid Carriers coated with Stearic Acid-Chitosan Oligomer for Transfollicular Delivery.

PhD Research Day, UCL School of Pharmacy, 7th April 2017, Oral presentation - Lipid-Based Nanoparticles for Dermal/Transfollicular Delivery of 5 $\alpha$ -reductase Inhibitors for the Treatment of Hair Loss